ELECTROCHEMICAL, OPTICAL AND PHOTOPHYSICAL PROPERTIES OF POLYPYRIDYL COMPLEXES OF RU (II) AND OS (II) IN POLYMER FILMS

By

BRIAN T. HAUSER

A DISSERTATION PRESENTED TO THE GRADUATE SCHOOL
OF THE UNIVERSITY OF FLORIDA IN PARTIAL FULFILLMENT
OF THE REQUIREMENTS FOR THE DEGREE OF
DOCTOR OF PHILOSOPHY

UNIVERSITY OF FLORIDA

1996

To Robin.

ACKNOWLEDGMENTS

The completion of this dissertation culminates many years of a long, often arduous process. Considerable instruction, encouragement, and understanding were offered by many people who deserve recognition. First, my undergraduate advisor, Dr. Raymond Dominey encouraged me to go to graduate school with his enthusiasm for chemistry and his faith in my abilities. Second, my graduate advisor, Dr. Kirk Schanze gave me the opportunity to get a taste of research at the graduate level as an undergraduate, then guided me through my graduate research and this dissertation. For making lab life a little easier and enjoyable, I need to thank the many members of the Schanze research group, past and present, including, Tom Perkins, Nancy Thornton, Lucian Lucia, Yingsheng Wang, Kevin Ley, Dr. Yibing Shen, whose patience helped me obtain the crystal structures, and especially Troy Bergstedt, who suffered with me through the early "lean" years of this project when *nothing* seemed to work. Finally, and most importantly, I need to thank my Mom and Dad for their love and support of me, and to my wife Robin, for her pep talks and for putting up with me as I wrote this thing. I can't think of anyone else with whom I'd rather spend my life.

TABLE OF CONTENTS

ACKNOWLEDGMENTS iii

LIST OF FIGURES vi

LIST OF TABLES x

ABSTRACT xi

CHAPTERS

I FABRICATION OF MICROSTRUCTURED REDOX FILMS FOR ELECTROCHEMICALLY SWITCHABLE DIFFRACTION GRATINGS 1

Introduction 1
Background 2
  Strategies for CME Fabrication 3
    Monolayer films 4
    Multilayer and polymer films 6
  Redox Film Modified Electrode Fabrication 16
    Electropolymerization 16
  Photolithography 20
  Spatial Control of CME Fabrication 22
  Diffraction Theory Basics 27
Description of the Present Study 30
Studies of *poly*-$[(bpy)_2Ru(vpy)_2]^{2+}$ and *poly*-$[Os(vbpy)_3]^{2+}$ Films 30
  PL-EP Method 32
  Electrochemical Characterization of Grating Patterned Redox Films 48
    Ideal electrochemical behavior 48
    Experimental results 50
  Optical Characterization of Grating Patterned Redox Films 58
    Spectroelectrochemistry 58
    Modulation of diffraction efficiencies through potential sweeping 61
    Modulation of diffraction efficiencies through potential stepping 75
Discussion and Interpretive Analysis 88
  Electrochemical Behavior of PL-EP Produced Grating Films 88
  Optical Behavior of PL-EP Produced Grating Films 92
Conclusions 105
Experimental 106

Materials and Syntheses 106
PL-EP Fabrication of Redox Grating Films 109
Instrumentation and Apparatus 113

2 TEMPERATURE DEPENDENT LUMINESCENCE PROPERTIES OF TWO NOVEL HETEROLEPTIC RUTHENIUM POLYPYRIDINE COMPLEXES 116

Background 116
Luminescence Applications 125
Description of the Present Study 143
Studies of the Temperature Sensitive Luminescence of Rutdp and Rutpm 144
Synthesis and Crystal Structure Determination 147
Photophysical Characterization of Rutdp and Rutpm Solutions and Coatings 152
UV-visible absorption spectroscopy 152
Steady state and time-resolved luminescence 152
Discussion 163
Conclusions 172
Experimental 173
Materials and Syntheses 173
Synthesis of [(2,2':6',2''-terpyridine)(4,7-diphenyl-1,10-phenanthroline) (pyridine) ruthenium (II)] hexafluorophosphate (Rutdp) 174
Synthesis of [(*tris*(1-pyrazolyl)methane)(4,7-diphenyl-1,10-phenantrholine) (pyridine) ruthenium] (II) hexafluorophosphate (Rutpm) 175
Formulation and Application Procedures for Rutdp and Rutpm Paints 176
Instrumentation and Apparatus 177

APPENDICES

A COULOMETRIC INTEGRATION CALCULATIONS 182

B INSTRUMENTAL PERFORMANCE TESTS 185

C DERIVATION OF DIFFRACTION EFFICIENCY EQUATIONS 190

D X-RAY CRYSTALLOGRAPHIC DATA 194

LIST OF REFERENCES 251

BIOGRAPHICAL SKETCH 258

LIST OF FIGURES

Figure page

1.1 Langmuir-Blodgett technique........5

1.2 Chemisorption of redox active species on Pt and carbon electrodes........7

1.3 Self-assembly techniques........8

1.4 Sequential adsorption-reaction technique affording monolayers........10

1.5 Sequential adsorption scheme affording multilayers........11

1.6 Structures of various conducting polymers........13

1.7 Electron transport schematic in redox polymer films........15

1.8 Examples of preassembled redox polymers........17

1.9 Examples of electrochemically polymerizable redox monomers........19

1.10 Photolithographic process used in semiconductor manufacturing........21

1.11 Meyer electrochemical/photochemical scheme........24

1.12 Structures used in photopolymerized system........26

1.13 Characteristics of a transmission grating........28

1.14 Cyclic voltammogram (CV) of a *poly*-VBV^{2+} grating film........31

1.15 Schematic diagram of PL-EP technique........34

1.16 Optical micrographs of p-MPS patterned films on ITO electrodes........36

1.17 Profilometry of p-MPS patterned film on glass........37

1.18 Structures of monomer complexes used in the PL-EP scheme........38

1.19 Synthetic scheme for redox monomers used in the PL-EP method........39

1.20 Mechanism for reductive electropolymerization........41

1.21 CV produced during PL-EP fabrication of a $[(bpy)_2Ru(vpy)_2]^{2+}$ grating film........42

1.22 CV produced during PL-EP fabrication of a $[Os(vbpy)_3]^{2+}$ grating film........43

1.23 Optical micrographs of *poly*-$[(bpy)_2Ru(vpy)_2]^{2+}$ grating films......45

1.24 Optical micrographs of *poly*-$[Os(vbpy)_3]^{2+}$ grating films......46

1.25 Scanning electron microscope images of grating films......47

1.26 Ideal reversible CV of an immobilized redox layer......49

1.27 Oxidative CV of a *poly*-$[(bpy)_2Ru(vpy)_2]^{2+}$ grating film......52

1.28 Oxidative CV of a *poly*-$[Os(vbpy)_3]^{2+}$ grating film......53

1.29 Profilometry of a *poly*-$[(bpy)_2Ru(vpy)_2]^{2+}$ grating film......54

1.30 Oxidative spectroelectrochemistry of a *poly*-$[(bpy)_2Ru(vpy)_2]^{2+}$ grating film......59

1.31 Reductive spectroelectrochemistry of a *poly*-$[(bpy)_2Ru(vpy)_2]^{2+}$ grating film......60

1.32 Oxidative spectroelectrochemistry of a *poly*-$[Os(vbpy)_3]^{2+}$ grating film......62

1.33 Reductive spectroelectrochemistry of a *poly*-$[Os(vbpy)_3]^{2+}$ grating film......63

1.34 Experimental apparatus for monitoring diffraction efficiencies......64

1.35 Electrochemical and optical data for a VBV^{2+} grating film......66

1.36 Diffraction modulation by oxidatively sweeping a *poly*-$[(bpy)_2Ru(vpy)_2]^{2+}$ grating film......67

1.37 Diffraction modulation by reductively sweeping a *poly*-$[(bpy)_2Ru(vpy)_2]^{2+}$ grating film......70

1.38 Reductive CV of the *poly*-$[(bpy)_2Ru(vpy)_2]^{2+}$ grating film during diffraction modulation......72

1.39 Diffraction modulation by oxidatively sweeping a *poly*-$[Os(vbpy)_3]^{2+}$ grating film......73

1.40 Diffraction modulation by reductively sweeping a *poly*-$[Os(vbpy)_3]^{2+}$ grating film......74

1.41 Reductive CV of the *poly*-$[Os(vbpy)_3]^{2+}$ grating film during diffraction modulation......76

1.42 Double potential step chronoamperometry......78

1.43 Diffraction modulation by oxidatively stepping a *poly*-$[(bpy)_2Ru(vpy)_2]^{2+}$ grating film in 10 second intervals......79

1.44 Diffraction modulation by oxidatively stepping a *poly*-$[(bpy)_2Ru(vpy)_2]^{2+}$ grating film in 2 second intervals......80

1.45 Diffraction modulation by reductively stepping a *poly*-$[(bpy)_2Ru(vpy)_2]^{2+}$ grating film in 10 second intervals 82

1.46 One cycle of a reductively stepped *poly*-$[(bpy)_2Ru(vpy)_2]^{2+}$ grating film in 2 second intervals 83

1.47 Diffraction modulation by oxidatively stepping a *poly*-$[Os(vbpy)_3]^{2+}$ grating film in 10 second intervals 85

1.48 One cycle of an oxidatively stepped a *poly*-$[Os(vbpy)_3]^{2+}$ grating film in 2 second intervals 86

1.49 Diffraction modulation by reductively stepping a *poly*-$[Os(vbpy)_3]^{2+}$ grating film in 10 second intervals 87

1.50 Plots of i_p vs.sweep rate, v, and i_p vs. $v^{1/2}$ 91

1.51 (a) Top view of grating film; (b) Cross-section of grating film 93

1.52 Diffraction pattern generated by He-Ne laser impinging on a grating film 94

1.53 Calculated effects of changes in *k* and *n* relative to changes in *DE* 101

1.54 Diagram of cell used in all electrochemical/optical experiments 111

2.1 Deactivation pathways for an excited molecule 118

2.2 Examples of organic lumiphores 119

2.3 a) Jablonski diagrams; (b) fluorescence; (c) phosphorescence 121

2.4 Orbital diagrams for weak and strong field ligands 123

2.5 Barton and Hartschorn's complexes for DNA sensing 126

2.6 Profiles of O_2 sensing capabilities of Demas' complex 127

2.7 Apparatus for detecting temperature dependence of luminescent complexes 129

2.8 Image of $Ru(bpy)_3^{2+}$ paint's emission versus temperature gradient 130

2.9 Luminescence vs. temperature profiles: (a) general case; (b) $Ru(bpy)_3^{2+}$ 133

2.10 State diagrams depicting importance of k_{ic} as controller of luminescence 135

2.11 Structure and luminescence vs. temperature profile for Rutrpy 136

2.12 Energy ordering of the lowest triplet states for $Ru(bpy)_3^{2+}$ and Rutrpy 138

2.13 Structures of modified Rutrpy complexes and their luminescence profiles 139

2.14 Examples of heteroleptic Rutrpy complexes 141

2.15 Examples of substituted Rutrpy complexes... 142

2.16 Structures of heteroleptic Ru complexes used in present study 145

2.17 Synthetic scheme for Rutdp... 148

2.18 Synthetic scheme for Rutpm.. 149

2.19 X-ray crystal structure for Rutdp... 150

2.20 X-ray crystal structure for [Ru(tpm)(dpph)Cl]Cl 151

2.21 UV-visible spectra of Rutdp, Rutpm, and Rutrpy 153

2.22 Room temperature emission spectra of Rutdp and Rutpm.................................... 155

2.23 Low temperature emission spectra of Rutdp glass at increasing temperatures 156

2.24 Low temperature emission spectra of Rutpm glass at increasing temperatures 157

2.25 Temperature dependence of the luminescence lifetimes of Rutdp and Rutpm....... 160

2.26 Relative orderings of the lowest triplet energies for Rutrpy, Rutdp, and Rutpm ... 162

2.27 Low temperature emission spectra of Rutdp coating at increasing temperatures... 164

2.28 Low temperature emission spectra of Rutpm coating at increasing temperatures.. 165

2.29 Luminescence vs. temperature calibrations for Rutdp, Rutpm, and Rutrpy paints. 166

2.30 dI/dT vs. temperature plots for Rutrpy, Rutdp, and Rutpm paints........................ 171

A.1 Current vs. Time profiles before and after baseline correction............................... 183

B.1 Temperature dependency of photodiodes... 186

B.2 Stability test of He-Ne laser.. 187

B.3 Linearity tests for photodiodes 188

LIST OF TABLES

Table

page

1.1 Summary of electrochemical data for 3 Ru grating films 56
1.2 Summary of electrochemical data for 3 Os grating films 57
1.3 Summary of optical data for Ru and Os grating films 69
1.4 Variable identification and equation where they first appear 96
2.1 UV-vis assignments for Rutdp, Rutpm, and related complexes 154
2.2 Summary of emission properties for Rutdp, Rutpm and related complexes 158
2.3 Temperature vs. lifetime data for Rutdp and Rutpm 161
2.4 $\Delta E'$ and k_0' values for Rutdp, Rutpm and related complexes 161
D.1 Crystal data and structure refinement for Rutdp 194
D.2 Atomic coordinates and equivalent isotropic displacement parameters for Rutdp .. 196
D.3 Bond lengths and angles for Rutdp 198
D.4 Anisotropic displacement parameters for Rutdp 207
D.5 Hydrogen coordinates and isotropic displacement parameters for Rutdp 209
D.6 Observed and calculated structure factors for Rutdp 211

Abstract of Dissertation Presented to the Graduate School
of the University of Florida in Partial Fulfillment of the
Requirements for the Degree of Doctor of Philosophy

ELECTROCHEMICAL, OPTICAL, AND PHOTOPHYSICAL PROPERTIES OF POLYPYRIDYL COMPLEXES OF RU (II) AND OS (II) IN POLYMER FILMS

By

Brian T. Hauser

December, 1996

Chairman: Kirk S. Schanze
Major Department: Chemistry

Polypyridine complexes containing transition metal ions such as Ru, Os, and Re possess a remarkable wealth of photochemical and electrochemical properties. This combination makes them versatile candidates for unique photonic and electronic applications. The first chapter details the use of two metal polypyridine complexes in the development of a two-step novel fabrication technique which combines photolithography and electropolymerization (PL-EP). This technique allows for the production of microstructured polymer-modified electrodes whose films may act as gratings which possess interesting electrochemical and optical properties. In the photolithographic step, a solution of *poly*-methylphenylsilane (p-MPS) is applied to an electrode surface and used as a photoresist, creating a patterned framework of p-MPS on the electrode. The second step in the method is the electropolymerization of a monomer solution of either $[(bpy)_2Ru(vpy)_2]^{2+}$ or $[Os(vbpy)_3]^{2+}$ where bpy = 2,2'-bipyridine, vpy = 4-vinylpyridine,

and vbpy = 4, methyl-4'-vinyl-2,2'-bipyridine. The polymer is grown on the electrode areas which are not covered by the patterned p-MPS. A final development step results in microstructured arrays of electroactive polymers with high spatial resolution on the order of 5 μm. Because of the periodicity of the polymer arrays, these films act as gratings, and diffract light. The interesting feature of these grating films is that the amount of light diffracted, the *diffraction efficiency*, *DE*, can be modulated by controlling the electrochemical potential applied to the electroactive polymer electrode, i.e., oxidation or reduction of the patterned film results in a decrease or increase in the film's diffraction efficiency, respectively. The origin of the observed dependency of the *DE* with the redox state of the film is attributed to a change in the film's refractive index upon applying an electrical potential. Grating films produced by the PL-EP method show excellent stability to repetitive electrochemical cycling and fast charge transport, allowing for their *DEs* to be optically switched at 2 sec intervals.

The versatility of such polypyridine complexes is further detailed in the second chapter which focuses on their interesting luminescence properties rather than their electrochemical properties. The luminescence of metal polypyridine complexes is often temperature dependent, and careful manipulation of their chemical structure can yield complexes whose emission properties may allow for their use as temperature sensitive probes. The successful synthesis and design strategy of two novel heteroleptic polypyridyl Ru complexes, Rutdp and Rutpm, (where Rutdp = ruthenium(II)(2,2':6',2"-terpyridine)(4,7-diphenyl-1,10-phenanthroline)(pyridine) hexafluorophosphate and Rutpm = ruthenium(II)(tris(1-pyrazolyl)methane)(4,7-diphenyl-1,10-phenanthroline)(pyridine) hexafluorophosphate) whose luminescence is temperature sensitive in the 100-298 K region is reported. The photophysics of these complexes is reported for room temperature solutions, low temperature glasses and for experiments where these complexes have been doped into a polymeric binder, allowing them to be painted on surfaces.

CHAPTER 1
FABRICATION OF MICROSTRUCTURED REDOX FILMS FOR ELECTROCHEMICALLY SWITCHABLE DIFFRACTION GRATINGS

Introduction

Metal polypyridine complexes possess an enormous amount of interesting chemistry arising from the bonding between the central metal atom and the polypyridine ligands. Beginning with the study and characterization of the complex, $Ru(bpy)_3^{2+}$ (where bpy = 2,2'-bipyridine), these complexes' unique combination of electrochemical, photochemical, and photophysical properties have made them excellent candidates for a variety of applications including solar-energy conversion, photocatalysis, and luminescence imaging. The remarkable feature of metal polypyridine complexes is the ability to fine tune their redox and spectroscopic properties by the straightforward chemical modification of their structures. With a desired application in mind, one can chemically design a polypyridine complex to perform the needed function. The present study details using Ru and Os metal polypyridine complexes whose structures have been synthetically modified for two different applications. In the first, incorporation of these complexes into patterned redox polymer films have produced films with interesting electrochemical and optical effects. In the second, the specifically designed polypyridine complexes have led to compounds whose temperature sensitive luminescence properties have attempted to be tweaked. Both studies only reinforce the versatility that these complexes offer to chemists in the fabrication of interesting electroactive and photoactive materials.

Background

Redox reactions, which involve oxidation and reduction processes, or the loss and gain of electrons respectively, have been studied for centuries. These processes can be found practically everywhere from the biological world to technology. Processes such as photosynthesis in plants, the formation of rust on metallic objects, and the electrical power supplied by batteries are just a few of the myriad examples of important redox reactions. Thus, scientists have endeavored to better comprehend the nature of such reactions in attempts to exploit their use in the development of new technology.

Controlling redox reactions predictably remains an issue that is at the forefront of many chemists' research. For example, the movement of electrons in redox reactions produces a flow of current. Exploiting the generation of this current in a reproducible manner could perhaps lead to a number of electrical and mechanical applications. In the last 20 years, chemists have begun to realize the enormous potential that lies in the ability to manipulate redox chemistry, with the promise that one day it might produce interesting materials and devices which can perform various functions *at the molecular level*, including storing electrical energy, allowing for chemical sensing of biochemical reactions in the body, and serving as memory devices.[1,2,3] Many of these so-called "molecular electronic devices" [4,5] promise device construction from the ground up, that is from the atomic and molecular scale, as opposed to present day miniaturization in the microelectronics industry. At present, devices of this nature are still in the early, formative stages, but the challenge their fabrication presents (and their potential commercialization) keeps scientists in chemistry, physics, materials science, engineering and many other disciplines chasing the dream.

In 1974 Murray and his colleagues began this pursuit by venturing from solution studies of redox reactions into synthesis of redox active molecules on electrode surfaces to produce what he called "chemically modified electrodes," [6,7] (CMEs) which allowed him to more carefully control the dynamics of the redox activity of surface-attached species by adjusting the applied potential at the electrode. By tuning an appropriate potential of the electrode, he was able to change the function of the attached species to an electron donor (oxidized form) or an electron acceptor (reduced form). By submerging this modified electrode into a solution containing an electroactive substrate, the substrate can react at the electrode surface and perform several functions, including, for example, catalysis of another chemical reaction, or binding of the solution species to the electrode, *depending on the electrochemical status of the modified surface.* Because of the tunability of the electrode, the reactivity of this substrate is now made more predictable and thus, more easily controlled. With this basic idea in mind, chemists have begun to explore the possibilities that electrodes chemically modified with electroactive molecules could prove useful in areas such as electrocatalysis,[8] electroanalysis,[9] biocompatible sensors,[10] electrochromic displays,[11] and molecular based electronics.[4]

Strategies for CME Fabrication

There are several approaches to CME fabrication which will be discussed below. The choice of any existing strategy or an invention of a new technique is specific to the desired application, but all strategies involve some form of attachment of an electroactive species to the electrode. In all techniques, there are several criteria to which one should adhere. Most importantly, the attached species should be physically and chemically stable. A stable electrode will not be washed off by solvent or when submerged into electrolyte solution. Also, continuous cycling of the electrode's potential in the attached layer's region of interest should not cause the electroactive layer to degrade. This is particularly important in catalysis or molecular device applications where repeated reversibility of applied potential and long term performance is crucial to the device's function. The growth of the electroactive layer, or film, on the electrode can be controlled by various modification procedures to produce films of various composition. Each of these film types and methods of fabrication will be addressed separately.

Monolayer films

The ability to create monolayer films has existed for decades, and its importance in investigating fundamental processes at the atomic level such as electron transport has made this a widely studied area of research.[12] With new improvements in analytical surface detection instrumentation, such as reflection infrared spectroscopy, atomic force microscopy, and surface near-edge X-ray absorption fine structure, highly detailed pictures of the surfaces of monolayer films can now be visualized and examined to further advance these studies.

The more than half-century-old Langmuir-Blodgett[13] technique, shown in Figure 1.1, provides a versatile way to hydrophobically bond an electroactive monolayer to an electrode surface. In Figure 1.1, a amphiphilic target molecule, which contains a long chained non-polar tail and a polar head group at one terminus, is spread on the air-water interface in a Langmuir trough. As the barrier is compressed, the target molecule is assembled on the surface, with the hydrophilic polar group soluble in the water, and the hydrophobic tail oriented away into the air. A substrate, usually a glass or metal electrode which has been previously submerged in the trough, is then pulled out of the solution. The electrode's hydrophilic oxide surface draws up the arranged monolayer as shown in the transfer step. In the case of electrodes modified in this manner, the nonpolar end is capped with an electroactive compound,[14] thus making the attached monolayer electroactive.

Chemisorption, the strong adhesion of substances to a substrate, is another method of forming monolayer coverage on electrode surfaces. Initial studies in 1973 by Lane and Hubbard[15] revealed the affinity of alkenes to irreversibly adsorb on Pt surfaces. Functionalizing alkenes with various ionic moieties (Figure 1.2a) incorporates an

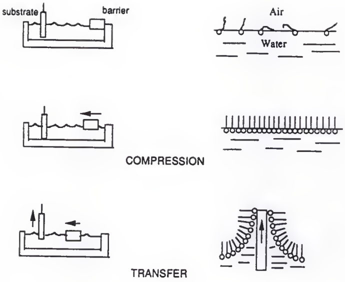

Figure 1.1 Langmuir-Blodgett technique for monolayer formation.(reproduced from ref. 12)

electroactive group into the monolayer, allowing for observation of surface charging effects when the modified electrode contacts species in solution. Anson expanded on these preliminary findings, demonstrating how additional aromatic π systems, such as ruthenium substituted phenanthrolines could also be chemisorbed onto carbon electrodes[16] (Figure 1.2b).

Self-assembled monolayers (SAMs) are a third method of achieving monolayer coverage on chemically modified electrodes. Self-assembly involves covalent bonding to the electrode's surface. The oxide surface of a glass or metal electrode contains hydroxyl groups which may form ester linkages to electroactive species terminated with carboxyl groups.[17] Other popular self-assembly methods include using organosilanes which undergo condensation reactions with surface hydroxyl groups to yield siloxane linked monolayers.[18] These organosilanes most often are terminated with some reactive group (i.e. amine, nitrile, halide) to allow for further functionalization with electroactive components with carboxyl substituents.[19] One last self-assembly technique is the assembly of thiol-terminated redox molecules to gold surfaces.[20] This type of self-assembly usually involves the formation of strong, covalent sulfur-gold bonds with high surface coverage of the redox-active component. These types of CMEs are gaining popularity for their highly oriented arrangement of surface bound redox species for utilization in molecular electronic devices.[21] Figure 1.3 summarizes each of these three self-assembly methods.

Multilayer and polymer films

The ability to modify electrode surfaces with greater amounts of electroactive materials has been significant in the development of CMEs and toward the goal of fabricating molecular electronic devices. CMEs designed with multilayer, or polymeric electroactive materials offer distinct advantages over their monolayer designed relatives. First, because of the greater coverage of redox sites, the electrochemical response is

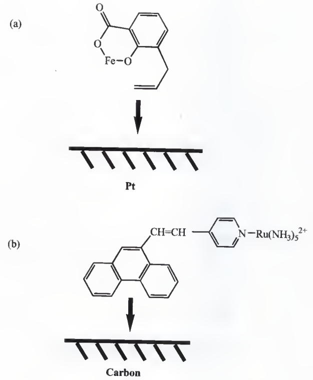

Figure 1.2. Chemisorption of redox active species on (a) Pt and (b) carbon.

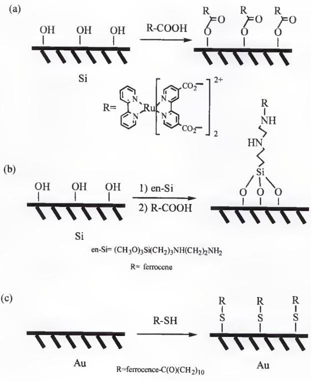

Figure 1.3. Self-assembly techniques. (a) hydroxyl functionalization (ref. 17); (b) organosilane assembly (ref. 18); (c) thiol on gold assembly (ref.19)

larger, which translates to a better signal to background noise ratio than that of monolayers. Equation 1.1 illustrates this dependence:

$$i_p = (n\mathcal{F})^2 A \Gamma_T \upsilon / 4RT \qquad 1.1$$

where i_p is the current at the electrode surface, n is the number of electrons involved in the process, $\mathcal{F}$ is Faraday's constant, A is the electrode area, Γ_T is the total electroactive coverage on the electrode in mol cm^{-2}, υ is the potential sweep rate, R is the molar gas constant, and T is temperature. Thus, from equation 1.1, the larger the value of Γ_T, the greater the i_p. A second advantage of multilayer films is because of this greater amount of electroactive material, they should better survive the repetitive cycling of the electrode's applied potential, crucial for possible catalysis and electronic device applications.

There are several types of electrodes modified with multilayers of electroactive material. The Langmuir-Blodgett technique described above (Figure 1.1) for monolayer formation can also be utilized to achieve multiple hydrophobic-hydrophilic based films by repetitive, alternating movement of the substrate into and out of the trough during transfer. However, one drawback that these types of films suffer is the chemical and mechanical instability inherent of the fragile nature of the film's polar/non-polar interaction. Another interesting, though somewhat intricate technique by Marks et al.,[22] expands upon using aforementioned organosilane self-assembly methods by the covalent reaction of a hemicyanine dye with an iodobenzyl-substituted silane (Figure 1.4). By repeating steps 1-5, multilayers films were prepared to study the film's second harmonic generation effects achieved by hyperpolarization. An additional self-assembled approach to multilayer films was introduced by Mallouk et al.,[23] who prepared films of zirconium alkanebisphosphonates by sequentially absorbing Zr^{4+} and phosphonic acid components on thiol or silane modified substrates (Figure 1.5). These films have possible applications in small molecule sensing devices,[24] as insulators in metal-insulator-semiconductor thin film

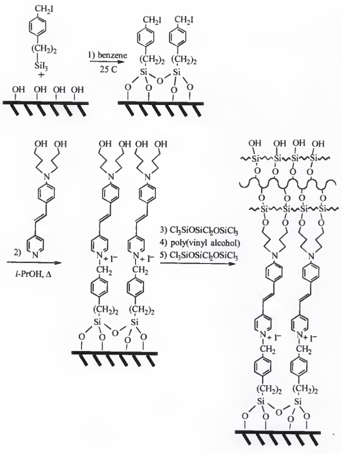

Figure 1.4. Sequential adsorption-reaction technique producing a monolayer of oriented hemicyanine molecules. Steps 1-5 can be repeated to produce multilayers. (From ref. 22)

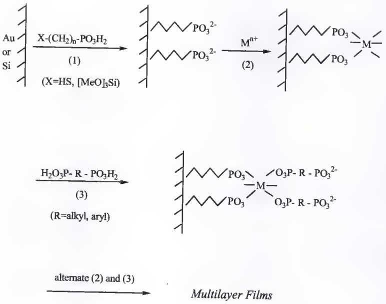

Figure 1.5. Sequential adsorption scheme for growing metal phosphonate multilayer films on electrode surfaces. (ref. 12, p. 224)

devices,[25] and as a backbone for incorporating azo dyes used to show second-order nonlinear optical effects.[26] Although these methodologies are widely used, and are being improved by chemists in the academic setting, the translation of these often time-consuming, intricate procedures to industry-based applications may be limited.

In contrast, multilayer materials comprised of *polymeric* electroactive components have several distinct advantages over the techniques discussed above. First, many of the fabrication methods, some of which will be examined, lead to more facile production of the modified electrodes. The ability to fabricate films which contain electroactive sites having several orders of magnitude greater coverage compared to monolayers, and the improved electrochemical signal which results, is another attractive feature. And with greater coverage, polymer films offer better chemical and physical stability in solution and during electrochemical cycling. Polymer films used for CMEs are generally categorized into two classes, conducting polymers and redox polymers. Each of these groups will be addressed separately, with a more thorough description of the latter type due to its relevance to this work.

Conducting polymers. π-conjugated polymers with delocalized electronic states over a broad energy range are usually referred to as conducting polymers. They are also sometimes called "organic metals" because of their highly conductive nature in the doped state.[27] These types of polymers include polypyrrole, polyaniline, and poly(3-methylthiophene) and their structures and other examples are given in Figure 1.6. All of these types of polymers can be switched between the fully reduced or insulating state, and the fully oxidized, or conducting state by electrochemical or chemical reagent doping methods. The difference in resistance between these two states can be as high as eight orders of magnitude, as is the case for poly(3-methylthiophene).[3] Coupling this with the fast switching times between the "off" and "on" states, the ease of preparation, and the stability of these materials, makes conducting polymers a very active area of research and a very desirable choice for molecular electronic devices.

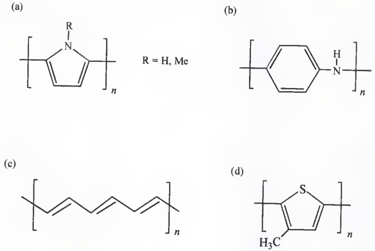

Figure 1.6. Structures of various conducting polymers. (a) polypyrrole; (b) polyaniline; (c) polyacetylene; (d) poly(3-methylthiophene)

Redox polymers. In contrast to the delocalized electronic states found in conducting polymers, redox polymers have distinct electron donor and acceptor sites incorporated into a polymer backbone. Although as a group they lack the high conductivities found in the organic based conducting polymers, they possess two unique characteristics; (1) they have greater potential to display molecular recognition, and (2) due to their well-defined surface formal potential, $E^{0'}$, they have well-defined "on" and "off" regions. In the former case, while conducting polymers may be sensitive to pH- or O_2-level fluctuations, redox films may be modified synthetically to be sensitive to metal ions such as Na^+, K^+, and others. This lends to incorporation of appropriate redox films into biochemical sensing devices. The concept of redox conductivity, first introduced by Murray,[28] helps to explain the latter point. This conductivity is a function of the charge transport mechanism in these films, usually described as electron hopping or self-exchange from adjacent redox sites. As the potential of the electrode nears $E^{0'}$, a concentration gradient begins to form, and a net current can flow. This conductivity (Eq. 1.2) is proportional to the rate of self exchange, k_{se}, and the concentrations of the oxidized and reduced sites, [ox] and [red], respectively.

$$\text{conductivity} \propto k_{se}\,[\text{ox}][\text{red}] \qquad 1.2$$

This narrow region where conductivity may be switched on or off arises from the fact that charge transport is only possible when [ox] = [red], and this requirement is only fulfilled at $E^{0'}$. Figure 1.7 shows a schematic representation of the charge transport in redox polymer films. An additional feature of redox films that can be coupled to this narrow region of conductivity is the synthetically accessible manner that this region can be tuned by synthetic additions of electron withdrawing or donating groups. Such synthetic modifications to the redox monomer can finely tune the $E^{0'}$ in intervals as small as 100

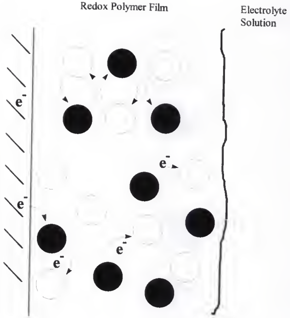

Figure 1.7. Electron transport in redox polymer films. *Top*: self-exchange; *bottom*: diffusional electron hopping. (From ref. 7)

mV, and over a wide range of $E^{0'}$s, thus allowing redox films to operate in potential regions where conducting polymers are inactive.

Redox Film Modified Electrode Fabrication

Redox polymer films can be prepared in various manners. The polymer can be made before applying it to the electrode surface, or it can be assembled from redox active monomers at the surface. Examples of the former type of redox films are illustrated in Figure 1.8. Preassembled redox polymers may involve pendant attachment of redox moieties such as $Fe(CN)_5^{3-}$,[29] and $Ru(bpy)(trpy)^{2+}$,[30] to poly(vinylpyridine) (Figure 1.8a). Other preassembled redox polymers, like poly(vinylferrocene) (b) can be polymerized first, and the resulting polymer applied to the surface of an electrode by spin-coating.[31] Monomers can polymerize via condensation reactions (c) and be applied by spin-coating as well. Ion-exchange polymers (d) use polymers such as protonated poly(vinylpyridine) whose cationic form acts as an ion exchanger, allowing incorporation of redox active ions into the cationic polymer backbone.[32]

Electropolymerization

Perhaps one of the most versatile methods to produce redox polymer films is by electrochemical polymerization, or electropolymerization. In this process, a potential is applied to an electrode submersed in a solution of an appropriate electroactive monomer and supporting electrolyte. The monomer is structurally modified to contain a polymerizable moiety, such as a vinyl- or amino- group, or as in the case of conducting polymers, a π-conjugated backbone. There are several features that make electropolymerization an especially attractive and widely-used fabrication technique. First, the amount of polymer deposited on the electrode can be controlled very carefully by controlling the amount of charge which is passed through the monomer solution. The amount of charge is controlled by the concentration of the monomer solution, and of the

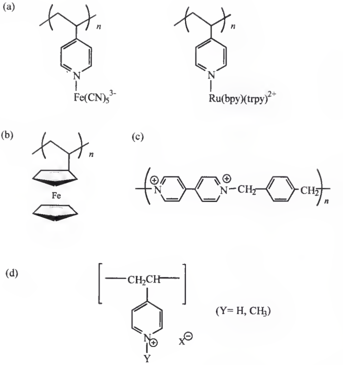

Figure 1.8. Preassembled redox polymers. (a) pendant attachment of redox active group; (b) polymerization followed by spin coating; (c) condensation to form polymer; (d) ion-exchange of redox site into polymer.

electrochemical potential. Electropolymerization can occur rapidly by potentiostatting, or holding the potential right at $E^{0'}$ of the monomer for a rapid film growth, or in a more controlled manner by scanning the applied potential oxidatively or reductively in a range which includes $E^{0'}$. Depositing redox polymeric layers in this manner helps enhance conductivity because of the homogeneous growth of new layers over existing conductive ones. This homogenous growth yields films which are free of defects such as pinholes, which are gaps large enough in the film that may allow molecules in solution to diffuse through the film and contact the bare electrode. Finally, recalling Equation 1.1, the ability to easily control the film's thickness easily allows adjustment of the amount of electrochemical response detected.

There are many types of molecules which can be electropolymerized, including polypyridine transition metal complexes,[33, 34] viologens,[35] porphyrins,[36] and the aforementioned π-conjugated polymers. Figure 1.9 illustrates some examples. The metal polypyridine transition complexes, like ruthenium *tris*-bipyridine, $Ru(bpy)_3^{2+}$, possess well-documented histories detailing their extensive redox photochemistry.[37] These studies have been the basis for many applications, including possible energy conversion photocatalysis schemes. Seeking to impart more control over the solution redox chemistry of these complexes has made them popular candidates for incorporation into electropolymerized redox films. In addition, the synthetic ease in altering these complexes to ready them as redox active monomers for polymerization has facilitated their use. Perhaps the most important aspect in their widespread use, however, is the observation that the redox properties of the monomeric solution species are maintained in the electrode bound polymer films.[38] This helps to predict how these polymeric analogues will function.

Although electropolymerization is a versatile and important technique to afford polymeric films for the reasons previously discussed, it does suffer from the disadvantage that it does not permit a direct means for production of polymer films that are patterned in two dimensions. Spatial definition of polymeric structures on the microscopic scale is

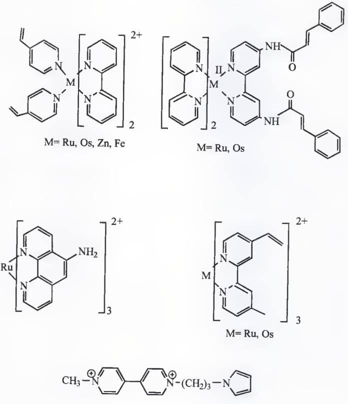

Figure 1.9. Example structures of electrochemically polymerizable redox monomers.

crucial toward development of molecular electronic devices and is certainly a requirement if such devices ever hope to compete with present devices based on solid-state semiconductor technology. Because of this, additional techniques are needed to integrate production of microstructured devices with existing electropolymerization methodology.

Photolithography

A popular method in which CMEs are spatially defined is photolithography. With the introduction of the integrated circuit in 1960, the era of microelectronics was born, and since then technology rapidly improved, allowing manufacturing of 64 megabyte semiconductor memory chips with submicron features.[39] This greater density of circuits on the semiconductor wafer has necessitated the need for smaller and smaller active elements. Photolithography, an art borrowed from the printing industry, has made highly resolved chips a reality. The technique involves the transfer of a patterned image, the circuit design for example, from a mask patterned with the desired image into a polymer film called a resist. After several development steps the image transfer is completed onto the underlying substrate. Figure 1.10 summarizes this process. The resist is the key component of this system. It is usually spin-coated as a thin film onto the silicon substrate, then brought into contact with the imaged mask. Exposure to a light source, often a Hg lamp, can impart one of two photochemical changes to the resist. Figure 1.10 shows these two types: positive and negative resists. In positive resists, the areas of the thin polymer film irradiated undergo photolytic cleavage of chemical bonds. These exposed areas become more soluble in an appropriate developer solution than the areas shielded from exposure, and are thus rinsed away. In negative type resists, the exposed areas are photocrosslinked (i.e., new bonds are formed), decreasing the solubility of these regions in the developer solution. The unexposed regions are washed away in negative type resists, creating the "negative" image of the mask. The resist then performs its

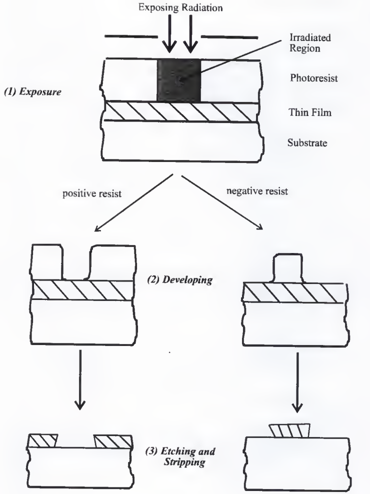

Figure 1.10. Photolithographic process used in semiconductor manufacturing. (ref. 38)

namesake duty, protecting the underlying silicon layer from a chemical etching step, thus allowing only the silicon layer not protected to be removed. A final stripping step removes the patterned resist, leaving behind the patterned integrated circuit, in either its "positive" or "negative" image. Although photolithography has traditionally been a fabrication technique used in the microelectronics industry, the method is gaining popularity in the creation of spatially defined films comprised of electrochemically active monomers.

Spatial Control of CME Fabrication

In the last several years, the need for spatial control of redox active polymer films has seen the development of several experimental techniques which combine electrochemical and photochemical techniques to create microstructured films on electrodes.[40, 41, 42] Most of these procedures have involved electropolymerization of a metal polypyridine complex followed by selective photochemical bond cleavage to yield microstructured arrays of polymer. For example, Meyer and coworkers[43] have shown that the established ligand loss chemistry of $Ru(bpy)_2(L)_2^{2+}$ complexes in solution[44, 45] shown in Equation 1.3:

$$[(bpy)_2Ru(py)_2]^{2+} + 2Cl^- \xrightarrow{h\nu} Ru(bpy)_2Cl_2 + 2\,py \qquad 1.3$$

can be observed in electropolymerized thin films on indium tin oxide (ITO) doped glass electrodes of *poly*-$[Ru(L)_2(vpy)_2]^{2+}$ where L is 2,2'-bipyridine (bpy), 4,4'-dimethyl-2,2'-bipyridine (dmb), or 4,4',5,5'-tetramethylbipyridine (tmb), and vpy is 4-vinylpyridine. Photochemical loss of vpy from the metal ion leads to loss of the metal ion from the polymer network (Equation 1.4). This disruption of the polymer makes it more soluble in these photolyzed regions and can be developed away, exposing the bare electrode. Thus,

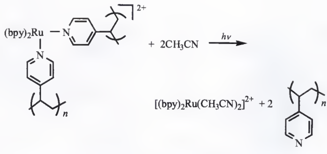

1.4

the metal polypyridine complex acts as a novel positive type photoresist. After the electrode has undergone this photochemical step, a second electroactive monomer, $[Os(vbpy)_3]^{2+}$ (vbpy = 4-methyl-4'-vinyl-2,2'bipyridine, Figure 1.9), can be reductively electropolymerized in the newly uncovered ITO electrode areas (See Figure 1.11). Because $[Os(vbpy)_3]^{2+}$ has a reduction potential more positive than that of $[Ru(tmb)_2(vpy)_2]^{2+}$ (-1.57 vs. -1.80 V, respectively), the $[Os(vbpy)_3]^{2+}$, will selectively bind at the electrode and not over existing $[Ru(tmb)_2(vpy)_2]^{2+}$. This technique has been further modified to produce bicomponent films whose oxidation potentials can be switched separately. Selecting either of the potentials induces a separate color change which could possibly be used in electrochromic displays.[46]

Bocarsly and coworkers[47] have designed a similar electrochemical/photochemical combinatorial approach involving polymeric films of a mixed Pt/Fe compound. A trinuclear complex, $[Pt(NH_3)_4]_2[(NC)_5Fe\text{-}CN\text{-}\ Pt(NH_3)_4\text{-}NC\text{-}Fe(CN)_5]$ can be oxidatively polymerized in the presence of additional $[Pt(NH_3)_4]^{2+}$ to give films of $[Fe^{II}(CN)_6\text{-}Pt^{IV}(NH_3)_4]_n$ on ITO electrodes. A two electron photoinduced intervalence charge transfer involving all three metal centers[48] can be invoked to simultaneously oxidize Fe from its 2+ to 3+ state and reduce the Pt from 4+ to 2+. During, this process, the -CN-

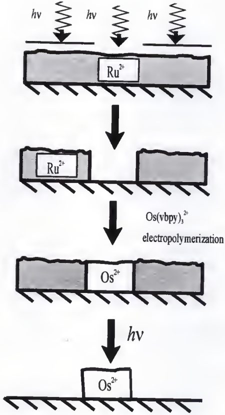

Figure 1.11. Meyer electrochemical/photochemical scheme to produce spatially resolved arrays of $[Os(vbpy)_3]^{2+}$. (From ref. 42)

ligand bonds to Pt are broken. Equations 1.5 and 1.6 summarize this process (with ligands omitted for clarity):

$$[\mathrm{Fe^{II}\text{-}Pt^{IV}}]_{2n+1} \xrightarrow{h\nu} 2[\mathrm{Fe^{III}\text{-}Pt^{IV}}]_n + [\mathrm{Pt(NH_3)_4}]^{2+} \qquad 1.5$$

$$[\mathrm{Fe^{II}\text{-}Pt^{IV}}]_n \xrightarrow{h\nu} n[\mathrm{Fe(CN)_6}]^{3-} + n[\mathrm{Pt(NH_3)_4}]^{2+} \qquad 1.6$$

The surface is thus an alternating array of defined regions; the unexposed [Fe-Pt]$_n$ film interdigitated between exposed areas of the mixed metal cyanometalate photochemical product, containing ferricyanide and platinum transition metal cations. Unlike other systems which use positive type resists, no subsequent developing step is needed. These types of materials are interesting because they display electrochromic properties due to the nature of the cyanometalate. By changing the potential applied to the cyanometalate, the color of this stripe can be changed to closely match the color of the unexposed [Fe-Pt]$_n$ stripes, thus making a substrate whose surface can be changed between striped and uniform coloring.

One final example of spatial control of electroactive films using photolithographic techniques is the previous work done in our lab by Bergstedt.[49, 50] In this procedure, a one-step approach involving *photo*polymerization of an electroactive ruthenium complex or viologen is used. A solution of compound (a) or (b) from Figure 1.12, pentaerythritol tetraacrylate (c), and a free-radical photoinitiator such as benzoin ethyl ether (d), is spin-coated onto an ITO electrode. The film is brought into contact with a mask and exposed to near-UV light. In this system, the ruthenium or viologen film acts as a negative photoresist, with compounds (a) or (b) crosslinking with (c), to form insoluble polymer. The unexposed regions are rinsed away leaving a patterned image of *poly*-a/c or *poly*-b/c. Resolution as high as 5 μm has been achieved via this method.

(a) RuAAP

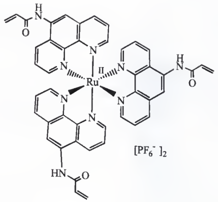

(b) VBV

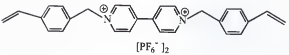

(c) BEE

(d) PETA

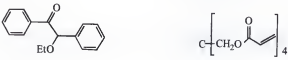

Figure 1.12. Abbreviations and structures of compounds used in photopolymerized system. (a) ruthenium polypyridyl based monomer; (b) vinyl benzyl viologen monomer; (c) benzoin ethyl ether photoinitiator; (d) pentaerythritol tetraacrylate crosslinking agent.

Diffraction Theory Basics

Because of the conceptual importance of diffraction to the work outlined in this chapter, a basic introduction to the principles of diffraction gratings is apropos. When light impinges upon a surface coated with a spatially periodic patterned thin film, it is diffracted in a manner depicted in Figure 1.13. This patterned film acts as a *transmission grating*, diffracting the incident light due to the periodic modulation of the film's complex refractive index ($\mathbf{n}(x,\lambda)$) in the plane of the substrate (x-axis, Figure 1.13). **n** is a complex expression, combining real and imaginary components at any position x, along the grating. The real and imaginary parts of the complex refractive index are represented in Equation 1.7 by $n(x,\lambda)$ and $k(x,\lambda)$ respectively:[51]

$$(\mathbf{n}(x,\lambda)) = n(x,\lambda) + ik(x,\lambda) \qquad 1.7$$

The variables n and k are functions of λ, the wavelength of light. k is the absorptivity of the film at wavelength λ and position x, while n is the film's refractive index. In Figure 1.13, a planar, monochromatic beam incident to the plane of the substrate at an angle θ to the normal, will be diffracted among several orders of output beams ($m = 0, \pm1, \pm2, \pm3, \ldots$). These diffracted beams appear at angles ϕ_m with respect to the normal as defined for the grating equation:[52]

$$\phi_m = \sin^{-1}[(m\lambda/d) - \sin\theta] \qquad \text{for } \theta = 0\text{:} \quad \phi_m = \sin^{-1}(m\lambda/d) \qquad 1.8$$

where m is the diffracted beam order, λ is the wavelength of the incident beam, and d is the spatial periodicity of the patterned film.

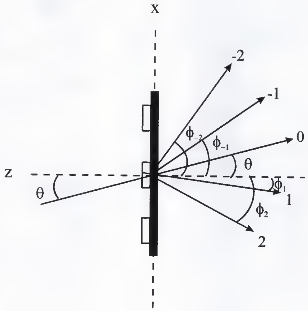

Figure 1.13. Characteristics of a transmission grating.

The diffraction efficiency (*DE*) of the grating is defined in Equation 1.9 as

$$DE = I_{diff}/I^{\circ} \qquad 1.9$$

which is a quantitative ratio of the sum of the intensities of all *m* diffracted beams (I_{diff}) to the intensity of the incident, or zero order beam (I°). The *DE* of a grating depends upon the variation in both components of the complex refractive index[53] in Equation 1.7,

$$DE \propto (\Delta k)^2 + (\Delta n)^2 \qquad 1.10$$

where Δk and Δn are the peak-null variations in *k* and *n* for the grating, respectively. Thus, a grating's behavior is a function of the changes in one or both of these components; modulation of *k* results in an *absorption* or *amplitude* grating, modulation in *n* results in a *phase* grating (named because a change in the refractive index subsequently changes the phase of the beam as it travels through the grating), and a modulation in both *k* and *n* results in a *mixed* grating. The derivation of Eq. 1.10, and its application to the data of the present study will be explored in a later section.

The work by Bergstedt in our group has focused on using grating patterned films produced by the above described photopolymerization technique to examine their electrochemically dependent optical properties. Because of the periodicity of the film's narrow line widths, the films behave as phase gratings, i.e., the films diffract light. The novel feature of these gratings is that the diffraction efficiency can be controlled as a function of the film's redox state. Electro-optic devices such as this, which can use an electrical signal to modulate an optical signal, are part of a burgeoning area of research.[54] In this Information Age, the need to process and store greater amounts of data is becoming a necessity. Photons can perform these tasks much faster and with higher efficiency than electrons. Totally photonic devices capable of optical processing and storage are still years from becoming a reality. However, preliminary studies of systems such as the one above and those described in the remainder of this chapter are fundamentally important in the initial creation of electro-optic transitional devices to allow the promise of photonic designs to be fulfilled.[55]

Description of the Present Study

The purpose of the work described in this chapter is to explore different types of redox films and fabrication techniques to improve upon existing optical diffraction gratings demonstrated in earlier work.[49,50] In order to achieve this, we have implemented a two step method that combines photolithography and electropolymerization (PL-EP) to produce spatially patterned redox arrays. The photolithographic step uses *poly*-methylphenylsilane (p-MPS) as a positive type photoresist, followed by a second electropolymerization step of a redox active transition metal complex. In theory, using p-MPS initially as a framework for subsequent electropolymerizations should allow any redox active species which can be electropolymerized to be spatially defined in any predesigned pattern. The premise of switching from photopolymerized to electropolymerized films is that the latter type should not only increase the stability of these films, but improve the electrochemical response as well. The rest of the chapter will be devoted to explanation of the PL-EP technique, a discussion of the resulting electrochemical and optical data acquired, and a more thorough discussion of the origin of the diffraction modulation and its theoretical application to the experimental data.

Studies of *poly*-$[(bpy)_2Ru(vpy)_2]^{2+}$ and *poly*-$[Os(vbpy)_3]^{2+}$ Films

Initial studies of ITO electrodes patterned with ruthenium and viologen films introduced in the preceding section revealed poor chemical and physical stability after only a few minutes of electrochemical cycling. Figure 1.14 shows the cyclic voltammogram of

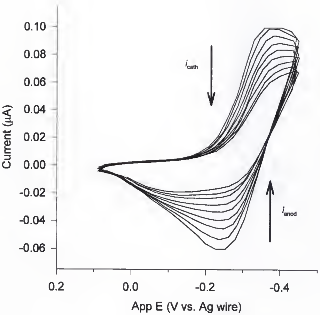

Figure 1.14. Cyclic voltammetry of *poly*-VBV^{2+} grating film on ITO reversibly scanned for 10 min through the $VBV^{2+/+\bullet}$ redox couple.

a patterned vinyl benzyl viologen film (VBV^{2+}) photopolymerized with the PETA co-monomer (Figure 1.12). This wave, obtained by reversibly scanning through the first reduction of the viologen compound, shows that after only 10 minutes of scanning, the cathodic and anodic currents (notated on the graph as i_{cath} and i_{anod} respectively) have decreased by 40 and 60%, respectively. The decreasing current was due in part to the loss of the film from the electrode, as confirmed by inspection under a microscope. Clearly these films suffer from problems associated with this photopolymerization process. First, it requires the use of the insulating PETA co-monomer to aid in creation of the cross-linked patterned substrates. Because of this, the electroactive sites are diluted by the presence of the PETA, and thus the current response is smaller than one would expect for a film comprised totally of electroactive species. Second, the diffusion of positively charged counterions into the films is needed to compensate for the electrochemical reduction. This diffusion is likely slowed by the highly cross-linked nature of these films formed in the photopolymerization process, resulting in poorer charge transport. This cross-linking tends to create a tightly bound polymer network which could slow the necessary ingress of counterions. Because of these problems and the physical instability of the photopolymerized films, we proposed to improve these characteristics by developing alternative systems.

PL-EP Method

Electropolymerized films, due to their physically stable nature, and superb electron transport properties as detailed in the introduction, seemed a logical choice to enhance the electrochemical and subsequently the optical properties of the redox films. However, as noted previously, the technique does not afford 2-D patterning of films on its own merit. A recent paper by Tachinaba[56] describes a two step process to fabricate patterned polythiophene films. This process utilizes *poly*-methylphenylsilane (p-MPS) as a positive type photoresist to initially pattern an ITO electrode. After UV exposure and development, the p-MPS patterned electrodes were placed in a solution containing a thiophene derivative. Electropolymerization was effected by applying a constant voltage to the electrode. Thus, patterned thiophene films were able to be grown only in the UV exposed areas. Figure 1.15 illustrates this process, which we have implemented to produce patterned films comprised wholly of electroactive redox type polymers.

The use of polysilanes as positive photoresists was not examined until the synthesis in the late 1970s of modified polysilanes that were soluble in organic solvents,[57] unlike their crystalline predecessors which were largely intractable. Introduction of substituents at intervals along the silicon backbone such as phenyl groups helps to break up this crystallinity so that the polymer becomes thermoplastic and soluble enough to be cast as films. Recall that in positive type resists, irradiated regions contain molecules in which bonds have been broken leading to better solubility. In particular, p-MPS is well-suited for use as a positive resist because the polymer is very soluble in non-polar solvents (e.g. hexane, toluene) and relatively insoluble in polar solvents (e.g. CH_3CN, DMF, H_2O).[56] The versatility and usefulness of p-MPS lies in the fact that the near-UV irradiated polymer is easily soluble in moderately polar solvents and can be selectively dissolved exposing the bare electrode surface. The unirradiated polymer is insoluble in the polar solvents typically used in most electrochemical experiments. The use of p-MPS and other polysilanes as resists is possible because of the nature of the silicon-silicon bond of the polymer backbone which undergoes photoscission:[58]

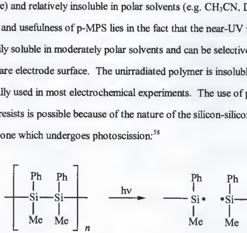

$$\left[-\underset{\mathrm{Me}}{\overset{\mathrm{Ph}}{\mathrm{Si}}}-\underset{\mathrm{Me}}{\overset{\mathrm{Ph}}{\mathrm{Si}}}- \right]_n \xrightarrow{h\nu} -\underset{\mathrm{Me}}{\overset{\mathrm{Ph}}{\mathrm{Si}}}\bullet \quad \bullet\underset{\mathrm{Me}}{\overset{\mathrm{Ph}}{\mathrm{Si}}}- \qquad 1.11$$

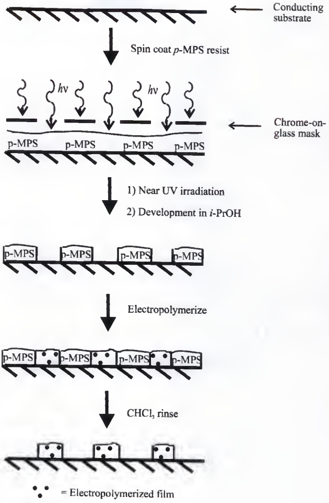

Figure 1.15. Schematic diagram of PL-EP technique.

Polysilanes typically have large absorption bands in the 300-350 nm range, and this mechanism for scission in Eq. 1.11 was proven by West and coworkers[59] by observation of the photochemical bleaching of the large band at 313 nm of a p-MPS film during irradiation. In the present study, p-MPS was synthesized by Wurtz coupling[60] of dichloromethylphenylsilane. Average M_w's of ≈ 3000 were routinely obtained by gel permeation chromatography. A complete synthetic procedure, as well as detailed procedures for the fabrication of patterned redox polymer modified electrodes are listed in the experimental section at the end of this chapter.

ITO electrodes are spin-coated with a solution of p-MPS in toluene. The coated electrodes are then exposed to near UV light through a patterned mask for 15 minutes, and developed in isopropanol. Figure 1.16 shows two magnifications of optical micrographs of developed target films patterned with p-MPS. This mask is patterned with a geometrically decreasing series of horizontal and vertical lines of known width, enabling determination of minimum resolution capabilities of a chosen photoresist. Resolution < 3 μm (Figure 1.16 (b), Group 7) can be achieved. To determine film thickness, profilometry was performed on 10 p-MPS modified electrodes patterned in a grating design. Results revealed thickness averaging 2.5 ± 0.5 μm. A representative plot is shown in Figure 1.17. This 0.5 μm variance may lead to reproducibility problems during the electropolymerizations as will be addressed in the experimental section.

The next step in the PL-EP method is the electropolymerization of an appropriate monomer. The two monomers investigated in this chapter are the metal polypyridine complexes $[(bpy)_2Ru(vpy)_2]^{2+}$ and $[Os(vbpy)_3]^{2+}$ whose structures are shown in Figure 1.18. There has been a great deal of literature describing the features of electropolymerized films of these and similar polypyridine complexes of Ru and Os.[30, 33, 34] Also, the relative ease of the syntheses of these compounds, shown in Figure 1.19, and our previous synthetic experience in this area make these complexes a logical choice to incorporate them into the PL-EP scheme to produce patterned, redox polymer films.

(a)

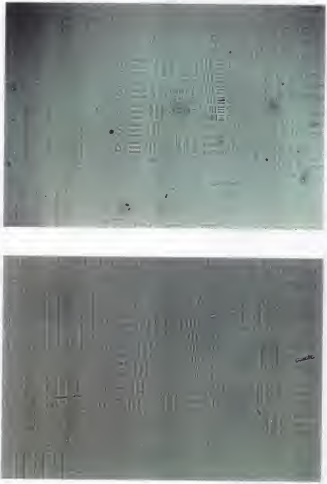

(b)

Figure 1.16. Optical micrographs of p-MPS patterned films on ITO electrodes produced by exposure through a target mask. (a) 4x magnification; (b) 20x magnification. Smallest clean electrode areas (Group 7, element 6) are 2.2 μm wide.

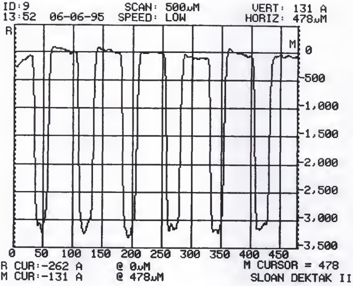

Figure 1.17. Profilometry of p-MPS patterned on glass. Films produced by exposing through a mask with 25 μm wide lines separated by 50 μm wide gaps. Y-axis measures p-MPS thickness in angstroms.

a) [$(bpy)_2Ru(vpy)_2]^{2+}$

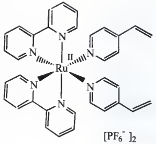

b) $[Os(vbpy)_3]^{2+}$

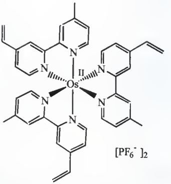

Figure 1.18. Structures of monomer complexes used in PL-EP scheme.

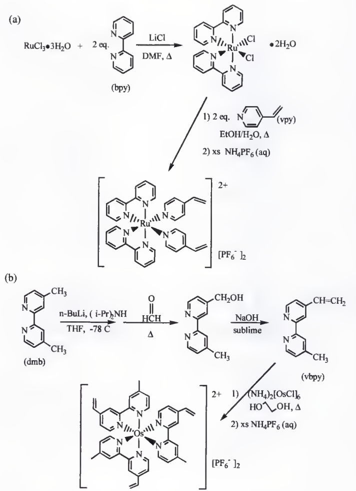

Figure 1.19. Synthetic scheme for redox monomers used in PL-EP method. (a) $[(bpy)_2Ru(vpy)_2]^{2+}$; (b) $[Os(vbpy)_3]^{2+}$.

Metal polypyridine complexes of this type have three one-electron reduction waves in the cathodic region with the third typically at much more negative potential of the first two. The first two are bipyridine ligand based reductions, while the third is that of the polymerizable vinyl ligand. Electropolymerization can often be effected by sweeping through the first wave, but is often faster when the potential is scanned through the second reduction wave. Electropolymerization is usually carried out by scanning 100-150 mV negative of the second ligand reduction, but not totally through the third vinyl based reduction. Scanning through this third wave often causes rapid and uncontrollable film growth, resulting in flaky, brittle films. Figure 1.20 shows the proposed free radical mechanism for reductive electropolymerization of $[(bpy)_2Ru(vpy)_2]^{2+}$ to give redox polymer modified electrodes.[61] The mechanism implies that polymerization is actually an indirect process; since the potential is swept positive of where the vpy ligand is reduced, thus avoiding polymerization by direct vpy free radical formation. It is the bpy ligand based reductions, which reduce the vpy through ligand orbital mixing, thus initiating this indirect free-radical process.[33]

When a p-MPS patterned ITO electrode is placed in an Ar degassed solution of either 2.5 mM $[(bpy)_2Ru(vpy)_2]^{2+}$ or 1.0 mM $[Os(vbpy)_3]^{2+}$ containing 0.1 M tetrabutylammonium hexafluorophosphate (TBAH) in CH_3CN, and the potential is scanned repeatedly at 100 mV/s approximately 100-200 mV past the second bpy based reduction, (−1.68 and −1.49 V vs. clean Ag wire for the Ru and Os films respectively) there is a steady increase in the current at the electrode. (Figures 1.21 and 1.22) This increase is attributable to the electroactivity of the growing polymer film and that of fresh, inward-diffusing monomer. Typically, under fixed conditions, the amount of polymer deposited per number of scans is approximately constant. (Figure 1.22, inset) A lower concentration was needed in electropolymerizations of $[Os(vbpy)_3]^{2+}$ than in $[(bpy)_2Ru(vpy)_2]^{2+}$ to produce films of similar quality. This may be due to the number of polymerizable groups: three in the Os, vs. two in the Ru. The variables in this process, such as concentration,

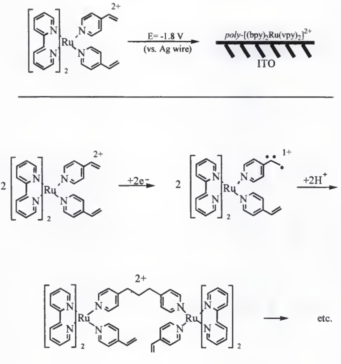

Figure 1.20. Mechanism for reductive electropolymerization of $[(bpy)_2Ru(vpy)_2]^{2+}$ affording redox polymer modified electrodes. (from ref. 60)

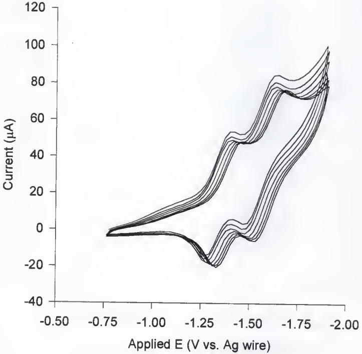

Figure 1.21. Cyclic voltammogram produced during the PL-EP fabrication of a grating patterned *poly*-$[(bpy)_2Ru(vpy)_2]^{2+}$ film on a p-MPS patterned ITO electrode using a 2.5 M monomer and a 0.1 M TBAH/CH_3CN electrolyte solution swept 7 times at 100 mV/s from −0.75 to −1.85 V. (Electrode area = 0.0396 cm^2)

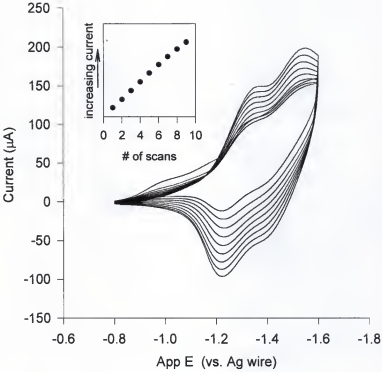

Figure 1.22. Cyclic voltammogram produced during the PL-EP fabrication of a grating patterned *poly*-[Os(vbpy)$_3$]$^{2+}$ film on a p-MPS patterned ITO electrode using a 1.0 M monomer and a 0.1 M TBAH/CH$_3$CN electrolyte solution swept 9 times at 100 mV/s from −0.8 to −1.6 V; (inset) linear response of current with # of scans. (Electrode area = 0.0396 cm^2)

sweep rate, and sweep range and their effects on the quality of the produced films will be addressed in the experimental section.

After electropolymerization the remaining p-MPS on the electrode is rinsed away by submersing it in chloroform, leaving a shiny faint orange (Ru) or faint green (Os) film. Typical optical micrographs for patterned films of *poly*-$[(bpy)_2Ru(vpy)_2]^{2+}$ and *poly*-$[Os(vbpy)_3]^{2+}$ produced by the PL-EP method are shown in Figures 1.23 and 1.24, respectively. If the p-MPS patterned electrode in Figure 1.16 is submersed in either monomer solution and electropolymerized as detailed above, the polymer will grow in the bare electrode areas, resulting in the target pattern shown in Figures 1.23(a) and 1.24(a). Thus, using a table corresponding to line widths for each group, one can estimate the resolution of the produced polymer lines. Groups 4 and 5 have line widths ranging from 25 to 8 μm. In Figures 1.23(b) and 1.24(b), actual grating patterned polymer films on ITO are illustrated, produced from a p-MPS film exposed through a mask with 5 μm lines and gaps. Figure 1.25 shows scanning electron microscope (SEM) photographs of the same grating patterned polymer films of *poly*-$[(bpy)_2Ru(vpy)_2]^{2+}$ and *poly*-$[Os(vbpy)_3]^{2+}$ at much higher magnification, illustrating that the polymer stripes are slightly narrower than the expected 5 μm lines of the grating mask.

Thus, the PL-EP technique is a versatile manner to produce patterned redox polymer films. The novelty of the method allows one to pattern virtually any electropolymerizable species, including the organic π-conducting polymers such as polypyrrole,[62] in any design, with resolution as high as a few microns. In addition, by controlling the number of scans and the concentration of the monomer solution, one can control the thickness of these films.

(a)

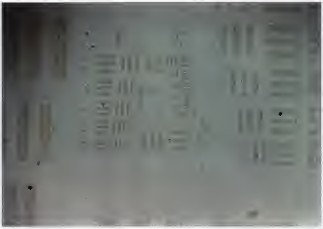

(b)

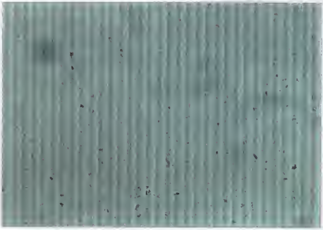

Figure 1.23 Optical micrographs of *poly*-$[(bpy)_2Ru(vpy)_2]^{2+}$patterned films on ITO electrodes. (a) Film produced by exposure through a target mask, 4x magnification; (b) Film produced by PL-EP technique, 40x magnification. Lines and gaps are ≈5 μm wide.

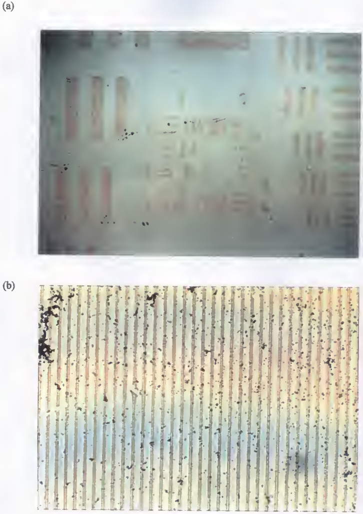

Figure 1.24. Optical micrographs of *poly*-$[Os(vbpy)_3]^{2+}$ patterned films on ITO electrodes. (a) Film produced by exposure through a target mask, 4x magnification; (b) Film produced by PL-EP technique, 40x magnification. Lines and gaps are ≈5 μm wide.

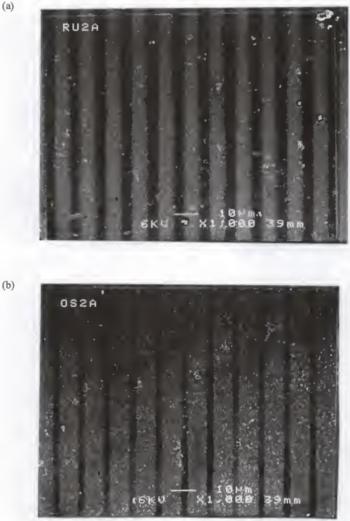

Figure 1.25. Scanning electron microscope images of grating patterned films of (a) *poly*-$[(bpy)_2Ru(vpy)_2]^{2+}$ and (b) $[Os(vbpy)_3]^{2+}$ on ITO electrodes. 1000x magnification.

Electrochemical Characterization of Grating Patterned Redox Films

Ideal electrochemical behavior

As an introduction to the electrochemical data in the present study, the electrochemical behavior of redox films modified onto electrode surfaces will be briefly reviewed. In an ideal electrochemical situation, electron transfer from the electrode surface to the immobilized redox film should be fast and reversible, and is governed by the Nernst equation[63]:

$$E = E^{0'} + \frac{RT}{nF}\ln\frac{C_O^*}{C_R^*} \qquad 1.12$$

where E is the potential of the electrode, $E^{0'}$ is the formal potential, and C_O^* and C_R^* are the bulk concentrations of the oxidized and reduced sites in the film. Equation 1.12. is very similar to Murray's definition of redox conductivity introduced back in Eq. 1.2. Recall that redox conductivity can only occur when the concentration gradient formed in the film has equilibrated (i.e., the concentrations of oxidized and reduced species become equal). This condition is satisfied at $E^{0'}$. In Eq. 1.12, setting C_O^* equal to C_R^* eliminates the right term leaving $E = E^{0'}$, which translates to the potential read at the electrode actually equaling the formal potential. However, this is not always the case. In solution, charge transport is a combination of self-exchange of electron and diffusion of redox sites to and from the electrode. In redox films however, the redox sites are covalently attached to a polymeric backbone, decreasing the amount of site diffusion, and charge transport is predominantly dictated by electron self-exchange or hopping, as was shown schematically in Figure 1.7. In truly Nernstian behavior, diffusion contributions are totally absent. An example of this ideal reversible electrochemical behavior in a redox film is illustrated in the cyclic voltammogram in Figure 1.26. The features of this wave which are of importance are $E_{p,a}$, $E_{p,c}$, $i_{p,a}$, and $i_{p,c}$, the potentials and currents at which the anodic and cathodic

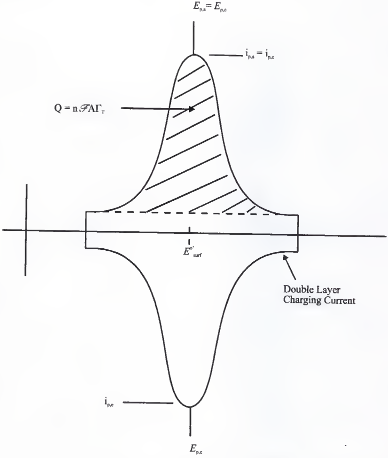

Figure 1.26. Ideal reversible cyclic voltammogram of an immobilized redox layer. (ref. 7)

(oxidative and reductive) processes take place, respectively. Ideal electron transport would be observed when $E_{p,a}$, = $E_{p,c}$, and $i_{p,a}$, = $i_{p,c}$ (i.e. ΔE_p and $\Delta i_p = 0$). This condition translates to all of the redox sites in the film being oxidized or reduced at the same applied potential, with equal amounts of current produced in each process, giving a perfectly symmetric, mirror image wave shape. Thus the reported potential at which the redox process occurs, $E^{0'}$, should be equal to either $E_{p,a}$, or $E_{p,c}$. However, in most electrodes modified with redox films, charge transport is somewhat less than ideal, allowing for contributions from diffusional effects. These may include several factors. First, although the polymer backbone is generally considered a tightly interwoven network of strands, the redox sites attached may still possess some mobility. This tightly knit polymeric network, and the thickness of the film itself, may also make counterion flow slower, which is important because of the necessity of counterion influx or egress to maintain charge neutrality. Also the size of the counterions may cause deviation from the ideal because of steric hindrance as they diffuse through the film. Any of these factors will increase diffusional contributions and in turn, cause $\Delta E_p \neq 0$. In these circumstances, $E^{0'}$ is more correctly reported as the half-potential, $E_{1/2}$, which is the average of the potentials at the individual redox processes:

$$E_{1/2} = 1/2(E_{p,a}, - E_{p,c}) \qquad 1.13$$

Therefore, ΔE_p is a good indication of the charge transport properties of these types of films. The larger this difference is, the greater the contribution of diffusion effects, and the poorer the charge transport through the film.

Experimental results

With this quantitative indicator in mind, the oxidative cyclic voltammograms (CVs) of patterned *poly*-$[(bpy)_2Ru(vpy)_2]^{2+}$ and *poly*-$[Os(vbpy)_3]^{2+}$ fabricated by PL-EP on ITO electrodes can be examined. These CVs, run in fresh 0.1 M TBAH/CH_3CN electrolyte at various sweep potentials, are illustrated in Figures 1.27 and 1.28, respectively. Both figures show reversible waves for the $Ru^{II/III}$ couple and $Os^{II/III}$ couple at $E_{1/2} = +1.34$ V and +0.80 V, respectively, vs. a Ag wire quasi-reference electrode. ($\approx +0.13$ V vs. SCE) which are very close to their $E_{1/2}$ values in solution of +1.31 V and +0.78 V, respectively. ΔE_p at a 10 mV/s sweep rate, ν, is 50 mV in the *poly*-$[(bpy)_2Ru(vpy)_2]^{2+}$ films, and 30 mV in the *poly*-$[Os(vbpy)_3]^{2+}$. This compares favorably to unpatterned Ru and Os films of comparable thickness on Pt electrodes whose ΔE_p values at this sweep rate also lie in the 30-50 mV range.[30, 33, 69] This agreement indicates near Nernstian response and fast charge transport.

The surface coverage, Γ_T, was calculated for 3 grating patterned Ru films and 3 grating patterned Os films fabricated using the conditions outlined in the experimental section. The coverage can be determined by integration of the current under the anodic and cathodic waves of each of the patterned films, like those in Figures 1.27 and 1.28 to establish the total charge passed during each process. This gives an effective surface concentration of electroactive sites. This is achieved by subtracting out the double layer charging current to baseline correct for the anodic and cathodic currents. Appendix A describes this process in more detail. Surface coverages on the order of 1×10^{-8} mol/cm^2 were found for both types of films. This corresponds to roughly 100 monolayers. (1 monolayer = 1×10^{-10} mol/cm^2) Profilometry measurements indicate thickness of Ru films averaging in the range of 80-100 nm. (Figure 1.29) The molar concentration of redox sites in these films, C(M), can be calculated by the following equation[64]:

$$C(\mathrm{M}) = \Gamma\ (\mathrm{mol/cm^2})/d\ (\mathrm{cm}) \qquad 1.14$$

where d is the film thickness obtained by profilometry. Using this relation gives molar concentrations of in the range of 1.0-1.5 M for films of *poly*-$[(bpy)_2Ru(vpy)_2]^{2+}$ and *poly*-

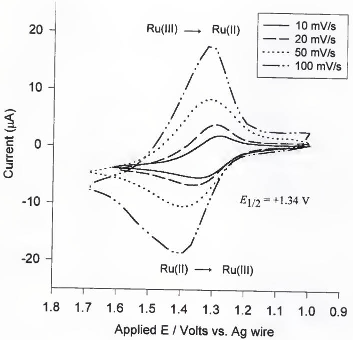

Figure 1.27. Oxidative cyclic voltammetry of a *poly*-$[(bpy)_2Ru(vpy)_2]^{2+}$ grating patterned film (100 lines/mm) at various sweep rates in 0.1 M TBAH/CH_3CN.

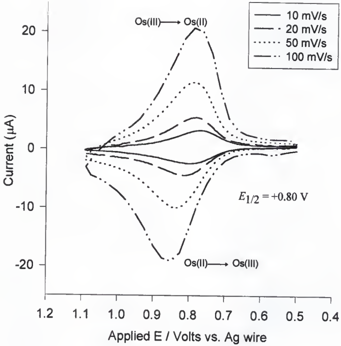

Figure 1.28. Oxidative cyclic voltammetry of a *poly*-[Os(vbpy)$_3$]$^{2+}$ grating patterned film (100 lines/mm) at various sweep rates in 0.1 M TBAH/CH$_3$CN.

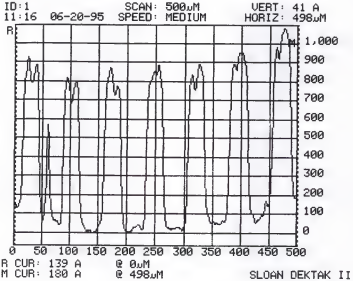

ID:1 SCAN: 500µM VERT: 41 A
11:16 06-20-95 SPEED: MEDIUM HORIZ: 498µM

R CUR: 139 A @ 0µM
M CUR: 180 A @ 498µM

SLOAN DEKTAK II

Figure 1.29. Profilometry of a *poly*-$[(bpy)_2Ru(vpy)_2]^{2+}$ grating film. Films produced by exposing through a mask with 25 µm wide Ru arrays separated by 50 µm wide bare electrode areas. Y-axis measures film thickness in angstroms.

$[Os(vbpy)_3]^{2+}$, which is typical for these types of films produced by similar conditions for electropolymerization.[33,64]

Several interesting conclusions can be inferred from the electrochemical data of these patterned films, which is summarized in Tables 1.1 and 1.2 for the Ru and Os films, respectively. The films seem to model near ideal electrochemical response, i.e., the charge transport is fast and reversible, inferring electron self-exchange to be dominant over diffusional control. This is noted from the relatively small ΔE_p's, (< 100 mV in almost all cases) and the near symmetric i_c's and i_a's which correspond to nearly equal Γ_a and Γ_c values. Also the amount of total charge passed under these waves should be equal regardless of sweep rate, v. Examination of the Γ_T values in Tables 1.1 and 1.2 at various sweep rates reflect relatively good agreement. One other observation from these tables indicates that surface coverages may vary even when using identical fabrication conditions for the respective films. This reproducibility problem is addressed further in the experimental section.

The other important feature of electropolymerized films along with their excellent electrochemical response is their stability toward repetitive cycling. Patterned films of *poly*-$[(bpy)_2Ru(vpy)_2]^{2+}$ and *poly*-$[Os(vbpy)_3]^{2+}$ have been cycled oxidatively for over 100 scans (> 4 hr) with no apparent loss in the current. This stability and improved response were the main impetus behind instituting the PL-EP technique to fabricate grating films comprised of redox polymers. Further analysis of the electrochemical data will follow in the discussion section immediately after the characterization of the pertinent optical data.

Electrode Film #	Sweep rate, ν (V/s)	$E_{1/2}$ (V)[a]	ΔE_p (mV)	Γ_a^b (mol/cm$^{2)}$	Γ_c^b (mol/cm^2)	Γ_T^b (mol/cm^2)
Ru 1	0.010	+1.31	50	9.38×10^{-9}	8.82×10^{-9}	1.82×10^{-8}
	0.020	+1.32	61	8.66×10^{-9}	8.81×10^{-9}	1.75×10^{-8}
	0.050	+1.34	87	9.13×10^{-9}	8.58×10^{-9}	1.77×10^{-8}
	0.100	+1.36	96	8.81×10^{-9}	9.59×10^{-9}	1.84×10^{-8}
Ru 2	0.010	+1.33	54	8.98×10^{-9}	1.07×10^{-8}	1.97×10^{-8}
	0.020	+1.35	66	7.90×10^{-9}	8.90×10^{-9}	1.68×10^{-8}
	0.050	+1.38	90	9.06×10^{-9}	8.74×10^{-9}	1.78×10^{-8}
	0.100	+1.40	103	8.74×10^{-9}	9.76×10^{-9}	1.85×10^{-8}
Ru 3	0.010	+1.33	56	9.10×10^{-9}	1.00×10^{-8}	1.91×10^{-8}
	0.020	+1.35	67	8.80×10^{-9}	1.13×10^{-8}	2.01×10^{-8}
	0.050	+1.36	86	1.26×10^{-8}	1.07×10^{-8}	2.33×10^{-8}
	0.100	+1.38	101	1.32×10^{-8}	1.42×10^{-8}	2.74×10^{-8}

Table 1.1. Summary of electrochemical data for 3 grating films of *poly*-$[(bpy)_2Ru(vpy)_2]^{2+}$ on ITO electrodes fabricated by sweeping reductively from −0.7 to −2.0 V in 2.5 mM $[(bpy)_2Ru(vpy)_2]^{2+}$ with 0.1 M TBAH/CH_3CN at 100 mV/s. [a]voltages vs. clean Ag wire (≈ +0.13 V vs. SCE) [b]See Appendix A for description of surface coverage calculations.

Electrode Film #	Sweep rate, ν (V/s)	$E_{1/2}$ (V)^a	ΔE_p (mV)	$\Gamma_a{}^b$ (mol/cm$^{2)}$	$\Gamma_c{}^b$ (mol/cm^2)	$\Gamma_T{}^b$ (mol/cm^2)
Os 1	0.010	+0.79	30	9.20×10^{-9}	1.15×10^{-8}	2.07×10^{-8}
	0.020	+0.80	40	9.24×10^{-9}	1.27×10^{-8}	2.19×10^{-8}
	0.050	+0.81	58	9.87×10^{-9}	1.03×10^{-8}	2.02×10^{-8}
	0.100	+0.83	66	9.39×10^{-9}	9.21×10^{-9}	1.86×10^{-8}
Os 2	0.010	+0.81	38	1.39×10^{-8}	1.17×10^{-8}	2.56×10^{-8}
	0.020	+0.82	42	1.80×10^{-8}	8.90×10^{-9}	2.69×10^{-8}
	0.050	+0.85	64	1.17×10^{-8}	1.08×10^{-8}	2.25×10^{-8}
	0.100	+0.86	73	1.51×10^{-8}	1.58×10^{-8}	3.09×10^{-8}
Os 3	0.010	+0.82	36	1.89×10^{-8}	1.69×10^{-8}	3.58×10^{-8}
	0.020	+0.83	43	1.66×10^{-8}	1.82×10^{-8}	3.48×10^{-8}
	0.050	+0.85	65	1.67×10^{-8}	1.50×10^{-8}	3.17×10^{-8}
	0.100	+0.89	80	1.86×10^{-8}	1.78×10^{-8}	3.64×10^{-8}

Table 1.2. Summary of electrochemical data for 3 grating films of *poly*-$[Os(vbpy)_3]^{2+}$ on ITO electrodes fabricated by sweeping reductively from –0.8 to –1.6 V in 1.0 mM $[Os(vbpy)_3]^{2+}$ with 0.1 M TBAH/CH_3CN at 100 mV/s. ^{a}voltages vs. clean Ag wire (≈ +0.13 V vs. SCE) ^{b}See Appendix A for description of surface coverage calculations.

Optical Characterization of Grating Patterned Redox Films

This section will present experimental results generated by studying the optical properties of grating films of *poly*-$[(bpy)_2Ru(vpy)_2]^{2+}$ and *poly*-$[Os(vbpy)_3]^{2+}$in relation to their relevant electrochemical properties. A more detailed analysis further explaining these results will follow.

Spectroelectrochemistry

One of the original reasons to modify electrodes with films comprised of metal polypyridines was to examine whether the interesting photochemical properties of the solution complexes would be retained. Thus, monitoring the absorption behavior of these films as they are oxidized or reduced is important. This can be achieved by performing spectroelectrochemical experiments on optically transparent electrodes. Since the films fabricated by the PL-EP technique are polymerized on ITO electrodes, this experiment is easily accomplished. In spectroelectrochemistry, the modified electrode is placed in the beam of a UV-visible spectrophotometer, and the potential of the electrode is slowly swept positively or negatively. Absorption data is periodically collected, monitoring changes in the absorption spectrum resulting from species produced or consumed in the redox process. Further detail can be found in the experimental section.

The spectroelectrochemical oxidation and reduction of grating films of *poly*-$[(bpy)_2Ru(vpy)_2]^{2+}$ on ITO electrodes is illustrated in Figures 1.30 and 1.31. Figure 1.30 shows overlaid absorption difference spectra taken at 100 mV steps as the potential is scanned through the $Ru^{2+/3+}$ redox couple. These spectra show bands in a downward growth, corresponding to the bleaching of the π-π^* and MLCT absorption bands at 340 nm and 450 nm, respectively. These bands are clearly seen in a UV-vis spectrum recorded at 0.0 V(Figure 1.30, inset). The reductively scanned spectra, shown in Figure 1.31, show the growth of two bands at 380 and 515 nm corresponding to new absorptions created by

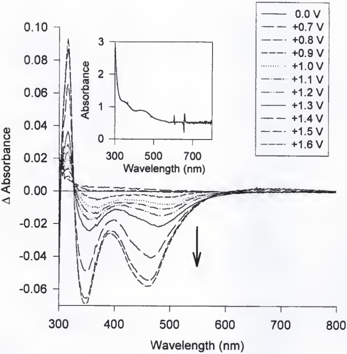

Figure 1.30. Spectroelectrochemistry of *poly*-$[(bpy)_2Ru(vpy)_2]^{2+}$ grating film scanned oxidatively from +0.7 V, plotted as difference spectra; (inset) UV-vis spectrum of same film at 0.0 V.

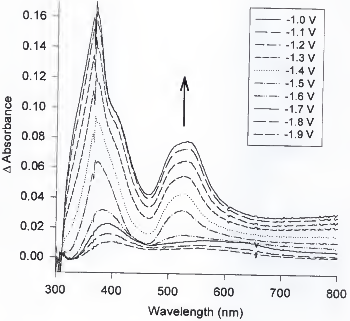

Figure 1.30. Spectroelectrochemistry of *poly*-$[(bpy)_2Ru(vpy)_2]^{2+}$ grating film scanned reductively from −1.0 V, plotted as difference spectra.

the first and second reductions of the bpy ligands, with positive and negative pointing arrows indicating direction of growth or bleaching, respectively.

Figures 1.32 and 1.33 display the oxidative and reductive spectroelectrochemistry of *poly*-$[Os(vbpy)_3]^{2+}$ patterned ITO electrodes. Again, comparing to the zero potential UV-vis spectrum (inset, Figure 1.32), the spectra show a large bleaching of the wide MLCT band at 500 nm, while in Figure 1.33, new absorptions appear at 350 and 550 nm, corresponding to the reduced vbpy ligands, as well as a bleaching centered at 650 nm.

Modulation of diffraction efficiencies through potential sweeping

As outlined in the introduction, the closely spaced patterned polymer arrays allow these films to diffract light. The efficiency of this diffraction can be regulated by switching the potential applied to the film coated electrode. Recalling Eq.1.10, the diffraction efficiency of a given grating film is a function of the film's refractive index, absorptivity, or a combination of these factors. So the observed electrochemically-induced modulation of this diffraction efficiency must be attributed to a change in one or both of these variables. The acquired optical experimental data exhibiting this behavior will be presented with an interpretive analysis pinpointing the origin of this phenomenon in a later section.

To monitor these events, we have created an experimental apparatus designed to digitally acquire diffraction data during the electrochemical switching process. This apparatus uses an electrochemical cell containing the modified electrode whose potential is controlled by an attached potentiostat, and a He-Ne laser, whose output impinges upon the surface of the film, resulting in diffraction whose intensity can be monitored by photodiodes. The apparatus, schematically depicted in Figure 1.34, is described in further detail in the experimental section. Four different analog signals, the transmitted, or zero order beam intensity, the first order diffracted beam intensity (recall Figure 1.13), the current, and the applied potential are sampled simultaneously, digitally converted, and their features monitored in real time.

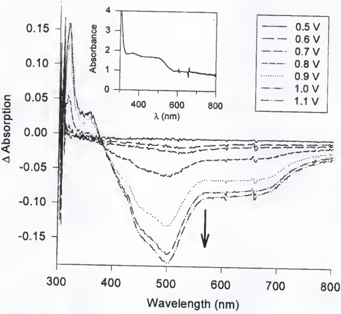

Figure 1.32. Spectroelectrochemistry of a *poly*-[Os(vbpy)$_3$]$^{2+}$ grating film scanned oxidatively from +0.5 V, plotted as difference spectra; (inset) UV-vis spectrum of same film at 0.0 V.

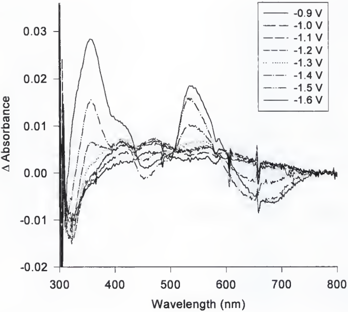

Figure 1.33. Spectroelectrochemistry of a *poly*-$[Os(vbpy)_3]^{2+}$ grating film scanned reductively from −0.9 V, plotted as difference spectra.

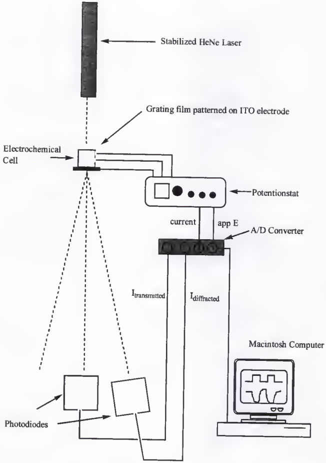

Figure 1.34. Experimental apparatus for electrochemically controlling diffraction efficiencies of grating patterned redox films.

A good example of the kind of data generated in a typical swept potential experiment is shown in Figure 1.35. These plots summarize the important features of the ability to electrochemically induce diffraction changes in the initial photopolymerized system using grating patterned films comprised of vinyl benzyl viologen. (poly-VBV^{2+}) Three of these signals are plotted versus time. The potential, swept negatively from +0.1 V to -0.4 V is displayed as a triangular wave, as it is reversibly and repeatedly cycled. The current response, which was plotted as a function of potential in the cyclic voltammogram back in Figure 1.14, clearly shows the same decreasing trend, now plotted versus time. The initial intensity of the diffracted beam is normalized to 100% and changes are reflected relative to this value. Films that diffract the He-Ne output better or worse as a result of an electrochemically induced change will show a respective increase or decrease in the diffraction intensity. In the case of the viologen system, as the potential is swept negatively, the diffraction signal increases, reaching a maximum when the film is wholly reduced. Upon subsequent re-oxidation of the film, the intensity returns to its initial value. This signal in this experiment also decreases over time, as the physical stability of the film on the electrode surface is poor.

An interesting aspect of the *poly*-$[(bpy)_2Ru(vpy)_2]^{2+}$ and *poly*-$[Os(vbpy)_3]^{2+}$ grating films in this study is that the diffraction efficiency can be decreased by sweeping oxidatively through the metal's 2+/3+ redox couple, or increased by reductively sweeping through the bpy ligand based reductions. Thus the modulation of the *DE* can be intentionally adjusted by sweeping in an appropriate positive or negative direction.

poly-$[(bpy)_2Ru(vpy)_2]^{2+}$ grating films. Figure 1.36 illustrates the responses of the transmitted beam, the diffracted beam, the current and the applied potential over time in an experiment in which the potential of a grating film comprised of *poly*-$[(bpy)_2Ru(vpy)_2]^{2+}$ (DE_0 = 0.026%) is oxidatively swept through the $Ru^{2+/3+}$ redox couple in fresh 0.1 M TBAH/CH_3CN electrolyte solution. The four responses are stacked vertically to easily display any observed dependencies of the optical and current responses on the redox

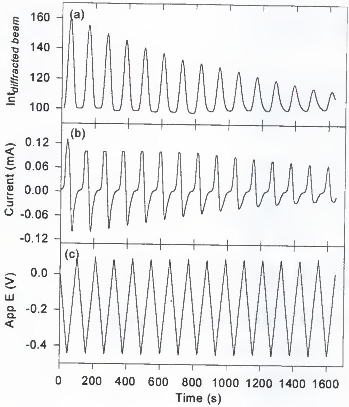

Figure 1.35. Electrochemical and optical data for a poly-VBV^{2+} grating film. (a) diffracted beam intensity; (b) current response; (c) applied potential swept through the VBV$^{2+/+\bullet}$ redox couple.

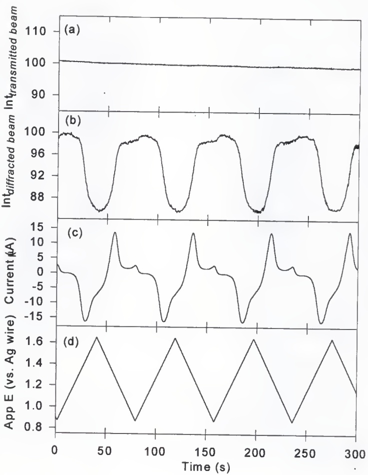

Figure 1.36. Diffraction modulation by oxidatively sweeping a *poly*-$[(bpy)_2Ru(vpy)_2]^{2+}$ grating film. (a) intensity of transmitted beam; (b) intensity of diffracted beam; (c) current response. (d) applied potential (20 mV/s sweep rate). $DE_0 = 0.026\%$.

potential of the film. The responses of the transmitted and diffracted beams are normalized for comparison convenience to other data presented later. The triangular wave in (d) represents the potential profile as it is swept repeatedly from +0.9 to +1.6 and reversed back to +0.9 V. A reversible, nicely shaped, stable current response (c) is observed and does not show any decrease, even after hours of scanning. The diffraction efficiency of the first order diffracted beam, shown in (b) shows that as the potential is swept positively, oxidation of the film results in an ≈15%, decrease of the diffracted beam signal. Reversing the potential, reduces the film from the Ru^{3+} to Ru^{2+}, and the diffracted signal rebounds to its initial value. This same 15% decrease and its subsequent return to its previous value is observed as the potential is swept reversibly over the course of the experiment. This absolute change in the *DE* is consistent with two other Ru grating films whose data is listed in Table 1.3. Table 1.3 gives a comparison of the pertinent numeric data for this optical experiment and those that follow. It will be referred to often as a survey of the data produced for experiments involving both Ru and Os grating films fabricated by the PL-EP method. Lastly, one other observation for the present experiment is the absence of change in the output of the transmitted or zero-order beam (Figure 1.36 (a)).

Scanning a film reductively through the bpy reductions produces the opposite effect in the diffracted beam response (Figure 1.37). Sweeping from −0.8 to −2.0 V (d) produces an average 28% *increase* (Table 1.3) in the diffracted beam response, and a concomitant small decrease in the response of the transmitted beam. Reversing the potential reveals a complete recovery to its initial diffraction efficiency, DE_0 of 0.047%. The current and optical responses however, are not as well shaped as in the oxidative experiments. This is not a problem associated with decreasing stability of the film, since the current and optical responses are not decreasing with number of redox cycles as was the case in the VBV photopolymerized system (Figure 1.35). This is most likely due to the relatively poor electrochemistry typically seen for reductively swept metal polypyridine

		% Absolute Changes in Diffraction Efficiency (ΔDE) During Designated Electrochemical Event			
Electrode Film #	DE_0 (%)	Oxidatively Swept[a]	Reductively Swept[a]	Oxidatively Stepped[b]	Reductively Stepped[b]
Ru 1	0.026	−15	+25	−13	+51
Ru 2	0.091	−13	----	----	----
Ru 3	0.053	−14	----	----	----
Ru 4	0.047	----	+30	−16	+60
Ru 5	0.039	----	+29	−15	+44
Average Ru film	0.033	−14.0	+28.0	−14.67	+51.67
Os 1	0.056	−18	+55	−30	+60
Os 2	0.094	−21	+59	−36	+53
Os 3	0.120	−23	----	−28	----
Os 4	0.076	----	+47	----	+49
Average Os film	0.0865	−17.33	+53.67	−31.33	+54.0

Table 1.3. Summary of optical data for 5 grating films of *poly*-$[(bpy)_2Ru(vpy)_2]^{2+}$ and 4 grating films of *poly*-$[Os(vbpy)_3]^{2+}$ on ITO electrodes fabricated by the PL-EP method. Films Ru 1 - Ru 3 and Os 1 - Os 3 are the same as those in Tables 1.1 and 1.2. Films Ru 4 and 5 were made similarly to Ru 1- Ru 3, and film Os 4 made similarly to Os 1-Os 3. [a]20 mV/s sweep rate; [b]10 sec interval switching times.

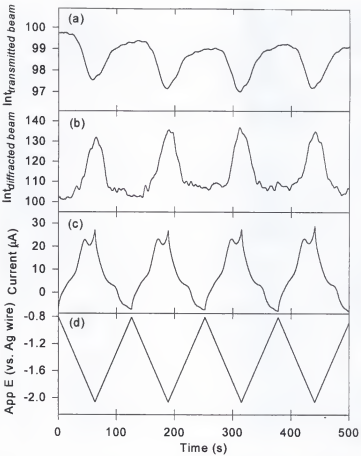

Figure 1.37. Diffraction modulation by reductively sweeping a *poly*-$[(bpy)_2Ru(vpy)_2]^{2+}$ grating film. (a) intensity of transmitted beam; (b) intensity of diffracted beam; (c) current response. (d) applied potential (20 mV/s sweep rate). $DE_0 = 0.047\%$.

films on ITO electrodes. Figure 1.38 shows the cyclic voltammogram produced by plotting the current and potential responses in Figure 1.37 versus each other. Note that while the current response is relatively retraceable over the course of the experiment, the wave shapes corresponding to the bpy reductions are not well-defined. A better current response would give two distinct reversible reductions, much like those illustrated in the reductive electropolymerization CV back in Figure 1.21. The poor wave shape produced in Figure 1.38 is observed in all other reductively swept cases involving grating patterned films of Ru.

poly-$[Os(vbpy)_3]^{2+}$ grating films. The diffraction characteristics of the grating films comprised of *poly*-$[Os(vbpy)_3]^{2+}$ films behave similarly to the Ru based films. Figure 1.39 shows the results of an experiment in which the potential is repetitively swept through the $Os^{2+/3+}$ redox couple at $E_{1/2} = +0.8$ V from +0.5 to 1.1 V and back (d). The current response (c) is well-shaped, and equal and opposite in magnitude as the film is electrochemically switched, and this magnitude is maintained over long (> 3 hr) sweep times. A slightly larger average decrease in the diffracted beam intensity of $\approx$17% as compared to *poly*-$[(bpy)_2Ru(vpy)_2]^{2+}$ films (Table 1.3) is observed as the film is oxidized. These films also display excellent recovery of the diffracted beam intensity to the initial level as the potential is reversed, and the film is re-reduced. In these films, unlike the analogous oxidative case of the Ru comprised films, a small dependence of the response of the transmitted beam on the potential is observed. This can be explained by referring back to the oxidative spectroelectrochemistry of the Os grating film in Figure 1.32. This figure shows that there is an overlap of the ground state absorption with the 633 nm output of the HeNe laser beam.

Reductively sweeping these films through the two bpy ligand reductions from –0.7 to –1.9 V as illustrated in Figure 1.40, gives a similar response to the reductively swept Ru comprised films, and reverse behavior of what is seen in the oxidative cases. An increase of nearly 60% of the *DE* is monitored when the film is fully reduced. A 2-3%

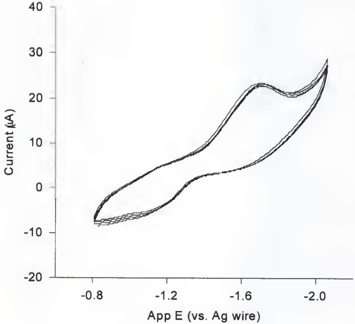

Figure 1.38. Cyclic voltammogram of the *poly*-$[(bpy)_2Ru(vpy)_2]^{2+}$ grating film produced by plotting the current and potential responses from Figure 1.37.

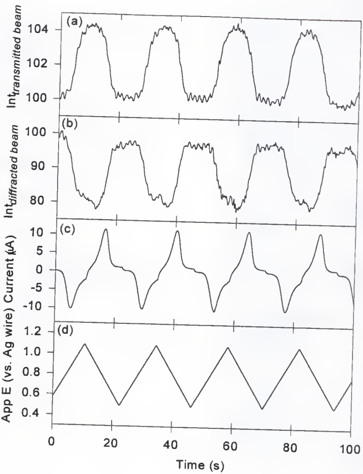

Figure 1.39. Diffraction modulation by oxidatively sweeping a *poly*-[Os(vbpy)$_3$]$^{2+}$ grating film. (a) intensity of transmitted beam; (b) intensity of diffracted beam; (c) current response; (d) applied potential (50 mV/s sweep rate). $DE_0 = 0.056\%$.

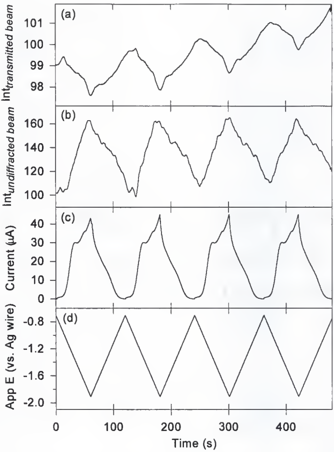

Figure 1.40. Diffraction modulation by reductively sweeping a *poly*-$[Os(vbpy)_3]^{2+}$ grating film. (a) intensity of transmitted beam; (b) intensity of diffracted beam; (c) current response; (d) applied potential (50 mV/s sweep rate). $DE_0 = 0.094\%$.

decrease of the transmitted beam when the potential is scanned negatively is also noted. The poor reductive current shape of the *poly*-$[Os(vbpy)_3]^{2+}$ films resulting in the cruder diffraction response (Figure 1.41) is similar to that recorded when the Ru based films were scanned reductively. One point which should be addressed is the relative disparity of the reductive wave of the films during electropolymerization and after it is completed. During reductive growth of the film, two distinct waveshapes corresponding to the bpy ligand reductions are easily observed (Figures 1.21 and 1.22). After film growth has been completed, and the film is developed and placed in fresh electrolyte solution for optical experiments, the reductive wave shapes are poorer, as observed in Figures 1.38 and 1.41. There are two possible explanations for this observed behavior. The first could be the difference in the morphology of between the growing film and the "finished" film. It may be that the growing polymer network is not as tightly bound as the "finished" polymer, allowing better diffusion of the electrolyte in the former case than the latter. The second rationale could be due to the inherent sensitivity of reductive processes to atmospheric O_2 quenching. Cyclic voltammograms which give evidence of O_2 susceptibility usually give a fairly well-defined reductive half-wave, but the re-oxidation wave is not distinct, as is the case in both figures.

Modulation of diffraction efficiencies through potential stepping

In contrast to the gradual changes in current and diffraction efficiency produced as the potential is swept, inducing a sudden potential change can produce transient effects in the current and optical signals, resulting from the switched electroactive properties of the redox film and their effects on the optical properties. This procedure, in which the potential is repeatedly stepped to and from a potential far enough past $E_{1/2}$ to produce an almost instantaneous change of redox state, and monitoring the subsequent current response as a function of time, is called double potential step chronoamperometry. Experiments of this nature are often used to investigate the charge transport kinetics

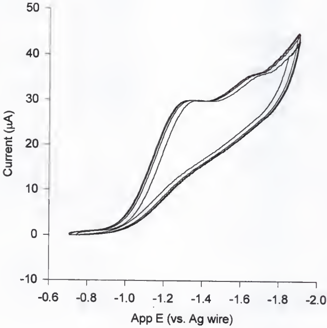

Figure 1.41. Cyclic voltammogram of the *poly*-$[Os(vbpy)_3]^{2+}$ grating film produced by plotting the current and potential responses from Figure 1.40.

through redox films. If the optical beams are monitored along with the current during the stepping cycles, the diffraction efficiency can be modulated to observe an increase or decrease depending on the potential applied to the film. These experiments would show how fast the diffracted beam intensity could recover after the potential had been switched. The ability to turn the diffraction "off" or "on" by inducing an electrochemical change is an attractive feature of these films. Quantifying the recovery times could help gauge the film's optical switching ability, crucial for eventual utilization in electro-optic molecular devices, and also in probing the mechanism of diffraction switching.

Figure 1.42 depicts the basic aspects of the double potential step chronomamperometric experiment involving an electroactive species, A, which is reduced as the potential is stepped from an arbitrary potential positive of $E^0(A/A^-)$, E_1, to a potential E_2, which is negative of $E^0(A^-/A)$ to ensure exhaustive reduction. The potential is held at E_1, and then suddenly changed to E_2. After a time interval, τ, the potential is reversed to its initial value. The current response in (b) shows a large spike corresponding to the flux of current to the electrode as the potential is stepped to E_2 and reduced sites are created. As the concentration gradient of reduced species moves past equilibrium, all remaining A sites are consumed, and the current decreases as this flux diminishes. As the potential is stepped back to E_1 the film is re-oxidized and current flows away from the electrode, producing a negative spike, which in turn decays until the film is fully re-oxidized. Thus the length of time needed for the decay to recover gives a quantitative measurement of the charge transport properties of the film. The shorter the decay times, the faster the charge transport through the film. This approach can be used to quantify how fast the optical beam can recover as well.

poly-$[(bpy)_2Ru(vpy)_2]^{2+}$ Grating Films. A representative data set from stepped potential experiments involving the oxidative switching of a *poly*-$[(bpy)_2Ru(vpy)_2]^{2+}$ grating film produced by the PL-EP method is shown in Figures 1.43 and 1.44 whose DE_0 is 0.026 %. The now familiar stacked plots display the four collected signals in the same

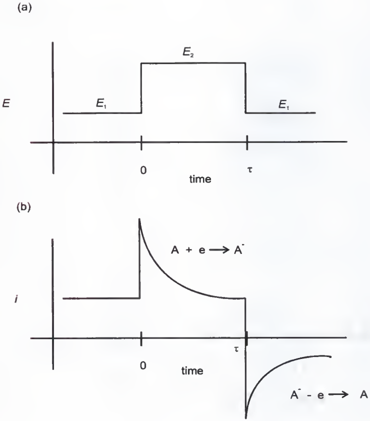

Figure 1.42. Double potential step chronamperometry. (a) Typical potential waveform; (b) current response. (from ref. 63.)

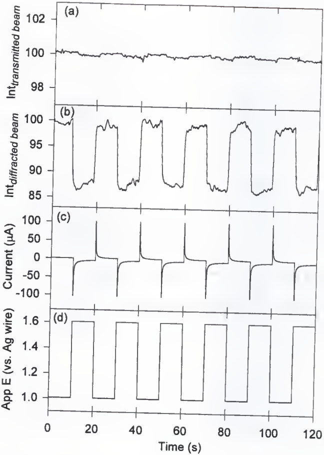

Figure 1.43. Diffraction modulation by oxidatively stepping a *poly*-$[(bpy)_2Ru(vpy)_2]^{2+}$ grating film repeatedly between 1.0 and 1.6 V in 10 second intervals. $DE_0 = 0.026\%$

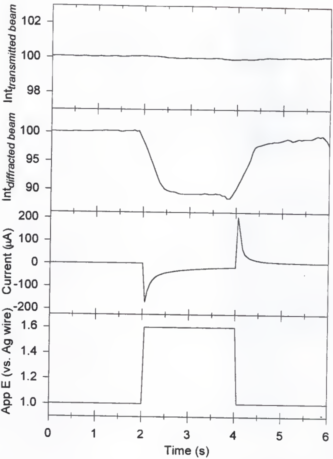

Figure 1.44. One complete cycle of an oxidatively stepped *poly*-$[(bpy)_2Ru(vpy)_2]^{2+}$ grating film between 1.0 and 1.6 V in 2 sec intervals.

manner as in the swept data, with the intensities of the undiffracted and diffracted beams, the current and the applied potential plotted from top to bottom. Both figures show effects on the optical and current signals as the potential is rapidly stepped from +1.0 to +1.6 V, through the $Ru^{2+/3+}$ couple at 1.32 V, at time intervals, τ, of 10 and 2 seconds, respectively, sampling at 100 samples/second. These intervals approach the limit of how fast the diffracted signal can recover. In both figures, the current spikes are relatively equal and opposite in value over the course of the experiment, indicating good electrochemical and physical stability of the film. In the diffracted signals, oxidative stepping induces an approximate 13% decrease in the *DE*, similar to the value obtained in the oxidatively swept experiments, and similar to in magnitude to other Ru grating films whose values are listed in Table 1.3. Also, good recovery of the intensity is observed after both steps using 10 sec intervals (Figure 1.43), judging from the relatively flat response. (The flatness can be visualized through the noise caused by the high sampling rate, and has been partially smoothed. See experimental for smoothing details.) Reducing the switching time to 2 sec in Figure 1.44 shows rounded signals which are just beginning to flatten before the subsequent step, indicating that this is the minimum time allowable for complete optical switching of these films.

The analogous reductive experiments were performed to observe if the nature of the redox process would dictate the kinetics of the electrochemical and optical processes. Figures 1.45 and 1.46 illustrate the results of such experiments for a film with DE_0 = 0.047% performed by stepping the potential from 0.0 to −2.0 V, through both bpy ligand reductions at −1.36 and −1.58 V. As was first observed in the swept cases, reducing these films causes the *DE* of the film to increase, by approximately 60% and 43% for switching intervals of 10 and 2 sec, respectively, which compare favorably to the reductively swept case above. The reductive steps show slightly better temporal response of the diffracted signal than the oxidatively stepped data, clearly illustrated by comparing the single cycle plots in Figure 1.44 to that in Figure 1.46, which shows the latter's diffracted signal

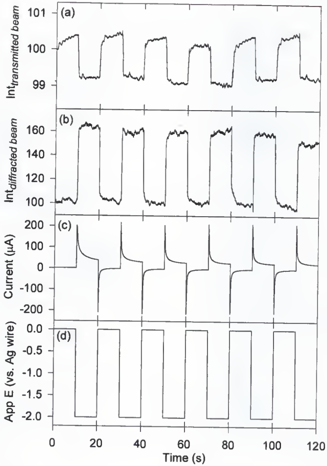

Figure 1.45. Diffraction modulation by reductively stepping a *poly*-$[(bpy)_2Ru(vpy)_2]^{2+}$ grating film repeatedly between 0.0 and –2.0 V in 10 second intervals. $DE_0 = 0.047\%$

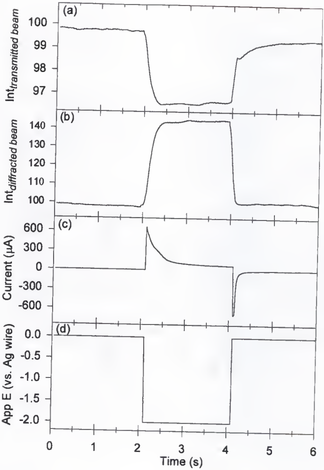

Figure 1.46. One complete cycle of a reductively stepped *poly*-$[(bpy)_2Ru(vpy)_2]^{2+}$ grating film between 0.0 and −2.0 V in 2 second intervals.

flattening more quickly. Also, the transmitted beam shows a larger dependence (2-3%) on the potential of the film than in the oxidative cases. In this case however, while the diffraction intensity increases as the film is reduced, the undiffracted intensity decreases. One other interesting feature of the undiffracted intensity is that it recovers more slowly than the diffracted intensity. The origin of this signal, easily observed in Figure 1.46 (top), and its behavior will be discussed in a later section.

poly-$[Os(vbpy)_3]^{2+}$ grating films. The oxidative stepping of a *poly*-$[Os(vbpy)_3]^{2+}$ grating patterned film at 10 sec intervals is shown in Figure 1.47. Like the similar case in the *poly*-$[(bpy)_2Ru(vpy)_2]^{2+}$ grating films, stepping from +0.5 to +1.2 V, results in the complete oxidation of Os^{2+} to Os^{3+} sites in the film, and produces a 36% decrease in the diffracted beam intensity. In the case involving a 2 sec step time, an approximate 25% decrease in the diffraction efficiency is noted. (Figure 1.48) These are slightly higher than the 17% average decrease reported in Table 1.3 for the swept cases. Re-reducing the film by stepping back the potential to +0.5 V restores the diffracted intensity to its initial full value of 0.094%. Both figures show a small $\approx$ 2% increase in the intensity of the transmitted beam occurring when the films are oxidized, and a subsequent return when the potential is switched back positively.

Reductively stepped *poly*-$[Os(vbpy)_3]^{2+}$ grating films display optical switching behavior as well. Figure 1.49 illustrates that when such a film is stepped in 10 second intervals from −0.6 to −1.6 V through both ligand reductions, a 25% increase of the diffracted beam intensity is achieved. The intensity of the transmitted beam behaves as in previous reductively swept and stepped experiments, showing a small 1% decrease when the film is reduced at the more negative potential. Shorter time intervals produced diffracted beam shapes which had not finished decaying before the subsequent potential step.

Table 1.3 summarizes the initial diffraction efficiency (DE_0) and absolute magnitude of the changes in *DE* for all four experiment types reported as percentages for

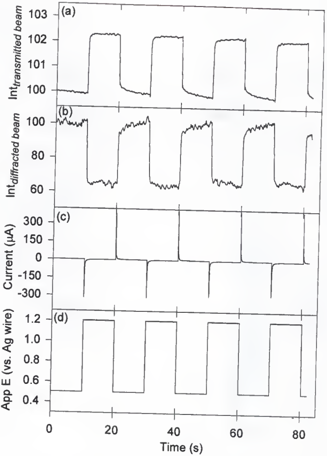

Figure 1.47. Diffraction modulation by oxidatively stepping a *poly*-$[Os(vbpy)_3]^{2+}$ grating film repeatedly between 0.5 and 1.2 V in 10 second intervals. $DE_0 = 0.094\%$

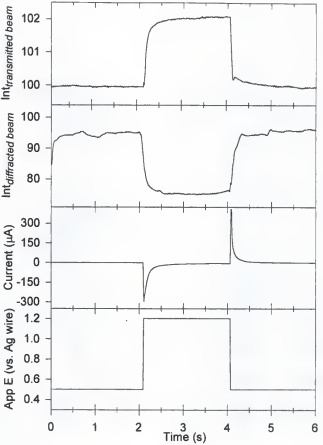

Figure 1.48. One complete cycle of the same *poly*-$[Os(vbpy)_3]^{2+}$ grating film in Figure 1.47 oxidatively stepped between 0.5 and 1.2 V in 2 second intervals.

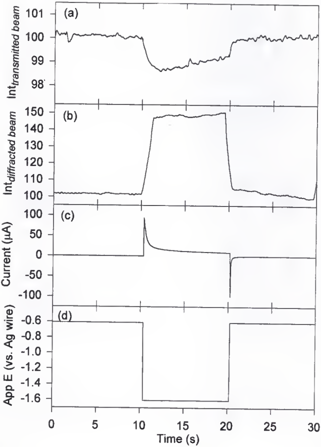

Figure 1.49. Diffraction modulation by reductively stepping a *poly*-$[Os(vbpy)_3]^{2+}$ grating film between -0.6 and -1.6 V in 10 second intervals. $DE_0 = 0.076\%$

representative Ru and Os films whose optical data was presented in this section. The oxidatively swept data for both Ru and Os type grating films is for the same set of films whose electrochemical data is presented in Tables 1.1 and 1.2, respectively. The remaining Ru film data is not from these exact films, but those produced in a similar fashion. Notice that there is a fairly wide distribution of DE_0's in each data set. This is most likely ascribed to the difficulty in exact film reproduction by employing the PL-EP technique. Further explanation of this problem is addressed in the experimental section.

The results of these stepped experiments illustrate that because of their relatively fast charge transport properties, *poly*-$[(bpy)_2Ru(vpy)_2]^{2+}$ and *poly*-$[Os(vbpy)_3]^{2+}$ grating films can be optically switched in 2 second intervals. This is much faster than the minute stepping times required for full signal recovery in the viologen films.[65] Also, all of the stepped experiments involving films of either type, excellent electrochemical and optical stability is established. This is demonstrated by strong, repetitive signals which do not diminish even after thousands of swept or stepped cycles. This feature, coupled with the superior minimum switching times, demonstrate that films produced by the PL-EP technique are better suited than their photopolymerized predecessors for optical devices whose diffraction efficiency can be electrochemically modulated.

Discussion and Interpretive Analysis

The following two sections will focus on providing an explanation for the electrochemical and optical behavior of the grating films presented above and their relevance and application to established theory.

Electrochemical Behavior of PL-EP Produced Grating Films

Charge transport in redox films occurs by a complex mechanism which involves several factors. These include self-exchange of electrons from the electrode to sites in the film, a subsequent inward diffusion of counterions into the film to maintain charge neutrality, and the distance between redox sites, which varies depending on concentration, and possible swelling and deswelling of the film.[66] Also, the film morphology is important. Ion -exchange polymers will have redox sites which diffuse more freely than redox sites which are tethered to a polymer network. The identity of the actual factor which is rate-controlling is the focus of many groups' research. As films become thicker, the diffusional contributions affecting charge transport become larger, adding yet another factor to consider. Determining the actual mode of transport and rates of diffusion are beyond the scope of this work, but several qualitative conclusions can be drawn from the existing data. Previous work in Murray's group studying charge transport on Pt electrodes modified with homogeneous films of *poly*-$[(bpy)_2Ru(vpy)_2]^{2+}$ and *poly*-$[Os(vbpy)_3]^{2+}$ with similar surface coverages and thickness to those reported in this study has shown the calculation of appreciable diffusion coefficients, indicating that diffusion contributions to charge transport are important.[33,34,36]

Recalling Figure 1.26, an ideal electrochemical process in a redox modified electrode with facile charge transport, should produce equal and opposite waves with $\Delta E_p = 0$ for the forward and backward processes. Also the amount of charge passed should be equal and independent of the sweep rate, ν. Tables 1.1 and 1.2 showed that although the ΔE_p's for these films are not zero, they are relatively small, and that the surface coverages are relatively equal and independent of ν, all indications that transport is fast and not diffusion controlled.

Another useful piece of information about the charge transport characteristics of these films can be revealed by plotting i_p, the peak current, vs. ν, and i_p vs. $\nu^{1/2}$. In redox films exhibiting facile charge transport, i_p varies linearly with ν, from Eq. 1.1.[7] When this dependency is observed, complete oxidation/reduction of the film's redox sites is believed to occur. If the transport process is slower, i_p varies linearly with $\nu^{1/2}$,[67] as is the case in solution, and thicker films. (Thicker films, where diffusion effects become greater are defined as films with surface coverages > 1×10^{-8} mol/cm^2.) This relation is derived from the Randles-Sevcik equation[68] (Eq. 1.15) which describes the semiinfinite diffusion of solution dissolved reactants diffusing to the electrode surface

$$i_p = 2.72 \times 10^5 n^{3/2} A D^{1/2} C^0 v^{1/2} \quad (\text{at } 25^\circ \text{C}) \qquad 1.15$$

where n is the number of electrons in the process, A is the area, D is the diffusion coefficient, and C^0 is the concentration. Figure 1.50 illustrates plots of both relationships using i_p's from the oxidative (Ru or Os $2^+/3^+$ redox couple) CVs in Figures 1.27 and 1.28. Inspection of these plots illustrates that a better fit is produced in the i_p vs. ν plot (a) than in the i_p vs. $v^{1/2}$ plot (b). This would infer transport closer to ideal than that governed by diffusion rates.

One important fact to note is that the standards that have been established for quantifying charge transport rates, especially those governed by diffusion, are based on homogenous films on electrodes in the infinite or semiinfinite case. In the present study, films produced by PL-EP are *not* in the infinite case, i.e., they have areas of bare electrode separating the arrays of polymeric redox film. Because of this, direct comparison to previous studies using similarly comprised metal polypyridine redox films by implementing the traditional methods of Murray,[69] or Pickup[70] which found significant diffusion contributions may not be totally valid. These exposed electrode areas between arrays could possibly allow for faster self-exchange rates by facilitating counterion flow into the film. This could be an indication why the present heterogeneous grating films show better correlation to v, when homogeneous films of similar concentration, coverage, and thickness show better fitting to $v^{1/2}$.

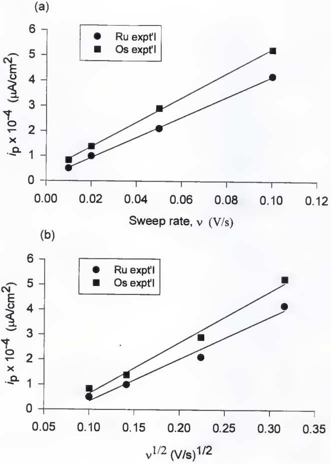

Figure 1.50. (a) i_p vs. sweep rate, ν, for $2^+/3^+$ oxidation process for Ru and Os grating films; (b) i_p vs. $\nu^{1/2}$ for same process. Lines represent the best linear fits to the experimental data used in Figures 1.27 and 1.28 divided by the electrode area.

Optical Behavior of PL-EP Produced Grating Films

For proper and meaningful analysis of the optical data presented, two key issues need to be addressed: 1) the basis for diffraction in these grating films, and (2) understanding the origin of the diffraction modulation resulting from induced changes of the film's redox potential. As briefly mentioned in the introduction section, the refractive index, *n*, plays an important role in the ability of these films to act as gratings. Before discussion of this role can commence, a definition of the refractive index is instructive.

The velocity of an electromagnetic wave, *v*, when traveling through a medium will be slower than its velocity through a vacuum, and is represented by equation 1.16:

$$v = \frac{c}{n} \qquad 1.16$$

where *c* is the speed of light in a vacuum. The refractive index of the medium, *n*, is the factor by which this velocity is reduced. Figure 1.51(a) shows a top view of a typical redox film grating patterned electrode. As light impinges the film's surface, the regions containing the film (higher *n*), will slow its speed, radiating a beam which lags *in phase* to the light which has traveled through the lower *n*, bare electrode areas. (Or, as in the case in the electrochemical cell, the electrolytic solution which fills these gaps.) This closely spaced array of alternating regions of high and low refractive index, causes the diffracted pattern seen in Figure 1.52. Notice the transmitted beam in the center with *m* orders of diffracted beams (recall Eq. 1.8, and Fig 1.13) of decreasing intensities relative to the zero-order, or undiffracted beam.

The data presented shows a clear dependence of these films' ability to diffract light on the redox state of the film. The crux of the research is understanding how an applied electrochemical change causes these films to behave as better or worse diffracting media. Recall from Eq.1.7 that because of the absorption of light from molecules dispersed within

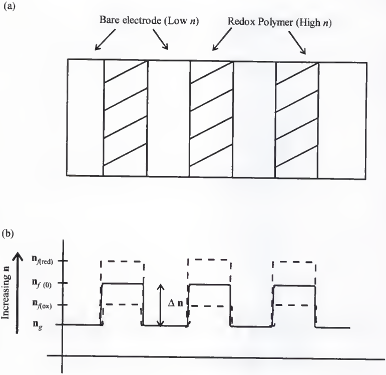

Figure 1.51. (a) Top view of grating showing areas of high and low *n*; (b) Cross section of grating film showing changes in the magnitude of the complex refractive index, **Δn**, monitored during electrochemical oxidation or reduction of the grating film.

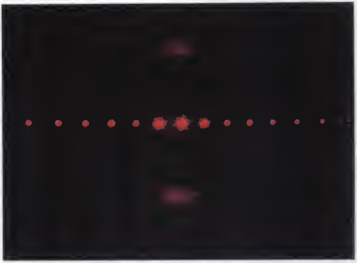

Figure 1.52. Diffraction patterned generated by He-Ne laser impinging on the surface of a grating film.

the film, the refractive index is a complex quantity, **n**, consisting of real and imaginary components, shown again here:

$$(\mathbf{n}(x,\lambda)) = n(x,\lambda) + ik(x,\lambda) \qquad 1.17$$

with n accounting for the real component of the refractive index, and k accounting for the absorption. (Refer to Table 1.4 to aid in the identification of the numerous variables used in equations presented in this section.) Modulation of the diffraction efficiency is caused by a change in either one or both of these components. For a sinusoidal grating, the diffraction efficiency, DE, at probe frequency, ω, is[53]

$$DE(\omega) = \exp\left[-\frac{2.3OD(\omega)}{\cos\theta}\right]\left[\sinh^2\frac{\pi\Delta k(\omega)T}{\lambda\cos\theta} + \sin^2\frac{\pi\Delta n(\omega)T}{\lambda\cos\theta}\right] \qquad 1.18$$

where the first term in brackets accounts for the average loss in optical density, OD, due to absorption, T is the film thickness, λ is the probe wavelength, and θ is the Bragg angle of diffraction. This can be simplified to the expression previously given in Eq. 1.10, shown here: (refer to Appendix C for derivation)

$$DE = (\Delta k)^2 + (\Delta n)^2 \qquad 1.19$$

The resting or initial DE of these grating films is then defined as

$$DE_0 = (\Delta k_0)^2 + (\Delta n_0)^2 \qquad 1.20$$

Table 1.4. Variable identification and equation in which they are first appear.

Variable	Definition	Equation
$\mathbf{n}$	complex refractive index (RI)	1.17
n	real (phase) component of $\mathbf{n}$	1.17
k	imaginary (absorptive) component of $\mathbf{n}$	1.17
DE	diffraction efficiency	1.18
ω	probe frequency	1.18
λ	probe wavelength (633 nm)	1.18
OD	optical density	1.18
Δn	change in real component of $\mathbf{n}$	1.18
Δk	change in imaginary component of $\mathbf{n}$	1.18
T	grating film thickness (≈100 nm)	1.18
DE_0	initial diffraction efficiency before electrochemical change	1.20
Δk_0	change in initial imaginary component of $\mathbf{n}$	1.20
Δn_0	change in initial real component of $\mathbf{n}$	1.20
$\mathbf{n}_{f(0)}$	initial value of grating film's complex RI	1.21
$n_{f(0)}$	initial value of grating film's real component of the complex RI = 1.749	1.21
n_g	actual refractive index of the electrolyte solution filling gaps between grating film stripes = 1.347	1.21
$k_{f(0)}$	initial value of grating film's imaginary component of $\mathbf{n}$	1.21
k_g	initial value of the gap solution's imaginary component of the complex RI = 0	1.21
DE_f	diffraction efficiency after an electrochemical event	1.23
$\mathbf{n}_{f(f)}$	value of grating film's $\mathbf{n}$ after an electrochemical event	1.23
$n_{f(f)}$	final value of grating film's real component of $\mathbf{n}$ after an electrochemical event	1.23
$k_{f(f)}$	final value of grating film's imaginary component of $\mathbf{n}$ after an electrochemical event	1.23
ΔDE	difference between final and initial diffraction efficiencies	1.24
$\Delta(\Delta\mathbf{n})$	change in the change of the complex RI after an electrochemical event	1.24
$\mathbf{n}_{f(\mathrm{red})}$	arbitrary value of grating film's complex RI after an applied reductive potential	Fig. 1.51
$\mathbf{n}_{f(\mathrm{ox})}$	arbitrary value of grating film's complex RI after an applied oxidative potential	Fig. 1.51
ΔOD	change in the grating film's optical density after an electrochemical event	Fig. 1.53

A schematic visualization of the changes in DE_0 as they relate to the film's initial complex index of refraction, $\mathbf{n}_{f(0)}$ during an electrochemical change is depicted in Figure 1.51(b). Using this scheme, equation 1.20 can be rewritten as:

$$DE_0 = \mathbf{n}_{f(0)} = (n_{f(0)} - n_g)^2 + (k_{f(0)} - k_g)^2 \qquad 1.21$$

and setting $k_g = 0$,

$$DE_0 = (n_{f(0)} - n_g)^2 + k_{f(0)}{}^2 \qquad 1.22$$

Expressing DE_0 in this manner takes into account both components of the complex refractive index at rest, related to that of the gap solution. An electrochemically induced change in DE_0 changes the DE to a new value, DE_f, defined (Figure 1.51) as the squared difference of the film's complex refractive index after the change, and the refractive index of the gap solution, n_g plus the final value of the grating film's absorptive component, $k_{f(f)}$ squared:

$$DE_f = \mathbf{n}_{f(f)} = (n_{f(f)} - n_g)^2 + k_{f(f)}{}^2 \qquad 1.23$$

Oxidatively swept or stepped experiments decreases the DE, with a concomitant decrease in $\mathbf{n}_{f(f)}$ to an arbitrary value, $\mathbf{n}_{f(ox)}$, while in the reductive cases, the opposite behavior is observed to an arbitrary value, $\mathbf{n}_{f(red)}$ (Figure 1.51(b)). The change in DE, ΔDE, for an oxidative or reductive applied potential results in a change in $\Delta\mathbf{n}$, or $\Delta(\Delta\mathbf{n})$, which is the difference of the final and initial diffraction efficiencies:

$$\Delta DE = \Delta(\Delta\mathbf{n}) = DE_f - DE_0 \qquad 1.24$$

which can be rewritten using Equations 1.22 and 1.23 to become:

$$\Delta DE = \Delta(\Delta \mathbf{n}) = (n_{f(\mathrm{f})} - n_g)^2 + k_{f(\mathrm{f})}{}^2 - [(n_{f(0)} - n_g)^2 + k_{f(0)}{}^2] \qquad 1.25$$

Experimentally, ΔDE is monitored by reading the signal of the diffracted beam collected at the photodiode.

In two detailed analyses of diffraction from laser-induced gratings, Fayer and coworkers[53,71] describe the relation between the phase and absorption contributions to the grating's diffraction efficiency. In these studies, they illustrate the wavelength dependence on the diffraction efficiency, concluding that the relative phase and absorption contributions depend only on the position of the probe wavelength relative to the absorption band maximum of the grating and the linewidth of the absorption band. When the probe beam and absorption maximum are on-resonance, phase effects are zero, and do not contribute to the diffraction. As the probe beam is moved off-resonance, the absorption effects diminish, and phase contributions increase until the probe beam is totally off-resonance with the absorption band, at which point phase effects dominate diffraction. Because of this, the film can be made to behave as an amplitude or phase grating simply by tuning the wavelength of the probe beam. Therefore, examination of the probe wavelength dependence on the present grating films is important in determining the origin of the diffraction. This can be ascertained by analysis of the spectroelectrochemical data coupled with the transmitted beam intensity in the diffraction modulation experiments.

In the present study, the probe wavelength of the He-Ne laser utilized in the experimental apparatus is 633 nm. Transmission grating behavior would be apparent from large contributions of k, the imaginary, absorptive component of $\mathbf{n}$, by observation of any absorption changes in the UV-vis spectra that are on resonance with the laser. Absence of spectral changes would suggest diffraction efficiency modulation by large changes in *n*, the refractive index.

The first spectroelectrochemical experiment involving grating films comprised of *poly*-$[(bpy)_2Ru(vpy)_2]^{2+}$ addresses this dependency question. In Figure 1.30, as the film is oxidized from Ru^{2+} to Ru^{3+}, the MLCT band is bleached, with the intensity of this bleaching approaching zero at 600 nm. There are no absorbance changes at 633 nm, the probe wavelength, indicating that the oxidized Ru films are optically transparent. This is supported by the diffraction modulation data in Figure 1.36, which shows no apparent change in the response of the transmitted beam intensity with changing redox potential. Therefore, in this case, the observed 15% change in diffraction intensity is most likely caused by a change in *n* and not *k*.

In such cases where there is no dependency on *k*, Eq. 1.19 can be simplified even further to:

$$\Delta DE = (\Delta n)^2 \qquad 1.26$$

Eliminating values of *k* from Eq. 1.25 results in the following expression

$$\Delta DE = DE_f - DE_o = (n_{f(f)} - n_g)^2 - (n_{f(0)} - n_g)^2 \qquad 1.27$$

All of the values in Eq. 1.27 are experimentally known except for $n_{f(f)}$. DE_o is determined by reading the ratio of the diffracted to the transmitted intensities at the outset of the experiment. DE_f is determined by extracting these same two parameters at the oxidized potential. n_g is the refractive index of the TBAH/CH_3CN electrolyte solution filling the gaps between polymerized film, determined to be 1.347 by measurement in a refractometer. $n_{f(0)}$, the refractive index of the *poly*-$[(bpy)_2Ru(vpy)_2]^{2+}$ or *poly*-$[Os(vbpy)_3]^{2+}$ grating film at its resting potential is 1.749 for either film type and its value is determined by a refractive index matching experiment. In this experiment, a grating film is affixed in the electrochemical cell and placed in the beam of the He-Ne laser in the experimental apparatus in Figure 1.34. A solvent of known refractive index is added to the cell, and a photodiode is aligned to capture the intensity of the diffracted beam. The intensity is noted, then the solvent is removed and replaced with another solvent of greater refractive index. If the *n* of this new solvent filling the gaps is closer to the *n* of the film, Δn decreases (Fig. 1.51(b)), and subsequently the diffraction intensity decreases. The solvents are replaced until the diffracted intensity is virtually undetectable, resulting in a "match" of the film's *n* to that of the solution ($n_g = n_f$).

Using Fayer's *DE* expression in Eq. 1.18 as a model, experimental values of ΔDE can be calculated based on the known properties of these films. In the oxidative case for the *poly*-$[(bpy)_2Ru(vpy)_2]^{2+}$ grating films, absorbance contributions from *k* are zero, and Eq. 1.18 takes the form: (Appendix C)

$$DE(\omega) = \left[\frac{\pi \bullet T}{\lambda \cos\theta}\right]^2 (\Delta n(\omega))^2 \qquad 1.28$$

and thus ΔDE, using Eq. 1.27 is

$$\Delta DE(\omega) = \left[\frac{\pi \bullet T}{\lambda \cos\theta}\right]^2 [(n_{f(f)} - n_g)^2 - (n_{f(0)} - n_g)^2] \qquad 1.29$$

Using the experimentally determined values of $n_{f(0)}$, n_g, T, and λ in Table 1.4, ΔDE can be calculated by incrementally varying the only unknown variable, $n_{f(f)}$. A plot constructed of the calculated values of ΔDE using this procedure versus the change in Δn is shown in Figure 1.53. Following the dashed lined, a 0.04 (4%) change in Δn, (corresponding to a change in the film's refractive index from its initial value of 1.749 to a final value of 1.679)

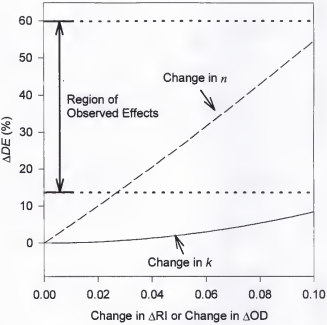

Figure 1.53. Calculated effects of changes in k (from ΔOD) and n on the changes in diffraction efficiency using Equation 1.18.

results in an approximate 20% change in the diffraction efficiency, a value close to those observed in the oxidative cases for *poly*-$[(bpy)_2Ru(vpy)_2]^{2+}$ grating films (Table 1.3).

In the calculated model above, ΔDE is determined by using the known values from Table 1.4 and incrementally varying $n_{f(f)}$. In the experiments, ΔDE values are obtained by monitoring intensity fluctuations detected by photodiodes. Since ΔDE values are experimentally known, it should be possible to use Eq. 1.18 in the reverse manner in which it was used above, this time solving for $n_{f(f)}$ using known ΔDE values instead of vice versa. Efforts to do this returned values of $n_{f(f)}$ which, by subtracting $n_{f(f)}$ from $n_{f(0)}$, produced changes in Δn which did not fit the model plotted in Figure 1.53. The probable cause of this discrepancy is the very low DE_0 values of these grating films listed in Table 1.3, determined at the outset of each experiment. Using Equation C.9, and measured values for T, $n_{f(0)}$, and n_g listed in Table 1.4, DE_0 values for these films should be 8%. This value is approximately a factor of 100 greater than the values listed in Table 1.3, causing significant deviation in $n_{f(f)}$ from the model. The low DE_0's are an outcome of the PL-EP fabrication method. Microscopic inspection of the grating films shows isolated domains where polymer growth is confined to the bare electrode regions dictated by the p-MPS, resulting in high resolution and better diffraction. However, over the larger region of the film probed by the laser, homogenous coverage of highly resolved alternating polymer stripes is not apparent. Thus, the overall DE_0 measured is an average of the total area probed, not just the homogenous region. This results in superficially low DE_0's, and subsequent $n_{f(f)}$'s which poorly fit the calculated model. However, the magnitude of the ΔDE's calculated by Eq. 18 and those observed experimentally *are* in good agreement, as noted by the designated region in Figure 1.53. This suggests that although the *absolute* DE values are low because of non-uniform film morphology, the magnitude change of the gratings' ΔDE fits the calculated model very well.

Treating the reductive case for the *poly*-$[(bpy)_2Ru(vpy)_2]^{2+}$ and both oxidative and reductive cases of the *poly*-$[Os(vbpy)_3]^{2+}$ by ignoring the contribution of k to the changes in the diffraction efficiency may not be appropriate. This is due to observably larger changes in the transmitted beam during the optical modulation experiments. If the changes in the film's absorption are large enough, the films could behave as mixed amplitude and phase gratings. The spectroelectrochemical data in the reductive case of the *poly*-$[(bpy)_2Ru(vpy)_2]^{2+}$, shown in Figure 1.31 shows new absorptions resulting from the reduction of these films, whose bands tail out into the red, encompassing the region of the probe beam. This growth explains why the intensity of the transmitted beam decreases when the film is reduced. In the oxidative spectroelectrochemistry of the *poly*-$[Os(vbpy)_3]^{2+}$ grating films, the bleaching of the MLCT band extends far enough into the red to affect the behavior of the transmitted beam. Since this absorption band is slowly bleached during oxidation, the transmitted beam should increase in intensity during this redox change. The response of the transmitted beam in Figures 1.39 and 1.46 confirm this expected behavior. The transmitted beam behavior in the reductive case for the Os films is analogous to the reductive case observed in the Ru films. These observed changes in the transmitted intensities may be enough to attribute the change in diffraction efficiency to absorptive effects resulting from modulation of k instead of n.

For amplitude grating behavior, expected changes in the diffraction efficiency can be calculated using Eq. 1.18 in a similar manner to that presented above for the changes due to modulation of the refractive index. In the case where k contributes solely, $n = 0$ and Eq. 1.18 can be rewritten as:

$$DE(\omega) = \exp\left[-\frac{2.3OD(\omega)}{\cos\theta}\right]\left[\frac{\pi \bullet T}{\lambda\cos\theta}\right]^2 [(\Delta k)]^2 \qquad 1.30$$

The optical density, OD, is related to k by the expression:

$$k = 2.3\lambda(OD)/(4\pi T) \qquad 1.31$$

Thus, for these grating films to act as amplitude gratings, changes in their optical density, and thus values of *k*, will determine ΔDE. By incrementally varying *OD*, (ΔOD) the concomitant changes in *k* can be calculated using Eq. 1.30, producing *k* values then used in Eq. 1.29 to calculate expected ΔDE values. The solid line in Figure 1.53 shows this expected effect. Even at a ΔOD of 0.10, the calculated ΔDE value is only approximately 8%, well below the region of the observed ΔDE whose experimental values are listed in Table 1.3. This is a strong piece of evidence supporting the notion that in the case of the Ru grating films, electrochemically induced changes in the diffraction efficiency are caused by changes in the film's refractive index and not changes in its optical density.

The data from the spectroelectrochemical experiments illustrated in Figures 1.30-1.33 help to corroborate this finding. At 633 nm, ΔOD can be read from the plots by subtracting the *OD* in its electrochemically changed state from the initial *OD*. These ΔOD values range from 0.0 (Ru oxidized state, Figure 1.30) to only 0.08 (Os oxidized state, Figure 1.32). These values closely model the expected behavior calculated and plotted in Figure 1.53. This infers that the absorption of the probe beam is significantly off-resonance and of low magnitude, therefore modulation of the diffraction efficiency in the Ru grating films is due solely to changes in the refractive index, resulting in films which act as phase gratings. In the Os grating films, however, Table 1.3, shows that for the oxidative process, higher *DE* values are observed. This may be a result of the higher ΔOD values which could add some contribution of *k* to the overall ΔDE. Thus, these Os films may be more properly be labeled as mixed amplitude/phase gratings rather than purely phase gratings.

Conclusions

The above studies of grating films comprised of either *poly*-$[(bpy)_2Ru(vpy)_2]^{2+}$ or *poly*-$[Os(vbpy)_3]^{2+}$ have demonstrated several interesting aspects. The first is that the PL-EP method affords the ability to produce microstructured arrays of electropolymerized films. These patterned films have enhanced electrochemical properties over the original viologen photopolymerized system in that they posses a higher concentration of redox sites, and as a result, exhibit faster charge transport. Two other important features demonstrated by PL-EP produced grating films are their improved stability during repetitive electrochemical cycling, and their faster optical switching rates compared to the viologen films. The improved electrochemical properties of these films subsequently improves the optical switching properties, as was shown in the stepped potential experiments. This feature makes them more desirable candidates for device applications. Minimum stepping times of 2 seconds observed in these films are much faster than the minute times needed in the photopolymerized scheme, although still not quite as fast as the millisecond time intervals for various conducting polymers.[3] Lastly, utilizing $[(bpy)_2Ru(vpy)_2]^{2+}$ or $[Os(vbpy)_3]^{2+}$ as monomers in the PL-EP method affords grating films with the added ability to modulate the film's diffraction efficiency positively or negatively. This is easily performed by either sweeping or stepping the potential applied to the film through its reductive or oxidative redox couples respectively.

The disadvantages of this technique involve the fabrication process. These are primarily two-fold. The first is that the PL-EP method suffers from a low success rate of usable films because of the uncertainty in determining when to stop the electropolymerization process. The second problem is the quality of the film coverage that is produced. Grating films' surfaces are not homogenous in the area probed by the beam, i.e. the probed region is not distinctly spatially defined, leading to areas of high and low resolution when observed under the microscope. This results in artificially low DE_0 values which are averaged over the total area probed by the laser. This is most likely the reason that experimental values do not fit Fayer's *DE* equation (Eq. 1.18). However, it is important to note that the magnitude of ΔDE calculated using the values of T, λ, $n_{f(0)}$, and n_g measured for these films *is* in good agreement with the observed *DE* changes in Table 1.3.

Lastly, we believe that this is the first set of studies which demonstrate modulation of the diffraction efficiency by electrochemical means. This phenomenon of modulating a grating's diffraction efficiency is not a new concept. However, previous examples from the literature have all utilized holographic gratings whose diffraction efficiency modulation relies on the effect of an electric field on the molecular orientation of birefringent liquid crystalline materials.[72,73,74] These holographic polymers are potentially valuable devices capable of optical storage, and optical amplification. Although the redox film based gratings in the present study are probably not suitable for these applications, their inherent redox properties could make them attractive in other areas, such as chemical/optical sensing. In such cases, addition of an reactive analyte could chemically oxidize or reduce the films, resulting in a modulation of the diffraction efficiency via a *chemical* rather than electrochemical change.

Experimental

Materials and Syntheses

All materials used in the syntheses were of reagent grade and used as received unless otherwise noted.. The electrolyte in all electrochemical experiments, tetrabutylammonium hexafluorophosphate (TBAH) (Aldrich) was recrystallized twice from 1/1 ethyl alcohol/water and dried in a vacuum oven before use. 4,4'-dimethyl-2,2'-bipyridine was synthesized by the reported procedure of Spiro and Ghosh.[75] All ITO coated glass electrodes were purchased from Delta Technologies, Stillwater, MN (No. CC-80IN-1509). Average ohmic resistances were on the order of 60 mΩ. ITO electrodes were cleaned by wiping them with acetone and blowing dry with N_2 before use. The syntheses of the compounds used in the PL-EP method is as follows.

poly-methylphenylsilane (p-MPS). This compound was synthesized via a modified method of Watanabe and Ito.[60] A clean, oven-dried 500 mL 3-neck roundbottom flask was fitted with a mechanical stirrer and a reflux condenser. N_2 was purged through the remaining joint and out the top of the condenser. Na pellets (0.92 g, 0.090 mol, Aldrich) were submersed in 50 mL freshly distilled toluene (Na, benzophenone) in a clean oven-dried beaker and quickly poured into the flask. A solution of 18-crown-6 (0.58 g, 2 mmol, Aldrich) in 5 mL dry toluene was then added to the Na slurry and the mixture was stirred. The N_2 inlet was replaced with an addition funnel containing dichloromethyl-phenylsilane (6.5 mL, 0.040 mol, Aldrich) in 7 mL dry toluene. The stirring Na slurry was heated to reflux under N_2, at which point the addition funnel was opened slightly, allowing the silane to add dropwise over a half-hour period. After all was added, the solution was refluxed for an additional 2 hr period and cooled to room temperature. The blue-gray supernatant was pipetted off and centrifuged, leaving a pale-yellow liquid. This liquid was then pipetted into a beaker of stirring methanol, precipitating the desired product as a powdery white solid. The solid was collected on a fritted funnel and re-precipitated twice by dissolving the solid in $CHCl_3$ and precipitating it in isopropanol. GPC characterization versus polystyrene standards revealed an M_w of 3500.

$[Os(vbpy)_3]^{2+}$. After initial problems with the synthesis of the vinylbipyridine ligand via the method of Abruña[76], better success was achieved via the following procedure of Guarr and Anson.[77] Because of the creation of a highly unstable dimethylbipyridine anion, extreme care was taken to ensure all glassware and syringes were cleaned and oven-dried overnight, and then flame-dried after assembly. The glassware apparatus was assembled using a 125 mL addition funnel inserted into the middle neck of a 300 mL 3-neck round bottomed flask. One of the remaining two necks was fitted with a new septum for syringe additions, while the other was fitted with a ground glass joint adapter which held a glass tube which could be utilized for solution bubbling. A brisk flow of N_2 was purged through the apparatus during all chemical additions. Diisopropylamine (5 mL, Aldrich) and 20 mL of freshly dried THF (over NaK, benzophenone) were syringed into the flask and stirred. *n*-BuLi (14 mL, 2.0 M, Aldrich) was then syringed in and the resulting mixture was stirred for 15 min at -78° C. In a separate clean, dry flask was placed dimethylbipyridine, dmb, (5.0 g, 0.027 mol) and a magnetic stir bar. With vigorous stirring, dry THF was cannula transferred from the still into the flask containing the dmb, approximately 150 mL. Because of relatively poor solubility of the dmb in THF, it takes a while for the dmb to dissolve. The solution of dmb is then cannula transferred into the addition funnel and is added dropwise over a 1 hr period, producing a deep green-black solution. A separate flask containing 2.0 g paraformaldehyde is connected to the glass transfer tube and the flask is warmed. A stream of Ar was used to bubble the paraformaldehyde vapors into the dmb anion solution over a 2 hr period. The temperature of the solution was allowed to rise to ambient during this transfer. Often times throughout this vapor bubbling, the glass transfer tube needed to be gently warmed with a heat gun to melt the solid that began to build up inside the tube, slowing the transfer. After this time period, the reaction was quenched with ice-water, creating a yellow solution. The solvent was rotary evaporated under vacuum leaving a yellow oil and a large amount of unreacted dmb solid. The oil was filtered and allowed to sit on the bench top overnight. The following day, more unreacted dmb had precipitated and was again removed by filtration. The yellow oil, an alcoholic intermediate, was dehydrated by adding ≈ 0.5 g of powdered NaOH to the oil in a vacuum sublimator and heating the mixture at 130° C under vacuum. The desired product, vinylbipyridine, vbpy, was collected over a 6 hr period as a white crystalline solid by periodically removing the cold finger and scraping the crystals off, then replacing and continuing the sublimation.

Complexation to form $[Os(vbpy)_3]^{2+}$ was achieved by a straightforward utilization of the method published by Gould and coworkers.[43]

The other complex used in this study, $[(bpy)_2Ru(vpy)_2]^{2+}$was synthesized easily according to previously reported procedures.[61] Both synthetic schemes are summarized pictorially in Figure 1.19.

PL-EP Fabrication of Redox Grating Films

Concentrations of p-MPS solutions in toluene were 0.1 mg/μl and spin-coated onto cleaned ITO electrodes by dropping ≈20 μl of the solution onto the electrode, manually spreading it out with a flattened glass rod, then spinning at 4500 rpm for 15 s to create an optically transparent film. The films were then exposed to near-UV light from a 450 W Hanovia medium pressure Hg immersion lamp in a water-cooled quartz immersion well through either a USAF target patterned chrome-on-glass reticle (Rolyn Optics) or a Ronchi grating patterned chrome-on-glass mask (Edmund Scientific) the latter having a spatial frequency of 100 lines/mm. This translates to electrodes patterned with 5 μm line and gap widths. The electrode's film side was clamped to mask's chrome side by a black metal paper clip, and the back of the electrode was covered with a piece of black construction paper to eliminate back-side exposure. This "sandwich" consisting of the p-MPS coated electrode between the mask and construction paper was placed 2 in from the outside wall of the immersion well and exposed for 15 min. Following exposure, the films were developed by gently swirling the ITO electrode for 1 min in a plastic beaker containing isopropyl alcohol. After drying the film coated electrode with a gentle stream of N_2, the films were inspected under a microscope to determine if the exposed p-MPS was fully removed, leaving stripes of bare electrode. Often times an additional rinse in isopropanol for 30 s was needed to complete the development. Inspection under the microscope revealed isolated regions where contrast between p-MPS film lines and bare electrode surface varied . An area with better p-MPS/clean electrode contrast was aligned with the cell opening and hole in the Viton seal shown in Figure 1.54.

Electropolymerizations were carried out by placing CH_3CN solutions containing either 2.5 mM -$[(bpy)_2Ru(vpy)_2]^{2+}$ or 1.0 mM $[Os(vbpy)_3]^{2+}$ with 0.1 M TBAH in a Teflon electrochemical cell. (Figure 1.54) The p-MPS patterned electrode and Viton seal is seated in the notch of the cell body. The electrode is covered with a teflon cover slip and is assembled to the rest of the cell with screws, carefully tightening so as not to apply too much pressure to break the electrode. The ITO electrode is cut longer than this slot so that the end of the lead from the potentiostat is easily affixed via an alligator clip to the ITO glass, making it the working electrode. The monomer solution is added to the reservoir, is capped with a septum, and the cell is gently purged with Ar for 10 min taking care that no monomer solution is bubbled out the top of the vent needle. The needles are removed and replaced with clean Ag wire and Pt wire reference and auxiliary electrodes, respectively. The Ag electrode is shrouded with a plastic sheath to protect against shorting the cell's circuit by contacting the Pt electrode. Often times an air bubble is trapped in the cell against the electrode, not allowing contact of the monomer solution with the ITO electrode. The cell can be gently tapped on the cover slip with a finger to remove this bubble. Once the bubble is removed, ohmic contact to all 3 electrodes is made by using alligator clips, and the working electrode is then scanned at a 100 mV/s rate 4-7 times from -0.7 to -2.0 V for the $[(bpy)_2Ru(vpy)_2]^{2+}$ solution, or 8-10 times from -0.8 to -1.6 V for the $[Os(vbpy)_3]^{2+}$. The potential of the Ag wire reference electrode is $\approx$ +0.13 V vs. SCE. After cathodic cycling, the ITO electrode patterned with polymer is rinsed in a plastic beaker of CH_3CN (film side up so as not to disturb the film) for 20 s to remove excess adhered monomeric solution, followed by immersion in a separate beaker of $CHCl_3$ (30 s) to dissolve any residual p-MPS, leaving a round spot of grating film whose size is approximated by the diameter of the cell aperture (0.32 cm). As in the p-MPS patterned electrodes, the development process was assessed by inspection under a

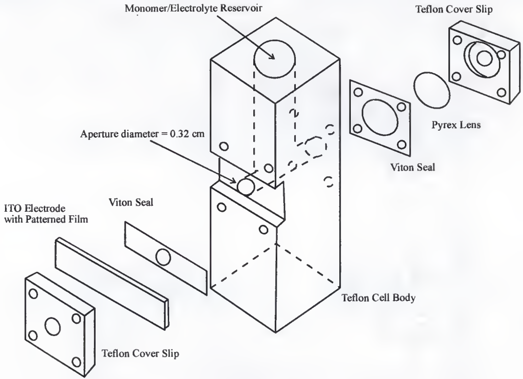

Figure 1.54. Expanded view of cell used in all electrochemical and optical experiments.

microscope. Also the films were placed in front of the HeNe laser to see how well they diffracted. Longer CH_3CN and $CHCl_3$ soak times (1 min or more) sometimes helped to improve the diffraction.

Unfortunately, the procedure above involves much trial and error and is by no means 100% reproducible. This is because of the many variables which must be considered when producing these grating films. Variables which affect film growth are concentration, potential sweep rate, potential sweep range, number of sweeps, and p-MPS thickness and development. Of these, the first four are seemingly easier to control than the latter two. The first three conditions used in these experiments were determined by trying various values and using the best combinations. Initial parameters for these three variables were chosen from literature procedures involving homogenous film growth on clean electrode surfaces.[32-34] These initial parameters were then varied when using the p-MPS patterned substrates by repetitive trial and error until satisfactory films were produced, as judged by appearance under the microscope, and diffraction capabilities when place in the path of the laser. For example, higher monomer concentrations electropolymerized more quickly, requiring less scans before overpolymerization of the films occurred, evidenced by polymer growth over the p-MPS film regions. Lower concentrations at lower scan rates with more sweeps were found to produce superior films. Also, sweeping too far negative of the second ligand reduction potential facilitated films whose rapid growth was harder to control, and often resulted in more brittle films.

Even with the above stated baseline set of parameters, exact reproducibility was difficult to attain and resulted in a low success rate of film production. For example, for a set of 10 p-MPS slides prepared in an identical manner, adhering in all cases to the best set of electropolymerization conditions, on average, 3 polymerized films would be judged acceptable for diffraction studies, and even these possessed film morphology which were not homogenous throughout the film. The low rate of usable films, and the non-uniform film growth is most likely associated with the thickness and appearance of the p-MPS film, which forms the template for where polymer can be grown. Because the quality of the p-MPS film is judged by the contrast between "clean" electrode and film, how clean these exposed areas actually are from film to film is unknown and arbitrarily determined by microscopic visualization. For example, two p-MPS films which are prepared in the same manner and electropolymerized in the presence of a monomer solution following the same set of circumstances will not, with a high probability give two usable films because of the differences in their p-MPS films.

An additional problem is knowing when to stop sweeping the potential. This again is trial and error. In homogenous film growth, watching the quality of the reductive cyclic voltammogram and its current increase is instructive as to how well the film is growing. However, in grating films on p-MPS patterned ITO electrodes, watching the waves like those in Figures 1.21 and 1.22 does not allow for absolute assurance as to the extent of the polymerization, i.e. knowing the difference between when the growing polymer has filled the gaps between the p-MPS, and when the two polymerized regions begin to grow together. Following the growth of the waves is only an arbitrary indicator that polymer is indeed growing. Even with strict adherence to p-MPS film preparation, i.e. solution concentration, spin coating volume, rate and length, exposure and development, two films electropolymerized using the same conditions may or may not yield films which are suitable for diffraction studies. The ambiguous nature of knowing when to stop sweeping and its effects on film homogeneity are problems associated with the PL-EP technique and contributes significantly to its low success rate of usable films.

Instrumentation and Apparatus

Optical micrographs were photographed using a Nikon Optiphot-POL microscope set in transmission mode, equipped with an Nikon F4s 35 mm SLR camera. Scanning electron microscope images were obtained on a Jeol JSM-6400 series microscope.

Profilometry measurements of the film's thickness were measured using a Sloan Dektak II model profilometer with a 12 µm stylus.

Electrochemical data were obtained using a BAS CV-27 potentiostat whose potential was controlled and current monitored by interface to a Maclab /4e 4-channel analog-to-digital converter (ADInstruments) and processed on a Macintosh Centris 610 computer.

Spectroelectrochemical experiments were performed by mounting the Teflon electrochemical cell in Figure 1.54 holding the patterned electrode in a Hewlett-Packard 8452A diode array UV-visible spectrophotometer. The potential was controlled by the above described potentiostat and swept at a 9.0 mV/s rate, and spectra were recorded every 100 mV through one cycle of the potential region of interest. These spectra are then subtracted from the spectrum at 0.0 V to produce difference files whose plots are illustrated in Figures 1.30-33.

Optical switching data was collected using the apparatus shown schematically in Figure 1.34. The output of a 2 mW stabilized Synchrolase 100 He-Ne laser(Aerotech) is focused through a homemade Teflon electrochemical cell in which the ITO electrode patterned with the redox polymer is affixed. For all experiments, the cell is Ar degassed for 15 min prior to mounting in the path of the laser. Once mounted, the position of the cell window was adjusted in attempt to find the region of the grating film which gave the most intense diffracted signal. The potential of the cell is controlled by the above potentiostat interfaced to the A/D converter. The undiffracted and diffracted beams are collected by silicon photodiodes (Motorola MRD500) housed in aluminum compartments which are temperature controlled by a circulating water bath (Lauda) set at 25°C, and self-powered by 4 AA size batteries wired in series. The 633 nm wavelength output of the He-Ne laser is isolated by placing an appropriate interference filter in front of the diode. To ensure operation in the linear region of the diodes, a combination of optical diffusers and or neutral density filters were used to attenuate the beam before collection by the photodiode. Appendix B describes the linearity and stability tests performed on the laser and the photodiodes to ensure the system met specifications. The outputs of each of the photodiodes are also connected to the A/D converter, allowing for real time visualization of all 4 sets of data during acquisition.

Before electrochemical switching of the redox potential of the patterned electrode, a measurement of the initial diffraction efficiency was taken. This was performed by reading the intensity of the undiffracted beam at the photodiode, using two 25% transmittance neutral density filters to ensure operation in the linear region of the photodiode (Appendix B), then aligning the *same* photodiode in the path of the diffracted beam, (also using the same combination of ND filters) and reading its intensity. The initial diffraction efficiency, DE_o, is calculated by the ratio of the diffracted intensity to the undiffracted intensity measurements.

CHAPTER 2

TEMPERATURE DEPENDENT LUMINESCENCE PROPERTIES OF TWO NOVEL HETEROLEPTIC RUTHENIUM POLYPYRIDINE COMPLEXES

Background

Luminescent objects are things which can emit light. In chemistry, there are many examples of molecules whose luminescent properties make them interesting for study. A very important topic to address is the relevance of chemical structure to luminescence ability, i.e., what are the structural differences which allow one compound to luminesce while another does not, and how can luminescence be affected by synthetically modifying chemical structure? If scientists can find the answers to these questions, this knowledge will help them create new luminescent compounds and materials with strict control on how this light is emitted. Why is this important? Luminescent materials have many potential real-world applications, from street signs which are easier to see at night to luminescent based biomedical sensors which can be designed to monitor the chemical levels in the body by changes in light intensities.[78,79] None of these commercial applications can be realized, however, without first fully understanding how luminescence is initiated, and thus, how it can be controlled and utilized.

When a molecule luminesces, the release of light corresponds to a release of energy in the form of a photon. In order to release this energy, it first must acquire it from the sun or a light source such as a laser. Molecules which absorb light are called chromophores and this absorption creates a higher energy state of the molecule called the excited state. The excited state is more unstable than the previous, so-called ground state, and will quickly release the extra energy, relaxing to the ground state. The duration of the excited state, the lifetime, becomes an important issue because if the extra energy is to be utilized to perform further chemical processes, it must be done before relaxation, or wasting of this inputted energy occurs.

An excited molecule can release its energy by several different deactivation processes, shown in Figure 2.1. It may disappear and be *photochemically* converted into a new product (i); it may react with a different molecule which acts as an energy drain and be *quenched* (ii); it may deactivate in a radiationless manner by releasing heat (iii), or it may relax by emitting a photon thus luminescing (iv). The problem for chemists is that all of these deactivation processes compete for the same absorbed energy contained in the excited state. Thus, if one's interest in using the excited state is to initiate further photochemistry, the lifetime of the excited state needs to be long enough to react with another chemical species before the energy is wasted by thermal or luminescent relaxation. If rather the intent is to utilize the compound's luminescence, the heat-releasing or non-radiative process must be minimized, and steps must be taken to guard against energy quenching by another species. The challenge then, is to chemically design a compound which is engineered to utilize the excited state energy to produce the desired effect.

There are many types of compounds that luminesce and many of them have familiar applications. Fluorescein, an organic lumiphore, is added to antifreeze to give its distinctive green color, allowing for easy detection under an ultraviolet lamp if it is accidentally ingested. Rhodamine, a red colored organic dye, is used in paints applied to fire engines to improve their visibility. The names and structures of other common organic lumiphores are shown in Figure 2.2. Another class of lumiphores are the complexes containing transition metal ions such as Ru, Os, Re, and Rh. These compounds are becoming increasing popular for use in luminescent applications because of several advantages they offer over their organic counterparts. Their excited state lifetimes are generally longer, often lasting for several microseconds compared to lifetimes of organic lumiphores which are a few nanoseconds. Since they last longer, these transient states are easier to detect. Another attractive feature of this class of compounds is that their

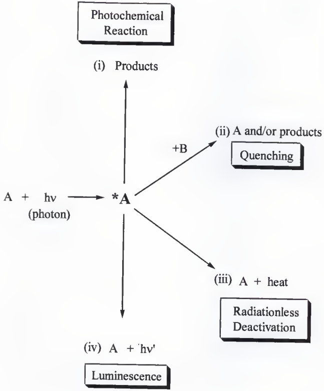

Figure 2.1. Possible deactivation pathways for an excited molecule, *A. (from ref 37.)

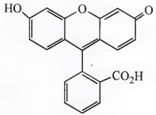

Fluorescein

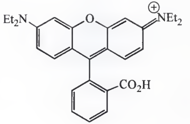

Rhodamine B

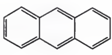

Anthracene

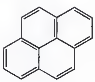

Pyrene

Figure 2.2. Structures and names of various organic lumiphores

chemical structure is easily modified to more accurately control their luminescent properties. This will be discussed later in greater detail.

One transition metal complex in particular, $Ru(bpy)_3^{2+}$ (bpy = 2,2'-bipyridine) has been the focus of decades of research.[37] This complex's relatively long-lived excited state, chemical stability, redox properties and luminescence emission, as well as the tuning of these properties by structural modification has led to a myriad of derivatives contributing a wealth of knowledge about their photochemical and photophysical tendencies. In order to molecularly engineer the structure of Ru polypyridyl complexes, it is important to first examine the molecular orbital structure of these compounds, and how structure may affect a complex's absorption and emission properties.

Absorption of a photon of light by a chromophore involves promotion of an electron into a higher energy state. In terms of spin multiplicities, this involves a ground state (Figure 2.3, S_0) to singlet excited state (S_1) transition, where electrons remain paired and the singlet spin multiplicity is preserved. Relaxation to the ground state may occur by any of the deactivation processes previously illustrated in Figure 2.1, but for the purpose of this chapter, the discussion will focus on the relationship between radiative and non-radiative modes of decay. From the singlet state, relaxation may occur by emission of a photon, called fluorescence, or via loss of heat. (Figure 2.3a, k_f and k_{nr} respectively). (Often times the excited single electron will undergo a rapid inversion of its spin state, called intersystem crossing (k_{isc}), into a lower energy triplet state (T_1)). Deactivation from the triplet state may also occur by either radiative or non-radiative means. Radiative decay from the triplet state is called phosphorescence (Figure 2.3c, k_p), and is characterized by longer lifetimes on the millisecond timescale.

The excited decay processes of Ru (II) polypyridine complexes described by the above spectroscopic states can be related to the complexes' molecular orbital diagrams. Ru is a d^6 metal with partially filled d orbitals, and Ru complexes of the formula MX_6 have octahedral symmetry. The bonding scheme involves d metal orbitals, σ-donor orbitals

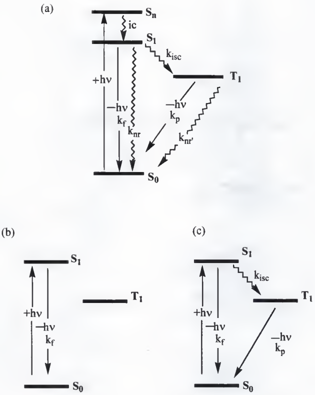

Figure 2.3 (a) Jablonski diagram summarizing excited-state processes which may occur for a chromophore; (b) Electronic spin configuration for excited singlet state before fluorescence; (c) Electronic spin configuration for excited triplet state before phosphorescence.

located on the nitrogen atoms, and π-donor and π*-acceptor orbitals on the aromatic bpy rings. The energetic ordering of these orbitals is illustrated in Figure 2.4. The absorption of a photon of light is a process involving a promotion of an electron from the highest occupied molecular orbital (HOMO), to the lowest energy unoccupied molecular orbital, (LUMO) whose identity largely depends on the ordering of energies of the ligand and metal orbitals. It is the energetic placement of the LUMO which dictates the luminescence properties of these types of transition metal complexes. Notice from Figure 2.4 that the five d metal orbitals are split into three degenerate t orbitals and a higher energy doubly degenerate e level. The energy splitting between these d orbitals, Δ, is determined by the ligand environment surrounding the central metal ion, called the crystal or ligand field. This parameter, Δ, is critical in determining the identity and placement of the LUMO. Δ is defined by a ligand's electron donor and acceptor capabilities, i.e., how well it forms bonds. In weak ligand fields, there is poor overlap of the electron densities between the metal and ligand orbitals. This results in a smaller value of Δ, and for Ru polypyridyl complexes, the degenerate d(e) orbitals become the LUMO for subsequent electronic transitions (Figure 2.4b). If Δ is large, a strong field case, orbital overlap is much improved, pushing the e orbitals higher than the π* orbitals of the ligands, (Figure 2.4c) making these π* orbitals the LUMO. This is the case in Ru polypyridyl complexes since polypyridyl ligands are usually strong field ligands; they are good σ-donators and their empty π* orbitals aid in accepting electron density by stabilizing it through delocalization in their aromatic rings.

Therefore, based on these arguments, the ligand splitting energy, Δ, determines the nature of the HOMO -LUMO interaction. In the weak field case, promotion of an electron from a d(t) to a d(e) orbital (hence referred to as a d-d transition) places an electron in an anti-bonding orbital, often resulting in destabilization of the complex, which generally leads to energy deactivation by ligand loss (Figure 2.1(i)) rather than luminescence. In Ru polypyridine complexes, a strong field situation, absorption of a

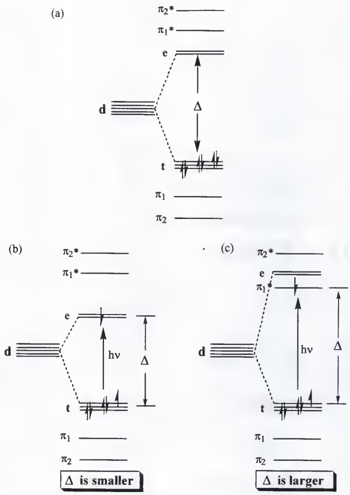

Figure 2.4. (a) General molecular orbital diagram for molecules of O_h type symmetry; (b) Weak ligand field splitting of d orbitals; (c) strong ligand field splitting of d orbitals.

photon of light involves shuttling the excited electron from the metal orbital into a ligand π^* orbital of singlet character. This type of transition is called metal-to-ligand charge transfer (MLCT). Rapid intersystem crossing occurs to a triplet MLCT state, which then deactivates by luminescence.[80, 81] Such deactivation would technically define phosphorescence, but is commonly referred to as luminescence due to spin-orbit coupling of the ^{1}MLCT and ^{3}MLCT states, resulting in emission lifetimes which are much faster and intermediate between fluorescence and phosphorescence decays. Further descriptions of the radiative decay of Ru polypyridine complexes will be referred to as luminescence rather than phosphorescence.

The lowest energy emitting state in Ru polypyridyl complexes, as described above, is ^{3}MLCT in nature, corresponding to relaxation from a bipyridine π^* orbital back to the metal d orbital. If either of these orbital energy levels is manipulated, the redox properties and luminescence energy of the complex will be shifted as well. The versatility of these complexes lies in the way that this energy can be finely tuned by functionalizing the bipyridine rings with donor or acceptor groups, commonly attached in the 4 and/or 4' positions. Attaching an electron withdrawing group will make the complex easier to reduce by lowering the energy of the π^* orbital, and subsequently red-shifting the wavelength of emission. An electron donating group will have the opposite effect, resulting in a complex which is easier to oxidize by raising the π^* orbital and thus blue-shifting the emission. This technique can prove to be quite useful in obtaining a complex whose energy levels must be distinctly defined for a desired redox or luminescent effect.

Luminescence applications

By understanding the ordering of the orbital energies, chemists have been able to design Ru polypyridyl complexes for unique applications involving their luminescence. Barton and Hartshorn[82] have synthesized several novel Ru polypyridine complexes which can molecularly recognize DNA. Two of these complexes are shown in Figure 2.5. These two complexes, $[Ru(bpy)_2(DPPZ)]^{2+}$ and $[Ru(phen)_2(DPPZ)]^{2+}$ (phen = 1,10-phenanthroline; DPPZ = dipyrido[3,2-a:2',3'c]phenazine) have no emission in aqueous solutions. If DNA is added to an aqueous solution containing one of these complexes, the solution will luminesce very brightly. They determined that the DPPZ ligand of the complex can bind to the base pairs on the DNA strands, effectively "turning on" the complex's luminescence. The interest in this field is the possible utilization of these complexes in biomedical diagnostic and therapeutic agents.[83, 84]

Another interesting application of the luminescence from Ru complexes involves devices for oxygen sensing. Demas and co-workers[85] have applied the knowledge that Ru luminescence is quenched by O_2 to develop devices that may be able to detect its presence or absence. In one illustrative experiment[86], $Ru(dpph)_3^{2+}$ (dpph = 4,7-diphenyl-1,10-phenanthroline) was dissolved in dichloromethane and the solution mixed into a silicone based sealant. After curing the Ru doped film, the film was placed in a fluorimeter to monitor its emission. In a normal atmosphere, there was little detectable luminescence. However, upon feeding nitrogen gas through the chamber, the intensity of emission greatly increased, as shown in Figure 2.6(a). As the N_2 stream was turned off, the emission intensity decreased, returning to its initial state. The sensitivity and versatility of these sensors was shown in an additional experiment whose results are illustrated in Figure 2.6(b). In this experiment, the device was breathed over, changing the immediate environment surrounding the sensor film between O_2 rich (inhalation) and CO_2

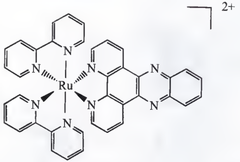

$[Ru(bpy)_2(DPPZ)]^{2+}$

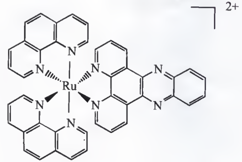

$[Ru(phen)_2(DPPZ)]^{2+}$

Figure 2.5. Two Ru polypyridyl complexes used as DNA sensors. From ref. 82.

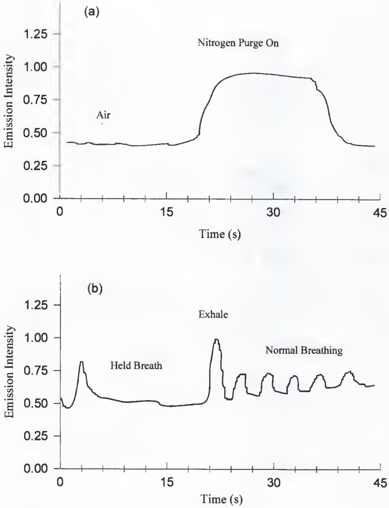

Figure 2.6. Application of fluorescence characteristics of $Ru(dpph)_3^{2+}$ doped polymer films as oxygen sensing devices. Reproduced from ref. 86.

(exhalation). The luminescence response followed accordingly, decreasing in high O_2 saturation and increasing upon exhaling.

The emission from Ru polypyridyl complexes is also temperature dependent. Because of this phenomenon, as will be explained below, these complexes are good choices for temperature sensing devices. One such application involves the mapping of the temperature of a surface. By coating an object with a luminescent complex, detected emission intensity changes are correlated to actual surface temperature. The recent advances in CCD (Charge Coupled Device) technology[87] has seen an enormous growth in imaging applications[88, 89] using these complexes as temperature sensitive coatings. CCD cameras which are the basis for emission detection, offer many advantages. They afford the ability to measure very small changes in emission with high resolution in a non-invasive manner. This non-invasive approach to imaging is important because it doesn't change the surface features being measured, as can occur when thermocouples are attached. Also, the camera can capture a real-time image of the temperature response of the total surface, whereas using thermocouples only allows data to be sampled where they have been affixed.

In one such experiment performed at the University of Florida Department of Aerospace Engineering,[90] the changes in emission intensity as a function of temperature from a $Ru(bpy)_3^{2+}$ painted steel surface were imaged. The apparatus used to record such measurements, pictured in Figure 2.7, uses a halogen lamp as an excitation source, and a 14-bit CCD camera to monitor emission. The painted substrate was mounted between two plates: a heat source (heater strips) and a heat drain (chilled water), to create a temperature gradient. A contour image of the substrate, shown in Figure 2.8, reveals the temperature dependency of the emission. At the hot end of the substrate, intensity was lower while at the cooler end, the intensity was much brighter.

The nature of the temperature dependence on emission intensity for Ru polypyridyl complexes like that illustrated in Figure 2.8 results from the competition of several

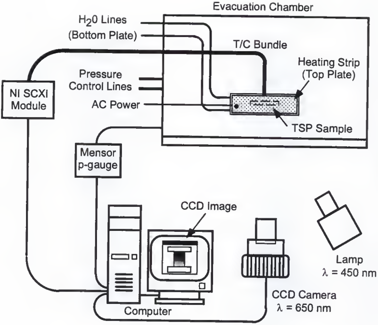

Figure 2.7. Experimental apparatus for imaging temperature sensitive coated substrates. (from ref. 90.)

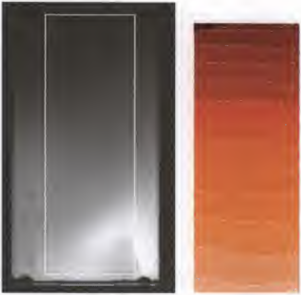

Figure 2.8. CCD image (left) of $Ru(bpy)_3Cl_2$ coated substrate and temperature contour (40 - 80 °C) Ref. 90.

deactivation modes which can quench emission. The quantum yield for luminescence, Φ_L, is an important quantitative measurement of the luminescence efficiency of lumiphores which indicates the number of photons emitted to the number of photons absorbed. Most transition metal complexes have Φ_L's in the range of 0.04-0.2, which is adequate for their use in temperature sensitive applications.[91] Φ_L for Ru (II) polypyridyl complexes is determined by the following expression which is derived from the competing nature of the rates of radiative decay, non-radiative decay, and decay from a thermally activated d-d transition which is non-luminescent:[92]

$$\Phi_L = \frac{k_r}{k_r + k_{nr} + k_{ic}} \qquad 2.1$$

where k_{ic} represents the rate of internal conversion to the non-luminescent ^{3}d-d state. For a constant illumination intensity, the luminescence intensity, I_L, is proportional to Φ_L. Radiative decay (k_r) is dictated by spin and orbital symmetry factors[93] and is only weakly temperature dependent. However, k_{ic} generally increases with increasing temperature, thus affecting Φ_L and therefore I_L. Modifying Eq 2.1 to reflect this significance yields the following expression (the temperature dependency of non-radiative decay is much weaker than k_{ic} and can be neglected)[94]:

$$I_L(T) \propto \Phi_L(T) = \frac{k_r}{k_r + k_{nr} + k_{ic}(T)} \qquad 2.2$$

where $I_L(T)$, $\Phi_L(T)$, and $k_{ic}(T)$ are notated to illustrate the temperature dependence of these variables. Because of its temperature dependence, $k_{ic}(T)$ can be expressed as an Arrhenius term:

$$k_{ic}(T) = k_{ic}^{o} \exp\left(\frac{-E_a}{RT}\right) \qquad 2.3$$

Figure 2.9(a) illustrates the temperature dependence of the Φ_L for a luminescent compound whose emission behavior is described by Eq 2.2. Notice that there are three distinct regions where the luminescence behaves differently: the temperature independent region (I), where there is little or no change in the intensity vs. change in temperature ($\delta I/\delta T$), a temperature dependent region (II), where the changes are greater than zero, and a region where there is little or no luminescence detected (III). These areas are determined from the competition between radiative decay and internal conversion. For practical temperature sensing applications, the sensitivity of the luminescent species, e.g., how well the emission intensity changes with small changes in temperature, is determined by $\delta I/\delta T$. In region I, one can monitor high luminescence intensities, but because of little temperature change, this region reveals little about the actual temperature of the object being imaged. At higher ratios, where the magnitude of k_r is more similar to that of k_{ic}, there is better sensing capability. This is evidenced by the higher contrast of the imaged intensities, like that for $Ru(bpy)_3^{2+}$ in Figure 2.8. The ability to produce higher contrast in the emission intensities is crucial for detecting very small changes in temperature. Thus a complex that is considered a good choice for temperature sensing will have a large $\delta I/\delta T$ in the temperature area of interest. In this study, we will use $\delta I/\delta T$ as a indicator of a complex's sensing potential in the 100-298 K range by calculating the slope of the synthesized complex's temperature versus emission intensity calibration plots like those in Figure 2.9.

The complex used in the above experiment, $Ru(bpy)_3^{2+}$, luminesces at room temperature, and its intensity increases to a maximum at ≈250K (Figure 2.9(b)) below which it remains unchanged with decreasing temperature. Luminescence increases as temperature decreases as determined by Eq. 2.2, where the temperature dependent term,

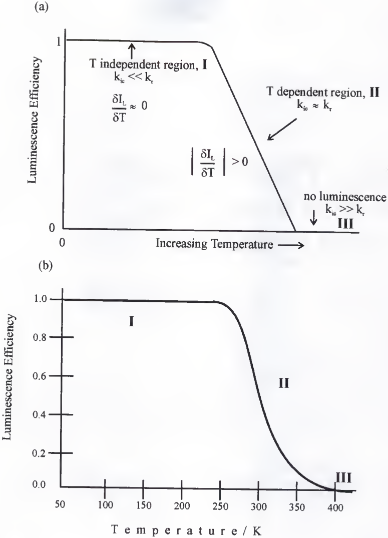

Figure 2.9. (a) Temperature dependence of the luminescence efficiency of a sample fluorophore, (b) Temperature dependence of $Ru(bpy)_3^{2+}$ luminescence efficiency.

k_{ic}, is smaller, thus increasing the value of I_L. As the temperature is increased above ambient, k_{ic} increases, resulting in a intensity decrease like that shown in Figure 2.8 approaching 80° C. Since the decay of luminescence, k_r, occurs from the lowest energy MLCT state, the energy difference between the emitting state and the thermally activated non-luminescent state becomes very important.

The observed temperature dependencies and the roles of k_{ic} and k_r are better understood by an illustrative examination of the energies of the two states involved in this process, shown in Figure 2.10(a). In $Ru(bpy)_3^{2+}$, the lowest energy HOMO-LUMO interaction results in the formation of a ^{1}MLCT state. After intersystem crossing to the ^{3}MLCT state, deactivation by luminescence (at room temperature) usually occurs. However, notice the figure shows that the thermally activated ^{3}d-d energy state is only slightly higher in energy than the ^{3}MLCT state, separated by an activation energy barrier, $\Delta E'$. As the temperature is raised (Figure 2.10(b)), enough thermal energy is present to overcome $\Delta E'$, and internal conversion to the non-luminescent ^{3}d-d state occurs. Thus, k_{ic} is greater than k_r and no emission is detected (Region III, Figure 2.9(b)). As discussed above in the case of ^{3}d-d deactivations, this may result in the loss of a bpy ligand from the complex. The proximity of the ^{3}d-d state to the emitting ^{3}MLCT state in $Ru(bpy)_3^{2+}$ makes it a poor choice for temperature sensing at very warm temperatures. Also, although at low temperature its quantum yield for luminescence (0.4) is high, and its emission lifetime (5 μs), τ is long, there is no change in its response[92] (Region I, Fig. 2.9b). Thus the optimal region for using the luminescence response of $Ru(bpy)_3^{2+}$ in temperature sensitive applications (Region II) is between 250 and 330K.

One Ru polypyridyl complex which has received much attention due to its peculiar luminescence properties is $Ru(trpy)_2^{2+}$, (Rutrpy, where trpy is 2,2':6',2''terpyridine).[95, 96, 97] As seen in Figure 2.11, trpy is a tridentate ligand, meaning it binds to Ru in three places. At room temperature Rutrpy has a lifetime of 250 ps and thus no detectable emission.[98] But at temperatures below 150 K, the complex luminesces quite intensely,

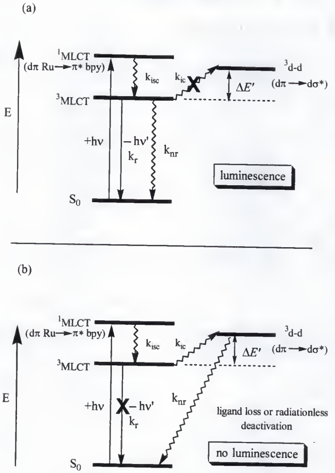

Figure 2.10. State diagrams depicting importance of k_{ic} as controller of luminescence. (a) luminescence of $Ru(bpy)_3^{2+}$ at room temperature; (b) $Ru(bpy)_3^{2+}$ at elevated temperature, showing lack of emission due to thermally activated ^{3}d-d state.

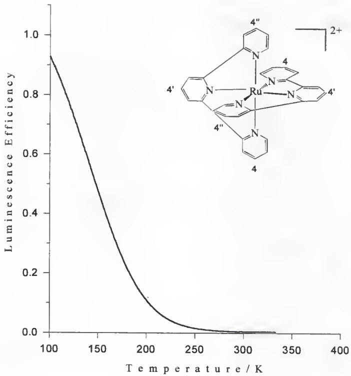

Figure 2.11. Structure and emission vs. temperature profile of Rutrpy.

shown by the luminescence vs. temperature profile[99] in Figure 2.11. The reason for this can be extracted from the state diagrams of Rutrpy and $Ru(bpy)_3^{2+}$, shown for comparison in Figure 2.12. The ^{3}d-d state of Rutrpy is lower in energy than it is in $Ru(bpy)_3^{2+}$. At room temperature, $\Delta E'$ is overcome, exciting the electron in the ^{3}MLCT state to the ^{3}d-d state and quenching luminescence. But as temperature decreases, k_{ic} also decreases, and emission from the ^{3}MLCT state is detected. (The temperature must however, be below 150 K before the radiative rate of decay, k_r can compete with k_{ic} and emission is detected.) The value of Δ is smaller in Rutrpy than in $Ru(bpy)_3^{2+}$. This is because trpy is a weaker field ligand than bpy. The orbital overlap between metal and trpy is much worse because of the severe distortion of the octahedral symmetry due to the strain induced in the tridentate ligand. The ligand wishes to remain planar, but because it bonds in three places, the "bite" angle at which the ligand bonds to the metal is strained. Because of this distortion, trpy is not only a poorer σ-donor than bpy, but also worse at accepting π electron density. This results in a smaller value of Δ, which ultimately reduces $\Delta E'$. From this discussion it is apparent that k_{ic} functions as a switch between the luminescent ^{3}MLCT state (the "on" position), and the non-luminescent ^{3}d-d state (the "off" position) shown in Figure 2.10, and that efforts to control the temperature dependence of the luminescence of Ru(II) polypyridine complexes should focus on slowing k_{ic} by tuning $\Delta E'$. This can be achieved by either raising the energy of the ^{3}d-d state by using stronger field ligands than trpy, thus increasing the ligand field splitting, Δ, or lowering the energy of the ^{3}MLCT emitting state by selecting a ligand with better π acceptor ability.

Several groups have attempted to make Rutrpy luminesce at higher temperatures by adjusting the energy barrier between ^{3}MLCT and ^{3}d-d states via synthetic modifications. These efforts have used three different synthetic strategies. The first is the introduction of different functional groups in the 4,4', and/or 4'' positions (Figure 2.13). McMillin [99] and Sauvage[100] have studied the effects of adding phenyl substituents to trpy ligands to create new Ru complexes based on modified trpy ligands such as those in Figure

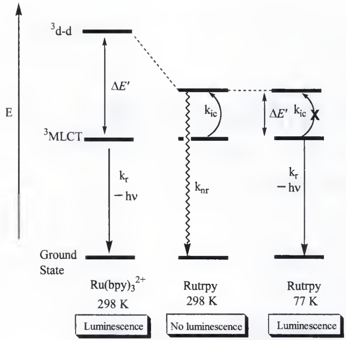

Figure 2.12. Relative energy ordering of the lowest triplet states and subsequent deactivation modes for $Ru(bpy)_3^{2+}$ and Rutrpy at room temperature and of Rutrpy at low temperature.

(a)

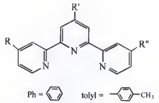

	R	R'	R"
trpy	H	H	H
dptrpy	H	Ph	Ph
tptrpy	Ph	Ph	Ph
ttrpy	H	tolyl	H

(b)

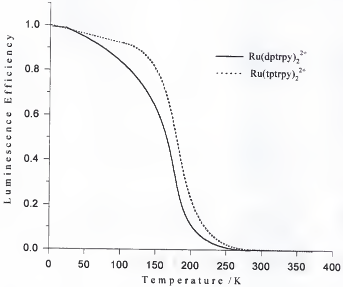

Figure 2.13. (a) Structures of modified trpy ligands; (b) emission profiles of $Ru(dptrpy)_2^{2+}$ and $Ru(tptrpy)_2^{2+}$. (from ref. 99)

2.13a. The luminescence versus temperature profiles in Figure 2.13b show that the temperature dependencies for Ru(dptrpy)$_2^{2+}$ and Ru(tptrpy)$_2^{2+}$ are shifted to higher temperatures as a result of greater phenyl substitution. From the figure, it is observed that Ru(tptrpy)$_2^{2+}$ has a small detectable room temperature emission, with a lifetime of $\approx$ 4 ns.[99] The investigators suggest that the energy of the π^* orbitals of the tptrpy is lower relative to trpy. This in turn widens the energy gap between the ^{3}MLCT and ^{3}d-d states, thus decreasing the contribution of k_{ic} to l_L in equation 2.2.

A second strategy to change the ligand environment of these complexes is to remove one of the trpy ligands and replace it with an altogether different ligand(s), thus changing the homoleptic complexes to heteroleptic, or mixed ones. These latter types are interesting for study because of the complexities that their electronic state manifolds present when determining the origin of emission. Complexes which have three different ligands instead of two aren't as well documented, but some examples using trpy do exist.[101, 61] Although tuning the temperature dependent emission properties of trpy complexes was not the primary motivation, Berger and McMillin synthesized the two heteroleptic Ru complexes shown in Figure 2.14 to determine the nature of the lowest excited state. They also indicated that the quantum yields for emission increased in comparison to Rutrpy due to the improved symmetry by removing one trpy and replacing it with two stronger field ligands.

A third strategy utilizes the previous two, forming heteroleptic complexes whose ligands are also functionalized. Maestri and co-workers[102] synthesized Ru complexes with two trpy ligands, but each ligand was functionalized at the 4' position with different electron donor and acceptor groups as illustrated in Figure 2.15a. Complexes with heteroleptic acceptor ligands showed increased room temperature emission quantum yields while those with heteroleptic donor ligands showed decreases in the quantum yields relative to Rutrpy. The same argument in terms of effects of the HOMO and LUMO orbitals in any particular case helps to explain this behavior. One final example of

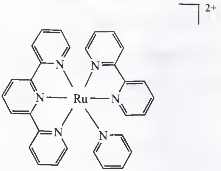

Ru(trpy)(bpy)(py)

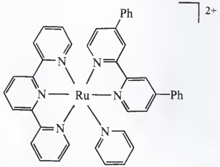

Ru(trpy)(4,4'-dph-bpy)(py)

Figure 2.14 Heteroleptic Ru trpy complexes.

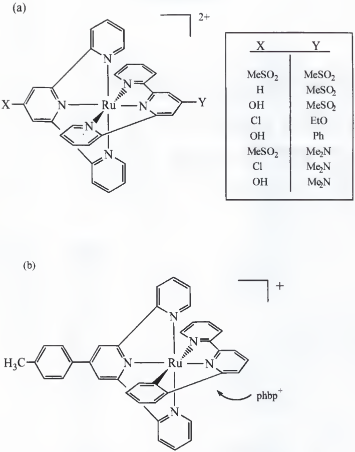

X	Y
MeSO$_2$	MeSO$_2$
H	MeSO$_2$
OH	MeSO$_2$
Cl	EtO
OH	Ph
MeSO$_2$	Me$_2$N
Cl	Me$_2$N
OH	Me$_2$N

Figure 2.15. (a) Substituted trpy complexes of Maestri; (b) Collin's Ru(ttrpy)(phbp)$^+$ complex.

combining functionalized trpy ligands and trpy ligand substitution is the work of Collin, et al.[103] describing the room temperature luminescence of the cyclometallated complex Ru(ttrpy)(phbp)$^+$ shown in Figure 2.15b. (phbp is the anion version of the C-N-N coordinating phbpH: 6-phenyl-2,2'-bipyridine). Because the phbp ligand is a tridentate ligand, the complex possesses similar symmetry to that seen in Rutrpy. Although room temperature emission was noticed, it was very weak. The authors comment that the emission is considerably red-shifted to ≈800 nm, indicating that the ^{3}MLCT band is much lower in energy, thus causing a dramatic increase in the non-radiative decay rate (loss of heat) as dictated by the energy gap law.[80]

Description of the Present Study

This chapter details the synthesis and photophysical characterization of new Ru (II) polypyridyl complexes whose emission properties are temperature dependent; these complexes may be useful as temperature sensors over broader temperature ranges (100 K-298 K). Our endeavors are based on the knowledge of the above studies, and understanding the synthetic manipulation of the complex's geometry and ligand field orbital energies, which can change a complex's emission properties. In order to be sensitive in the low temperature regime, the complexes have been based on mono-coordination of one of two tridentate ligands, trpy and *tris*(1-pyrazolyl)methane. Previous low temperature studies involving trpy substituted ruthenium complexes have been reported using *bis*-trpy coordination. Our strategy described in this chapter has sought to widen the range of temperature dependent emission, and its sensitivity over this range by synthesizing Ru complexes with one tridentate ligand thereby improving symmetry. By judiciously choosing the ligands which may occupy the three vacant Ru coordination spots, we have increased the temperature range and sensitivity at which emission can be detected. The successful syntheses of these two new heteroleptic Ru polypyridyl complexes, Rutdp, and Rutpm [Rutdp = Ru(2,2':6',2''-terpyridine)(4,7-diphenyl-1,10-phenanthroline)(pyridine) and Rutpm = Ru(tris(1-pyrazolyl)methane)(4,7-diphenyl-1,10-phenanthroline)(pyridine), Figure 2.16], and the strategy for their syntheses are described, as well as the important results testing their temperature sensitive emission properties in solution, low temperature glasses, and incorporated into a polymeric binder. The latter studies suggest that these complexes can be applied in luminescent coatings which may ultimately be used for luminescence imaging of temperature distributions.

Studies of the Temperature Dependence of the Luminescence of Rutdp and Rutpm

As mentioned above, the deviation from octahedral symmetry in Rutrpy is caused by two orthogonal trpy ligands which are planar. Because of the tridentate nature of the ligand, the central Ru metal atom binds to the three N atoms at angles less than the octahedral ideal of 90°. This geometric distortion is observed in other *bis*-trpy complexes of Ru[104, 105] and Cr^{3+} [106], and mono trpy complexes of Ga,[107] Zn,[108] Sn.[109] The distortion induces strain in the complex, resulting in poor σ- and π- type overlap between metal and ligand orbitals. Thus trpy is a weaker field ligand than bpy, inducing a ligand field splitting, Δ, which is decreased relative to $Ru(bpy)_3^{2+}$. This effect leads to the temperature dependence of its luminescence detailed above. Our motivation in the synthetic design of the two new heteroleptic complexes reported in this chapter attempts to control the temperature dependent term in Equation 2.2, k_{ic}. As outlined in the introduction, controlling the rate of internal conversion is a function of the activation barrier, $\Delta E'$ (Figure 2.10), and efforts to limit k_{ic} should focus on adjusting the energy levels of either the ^{3}MLCT or ^{3}d-d states. Our approach attempts to modulate both of these states. First, the removal of one of the trpy ligands could alleviate some symmetry-induced strain in the complex, and occupation of the vacant coordination sites by stronger field ligands could help to increase the energy of the ^{3}d-d state by increasing Δ. This should help in raising

(a)

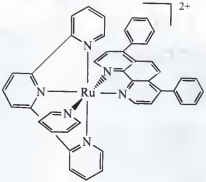

Rutdp

(b)

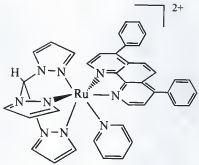

Rutpm

Figure 2.16. Structures of Ru heteroleptic complexes in present study.

the temperature at which luminescence is detected, but should also maintain the low temperature end by retaining one weaker field ligand (trpy or tpm). The diphenylphenanthroline (dpph) and pyridine (py) ligands which have filled trpy's vacated coordination sites are both stronger field ligands. The dpph ligand was selected in particular, because its extended π-conjugation makes it an excellent chromophoric ligand in Ru complexes like $Ru(dpph)_3^{2+}$. This complex, used by Demas as an oxygen sensor detailed above, has an MLCT absorption possessing a very high extinction coefficient, which is an indicator of absorption strength. Also, the extended π system should aid in delocalization, making dpph a better π acceptor ligand. Complexes incorporating dpph should therefore help to stabilize the energy of the ^{3}MLCT emitting state (explicitly the π* orbital), ultimately increasing $\Delta E'$.

The second heteroleptic complex, Rutpm, is different from Rutdp only in that its tridentate ligand has been changed from trpy to *tris*-(1-pyrazolyl)methane (tpm). This ligand has been widely used as a tripodal nitrogen donor ligand in organometallic complexes of Pd,[110,111] but its use as a ligand in Ru complexes is far less extensive.[112,113] Of the known Ru complexes containing tpm, those whose photophysical properties have been investigated are limited.[114,115] Like trpy, tpm is a weaker field ligand than bpy, and Ru (II) complexes of tpm possess luminescence properties which are temperature dependent.[114] The interesting feature of the tpm ligand however, is that it is a facially coordinating ligand, rather than the planar, meridional coordination adopted by the trpy ligand. Although this helps to alleviate the geometric strain observed in trpy, its structure, with three pyrazolyl-linked molecules, is less conjugated, making it a poorer acceptor of electron density when coordinated to Ru. These interesting structural differences between Rutdp and Rutpm (Figure 2.16) make them interesting choices in investigating their temperature dependent luminescence.

Synthesis and Crystal Structure Determination

The syntheses of the two heteroleptic complexes are outlined in Figures 2.17 and 2.18, and are described in greater detail in the experimental section at the end of this chapter. Forming complexes of Ru (II) containing three different ligands is a straight forward process involving the stepwise addition of the three ligands to ruthenium (III) trichloride. The tridentate ligand is attached first, followed by the bidentate dpph ligand, followed lastly by the addition of pyridine. The final step is accomplished by addition of silver trifluoromethanesulfonate, which forms an intermediate triflato complex, resulting in the precipitation of AgCl. The triflato ligand is an excellent leaving group and is readily replaced by excess pyridine present in the reaction. The complexes are isolated as the hexafluorophosphate salt by metathesis with NH_4PF_6, and purified by column chromatography.

Crystals of Rutdp and the precursor to Rutpm, $Ru(tpm)(dpph)(Cl)^+$ were successfully grown, resulting in the determination of chemical structure by X-ray diffraction. The crystal structures for these complexes are shown in Figures 2.19 and 2.20. The trpy ligand adopts the meridional coordination (Figure 2.19) while the tpm is coordinated facially (Figure 2.20). Further examination of the structure will be presented in a later section. Although satisfactory crystals of the final Rutpm complex could not be grown, the precursor complex gives the symmetry expected for Rutpm by substitution of the chloride ligand for pyridine.

The temperature dependent luminescence properties were studied in solution, in low temperature glasses and in a polyurethane polymeric binder supported on aluminum substrates. The coatings were applied by airbrushing them onto white primer-coated aluminum substrates. Refer to the experimental section for a thorough detail of the coating formulation and airbrush application.

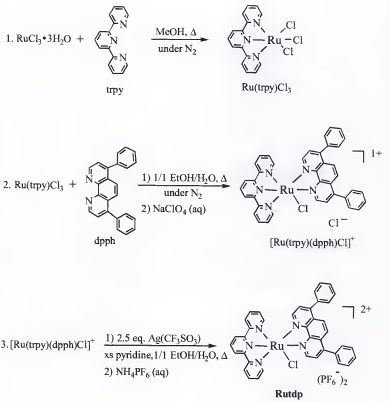

Figure 2.17. Synthetic scheme for Rutdp complex.

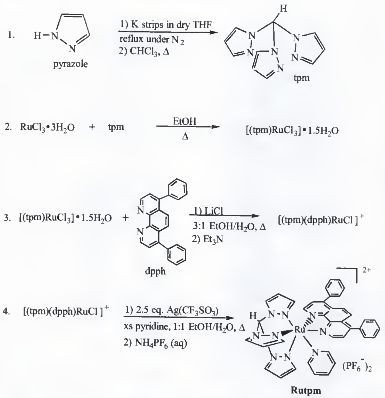

Figure 2.18. Synthetic scheme for Rutpm complex.

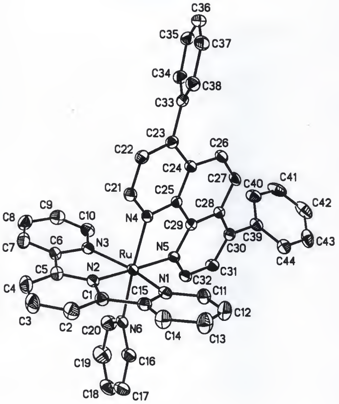

Figure 2.19. X-ray crystal structure of Rutdp.

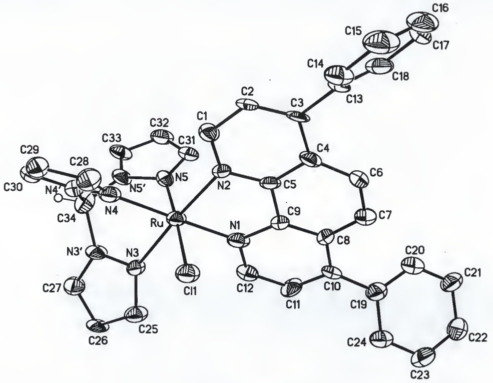

Figure 2.20. X-ray crystal structure of [Ru(tpm)(dpph)Cl]$^+$.

Photophysical Characterization of Rutdp and Rutpm Solutions and Coatings

UV-visible absorption spectroscopy

The UV-visible absorption data for equimolar concentrations of Rutdp and Rutpm are shown in Figure 2.21, overlaid with the spectrum of Rutrpy for comparison. The absorption maxima, assignments and molar absorptivities, ε, for all three complexes are listed in Table 2.1. The spectrum for Rutrpy shows the lowest energy MLCT $d\pi$ (Ru) → π^* (trpy) transition at 474 nm with ε equal to 10,662 (M^{-1} cm^{-1}). Addition of the dpph ligand in Rutdp results in a higher ε of 14,128 (M^{-1} cm^{-1}) and a second MLCT $d\pi$ (Ru) → π^* (dpph) transition at 416 nm. The appearance of two closely spaced MLCT absorptions for mixed Ru (II) polypyridyl ligand complexes has been documented previously.[116] In Rutpm, the dpph ligand also leads to the higher intensity absorptions of the $d\pi$ (Ru) → π^* (dpph) and $d\pi$ (Ru) → π^* (tpm) transitions at 416 and 356 nm, respectively.

Steady-state and time resolved luminescence

Room temperature and low temperature studies in solution. $Ru(trpy)_2Cl_2$ does not give detectable emission in solution at room temperature.[117] Figure 2.22 reveals that at room temperature, solutions of Rutdp or Rutpm in CH_3CN do give detectable, albeit very weak broad-band emission, whose emission maxima are both centered at approximately 650 nm. By taking the area underneath the respective emission bands, and using Eq. 2.5 (in experimental section), Φ_L values of $< 4 \times 10^{-3}$ (Table 2.2) were calculated for both solutions. For comparison, $Ru(bpy)_3^{2+}$, considered a good room temperature emitter, has a Φ_L approximately 10 times greater.[37]

Rutdp and Rutpm solutions were made in 4:1 EtOH/MeOH which produced transparent glasses at low temperature allowing investigation of their emission properties. Figures 2.23 and 2.24 illustrate the overlaid emission spectra of Rutdp and Rutpm glasses, respectively, taken as the temperature was increased. The emission maxima at 610 and 625 nm for Rutpm and Rutdp, respectively is ^{3}MLCT in nature, and is typical of Ru

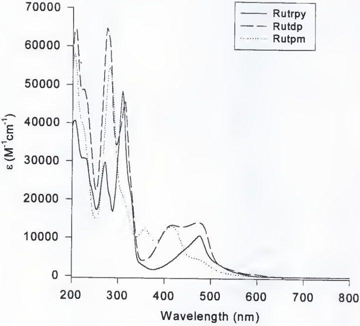

Figure 2.21. UV-visible absorption spectra of Rutrpy, Rutdp, and Rutpm complexes. (All solutions 2 x 10^{-5} M in CH_3CN.)

Table 2.1. UV-visible absorption characteristics of Rutdp, Rutpm, and related complexes.

Complex[a]	λ_{max} (nm)	ε (M^{-1} cm^{-1})	Assignment
Rutdp[b]	476	14 128	MLCT (Ru→ trpy)
	416	13 389	MLCT (Ru→ dpph)
	314	45 548	$\pi \rightarrow \pi^*$ (trpy)
	274	64 702	$\pi \rightarrow \pi^*$ (dpph)
	226	48 632	$\pi \rightarrow \pi^*$ (trpy, dpph)
	208	64 277	$\pi \rightarrow \pi^*$ (trpy, dpph)
Rutpm[b]	476 (sh)	4550	MLCT (Ru→ dpph)
	416	13 107	MLCT (Ru→ dpph)
	356	12 282	MLCT (Ru→ tpm)
	278	53 485	$\pi \rightarrow \pi^*$ (dpph)
	224	38 970	$\pi \rightarrow \pi^*$ (tpm, dpph)
	206	57 771	$\pi \rightarrow \pi^*$ (tpm, dpph)
Rutrpy[b]	474	10 662	MLCT (Ru→ trpy)
	308	48 345	All $\pi \rightarrow \pi^*$ (trpy)
	282	20 615	
	270	29 705	
	232	30 177	
	204	39 765	
[Ru(tpm)(4,4'-dph-bpy)(py)]$^{2+}$[b, d, f]	480(sh)	3360	MLCT (Ru→ bpy)
	428	6870	MLCT (Ru→ bpy)
	352	16 500	MLCT (Ru→ tpm, bpy)
	313	35 000	$\pi \rightarrow \pi^*$ (tpm, bpy)
	256	39 800	$\pi \rightarrow \pi^*$ (tpm, bpy)
[Ru(trpy)(4,4'-dph-bpy)(py)]$^{2+}$[c,e, f]	484	16 000	MLCT (Ru→ trpy)
	424	---	
	353	---	

[a] All solutions 2.0 x 10^{-5} M in CH_3CN except where noted..

[b] Complex is PF_6^- salt. (e.g. $[Ru]^{2+}[PF_6^-]_2$).

[c] Complex is Cl^- salt. (e.g. $[Ru]^{2+}[Cl^-]_2$).

[d] UV data from ref. 114.

[e] 1.0 mM solution in DMF; UV data from ref. 101.

[f] (4,4'-dph-bpy) = 4,4'-diphenyl-2,2'-bipyridine.

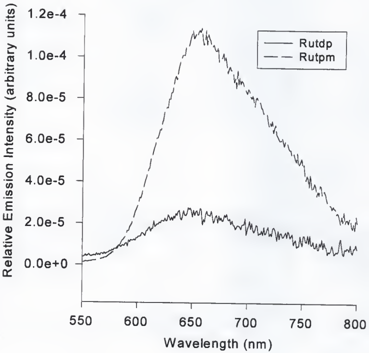

Figure 2.22. Emission spectra of Rutdp and Rutpm in CH_3CN at 295 K. $\lambda_{ex} = 470$ nm.

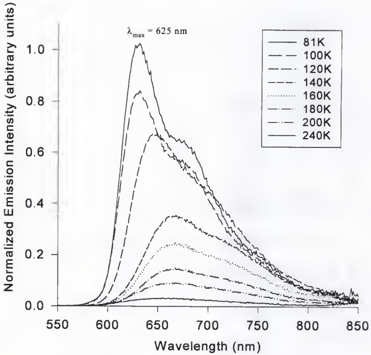

Figure 2.23. Emission spectra of Rutdp in 4:1 EtOH/MeOH at increasing temperature.

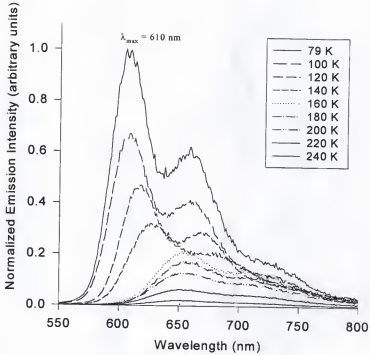

Figure 2.24. Emission spectra of Rutpm in 4:1 EtOH/MeOH at increasing temperature.

Table 2.2. Summary of Emission Characteristics for Rutdp and Rutpm and Related Ru Complexes.

	298 K			77 K	
Complex	$\lambda_{max, em}$ (nm)	τ (ns)	Φ_L	$\lambda_{max, em}$ (nm)[b]	τ (μs)[b]
Rutdp	647[a]	< 30[b]	0.0015[c]	625	6.46
Rutpm	650[a]	< 30[b]	0.0028[c]	610	7.05
Rutrpy	none	250 ps[d]	≈ 0	598[e]	11.0[e]
$[Ru(trpy)(4,4'\text{-}dph\text{-}bpy)(py)]^{2+}$	660[f]	---	≈ 0.0016[f]	---	---
$[Ru(tpm)(4,4'\text{-}dph\text{-}bpy)(py)]^{2+}$	661[g]	78[g]	0.0021[g]	630[g]	4.06[g]
$Ru(tptrpy)^{2+}$[h]	648[d]	4[d]	0.00075[d]	633[e]	7.8[e]
$Ru(tt)(phbp)^{+}$[i]	808[j]	60[j]	5 x 10^{-6}[j]	792[j]	0.9[j]

[a] measured in Ar degassed CH_3CN.
[b] all measured in 4:1 (v/v) EtOH/MeOH.
[c] calculated relative to $Ru(bpy)_3Cl_2$ (aq) using Eq 2.5 in the experimental section.
[d] measured in deoxygenated EtOH, ref. 105.
[e] ref. 96.
[f] measured in DMF, ref. 99.
[g] ref. 114.
[h] refer to Figure 2.13 for structure.
[i] refer to Figure 2.15b for structure.
[j] ref. 105.

polypyridyl complexes.[118] Both complexes' emission maxima are also lower than Rutrpy, whose emission maximum is at 598 nm (Table 2.2). At low temperatures, the emission bands possess more fine structure. This is a commonly observed feature of Ru polypyridyl complexes, resulting from the well-defined progression of vibrational states with similar energies.[119] As temperature increases, each of these discrete vibronic states broaden due to increased inhomogeneous solvent-sample interactions, and a single broad emission band results as shown in both Figures 2.23 and 2.24. The shift to lower energies in both emission spectra is a common feature for MLCT emission,[120] and is attributed to solvent dipoles which are frozen in the ground state rather than excited state orientation at low temperatures. Upon warming, these dipoles reorganize as the rigid glass matrix melts in the 140-160 K region, lowering the energy of emission,

Luminescence lifetimes, τ, were measured as a function of temperature for Rutdp and Rutpm in 4:1 EtOH/MeOH glasses. The data were fit using the method of Caspar[92] utilizing the following expression:

$$1/\tau\ (T) = k_1 + k_0'\exp(-\Delta E'/RT) \qquad 2.4$$

where k_1 is the sum of the radiative and non-radiative rates of decay, k_0' is the pre-exponential factor for internal conversion to the non-luminescent ^{3}d-d state, $\Delta E'$ is the activation barrier for internal conversion, R is the gas constant in joules, and T is temperature. Table 2.3 lists temperature vs. lifetime data for both complexes which are plotted with their fitted curves in Figure 2.25. The lifetimes of both complexes increase with decreasing temperature. Table 2.4 lists k_0' and $\Delta E'$ values for both Rutdp and Rutpm determined from fits to Eq. 2.4, and those reported for Rutrpy and $Ru(bpy)_3^{2+}$. A better fit to the data for Rutdp was obtained by adding a second exponential term. Comparison of various lifetime values at 77 K for tpm and trpy related complexes of Ru (II) are listed in Table 2.2. Both complexes give comparable lifetimes to Rutrpy.

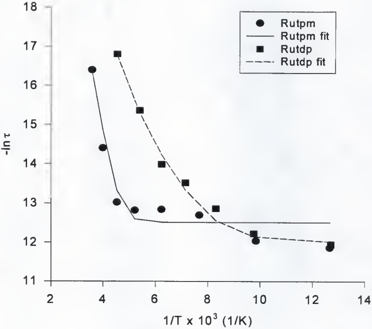

Figure 2.25. Temperature dependence of the luminescence lifetimes of Rutdp and Rutpm measured in 4:1 EtOH/MeOH.

Table 2.3. Temperature vs. lifetime data for Rutdp and Rutpm in 4/1 (v/v) EtOH/MeOH.

Rutdp		Rutpm	
Temp (K)	τ (μs)	Temp (K)	τ (μs)
79	6.46	79	7.05
102	4.91	102	5.89
121	2.59	130	3.06
140	1.34	160	2.65
161	0.838	192	2.70
185	0.220	221	2.20
221	≈ 0.060	251	0.550
260	< 0.050	280	≈ 0.075

Table 2.4. $\Delta E'$ and k_0' values for Rutdp, Rutpm and related complexes.

Complex	10^{-13} x k_0' (s^{-1})	$\Delta E'$ (cm^{-1})
Rutrpy	1.9[a]	1500[a]
Rutdp	0.019	1852
Rutpm	1.1	2622
$Ru(bpy)_3^{2+}$	4.5[b]	3563[b]

[a] ref 99.
[b] ref 92.

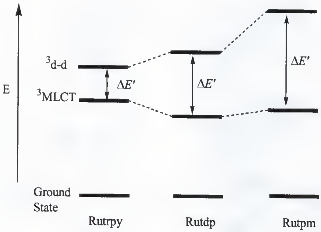

Figure 2.26. Relative orderings of the energies of the lowest triplet states for Rutrpy, Rutdp, and Rutpm.

Rutdp and Rutpm coated substrates. The temperature dependent luminescence properties of Rutdp and Rutpm coatings applied to aluminum substrates were investigated as well. Figures 2.27 and 2.28 illustrate the emission spectra taken of Rutdp and Rutpm coatings, respectively as temperature is increased. The most dramatic finding is than upon incorporation into the urethane binder, room temperature emission is approximately a factor of 50 times greater than observed in solution. The distinct fine structure and the red-shifting of the spectra are both observed, but not nearly as apparent as was observed in the rigid glass matrices. Calibration plots of the emission intensity vs. temperature of these two coatings are shown in Figure 2.29, compared to a substrate painted with Rutrpy. The synthetic modification of the two heteroleptic complexes on the temperature dependence is easily observed in that at 250 K, the emission intensity of the Rutrpy paint is practically zero, while the intensities of the two others is still relatively strong.

Discussion

Examining the crystal structures of the two complexes in Figures 2.19 and 2.20 allows for some interesting observations. The first is the obvious difference between the coordination preferences for the two tridentate ligands. As expected, Figure 2.19 shows that the trpy ligand attaches in a planar, meridional fashion, while Figure 2.20 shows that the tpm adopts a facial coordination. The geometric strain in the trpy ligand in its coordinated form results in a N1-Ru-N3 bond of angle of 158° (Table D.3), less than the ideal case in octahedral type symmetry of 180°, resulting in trpy being a weak field ligand. This also compares favorably to other trpy complexes of Ru.[105] Although the structural parameters for the crystal in Figure 2.20 could not be refined due to disorder caused by the presence of diethyl ether, similar tpm complexes of Ru[112, 113] show facial tpm coordination and octahedral symmetry.

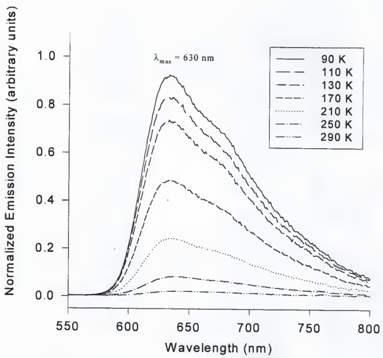

Figure 2.27. Emission spectra of Rutdp coated substrate at increasing temperature.

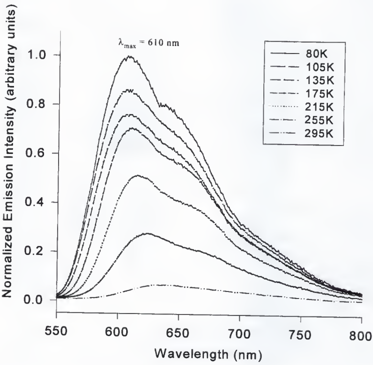

Figure 2.28. Emission spectra of Rutpm coated substrate with increasing temperature.

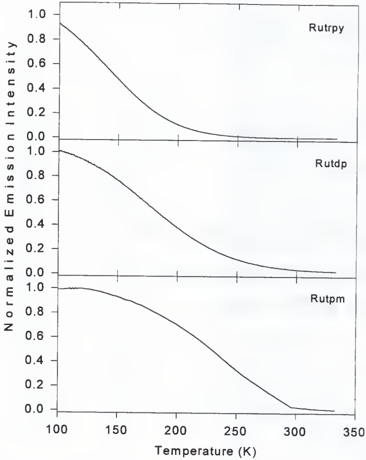

Figure 2.29. Calibration plots for temperature sensitive coated substrates plotting emission intensity versus temperature. $\lambda_{ex} = 470$ nm, $\lambda_{em} = 620$ nm.

As we had hoped, the structural modifications designed for both Rutdp and Rutpm have increased the temperature where emission can be detected. From the criteria detailed above in controlling k_{ic} (increasing or decreasing the energies of the ^{3}d-d or ^{3}MLCT states, respectively), and the photophysical data, several conclusions can be made. The most significant indication of this improvement is the increase in the activation barrier, $\Delta E'$, listed in Table 2.4 as determined by the temperature dependent lifetime experiments. These values, in decreasing order of energy, are $Ru(bpy)_3^{2+}$ > Rutpm > Rutdp > Rutrpy. For each of the new complexes, different arguments can be made as to the determination of whether increasing the ^{3}d-d or decreasing the ^{3}MLCT state, or perhaps some combination of both, is the reason for the increase in the temperature where emission can be detected.

In determining the role of the energy of the ^{3}MLCT state and its contribution to $\Delta E'$, the origin of the chromophoric ligand (that from which emission results), must first be determined. Recall in Ru(II) polypyridine complexes emission results from the lowest energy ^{3}MLCT state, after intersystem crossing from the lowest energy ^{1}MLCT state has occurred (Figure 2.10). The UV-visible absorption data in Table 2.1 lists the lowest energy absorptions and assignments which identify the chromophoric ligand in each case. The lowest excited state absorption in both Rutrpy and Rutdp is ^{1}MLCT in nature, and has been assigned as a $Ru(d\pi) \rightarrow trpy(\pi^*)$ transition at the same approximate energy. It is interesting to note that an almost structurally identical complex to Rutdp, $[Ru(trpy)(4,4'\text{-}dph\text{-}bpy)(py)]^{2+}$, where the bidentate ligand is the only difference, has a lowest MLCT absorption of the same transition and of approximate energy and ε as Rutdp. In the case of Rutpm, the lowest energy absorption is also MLCT in nature, but it is a $Ru(d\pi) \rightarrow dpph(\pi^*)$ transition rather than a $Ru(d\pi) \rightarrow tpm(\pi^*)$ transition. This is probably because tpm is a less conjugated ligand than dpph, and its π^* orbital is therefore at higher energy. This is corroborated by the assigned Ru → tpm MLCT absorption observed at 356 nm, and the presence of a similar band reported for a structurally similar complex,

$[Ru(tpm)(4,4'\text{-}dph\text{-}bpy)(py)]^{2+}$ (Table 2.1). Like Rutpm, the lowest energy absorption in this similar complex is MLCT in nature, with the transition to the functionalized bpy, rather than the tpm ligand orbital.

The emission properties of the two new complexes and other related complexes appear in Table 2.2. The most important observation is the enhanced room temperature emission of the two new complexes in solution versus Rutrpy. Figure 2.22 reveals that weak emission can be detected, whereas in Rutrpy, there is none. The two structurally similar complexes first listed in Table 2.1 also show detectable, albeit weak emission at room temperature[101,114] whose quantum yields compare favorably. One last complex to compare is the *bis*-(triphenyl)-substituted Ru trpy complex, $Ru(tptrpy)^{2+}$ (See Figure 2.13a for structure), whose quantum yield is even smaller than Rutdp or Rutpm. This complex is included to show that the first strategy for design of trpy complexes mentioned previously, substituting on both trpy rings, may not be as effective as the heteroleptic design employed for Rutdp and Rutpm, which removes one trpy ligand and replaces it with stronger field ligands.

The assignment of the chromophoric ligands from the absorption data for Rutdp and Rutpm should aid in identifying the ligand from which emission results. Analysis of the emission maxima of the complexes reveals the energy level of the ^{3}MLCT state, and therefore its contribution to the energy barrier. Rutrpy emits (at 77 K) at 598 nm, with emission relaxing from the trpy ligand. In Rutdp, the energy of emission has red-shifted to 625 and 647 nm for low and room temperatures, respectively. Emission in Rutdp should be from the trpy ligand as well, as determined in the absorption data. However, since the emission energy has decreased, there may be some stabilization of the trpy π^* orbital due to the presence of the dpph electronic manifold, whose Ru → dpph MLCT absorption is only 60 nm higher in energy than the Ru → trpy MLCT transition. This overlapping of orbital energies may provide stabilization which results in the red-shift of Rutdp's emission energy. In Rutpm, the tridentate tpm ligand MLCT absorption is higher in energy than the Ru → trpy transition, and thus the dpph is the ligand from which emission results.

These results suggest that the dominant factor contributing to the larger values of $\Delta E'$ for Rutdp or Rutpm versus Rutrpy in Table 2.4 is the increased energy level of the ^{3}d-d state. In the case of Rutdp, the increase in $\Delta E'$ is smaller than in Rutpm and is probably due to the presence of the trpy ligand. Trpy, with its planar geometry and strained bite angle upon bonding, is a weaker field than tpm, which coordinates facially. Thus the ligand field splitting, Δ, is larger in Rutpm than in Rutdp, with a concomitant increase in $\Delta E'$. Figure 2.26 illustrates the approximate energy levels of the relevant triplet states involved in the decay process for Rutrpy, Rutdp, and Rutpm.

Temperature sensitive coatings. Judging from the spectra in Figures 2.27 and 2.28, application of Rutdp and Rutpm as coatings seems to increase the intensity of emission even at higher temperatures. The urethane binder most likely provides the explanation. In solution the amount of vibronic coupling between the excited and ground states is increased, which increases the non-radiative rate of decay.[37] In the binder, however, vibrational effects are reduced because the substantial rigidity of the polyurethane matrix. This results in a slower rate of internal conversion k_{ic}, as a deactivation process (Eq. 2.2), and a concomitant increase in the emission intensity at room temperature versus that observed in fluid solution. This role of the binder also explains why the emission spectra of the coated substrates show a less pronounced red-shifting of the spectra, and less fine structure at higher temperature. In solution, recall that at low temperature the solvent dipoles are frozen and can not reorganize to a more favorable energy interaction with the excited complex, resulting in emission at a higher energy. As the glass melts, reorganization of the solvent dipoles around the excited state dipoles red-shifts the emission. By mixing these complexes in the binder, the effects of solvent reorganization energy in lowering the emission energy are less pronounced.

As outlined in the introduction, the purpose of this study was to find complexes whose temperature dependent luminescence characteristics would vary over a broader range than Rutrpy, including the region near ambient conditions. The emission profile of a generic fluorophore in Figure 2.9a indicated three regions where temperature dependence on the emission intensity behaves differently. Calculating the response in region II, where the changes in intensity vs. temperature (dI/dT) are the greatest, is probably the most important criterion for judging a particular complex as a good candidate for temperature sensing. Calculated values of dI/dT, which correspond to the fractional change in the normalized emission intensity per degree K, vs. temperature are an indicator of the expected contrast imaged for areas with different temperatures. The greater the magnitude of dI/dT, the better the expected contrast able to be detected by the CCD camera. Using the data in the three paint calibration curves in Figure 2.29, the calculated dI/dT vs. temperature plots in Figure 2.30 help to identify the temperature regions in which these coatings are most sensitive. The absolute luminosity of all three coatings is approximately equal at 100 K, so a quantitative measure of the imaged contrast that can be anticipated by comparing these coatings in any particular temperature region is reasonable. Analysis of the three plots reveals that Rutdp and Rutpm show significant dI/dT over a broader temperature range than Rutrpy, indicating the possibility of using the two designed complexes over a larger temperature region. Also notice that both Rutdp and Rutpm plots track the temperature dependent lifetime data well. From Table 2.3, Rutpm's lifetime is longer than Rutdp at higher temperature. This is reflected in the dI/dT plots showing the absolute dI/dT maximum shifted to higher temperature for Rutpm. Although the profile of Rutrpy is more narrow, it does show a greater slope (max $|dI/dT| \approx 0.012$ per K) compared to the maximum of either of the other two (max $|dI/dT| \approx 0.008$). This indicates that in the 120 -200 K region, Rutrpy coatings are a better choice for sensing, while Rutdp or Rutpm are the better options at higher temperature.

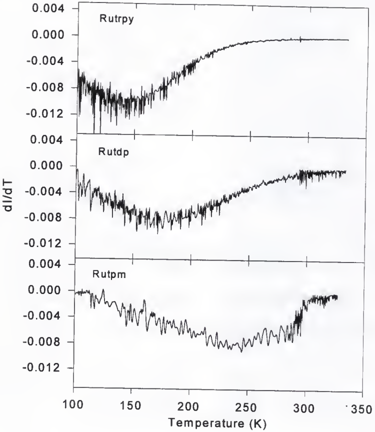

Figure 2.30. Comparison of the dI/dT vs. temperature plots for various coated substrates.

Conclusions

Two unique applications detailing the versatility of polypyridyl complexes of Ru and Os have been presented in this dissertation. In both studies, strategic chemical modification to the structure of the core metal complex has been the motivation for their use in electrochemical devices and photochemical probes. In the first study, polypyridyl complexes of Ru and Os were chosen because of their facile incorporation into microstructured polymer films via a new fabrication technique, resulting in optical switching devices. These polymer films behave as diffraction gratings whose diffraction efficiency can be modulated by altering the inherent electrochemical properties these polypyridyl complexes possess.

In the second study, the syntheses of two new heteroleptic polypyridyl complexes of Ru (II) are reported, whose strategy for their design has focused on their photophysical, instead of electrochemical properties. Understanding the importance of chemical structure in this case has led to the tuning of their photophysical properties. By examining the temperature dependence of the luminescence of the model complexes, $Ru(bpy)_3^{2+}$ and $Ru(trpy)_2^{2+}$, we have designed new complexes which act as temperature sensors over larger temperature regions than Rutrpy. Rutrpy, with its low lying ^{3}d-d energy level is thermally populated by internal conversion at room temperature, and has no radiative means of decay. By designing complexes which have stronger field ligands and greater conjugation, the energy of activation, $\Delta E'$, between the emitting and non-emitting states has been increased. The ligand field splitting, Δ, in Rutdp and Rutpm has increased by using stronger field ligands than trpy. The overall effect of this substitution is to increase the energy separating the two competing states by raising the energy level of the ^{3}d-d state, allowing for weak, but detectable emission at room temperature.

Incorporation of Rutdp or Rutpm into urethane based binders allows the complexes to be applied to surfaces as coatings for use as temperature sensors. The coatings have even greater room temperature emission intensities than the complexes in solution. Their application to temperature sensing at higher temperatures has been determined from plots of emission intensity vs. temperature. These plots indicate, along with plots of dI/dT vs. temperature, that Rutdp and Rutpm coatings are good choices as sensors at temperature ranges higher than Rutrpy.

Experimental

Materials and Syntheses

All materials used in the syntheses of the Ru complexes were of reagent grade and used as received unless otherwise noted. $RuCl_3{\bullet}3H_2O$, 2,2':6',2''-terpyridine and pyrazole, pyridine, and NH_4PF_6 (Sigma Aldrich), and 4,7-diphenyl-1,10-phenanthroline (Acros) were used as received. *Bis*-(2,2':6,2''-terpyridine)ruthenium (II) dichloride was synthesized as previously reported.[121] THF (tetrahydrofuran, Fisher) was pre-dried over molecular sieves, then distilled over Na/K benzophenone immediately before use. Alumina (Fisher, Brockman activity III) was used for column chromatography.

Positive FAB (fast atom bombardment) mass spectra were obtained on a Finnegan MAT 95 high-resolution mass spectrometer.

Diffraction quality crystals were obtained by using a slow diffusion of solvents. For Rutdp, ≈40 mg of the complex was placed in a clean vial and 2 mL of CH_3CN was added to dissolve it. The uncapped vial was then placed in a larger jar containing 2 mL ether. The jar was tightly capped and stored in the dark for a period of 4 days. Crystals of $[Ru(tpm)(dpph)Cl]^+$ were grown by dissolving ≈3 mg in 1.0 mL CH_3CN in an NMR tube, and carefully layering 1.0 mL diethyl ether on top. The tube was capped and placed in the freezer for 1 week.

Synthesis of [(2,2':6',2''-terpyridine)(4,7-diphenyl-1,10-phenanthroline)(pyridine) ruthenium (II)] hexafluorophosphate (Rutdp).

1) (2,2':6',2''-terpyridine) ruthenium(II) trichloride.(Ru(trpy)Cl$_3$) This known complex was synthesized by the procedure reported by Leising, et al.[122]

2) [(2,2':6',2''-terpyridine)(4,7-diphenyl-1,10-phenanthroline) chloro-ruthenium(II)] chloride.(**2**) This complex was prepared using a procedure for the similar though not identical Ru complex [Ru(trpy)(η^2-tpt)Cl]Cl (where the bidentate tpt ligand = 2,4,6-tripyridyltriazine) reported by Gupta, et al.[123] In an oven dried 100mL round bottom flask, Ru(trpy)Cl$_3$ (0.220g, 0.50mmol) and dpph (0.166g, 0.50mmol) were dissolved in 40mL of 1/1 (v/v) ethanol/water. The stirring solution was refluxed for 24 hr. After cooling to room temperature, an aqueous solution containing 80mg of NaClO$_4$ was added, and the total volume was reduced in half by rotary evaporation. The red-black solution was placed in the freezer overnight. A red-black precipitate which had formed was collected on a medium porosity fritted funnel, washed with excess cold water and dried in a vacuum dessicator. The crude material (320 mg recovered) was chromatographed on a column of alumina using a 65/35 ratio (v/v) of CH$_3$CN/toluene as the eluant. The desired product comes off the column as a red-brown band, following a thin orange band. The solid was recrystallized in boiling EtOH, resulting in red-black crystals. Amount recovered: 120 mg (28%). Mass spec (pos FAB) data: m/z = 702, corresponds to Ru (1+) cation; CHN analysis, calculated for C$_{39}$H$_{27}$N$_5$Cl$_2$Ru: C, 63.50; H, 3.69; N, 9.49. Found: C, 63.61; H, 3.72; N, 9.42.

3) Rutdp. In a clean, oven-dried 100 mL roundbottom flask was placed **2** (100 mg, 0.1 mmol), silver trifluoromethanesulfonate (69 mg, 0.2 mmol, Aldrich) and 40 mL of 1/1 (v/v) ethanol/H$_2$O. Pyridine (4 mL, , Fisher) was added to the stirring red-black solution and the resulting solution was refluxed under N$_2$. The reaction was followed by thin layer chromatography on silica plates using 9/1 (v/v) CH$_2$Cl$_2$/CH$_3$CN until a dark spot at R$_f$ = 0.51 appeared (≈ 6 hr). At this point, the now red-orange colored solution was

refluxed another 2 hr and then cooled to ambient temperature. A gray solid (AgCl) was filtered and the red-orange filtrate was rotovapped to dryness. The red-orange residue was dissolved in 0.5 mL acetone, and 2 mL of a saturated aqueous solution of NH_4PF_6 was added causing a precipitate to form. The precipitate was collected on a fritted funnel, dissolved in a minimum amount of acetone, and re-precipitated by pipetting the solution into 300 ml of ether. The red powdery solid was collected by filtration and dried overnight in a vacuum dessicator. The complex was purified by column chromatography using alumina and 2/1 (v/v) CH_3CN/toluene as the eluant. Yield: 50 mg (39%). Mass spec (pos FAB) data: m/z = 891, corresponds to Ru (1+) salt (2+ cation and 1 PF_6^-). CHN analysis, calculated for $C_{44}H_{32}N_6RuP_2F_{12}$: C, 51.0; H, 3.11; N, 8.11. Found: C, 50.45; H, 2.97; N, 7.91.

Synthesis of [(*tris*(1-pyrazolyl)methane)(4,7-diphenyl-1,10-phenantrholine)(pyridine) ruthenium] (II) hexafluorophosphate (Rutpm).

Preparation of this complex proceeds via the scheme outlined in Figure 2.16 and involves the stepwise attachment of ligands to $RuCl_3{\bullet}3H_2O$, after initial preparation of the tpm ligand. Synthesis of *tris*(1-pyrazolyl)methane) was accomplished using the method of Byers, Canty and Honeyman.[111]

1) Ru(tpm)Cl_3. This known complex was synthesized by the procedure reported by Llobet and co-workers.[113]

2) [Ru(tpm)(dpph)Cl]Cl. This precursor complex was prepared according to the procedure reported for the synthesis of [Ru(tpm)(phen)Cl]Cl.[113] (phen = 1,10-phenanthroline). In a clean and oven-dried 50 mL round bottomed flask was placed Ru(tpm)Cl_3 (0.5 g, 1.19 mmol), dpph (0.393 g, 1.20 mmol), and LiCl (0.5 g 11.8 mmol). 10 mL of 3:1 (v/v) $EtOH/H_2O$ was added and the mixture was stirred to create a green-brown solution. The solution was heated at reflux for 10 min at which time triethylamine (12 drops) was added and the solution was refluxed for an additional hour. The solution

was filtered hot and the solvent was rotary evaporated to ¼ of its original volume. The solution was placed in the freezer overnight. The black precipitate which had formed was collected by filtration using a fritted funnel. A portion of the solid was recrystallized in boiling absolute ethanol, resulting in black crystals. Amount recovered 0.78 g (91.3%) Mass spec (pos FAB) data: m/z = 683, corresponds to Ru (1+) salt. CHN analysis, calculated for $C_{34}H_{30}N_8O_2RuCl_2$ (dihydrate): C, 54.1; H, 3.87; N, 14.81. Found: C, 52.68; H, 3.74; N, 13.83.

3) Rutpm. This complex was synthesized in the same manner as the procedure for Rutdp stated above, substituting [Ru(tpm)(dpph)Cl]Cl for [Ru(trpy)(dpph)Cl]Cl. The green brown complex was purified by column chromatography using alumina and 2/1 (v/v) CH_3CN/toluene as the eluant. Amount recovered: 34 mg (24%). Mass spec (pos FAB) data: m/z = 872, corresponds to Ru (1+) salt (2+ cation and 1 PF_6^-). CHN analysis, calculated for $C_{39}H_{31}N_9RuP_2F_{12}$: C, 46.07; H, 3.07; N, 12.40. Found: C, 45.18; H, 2.89; N, 12.17. ^1H NMR results (CD_3CN): δ 6.19 (t, 3H), 6.82 (t, 3H), 7.08 (t, 2H), 7.36 (d, 2H), 7.71 (m, 10H), 7.83 (d, 2H), 8.06 (d, 2H), 8.32 (s, 1H), 8.35 (t, 1H) 8.59 (d, 3H), 9.07 (d, 2H).

Formulation and Application Procedures for Rutdp and Rutpm Coatings

Substrates were prepared for coating in the following process. Aluminum metal plates (≈1.5 in by 0.75 in) were lightly sanded on one side with very fine grain sand paper, then soaked briefly in $CHCl_3$ to remove any grit, wiped with a clean lab tissue, and air dried. A white primer coat was prepared by thoroughly blending 5 mL of DuPont Prime 'n' Seal 2603S activator and 5 mL 2680S white primer-sealer. The blended mix was poured into the reservoir of a Paasche single-action airbrush fitted with a size 2 nozzle and applied to the cleaned aluminum substrates in a fume hood. The airbrush was charged with 20 psi N_2 and sprayed at a distance of ≈ 8 in using a left-to-right motion. Several coats of primer were applied just until the painted surface hinted at becoming runny (typically 4-5 coats). The primer coated slides were then dried in a 60° C oven for 30 min.

Temperature sensitive coatings were formulated in the following manner. Concentrations of coatings were all approximately I mM, based on 5 mL total volume of the polymeric binder mixture (4 mL DuPont Chromaclear 7500s Urethane Clear and I mL Chromaclear 7575s Activator-Reducer) For either Rutpm or Rutdp, 5 mg was dissolved in 0.5 mL of 20% CH_3CN/MeOH in a clean vial. The pre-mixed 4:1 Chromaclear binder (5 mL) was then added and stirred thoroughly. Coating formulations were filtered through a glass pipette with a bit of tissue plugging the bottom. When larger coating volumes (> 10 mL) were necessary, they were filtered through a glass syringe equipped with a filter adapter housing a micropore filter. The filtered coatings were then poured into the airbrush reservoir and applied to the primer coated aluminum substrates. 7-8 coats were usually applied using the same left-to-right painting motion used for primer application, often waiting a minute or so between coats to allow for partial drying to prevent premature running. Coating continued in this manner until the onset of "framing" occurred, i.e., the buildup of applied coating which produced a darker colored border at the edges. The coated substrates were finally dried in a 60° C oven for 30 min before use.

Instrumentation and Apparatus

X-ray data were collected at 173 K on a Siemens SMART PLATFORM equipped with A CCD area detector and a graphite monochromator utilizing MoK_α radiation (λ = 0.71073 Å). Cell parameters were refined using up to 8192 reflections. A hemisphere of data (1381 frames) was collected using the ω-scan method (0.3° frame width). The first 50 frames were re-measured at the end of data collection to monitor instrument and crystal stability (maximum correction on I was < 1 %). Psi scan absorption corrections were applied based on the entire data set.

The structures were solved by the Direct Methods in *SHELXTL5*,[124] and refined using full-matrix least squares. The structure of Rutdp consists of the Ru complex cation and PF_6 anions in a 1:2 ratio. The PF_6 anions are both disordered each along a 4-fold axis passing through two axial F atoms. The axial F atoms are not disordered while the four equatorial atoms are refined in two positions. For one PF_6 anion the site occupation factors were 0.74(4) and 0.26(4), respectively, and 0.55(4) and 0.45(4) for the second. The non-H atoms were treated anisotropically, whereas the hydrogen atoms were calculated in ideal positions and were riding on their respective carbon atoms. 789 parameters were refined in the final cycle of refinement using 7168 reflections with $I > 2\sigma(I)$ to yield R_1 and wR_2 of 3.48 and 6.66, respectively. Refinement was done using F^2. Complete crystal data for Rutdp including tables of bond lengths and angle appear in Appendix D.

Crystals of the precursor complex [Ru(tpm)(dpph)Cl]Cl were monoclinic with space group C2/c, a = 27.329(1), b = 16.476(1), c = 17.795(1) Å and $\beta = 93.705(1)$. The structure was also solved by the Direct Methods in *SHELXTL5*, and refined using full-matrix least squares. The structure consists of the Ru complex cation and Cl anion in a 1:1 ratio. The crystal structure also revealed the presence of ether molecules in two positions. One in a general position and disordered while the other is disordered around a 2-fold rotation axis passing through the O atom. The structure has severe disorder that could not be modeled. This lead to a partial refinement structure that used 472 parameters and 2801 reflections with $I > 2\sigma(I)$ to yield R_1 and wR_2 of 9.05 and 28.49 , respectively. Refinement was done using F^2. Due to this partial refinement, complete bond angle, length and refinement parameters like those for Rutdp in Appendix D could not be calculated with a high degree of confidence.

UV-visible spectra were recorded using a HP 8452A diode-array spectrophotometer. Steady-state emission spectra were recorded using a Spex F-112 photon counting fluorimeter at room and low temperatures. For temperature measurement in 77 - 300 K region, an Oxford Instruments model DN-1704 optical cryostat was used which fits into the sample compartment of the fluorimeter, and whose temperature was controlled by an Omega instruments CYC3200 digital temperature controller. For solvent glasses, ≈ 2 mL of the desired Ru solution was pipetted into a Pyrex tube (0.25 in inner diameter, 18 in length) and Ar degassed for 1 hr, septum capped and inserted through a septum cap into the cryostat chamber which had been purged with He for 30 min. For coated substrates, the samples were measured by affixing the coated substrate secured at a 45° angle into the probe stick and inserting into the cryostat. An Omega type T thermocouple was affixed to either the back side of the painted substrate or around the Pyrex tube to record temperature, which was displayed on an Omega Monogram digital thermometer. This thermometer was equipped with a serial interface to a 486/33 PC for automated digital temperature acquisition.

The Spex fluorimeter is interfaced to the 486 PC and has the capability to collect luminescence intensity data as a function of time with data continuously being streamed onto the hard drive. Temperature data collected by the Omega thermometer is also continuously streamed and stored on the hard drive. Once the cryostat is cooled to 95 K, the temperature controller is programmed to linearly increase the temperature of the cryostat at a rate of 2.0 K/min. Data acquisition is started, simultaneously collecting luminescence intensity and temperature independently as a function of time. Luminescence and temperature data are sampled at a 1 and 10 Hz rate respectively over two hours. This period of time is generally required to reach ambient temperature, resulting in data sets consisting of approximately 7200 and 720 points, for the luminescence intensity and temperature, respectively.

Since the cryostat can only be used in the temperature range up to 300 K, the 300-340 K range was probed using a separate cell mount. A block of aluminum metal (a 4 in cube) was designed with an open face where the painted aluminum substrate could be affixed and fitted into the sample compartment of the fluorimeter allowing for front-face configuration of the excitation beam and monitored emission. A ¼" canal was machined out behind the area where the painted substrate was affixed to allow a water/ethylene glycol mixture to circulate whose temperature could be varied using a Lauda recirculating bath. Temperature was controlled by heating the circulating bath to 340 K, then setting the temperature to 263 K, (-10 °C) and initiating acquisition, allowing the temperature of the bath to slowly decrease to 273 K as monitored by the Type K thermocouple and digital thermometer. Both temperature and intensity were collected at the same rates as in the low temperature case over an hour period, resulting in sets of approximately 3600 and 360 points for intensity and temperature, respectively.

Calibration plots like those in Figures 2.25 were produced by combining the two datasets from the low temperature (LT) run into a single set of points comprising about 7200 x,y pairs (number will vary depending on exact duration of experiment, where x = temperature (T) and y = emission intensity(I_{em})) by interpolation of the temperature data to produce the same number of points as the intensity data. I_{em} was normalized and plotted versus T. The warm temperature (WT) data set was processed in the same manner and was appended to the LT data by averaging 100 I_{em} points from the WT data at the temperature where the LT data was stopped and normalizing them to the average of the last 100 I_{em} points taken at LT. This method produces a single plot of data taken for both temperature regimes. For dI_{em}/dT vs. T plots, in both LT and WT cases, I_{em} and T datasets were smoothed and the number of points reduced by interpolation. These reduced data sets were imported into a spreadsheet used to calculate the dI_{em}/dT values which were finally plotted versus T producing plots like those in Figure 2.26.

Room temperature quantum yields for luminescence, Φ_L, were measured relative to $[Ru(bpy)_3]^{2+}[Cl^-]_2$ for which Φ_L in an air saturated aqueous solution at 295 K is 0.0379, and then calculated using the following formula:

$$\Phi_L = \Phi_r (F_r / F_s)(I_r / I_s)(n_s / n_r)^2 \qquad 2.5$$

were F is the fraction of light absorbed at the excitation wavelength (F = (1-10^{-A}, where A = absorption), I is the integrated area of the emission band, calculated by taking the area under the emission band from 515-800 nm, and n is the refractive index for the sample (s) and reference (r) solutions.

Low temperature emission lifetimes were obtained using the time-correlated single photon counting technique[125] on a instrument manufactured by Photochemical Research Associates (PRA). Temperature inside the cryostat was controlled and monitored as described for the steady-state emission experiments. Solutions of either Rutdp or Rutpm in 4:1 (v/v)EtOH/MeOH (1 x 10^{-4} M) were degassed for 1 hr in the Pyrex tube used above then placed in the cryostat and aligned in the sample compartment. Excitation was produced from a H_2-filled spark gap and filtered through a Schott UG-11 near-UV band pass filter with maximum transmittance at 350 nm. Emission was filtered through a long wavelength pass interference filter ($\lambda > 600$ nm, Corion LL-600). In the 77-150 K temperature range the samples were excited at a rate of 10 kHz while warmer temperature measurements were excited at a 30 kHz rate. Decay data were collected by interfacing to an EG&G Ortec multi-channel analyzer board housed in a 486/66 PC. The number of counts collected in the maximum channel was at least 2000. The data was analyzed using the DECAN (v. 1.0, 1993) single wavelength luminescence lifetime analysis software.

APPENDIX A
COULOMETRIC INTEGRATION CALCULATIONS

Integration of the oxidative waves of electrodes patterned with *poly*-$[(bpy)_2Ru(vpy)_2]^{2+}$ and *poly*-$[Os(vbpy)_3]^{2+}$ films such as those illustrated in Figures 1.27 and 1.28 were calculated in a spreadsheet in the following manner. The area under the curve is equal to total charge, Q, which is a measurement of the current multiplied by time:

$$A = Q = it \qquad \text{A.1}$$

If the area under the curve is broken up into very small blocks of charge, the sum of each of these blocks is equal to the total charge contained under the wave. Because the data was acquired at a reasonably fast rate, (4 samples/ second, or one point every 0.25s), this method of summing small blocks of charge can be executed. The current generated in the waves in Figs. 1.27 and 1.28 was divided into each half-wave process, i_a and i_c, and was integrated separately by subtracting the charging current (Figure 1.26) to produce a flat baseline. (Figure A.1.) This baseline correction was achieved by choosing two points on each side of the base of the wave and mathematically performing a linear regression. The equation of the regression line was then used to calculate the points on the new baseline. The new baseline points were subsequently subtracted from the experimentally acquired data points to give the corrected current values. Each of these corrected current values was multiplied by the time division, (0.25 s)to give the charge in each block. The sum of these individual slices of the area is the total charge passed under the wave in coulombs.

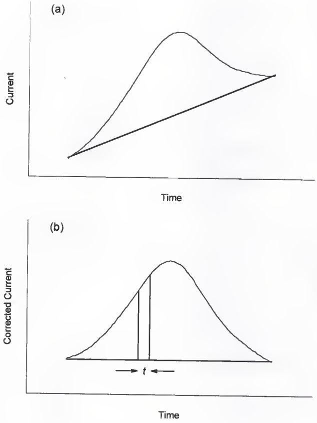

Figure A.1. (a) Initial current vs. time profile of a representative cathodic half-wave before baseline correction; (b) baseline corrected by subtracting the charging current.

The surface coverage, Γ_T, in units of moles per unit area, is calculated from the following equation:

$$\Gamma_T = \frac{Q}{nFA_f} \qquad A.2$$

where n is the number of electrons oxidized or reduced, F is Faraday's constant, in units of coulombs/mol, and A_f is the area of the film. This area can be fairly accurately approximated by a modified formula for the area of a circle:

$$A_f = (\Pi r^2)/2 \qquad A.3$$

where *r* is the radius of the film, and is measured by taking half of the electrochemical cell aperture of 0.3175 cm. The area is divided by two since only half of the electrode's surface is covered with polymer, due to alternating lines and gaps of the film's grating pattern, resulting in an electrode area of 0.0396 cm^2. The results, reported in Table 1.1, show coverage averages of Γ_c, Γ_a, and Γ_T of three similarly produced films of each polymer type at various sweep rates.

APPENDIX B
INSTRUMENTAL PERFORMANCE TESTS

The apparatus designed for collecting electrochemically modulated diffraction data from grating patterned redox films (Figure I.34) was tested periodically to ensure system stability and performance to the laser's specifications. Poor initial experimental results revealed drifting baselines in the diffracted and undiffracted optical signals collected at the photodiodes. In determining the source of instability, we focused on two areas: (1) the light source, initially a laser diode, and (2) the photodiodes. In the first case, the diode laser was replaced with a stabilized He-Ne laser which was after an hour warm-up period was specified to operate at less than 0.1 % noise on an hour timescale. In the second case, the photodiodes were found to have a noticeable temperature dependence. The room where the apparatus is located has temperature fluctuations as great at 3° C. To demonstrate the effect of room temperature on the photodiode's outputted signal, a simple experiment was performed which monitored the photodiode output and the temperature of the lab simultaneously over time. The temperature was monitored with high sensitivity using a thermocouple wired to the A/D converter, allowing for tenths of millivolt changes to be recorded. A noticeable effect was recorded. (Figure B.1) This temperature dependence was eliminated by redesigning the metal photodiode housing to be temperature regulated. This was achieved by attaching the diode in a brass plate which had been modified to allow for circulating water from a temperature controlled bath to surround and stabilize the diode, and inserted into a teflon sleeve, insulating it from the room's environment. Setting the temperature of the bath typically 5° C colder than room temperature would eliminate any fluctuations caused by changes in room temperature.

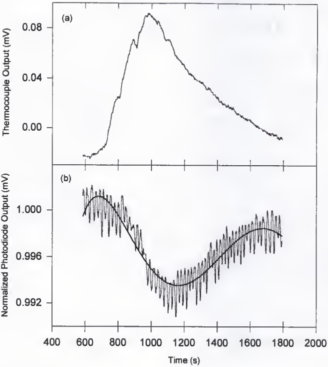

Figure B.1. Plots of (a) thermocouple output and (b) photodiode output vs. time, demonstrating fluctuation in room temperature and subsequent photodiode intensity dependency.

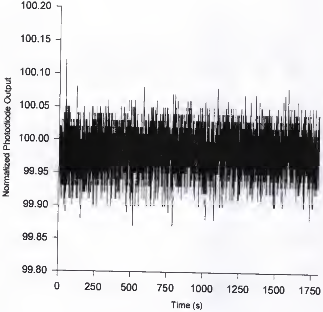

Figure B.2. Output of stabilized He-Ne laser detected by temperature controlled photodiodes.

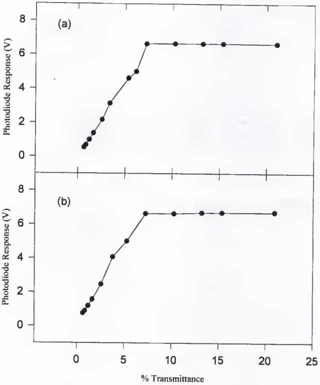

Figure B.3. Linearity tests of temperature regulated photodiodes/ (a) undiffracted beam diode; (b) diffracted beam diode. Tests performed without placing a grating film patterned electrode in the path of the He-Ne beam.

A typical experiment to test the laser and diodes involves warming up the laser for an hour, then directing the laser output into the photodiode and recording the signal for 30 min. Laser and photodiode response was deemed acceptable if noise levels met manufacturer's technical specifications for the laser of <0.1%. A typical plot of such a stabilization run is shown in Figure B.2.

After the experimental operating conditions were judged acceptable, tests were performed to find the linear portion of the photodiode's response, i.e. the maximum allowable voltage before saturation. This was executed by placing a series of neutral density filters in front of the photodiodes to attenuate the intensity of the laser being detected, and reading the subsequent voltage. A plot of photodiode response versus % transmittance (Figure B.3) indicates that to ensure linearity, experiments can be safely and accurately run with detected voltages less than 5 volts. Placing the patterned film coated electrode in the path of the laser considerably attenuates the signal initially. By using a combination of neutral density filters or by adjusting the position of an optical diffuser in front of the photodiodes, this attenuation can be finely tuned to guarantee operation in the linear region. Average initial readings of 3-4 V for the transmitted beam and 5-30 mV for the first order diffracted beam were typical for these types of redox films.

APPENDIX C
DERIVATION OF DIFFRACTION EFFICIENCY EQUATIONS

The equations used in calculating the refractive indices of the films in their electrochemically altered states are derived from the Fayer study[53] and have been simplified in the following manner. Refer to Table 1.4 for identification of all variables used in the ensuing equations.

The original equation involving the diffraction efficiency of a sinusoidal grating at probe wavelength, ω, is:

$$DE(\omega) = \exp\left[-\frac{2.3 \bullet OD(\omega)}{\cos\theta}\right]\left[\sinh^2\frac{\pi \bullet \Delta k(\omega)T}{\lambda\cos\theta} + \sin^2\frac{\pi \bullet \Delta n(\omega)T}{\lambda\cos\theta}\right] \qquad \text{C.1}$$

where T is the film thickness, λ is the probe wavelength, θ is the Bragg angle of diffraction, and the first term in brackets accounts for the average loss in optical density, *OD*, due to absorption. This equation can be reduced to Eq. C.2 which simplifies its application to experimental data. This equation can determine which factor, the absorption or the phase effects, is the origin of the diffraction changes observed in the grating films presented in this study.

$$DE = (\Delta k)^2 + (\Delta n)^2 \qquad \text{C.2}$$

The optical density of the film, *OD*, is related to the imaginary part of the complex refractive index, *k* (a unitless number), by:

$$k = (2.3\lambda OD)/(4\pi T) \qquad \text{C.3}$$

If the assumptions are made that $k << 1$, which is valid for relatively thin films of this type where $0 \leq OD \leq 0.1$, (valid from the results of the spectroelectrochemistry experiments) and that the overall *DE* is low, (< 0.01), which is the case in most experimental grating situations, then C.1 can be written as:

$$DE_{(\omega)} = \exp\left[-\frac{2.3 \bullet OD(\omega)}{\cos\theta}\right]\left[\frac{\pi \bullet T}{\lambda \cos\theta}\right]^2\left[(\Delta k(\omega))^2 + (\Delta n(\omega))^2\right] \qquad \text{C.4}$$

since $sinh^2 x \approx x$ and $sin^2 x \approx x$ for $x << 1$. In the oxidative case of the grating films of *poly*-$[(bpy)_2Ru(vpy)_2]^{2+}$, there is no absorptive loss in the film, and $OD(\omega) = 0$ and $\Delta k = 0$, leaving

$$DE_{(\omega)} = \left[\frac{\pi \bullet T}{\lambda \cos\theta}\right]^2 (\Delta n(\omega))^2 \qquad \text{C.5}$$

Recall that Δn is the difference between the value of the refractive index of the grating film, $n_{f(0)}$, and the electrolyte solution filling the gaps, n_g:

$$\Delta n = n_{f(0)} - n_g \qquad \text{C.6}$$

Substituting this expression into C.5 results in the equation

$$DE_{(\omega)} = \left[\frac{\pi \bullet T}{\lambda \cos\theta}\right]^2 [n_{f(0)} - n_g]^2 \qquad \text{C.7}$$

An electrochemically induced change in the diffraction efficiency, ΔDE, is reflected by a change in Δn, ($\Delta(\Delta n)$) which is the difference in the final and initial values of the film's refractive indices relative to the refractive index of the gap solution:

$$\Delta DE_{(\omega)} = \left[\frac{\pi \bullet T}{\lambda \cos\theta}\right]^2 [\Delta(\Delta n)]^2$$

C.8

$$\Delta(\Delta n) = (n_{f(f)} - n_g)^2 - (n_{f(0)} - n_g)^2 \qquad \text{C.9}$$

$$\Delta DE_{(\omega)} = \left[\frac{\pi \bullet T}{\lambda \cos\theta}\right]^2 [(n_{f(f)} - n_g)^2 - (n_{f(0)} - n_g)^2] \qquad \text{C.10}$$

All of the values in Eq. C.10 are known except for the refractive index of the film after the induced change, $n_{f(f)}$. The calculated changes in DE plotted versus changes in ΔRI, where RI is the refractive index of the grating film, are displayed in Figure 1.53.

Experimental values of $n_{f(f)}$ were calculated by solving Eq. C.10 for $n_{f(f)}$. This value was determined by expanding Eq. C.10, putting it into a quadratic expression of the form $ax^2 + bx + c = 0$, and solving for $n_{f(f)}$:

$$\left[\frac{\pi \bullet T}{\lambda \cos\theta}\right]^2 [(n_{f(f)})^2 + (-2n_{f(f)}\, n_g) + (2n_{f(0)}\, n_g - (n_{f(0)})^2 - \Delta DE)] = 0 \qquad \text{C.11}$$

Eq C.11 can be solved for $n_{f(f)}$ using the quadratic equation:

$$\mathrm{x} = n_{f(f)} = -b \pm \frac{\sqrt{b^2 - 4ac}}{2a} \qquad \text{C.12}$$

where

$$a = \left[\frac{\pi \bullet T}{\lambda \cos\theta}\right]^2 \qquad \text{C.13}$$

$$b = (\text{-}2n_g)\left[\frac{\pi \bullet T}{\lambda \cos\theta}\right]^2 \qquad \text{C.14}$$

$$c = \left[\frac{\pi \bullet T}{\lambda \cos\theta}\right]^2 (2n_{f(0)}\, n_g - (n_{f(0)})^2 - \Delta DE) \qquad \text{C.15}$$

As mentioned in the discussion, experimental values poorly fit the model plot. This is a function of the very low experimentally determined DE_0 values, which in turn result in very small ΔDE's. These low values are used in equation C.11, causing $n_{f(f)}$ values to deviate largely from the calculated model.

Calculation of the effects of changes in k due to changes in the film's absorption properties plotted in Figure 1.53 were performed by setting the value of n in Eq. C.4 equal to zero, simplifying to:

$$DE_{(\omega)} = \exp\left[-\frac{2.3 \bullet OD(\omega)}{\cos\theta}\right]\left[\frac{\pi \bullet T}{\lambda \cos\theta}\right]^2\left[(\Delta k(\omega))^2\right] \qquad \text{C.16}$$

Values of k were calculated by using equation C.3 and incrementally varying OD values.

APPENDIX D
CRYSTALLOGRAPHIC DATA FOR RUTDP

Table D.1. Crystal data and structure refinement for Rutdp.

Empirical formula	C44 H32 F12 N6 P2 Ru
Formula weight	1035.77
Temperature	173(2) K
Wavelength	0.71073 Å
Crystal system	Monoclinic
Space group	P2(1)/c
Unit cell dimensions	a = 11.4298(1) Å a = 90°
	b = 33.3446(6) Å b = 115.038(1)°
	c = 11.9240(2) Å g = 90°
Volume, Z	4117.44(11) Å^3, 4
Density (calculated)	1.671 Mg/m^3
Absorption coefficient	0.556 mm^{-1}
F(000)	2080
Crystal size	0.32 x 0.12 x 0.08 mm
Theta range for data collection	1.97 to 27.50 deg.
Limiting indices	-15<=h<=13, 0<=k<=44, 0<=l<=15
Reflections collected	9390
Table D.1. continued	
Independent reflections	9390 [R(int) = 0.0000]
Absorption correction	Psi scan

Table D.1. continued.

Refinement method	Full-matrix least-squares on F^2
Data / restraints / parameters	9328 / 0 / 789
Goodness-of-fit on F^2	1.045
Final R indices [I>2sigma(I)]	R1 = 0.0348, wR2 = 0.0666
R indices (all data)	R1 = 0.0583, wR2 = 0.0754
Extinction coefficient	0.00042(8)
Largest diff. peak and hole	0.443 and -0.604 $e.A^{-3}$

Table D.2. Atomic coordinates (x 10^4) and equivalent isotropic displacement parameters ($Å^2$ x 10^3) for Rutdp. U(eq) is defined as one third of the trace of the orthogonalized Uij tensor.

Atom	x	y	z	U(eq)
Ru	8782(1)	6455(1)	5647(1)	18(1)
N(1)	9477(2)	7026(1)	5597(2)	21(1)
N(2)	7806(2)	6772(1)	6351(2)	20(1)
N(3)	7598(2)	6014(1)	5838(2)	21(1)
N(4)	7551(2)	6511(1)	3806(2)	19(1)
N(5)	9783(2)	6139(1)	4813(2)	18(1)
N(6)	10163(2)	6343(1)	7477(2)	22(1)
C(1)	8029(2)	7171(1)	6524(2)	23(1)
C(2)	7422(3)	7394(1)	7110(3)	32(1)
C(3)	6598(3)	7199(1)	7511(3)	37(1)
C(4)	6385(3)	6792(1)	7327(3)	33(1)
C(5)	6992(2)	6580(1)	6727(2)	24(1)
C(6)	6840(2)	6151(1)	6394(2)	22(1)
C(7)	5969(3)	5902(1)	6571(3)	32(1)
C(8)	5842(3)	5510(1)	6188(3)	33(1)
C(9)	6588(3)	5373(1)	5615(3)	31(1)
C(10)	7452(3)	5630(1)	5457(2)	27(1)
C(11)	10312(2)	7141(1)	5126(2)	25(1)
C(12)	10631(3)	7534(1)	5075(3)	34(1)
C(13)	10092(3)	7830(1)	5519(3)	38(1)
C(14)	9231(3)	7719(1)	5999(3)	31(1)
C(15)	8936(2)	7320(1)	6033(2)	23(1)
C(16)	10905(2)	6632(1)	8224(2)	28(1)
C(17)	11810(3)	6560(1)	9428(2)	33(1)
C(18)	11962(3)	6178(1)	9888(3)	39(1)
C(19)	11228(3)	5880(1)	9131(3)	45(1)
C(20)	10341(3)	5969(1)	7947(3)	34(1)
C(21)	6383(2)	6679(1)	3331(2)	23(1)
C(22)	5608(2)	6691(1)	2061(2)	24(1)
C(23)	6026(2)	6531(1)	1229(2)	21(1)
C(24)	7289(2)	6364(1)	1705(2)	19(1)
C(25)	7998(2)	6352(1)	3002(2)	18(1)
C(26)	7895(2)	6205(1)	963(2)	22(1)
C(27)	9075(2)	6031(1)	1482(2)	24(1)
C(28)	9762(2)	5982(1)	2800(2)	20(1)
C(29)	9223(2)	6156(1)	3544(2)	18(1)
C(30)	10945(2)	5770(1)	3397(2)	22(1)
C(31)	11480(2)	5751(1)	4671(2)	25(1)
C(32)	10888(2)	5936(1)	5343(2)	23(1)

Table D.2. continued.

Atom	x	y	z	U(eq)
C(33)	5148(2)	6525(1)	-116(2)	20(1)
C(34)	4779(2)	6161(1)	-743(2)	24(1)
C(35)	3897(2)	6156(1)	-1980(2)	25(1)
C(36)	3416(2)	6512(1)	-2594(2)	28(1)
C(37)	3770(2)	6875(1)	-1983(2)	27(1)
C(38)	4627(2)	6881(1)	-735(2)	24(1)
C(39)	11607(2)	5564(1)	2720(2)	24(1)
C(40)	11006(3)	5257(1)	1878(2)	32(1)
C(41)	11671(3)	5056(1)	1303(3)	40(1)
C(42)	12918(3)	5163(1)	1545(3)	43(1)
C(43)	13525(3)	5464(1)	2378(3)	39(1)
C(44)	12880(3)	5663(1)	2974(3)	29(1)
P(1)	3136(1)	6943(1)	3836(1)	31(1)
F(1)	4064(2)	6571(1)	4441(2)	63(1)
F(2)	2229(2)	7321(1)	3253(2)	51(1)
F(3)	4312(11)	7193(3)	3767(18)	56(2)
F(4)	2847(9)	6756(3)	2539(9)	57(2)
F(5)	1974(14)	6702(4)	3879(16)	69(3)
F(6)	3450(12)	7133(4)	5155(9)	69(3)
F(3')	4448(27)	7155(9)	4205(35)	43(5)
F(4')	2938(27)	6873(20)	2398(33)	74(10)
F(5')	1832(45)	6707(15)	3569(65)	91(12)
F(6')	3279(37)	7051(14)	5170(27)	74(9)
P(2)	7131(1)	9931(1)	-2741(1)	35(1)
F(11)	6594(2)	10076(1)	-1762(2)	58(1)
F(12)	7679(2)	9792(1)	-3711(2)	62(1)
F(13)	8374(15)	9750(6)	-1613(15)	83(4)
F(14)	6452(18)	9516(4)	-2760(22)	70(3)
F(15)	5923(11)	10114(6)	-3738(12)	86(4)
F(16)	7906(13)	10334(3)	-2540(15)	60(3)
F(13')	8168(21)	9668(6)	-1748(16)	71(5)
F(14')	6123(26)	9570(8)	-3287(28)	81(5)
F(15')	6089(19)	10206(6)	-3839(15)	84(5)
F(16')	8081(20)	10298(6)	-2343(20)	89(5)

Table D.3. Bond lengths [Å] and angles [deg] for Rutdp.

Bond	Angle
Ru-N(2)	1.965(2)
Ru-N(4)	2.054(2)
Ru-N(1)	2.073(2)
Ru-N(3)	2.075(2)
Ru-N(5)	2.090(2)
Ru-N(6)	2.116(2)
N(1)-C(11)	1.352(3)
N(1)-C(15)	1.373(3)
N(2)-C(5)	1.353(3)
N(2)-C(1)	1.355(3)
N(3)-C(10)	1.345(3)
N(3)-C(6)	1.373(3)
N(4)-C(21)	1.332(3)
N(4)-C(25)	1.370(3)
N(5)-C(32)	1.332(3)
N(5)-C(29)	1.373(3)
N(6)-C(16)	1.342(3)
N(6)-C(20)	1.346(3)
C(1)-C(2)	1.390(3)
C(1)-C(15)	1.476(3)
C(2)-C(3)	1.386(4)
C(2)-H(2)	0.97(3)
C(3)-C(4)	1.380(4)
C(3)-H(3)	0.94(3)
C(4)-C(5)	1.382(4)
C(4)-H(4)	0.93(3)
C(5)-C(6)	1.475(3)
C(6)-C(7)	1.380(4)
C(7)-C(8)	1.372(4)
C(7)-H(7)	0.92(3)
C(8)-C(9)	1.377(4)
C(8)-H(8)	0.94(3)
C(9)-C(10)	1.380(4)
C(9)-H(9)	0.93(3)
C(10)-H(10)	0.92(3)
C(11)-C(12)	1.370(4)
C(11)-H(11)	0.92(2)
C(12)-C(13)	1.382(4)
C(12)-H(12)	0.91(3)
C(13)-C(14)	1.382(4)
C(13)-H(13)	0.90(3)
C(14)-C(15)	1.379(4)

Table D.3. continued.

Bond	Length
C(14)-H(14)	0.89(3)
C(16)-C(17)	1.390(4)
C(16)-H(16)	0.99(3)
C(17)-C(18)	1.368(4)
C(17)-H(17)	0.93(3)
C(18)-C(19)	1.364(5)
C(18)-H(18)	0.91(3)
C(19)-C(20)	1.377(4)
C(19)-H(19)	0.87(3)
C(20)-H(20)	0.96(3)
C(21)-C(22)	1.395(3)
C(21)-H(21)	0.95(3)
C(22)-C(23)	1.377(3)
C(22)-H(22)	0.92(3)
C(23)-C(24)	1.424(3)
C(23)-C(33)	1.490(3)
C(24)-C(25)	1.410(3)
C(24)-C(26)	1.435(3)
C(25)-C(29)	1.429(3)
C(26)-C(27)	1.354(3)
C(26)-H(26)	0.94(2)
C(27)-C(28)	1.439(3)
C(27)-H(27)	0.90(2)
C(28)-C(29)	1.401(3)
C(28)-C(30)	1.422(3)
C(30)-C(31)	1.378(3)
C(30)-C(39)	1.488(3)
C(31)-C(32)	1.393(3)
C(31)-H(31)	0.99(3)
C(32)-H(32)	0.96(2)
C(33)-C(38)	1.393(3)
C(33)-C(34)	1.393(3)
C(34)-C(35)	1.390(3)
C(34)-H(34)	0.92(2)
C(35)-C(36)	1.381(4)
C(35)-H(35)	0.96(2)
C(36)-C(37)	1.382(4)
C(36)-H(36)	0.92(3)
C(37)-C(38)	1.393(3)
C(37)-H(37)	0.90(3)
C(38)-H(38)	0.92(3)
C(39)-C(40)	1.394(4)

Table D.3. continued.

Bond	Length
C(39)-C(44)	1.395(4)
C(40)-C(41)	1.392(4)
C(40)-H(40)	0.92(3)
C(41)-C(42)	1.376(5)
C(41)-H(41)	0.93(3)
C(42)-C(43)	1.376(5)
C(42)-H(42)	0.92(3)
C(43)-C(44)	1.390(4)
C(43)-H(43)	0.89(3)
C(44)-H(44)	0.90(3)
P(1)-F(3')	1.54(3)
P(1)-F(4)	1.567(9)
P(1)-F(5)	1.571(12)
P(1)-F(6')	1.57(3)
P(1)-F(6)	1.589(8)
P(1)-F(1)	1.591(2)
P(1)-F(5')	1.59(4)
P(1)-F(2)	1.594(2)
P(1)-F(3)	1.613(9)
P(1)-F(4')	1.65(3)
P(2)-F(15)	1.518(11)
P(2)-F(13')	1.545(14)
P(2)-F(16')	1.57(2)
P(2)-F(16)	1.572(12)
P(2)-F(14)	1.582(14)
P(2)-F(12)	1.599(2)
P(2)-F(14')	1.60(2)
P(2)-F(13)	1.604(14)
P(2)-F(11)	1.607(2)
P(2)-F(15')	1.63(2)

Bond	Angle
N(2)-Ru-N(4)	98.67(7)
N(2)-Ru-N(1)	79.12(8)
N(4)-Ru-N(1)	89.01(7)
N(2)-Ru-N(3)	79.60(8)
N(4)-Ru-N(3)	89.93(7)
N(1)-Ru-N(3)	158.28(8)
N(2)-Ru-N(5)	176.84(8)
N(4)-Ru-N(5)	78.69(7)
N(1)-Ru-N(5)	99.01(7)
N(3)-Ru-N(5)	102.05(8)

Table D.3. continued.

Bond	Angle
N(2)-Ru-N(6)	87.96(8)
N(4)-Ru-N(6)	173.22(7)
N(1)-Ru-N(6)	93.62(8)
N(3)-Ru-N(6)	89.92(8)
N(5)-Ru-N(6)	94.72(7)
C(11)-N(1)-C(15)	117.6(2)
C(11)-N(1)-Ru	128.2(2)
C(15)-N(1)-Ru	114.0(2)
C(5)-N(2)-C(1)	121.7(2)
C(5)-N(2)-Ru	118.8(2)
C(1)-N(2)-Ru	119.3(2)
C(10)-N(3)-C(6)	117.9(2)
C(10)-N(3)-Ru	129.0(2)
C(6)-N(3)-Ru	113.0(2)
C(21)-N(4)-C(25)	117.9(2)
C(21)-N(4)-Ru	127.1(2)
C(25)-N(4)-Ru	114.96(14)
C(32)-N(5)-C(29)	116.7(2)
C(32)-N(5)-Ru	129.1(2)
C(29)-N(5)-Ru	114.20(14)
C(16)-N(6)-C(20)	116.5(2)
C(16)-N(6)-Ru	123.0(2)
C(20)-N(6)-Ru	120.5(2)
N(2)-C(1)-C(2)	120.0(2)
N(2)-C(1)-C(15)	112.8(2)
C(2)-C(1)-C(15)	127.2(2)
C(3)-C(2)-C(1)	118.6(3)
C(3)-C(2)-H(2)	123(2)
C(1)-C(2)-H(2)	119(2)
C(4)-C(3)-C(2)	120.5(3)
C(4)-C(3)-H(3)	122(2)
C(2)-C(3)-H(3)	118(2)
C(3)-C(4)-C(5)	119.3(3)
C(3)-C(4)-H(4)	122(2)
C(5)-C(4)-H(4)	119(2)
N(2)-C(5)-C(4)	119.8(2)
N(2)-C(5)-C(6)	112.8(2)
C(4)-C(5)-C(6)	127.3(2)
N(3)-C(6)-C(7)	121.1(2)
N(3)-C(6)-C(5)	115.3(2)
C(7)-C(6)-C(5)	123.6(2)
C(8)-C(7)-C(6)	120.4(3)

Table D.3. continued.

Bond	Angle
C(8)-C(7)-H(7)	120(2)
C(6)-C(7)-H(7)	119(2)
C(7)-C(8)-C(9)	118.7(3)
C(7)-C(8)-H(8)	121(2)
C(9)-C(8)-H(8)	121(2)
C(8)-C(9)-C(10)	119.4(3)
C(8)-C(9)-H(9)	126(2)
C(10)-C(9)-H(9)	115(2)
N(3)-C(10)-C(9)	122.6(3)
N(3)-C(10)-H(10)	117(2)
C(9)-C(10)-H(10)	121(2)
N(1)-C(11)-C(12)	122.6(2)
N(1)-C(11)-H(11)	114(2)
C(12)-C(11)-H(11)	123(2)
C(11)-C(12)-C(13)	119.7(3)
C(11)-C(12)-H(12)	118(2)
C(13)-C(12)-H(12)	122(2)
C(12)-C(13)-C(14)	118.6(3)
C(12)-C(13)-H(13)	121(2)
C(14)-C(13)-H(13)	121(2)
C(15)-C(14)-C(13)	119.7(3)
C(15)-C(14)-H(14)	119(2)
C(13)-C(14)-H(14)	121(2)
N(1)-C(15)-C(14)	121.6(2)
N(1)-C(15)-C(1)	114.5(2)
C(14)-C(15)-C(1)	123.9(2)
N(6)-C(16)-C(17)	123.0(3)
N(6)-C(16)-H(16)	115(2)
C(17)-C(16)-H(16)	122(2)
C(18)-C(17)-C(16)	119.3(3)
C(18)-C(17)-H(17)	123(2)
C(16)-C(17)-H(17)	118(2)
C(19)-C(18)-C(17)	118.2(3)
C(19)-C(18)-H(18)	121(2)
C(17)-C(18)-H(18)	121(2)
C(18)-C(19)-C(20)	120.1(3)
C(18)-C(19)-H(19)	123(2)
C(20)-C(19)-H(19)	117(2)
N(6)-C(20)-C(19)	122.8(3)
N(6)-C(20)-H(20)	114(2)
C(19)-C(20)-H(20)	124(2)
N(4)-C(21)-C(22)	122.4(2)

Table D.3. continued.

Bond	Angle
N(4)-C(21)-H(21)	117(2)
C(22)-C(21)-H(21)	120(2)
C(23)-C(22)-C(21)	121.1(2)
C(23)-C(22)-H(22)	121(2)
C(21)-C(22)-H(22)	117(2)
C(22)-C(23)-C(24)	117.9(2)
C(22)-C(23)-C(33)	120.0(2)
C(24)-C(23)-C(33)	122.1(2)
C(25)-C(24)-C(23)	117.6(2)
C(25)-C(24)-C(26)	117.6(2)
C(23)-C(24)-C(26)	124.8(2)
N(4)-C(25)-C(24)	123.0(2)
N(4)-C(25)-C(29)	116.5(2)
C(24)-C(25)-C(29)	120.4(2)
C(27)-C(26)-C(24)	121.6(2)
C(27)-C(26)-H(26)	120(2)
C(24)-C(26)-H(26)	118(2)
C(26)-C(27)-C(28)	121.7(2)
C(26)-C(27)-H(27)	120(2)
C(28)-C(27)-H(27)	118(2)
C(29)-C(28)-C(30)	117.9(2)
C(29)-C(28)-C(27)	117.5(2)
C(30)-C(28)-C(27)	124.6(2)
N(5)-C(29)-C(28)	123.8(2)
N(5)-C(29)-C(25)	115.3(2)
C(28)-C(29)-C(25)	120.8(2)
C(31)-C(30)-C(28)	117.3(2)
C(31)-C(30)-C(39)	119.2(2)
C(28)-C(30)-C(39)	123.5(2)
C(30)-C(31)-C(32)	121.2(2)
C(30)-C(31)-H(31)	120(2)
C(32)-C(31)-H(31)	119(2)
N(5)-C(32)-C(31)	123.1(2)
N(5)-C(32)-H(32)	115.1(14)
C(31)-C(32)-H(32)	121.8(14)
C(38)-C(33)-C(34)	119.6(2)
C(38)-C(33)-C(23)	120.0(2)
C(34)-C(33)-C(23)	120.2(2)
C(35)-C(34)-C(33)	119.9(2)
C(35)-C(34)-H(34)	121(2)
C(33)-C(34)-H(34)	119.6(14)
C(36)-C(35)-C(34)	120.0(2)

Table D.3. continued.

Bond	Angle
C(36)-C(35)-H(35)	123.4(14)
C(34)-C(35)-H(35)	116.6(14)
C(35)-C(36)-C(37)	120.7(2)
C(35)-C(36)-H(36)	118(2)
C(37)-C(36)-H(36)	121(2)
C(36)-C(37)-C(38)	119.5(2)
C(36)-C(37)-H(37)	122(2)
C(38)-C(37)-H(37)	118(2)
C(33)-C(38)-C(37)	120.2(2)
C(33)-C(38)-H(38)	121(2)
C(37)-C(38)-H(38)	119(2)
C(40)-C(39)-C(44)	118.8(2)
C(40)-C(39)-C(30)	121.4(2)
C(44)-C(39)-C(30)	119.7(2)
C(41)-C(40)-C(39)	120.1(3)
C(41)-C(40)-H(40)	117(2)
C(39)-C(40)-H(40)	122(2)
C(42)-C(41)-C(40)	120.4(3)
C(42)-C(41)-H(41)	122(2)
C(40)-C(41)-H(41)	118(2)
C(41)-C(42)-C(43)	120.1(3)
C(41)-C(42)-H(42)	120(2)
C(43)-C(42)-H(42)	120(2)
C(42)-C(43)-C(44)	120.2(3)
C(42)-C(43)-H(43)	122(2)
C(44)-C(43)-H(43)	118(2)
C(43)-C(44)-C(39)	120.3(3)
C(43)-C(44)-H(44)	122(2)
C(39)-C(44)-H(44)	118(2)
F(4)-P(1)-F(5)	90.1(6)
F(3')-P(1)-F(6')	86(2)
F(4)-P(1)-F(6)	179.2(6)
F(5)-P(1)-F(6)	90.6(6)
F(3')-P(1)-F(1)	81.2(13)
F(4)-P(1)-F(1)	87.7(4)
F(5)-P(1)-F(1)	89.9(6)
F(6')-P(1)-F(1)	87.4(14)
F(6)-P(1)-F(1)	91.9(5)
F(3')-P(1)-F(5')	175(2)
F(6')-P(1)-F(5')	90(2)
F(1)-P(1)-F(5')	95(2)
F(3')-P(1)-F(2)	97.8(13)

Table D.3. continued.

Bond	Angle
F(4)-P(1)-F(2)	93.3(4)
F(5)-P(1)-F(2)	90.9(6)
F(6')-P(1)-F(2)	91.7(14)
F(6)-P(1)-F(2)	87.1(5)
F(1)-P(1)-F(2)	178.70(12)
F(5')-P(1)-F(2)	86(2)
F(4)-P(1)-F(3)	89.3(5)
F(5)-P(1)-F(3)	179.0(8)
F(6)-P(1)-F(3)	90.0(6)
F(1)-P(1)-F(3)	90.9(5)
F(2)-P(1)-F(3)	88.3(4)
F(3')-P(1)-F(4')	92.9(13)
F(6')-P(1)-F(4')	175(2)
F(1)-P(1)-F(4')	98(2)
F(5')-P(1)-F(4')	91(2)
F(2)-P(1)-F(4')	83(2)
F(13')-P(2)-F(16')	90.1(10)
F(15)-P(2)-F(16)	92.4(8)
F(15)-P(2)-F(14)	93.6(7)
F(16)-P(2)-F(14)	172.7(8)
F(15)-P(2)-F(12)	93.2(6)
F(13')-P(2)-F(12)	88.9(5)
F(16')-P(2)-F(12)	90.7(6)
F(16)-P(2)-F(12)	89.5(4)
F(14)-P(2)-F(12)	94.4(7)
F(13')-P(2)-F(14')	94.2(10)
F(16')-P(2)-F(14')	174.2(10)
F(12)-P(2)-F(14')	85.6(7)
F(15)-P(2)-F(13)	175.8(8)
F(16)-P(2)-F(13)	87.2(8)
F(14)-P(2)-F(13)	86.5(8)
F(12)-P(2)-F(13)	91.0(5)
F(15)-P(2)-F(11)	86.9(6)
F(13')-P(2)-F(11)	91.1(5)
F(16')-P(2)-F(11)	88.4(6)
F(16)-P(2)-F(11)	89.7(4)
F(14)-P(2)-F(11)	86.5(7)
F(12)-P(2)-F(11)	179.13(12)
F(14')-P(2)-F(11)	95.3(7)
F(13)-P(2)-F(11)	88.9(6)
F(13')-P(2)-F(15')	176.4(9)
F(16')-P(2)-F(15')	88.9(9)

Table D.3. continued.

Bond	Angle
F(12)-P(2)-F(15')	87.6(6)
F(14')-P(2)-F(15')	86.6(10)
F(11)-P(2)-F(15')	92.3(6)

Table D.4. Anisotropic displacement parameters (Å^2 x 10^3) for Rutdp. The anisotropic displacement factor exponent takes the form: $-2\pi^2[h^2 a^{*2} U11 + 2 h k a^* b^* U12]$

Atom	U11	U22	U33	U23	U13	U12
Ru	19(1)	21(1)	15(1)	0(1)	8(1)	1(1)
N(1)	21(1)	23(1)	16(1)	0(1)	7(1)	3(1)
N(2)	19(1)	25(1)	17(1)	0(1)	8(1)	0(1)
N(3)	23(1)	23(1)	17(1)	-1(1)	8(1)	-2(1)
N(4)	18(1)	21(1)	18(1)	-1(1)	9(1)	1(1)
N(5)	18(1)	21(1)	16(1)	-1(1)	7(1)	0(1)
N(6)	22(1)	27(1)	16(1)	1(1)	9(1)	4(1)
C(1)	23(1)	24(1)	22(1)	-3(1)	10(1)	1(1)
C(2)	36(2)	27(2)	38(2)	-7(1)	21(1)	0(1)
C(3)	41(2)	35(2)	46(2)	-11(1)	31(2)	0(1)
C(4)	33(2)	39(2)	36(2)	-6(1)	24(1)	-2(1)
C(5)	23(1)	27(1)	24(1)	-1(1)	12(1)	-1(1)
C(6)	23(1)	26(1)	20(1)	-1(1)	11(1)	0(1)
C(7)	30(2)	36(2)	35(2)	-1(1)	19(1)	-2(1)
C(8)	28(2)	34(2)	36(2)	4(1)	12(1)	-7(1)
C(9)	34(2)	24(2)	33(2)	-1(1)	12(1)	-3(1)
C(10)	31(1)	26(1)	24(1)	-2(1)	12(1)	0(1)
C(11)	27(1)	25(1)	27(1)	-1(1)	14(1)	1(1)
C(12)	36(2)	34(2)	41(2)	2(1)	24(1)	-4(1)
C(13)	47(2)	26(2)	50(2)	1(1)	29(2)	-5(1)
C(14)	37(2)	24(1)	38(2)	-2(1)	21(1)	1(1)
C(15)	22(1)	25(1)	20(1)	-1(1)	7(1)	0(1)
C(16)	26(1)	35(2)	22(1)	-4(1)	9(1)	4(1)
C(17)	29(1)	46(2)	23(1)	-8(1)	8(1)	6(1)
C(18)	34(2)	57(2)	21(1)	7(1)	8(1)	13(1)
C(19)	49(2)	46(2)	35(2)	18(2)	11(2)	5(2)
C(20)	35(2)	34(2)	28(1)	6(1)	9(1)	2(1)
C(21)	22(1)	27(1)	23(1)	-1(1)	11(1)	3(1)
C(22)	17(1)	27(1)	26(1)	1(1)	8(1)	4(1)
C(23)	18(1)	21(1)	21(1)	1(1)	7(1)	0(1)
C(24)	19(1)	20(1)	17(1)	0(1)	8(1)	1(1)
C(25)	18(1)	19(1)	18(1)	-1(1)	9(1)	-1(1)
C(26)	24(1)	27(1)	16(1)	1(1)	9(1)	3(1)
C(27)	25(1)	30(1)	19(1)	-1(1)	14(1)	5(1)
C(28)	20(1)	21(1)	19(1)	-1(1)	9(1)	-1(1)
C(29)	18(1)	20(1)	18(1)	0(1)	7(1)	0(1)
C(30)	20(1)	24(1)	22(1)	-1(1)	10(1)	2(1)
C(31)	19(1)	31(2)	21(1)	1(1)	6(1)	7(1)
C(32)	22(1)	28(1)	17(1)	-1(1)	7(1)	1(1)

Table D.4. continued.

Atom	U11	U22	U33	U23	U13	U12
C(33)	15(1)	25(1)	20(1)	1(1)	7(1)	2(1)
C(34)	21(1)	25(1)	24(1)	1(1)	8(1)	2(1)
C(35)	21(1)	31(2)	24(1)	-7(1)	9(1)	-4(1)
C(36)	21(1)	41(2)	18(1)	-1(1)	5(1)	-1(1)
C(37)	24(1)	31(2)	23(1)	8(1)	8(1)	6(1)
C(38)	26(1)	24(1)	23(1)	-2(1)	11(1)	0(1)
C(39)	25(1)	29(1)	19(1)	4(1)	9(1)	10(1)
C(40)	28(2)	39(2)	25(1)	0(1)	8(1)	10(1)
C(41)	47(2)	45(2)	23(1)	-4(1)	9(1)	21(2)
C(42)	49(2)	57(2)	29(2)	10(2)	22(2)	33(2)
C(43)	33(2)	52(2)	40(2)	18(2)	24(1)	18(2)
C(44)	28(1)	31(2)	29(1)	4(1)	13(1)	6(1)
P(1)	30(1)	31(1)	34(1)	-1(1)	17(1)	1(1)
F(1)	64(1)	39(1)	77(1)	9(1)	21(1)	17(1)
F(2)	47(1)	53(1)	55(1)	10(1)	23(1)	20(1)
F(3)	48(3)	34(2)	105(7)	3(3)	51(4)	3(2)
F(4)	77(4)	59(4)	36(3)	-13(2)	26(2)	9(2)
F(5)	70(7)	52(3)	119(6)	-15(3)	74(6)	-15(4)
F(6)	90(4)	68(4)	37(4)	-18(3)	14(3)	11(3)
F(3')	32(6)	29(7)	68(13)	-6(8)	22(8)	-14(5)
F(4')	41(8)	143(27)	47(9)	-4(14)	25(6)	31(12)
F(5')	39(9)	70(14)	160(32)	-14(16)	39(14)	-31(8)
F(6')	79(13)	127(22)	33(11)	35(12)	41(11)	55(14)
P(2)	38(1)	28(1)	43(1)	-2(1)	21(1)	0(1)
F(11)	63(1)	61(1)	66(1)	- 10(1)	43(1)	7(1)
F(12)	85(2)	61(1)	59(1)	-2(1)	49(	8(1)
F(13)	48(4)	133(10)	66(5)	35(5)	21(4)	28(5)
F(14)	91(7)	34(3)	112(9)	-20(5)	70(7)	-21(4)
F(15)	45(4)	131(10)	49(4)	8(4)	-13(3)	12(5)
F(16)	72(5)	29(4)	101(8)	-1(4)	58(5)	-7(4)
F(13')	117(12)	63(6)	59(6)	42(4)	62(8)	70(7)
F(14')	89(10)	71(9)	111(11)	-46(8)	71(9)	-47(7)
F(15')	118(11)	69(7)	52(5)	7(4)	22(6)	64(7)
F(16')	96(8)	97(11)	64(6)	-37(7)	26(5)	-61(7)

Table D.5. Hydrogen coordinates (x 10^4) and isotropic displacement parameters (Å^2 x 10^3) for Rutdp.

Atom	x	y	z	U
H(2)	7586(26)	7679(9)	7212(25)	36(8)
H(3)	6150(28)	7354(9)	7853(26)	42(8)
H(4)	5835(27)	6655(8)	7587(25)	35(8)
H(7)	5445(25)	6005(8)	6907(24)	28(7)
H(8)	5244(27)	5339(9)	6304(25)	39(8)
H(9)	6588(26)	5113(9)	5338(25)	34(8)
H(10)	7969(27)	5544(9)	5088(26)	38(8)
H(11)	10631(23)	6934(8)	4835(22)	21(7)
H(12)	11195(27)	7590(8)	4745(25)	36(8)
H(13)	10296(26)	8091(9)	5493(25)	34(8)
H(14)	8855(27)	7902(9)	6286(26)	38(8)
H(16)	10786(28)	6903(9)	7847(26)	43(9)
H(17)	12286(29)	6778(9)	9882(28)	46(9)
H(18)	12547(29)	6122(9)	10675(28)	46(9)
H(19)	11289(27)	5631(9)	9352(26)	35(8)
H(20)	9795(29)	5773(9)	7380(28)	48(9)
H(21)	6083(26)	6786(8)	3895(25)	36(8)
H(22)	4779(26)	6790(8)	1806(24)	29(7)
H(26)	7461(22)	6230(7)	99(22)	18(6)
H(27)	9431(23)	5930(7)	1002(22)	18(6)
H(31)	12294(25)	5603(8)	5126(23)	28(7)
H(32)	11246(22)	5921(7)	6232(22)	18(6)
H(34)	5102(22)	5924(7)	-326(21)	15(6)

H(35)	3653(22)	5896(7)	-2363(21)	18(6)
H(36)	2881(25)	6501(8)	-3426(25)	30(7)
H(37)	3490(25)	7111(8)	-2373(24)	29(7)
H(38)	4860(24)	7124(8)	-329(23)	24(7)
H(40)	10181(27)	5169(8)	1708(25)	34(8)
H(41)	11249(30)	4845(9)	768(28)	48(9)
H(42)	13363(28)	5023(9)	1180(26)	42(8)
H(43)	14316(28)	5546(8)	2533(25)	35(8)
H(44)	13247(26)	5866(9)	3502(25)	36(8)

Table D.6. Observed and calculated structure factors for Rutdp

h	k	l	10Fo	10Fc	10s
1	0	0	1220	1196	17
2	0	0	2246	2224	32
3	0	0	638	625	11
4	0	0	1341	1316	20
5	0	0	450	458	10
6	0	0	238	233	9
7	0	0	181	208	13
8	0	0	496	484	8
9	0	0	704	684	9
10	0	0	543	541	11
11	0	0	206	184	26
12	0	0	419	408	19
1	1	0	608	599	6
2	1	0	1514	1472	15
3	1	0	220	226	8
4	1	0	106	85	14
5	1	0	111	155	13
6	1	0	456	479	5
7	1	0	1193	1179	8
8	1	0	222	235	8
9	1	0	493	488	6
10	1	0	417	415	6
11	1	0	256	244	15
12	1	0	125	168	29
1	2	0	329	329	4
2	2	0	1161	1178	9
3	2	0	203	203	6
4	2	0	304	282	5
5	2	0	112	144	11
6	2	0	169	171	8
7	2	0	358	344	8
8	2	0	68	78	23
9	2	0	473	474	5
10	2	0	54	16	54
11	2	0	185	185	15
12	2	0	173	221	21
1	3	0	936	932	8
2	3	0	861	864	6
3	3	0	204	182	4
4	3	0	18	26	18
5	3	0	586	539	7
6	3	0	91	114	15
7	3	0	95	90	15
8	3	0	0	33	1
9	3	0	129	123	11
10	3	0	544	544	7
13	6	0	258	250	26
1	7	0	820	813	6
2	7	0	156	128	8
3	7	0	376	370	5
4	7	0	658	649	6
5	7	0	8	35	7
6	7	0	214	203	7
7	7	0	292	297	6
8	7	0	0	3	1
9	7	0	381	389	8
10	7	0	0	13	1
11	7	0	28	43	28
12	7	0	106	57	39
13	7	0	224	246	30
0	8	0	1186	1207	17
1	8	0	1540	1562	13
2	8	0	90	88	16
3	8	0	558	573	5
4	8	0	276	234	5
5	8	0	300	313	6
6	8	0	362	362	6
7	8	0	265	258	6
8	8	0	551	554	7
9	8	0	162	159	15
10	8	0	300	296	10
11	8	0	150	40	36
12	8	0	214	189	20
13	8	0	284	268	18
1	9	0	2307	2321	20
2	9	0	1080	1113	10
3	9	0	366	372	5
4	9	0	565	562	5
5	9	0	716	746	6
6	9	0	1778	1782	15
7	9	0	505	491	7
8	9	0	0	27	1
9	9	0	272	249	14
10	9	0	462	436	9
11	9	0	535	533	12
12	9	0	0	3	1
13	9	0	138	148	32
0	10	0	386	381	10
1	10	0	227	260	11
2	10	0	608	579	5
3	10	0	1714	1762	13
4	10	0	1265	1274	10
8	13	0	223	236	11
9	13	0	102	130	39
10	13	0	96	106	40
11	13	0	265	264	17
12	13	0	0	39	1
0	14	0	909	955	15
1	14	0	752	752	8
2	14	0	0	25	-1
3	14	0	404	384	7
4	14	0	884	910	14
5	14	0	987	986	10
6	14	0	91	82	31
7	14	0	1075	1064	10
8	14	0	655	644	8
9	14	0	291	269	15
10	14	0	107	113	27
11	14	0	234	225	15
12	14	0	374	371	15
1	15	0	612	631	8
2	15	0	1111	1119	14
3	15	0	164	184	11
4	15	0	0	15	1
5	15	0	306	330	8
6	15	0	1106	1089	11
7	15	0	451	461	8
8	15	0	70	45	41
9	15	0	355	360	10
10	15	0	131	111	29
11	15	0	557	553	10
12	15	0	183	198	25
0	16	0	1310	1301	20
1	16	0	586	585	7
2	16	0	744	737	8
3	16	0	668	675	10
4	16	0	898	874	14
5	16	0	279	285	9
6	16	0	247	268	10
7	16	0	115	122	20
8	16	0	421	435	9
9	16	0	526	524	9
10	16	0	80	88	45
11	16	0	165	146	20
12	16	0	0	34	1
1	17	0	365	335	9
2	17	0	650	643	7
3	17	0	486	450	7
8	20	0	489	500	15
9	20	0	93	76	38
10	20	0	63	35	62
11	20	0	411	411	14
1	21	0	129	188	14
2	21	0	700	692	9
3	21	0	101	95	33
4	21	0	184	195	13
5	21	0	482	469	8
6	21	0	471	464	8
7	21	0	366	363	13
8	21	0	120	102	31
9	21	0	293	298	11
10	21	0	223	224	19
11	21	0	227	245	17
0	22	0	231	219	17
1	22	0	144	93	15
2	22	0	191	120	15
3	22	0	72	43	34
4	22	0	308	315	9
5	22	0	50	12	50
6	22	0	69	13	48
7	22	0	171	156	23
8	22	0	361	347	13
9	22	0	282	283	13
10	22	0	79	45	79
11	22	0	0	65	1
1	23	0	847	826	9
2	23	0	922	933	11
3	23	0	417	407	8
4	23	0	0	25	1
5	23	0	225	205	11
6	23	0	650	649	9
7	23	0	787	780	9
8	23	0	97	110	97
9	23	0	135	125	22
10	23	0	294	284	13
11	23	0	382	367	12
0	24	0	922	936	16
1	24	0	647	651	8
2	24	0	208	144	35
3	24	0	590	612	8
4	24	0	500	495	11
5	24	0	706	718	13
6	24	0	232	248	12
7	24	0	381	388	10
7	28	0	267	248	13
8	28	0	522	523	13
9	28	0	315	322	16
10	28	0	110	111	47
1	29	0	679	691	16
2	29	0	612	617	9
3	29	0	178	139	15
4	29	0	280	275	12
5	29	0	391	405	11
6	29	0	569	573	10
7	29	0	331	350	12
8	29	0	20	111	19
9	29	0	0	9	-1
1	30	0	123	99	29
2	30	0	343	323	13
3	30	0	242	238	16
4	30	0	607	598	14
5	30	0	0	74	1
6	30	0	87	70	72
7	30	0	67	74	67
8	30	0	372	364	16
9	30	0	134	141	28
1	31	0	176	179	19
2	31	0	144	118	25
3	31	0	272	288	12
4	31	0	199	167	30
5	31	0	137	139	21
6	31	0	156	96	21
7	31	0	0	13	1
8	31	0	109	70	34
9	31	0	32	44	31
0	32	0	61	48	61
1	32	0	377	387	12
2	32	0	70	35	70
3	32	0	254	234	13
4	32	0	366	368	11
5	32	0	289	306	13
6	32	0	139	135	24
7	32	0	0	101	1
8	32	0	313	279	14
9	32	0	197	217	23
1	33	0	410	390	12
2	33	0	520	536	30
3	33	0	758	767	10
4	33	0	129	91	25
5	33	0	113	145	28

11	3	0	172	144	31
12	3	0	43	81	42
0	4	0	1535	1520	17
1	4	0	1296	1310	11
2	4	0	1203	1205	8
3	4	0	1169	1180	8
4	4	0	552	586	4
5	4	0	363	380	4
6	4	0	194	186	6
7	4	0	290	288	5
8	4	0	965	958	6
9	4	0	519	511	5
10	4	0	351	346	8
11	4	0	272	252	12
12	4	0	324	332	15
13	4	0	238	219	28
1	5	0	1445	1436	12
2	5	0	1798	1840	13
3	5	0	921	949	7
4	5	0	142	138	6
5	5	0	424	442	4
6	5	0	1026	1015	7
7	5	0	715	709	5
8	5	0	254	256	9
9	5	0	483	491	6
10	5	0	679	665	8
11	5	0	499	477	10
12	5	0	78	5	50
13	5	0	376	393	22
0	6	0	2903	2925	31
1	6	0	1645	1663	14
2	6	0	1642	1674	14
3	6	0	138	131	7
4	6	0	851	864	6
5	6	0	409	448	5
6	6	0	422	428	5
7	6	0	516	527	5
8	6	0	202	197	7
9	6	0	203	196	9
10	6	0	259	260	10
11	6	0	157	105	28
12	6	0	483	483	13
5	10	0	100	87	13
6	10	0	448	451	6
7	10	0	210	203	12
8	10	0	1028	1053	10
9	10	0	466	458	8
10	10	0	52	71	52
11	10	0	176	151	21
12	10	0	182	203	21
13	10	0	500	493	14
1	11	0	289	285	7
2	11	0	1116	1089	10
3	11	0	701	719	6
4	11	0	138	90	8
5	11	0	428	442	7
6	11	0	767	760	8
7	11	0	412	403	8
8	11	0	170	156	28
9	11	0	364	361	9
10	11	0	413	397	10
11	11	0	451	444	12
12	11	0	36	33	36
13	11	0	157	9	46
0	12	0	306	308	8
1	12	0	117	109	12
2	12	0	497	499	6
3	12	0	369	361	6
4	12	0	261	227	5
5	12	0	550	554	6
6	12	0	703	675	8
7	12	0	329	321	8
8	12	0	169	180	14
9	12	0	269	272	11
10	12	0	20	7	19
11	12	0	128	145	28
12	12	0	0	36	1
1	13	0	706	707	12
2	13	0	1400	1425	12
3	13	0	625	636	6
4	13	0	105	106	9
5	13	0	429	429	7
6	13	0	443	424	7
7	13	0	536	525	8
4	17	0	621	620	8
5	17	0	194	201	11
6	17	0	64	31	50
7	17	0	235	247	12
8	17	0	112	128	21
9	17	0	147	124	19
10	17	0	53	13	53
11	17	0	0	3	1
12	17	0	204	198	23
0	18	0	326	262	12
1	18	0	978	1011	9
2	18	0	77	36	30
3	18	0	565	563	7
4	18	0	697	688	8
5	18	0	840	835	9
6	18	0	36	45	36
7	18	0	314	310	10
8	18	0	499	503	10
9	18	0	338	325	11
10	18	0	38	73	37
11	18	0	375	359	12
12	18	0	257	306	36
1	19	0	541	545	9
2	19	0	814	842	8
3	19	0	837	837	9
4	19	0	768	760	9
5	19	0	395	390	9
6	19	0	551	550	8
7	19	0	728	730	9
8	19	0	178	203	18
9	19	0	443	442	10
10	19	0	309	310	12
11	19	0	397	406	11
12	19	0	0	54	1
0	20	0	901	912	15
1	20	0	216	229	10
2	20	0	222	223	10
3	20	0	300	298	9
4	20	0	737	736	8
5	20	0	912	906	9
6	20	0	107	50	24
7	20	0	516	508	11
8	24	0	705	707	17
9	24	0	410	406	10
10	24	0	0	108	1
11	24	0	262	256	22
1	25	0	169	116	37
2	25	0	1157	1182	11
3	25	0	685	698	9
4	25	0	264	240	11
5	25	0	229	205	13
6	25	0	352	347	10
7	25	0	413	427	10
8	25	0	128	130	30
9	25	0	387	372	11
10	25	0	331	337	13
0	26	0	438	464	14
1	26	0	299	314	13
2	26	0	178	176	24
3	26	0	0	8	1
4	26	0	379	391	10
5	26	0	534	526	9
6	26	0	80	91	41
7	26	0	70	77	70
8	26	0	67	9	66
9	26	0	0	53	1
10	26	0	212	226	17
1	27	0	448	429	22
2	27	0	238	247	12
3	27	0	57	38	57
4	27	0	341	341	10
5	27	0	393	407	10
6	27	0	41	121	40
7	27	0	148	152	20
8	27	0	297	307	26
9	27	0	167	171	21
10	27	0	277	236	15
0	28	0	534	560	14
1	28	0	565	566	10
2	28	0	61	7	60
3	28	0	370	374	9
4	28	0	336	325	13
5	28	0	267	255	12
6	28	0	105	102	29
6	33	0	316	318	13
7	33	0	210	239	23
8	33	0	79	77	79
0	34	0	454	465	16
1	34	0	454	437	11
2	34	0	101	77	41
3	34	0	575	576	12
4	34	0	455	441	10
5	34	0	302	314	12
6	34	0	149	126	35
7	34	0	94	101	57
8	34	0	481	482	12
1	35	0	421	427	12
2	35	0	212	198	20
3	35	0	282	262	17
4	35	0	220	239	21
5	35	0	0	6	1
6	35	0	389	363	12
7	35	0	188	199	19
0	36	0	127	95	50
1	36	0	95	59	94
2	36	0	80	52	80
3	36	0	119	27	38
4	36	0	170	171	21
5	36	0	90	104	45
6	36	0	135	140	31
7	36	0	131	142	29
1	37	0	227	182	18
2	37	0	270	263	18
3	37	0	265	290	18
4	37	0	198	167	18
5	37	0	176	193	21
6	37	0	293	293	16
7	37	0	182	148	28
0	38	0	531	557	17
1	38	0	258	247	18
2	38	0	117	36	36
3	38	0	168	137	42
4	38	0	369	367	24
5	38	0	409	393	16
6	38	0	0	10	1
1	39	0	177	169	24

Table D.6. Observed and calculated structure factors for Rutdp

h	k	l	10Fo	10Fc	10s
2	39	0	457	460	12
3	39	0	494	509	13
4	39	0	242	214	20
6	3	1	908	922	9
7	3	1	578	567	6
8	3	1	548	543	7
-6	7	1	413	394	5
-5	7	1	150	168	9
-4	7	1	1240	1283	9
4	10	1	393	396	5
5	10	1	376	374	5
6	10	1	795	787	8
-11	14	1	69	39	68
-10	14	1	280	265	18
-9	14	1	99	137	25

5	39	0	192	184	42
0	40	0	106	95	75
1	40	0	208	208	24
2	40	0	0	42	1
3	40	0	202	199	24
4	40	0	311	289	23
5	40	0	115	135	45
1	41	0	112	49	40
2	41	0	176	202	27
3	41	0	99	21	49
4	41	0	61	96	60
0	42	0	399	412	21
1	42	0	191	206	26
2	42	0	98	134	63
3	42	0	112	137	46
1	43	0	159	177	32
-13	1	1	168	140	25
-12	1	1	0	25	-1
-11	1	1	230	232	13
-10	1	1	361	374	8
-9	1	1	583	575	6
-8	1	1	411	402	8
-7	1	1	494	513	6
-6	1	1	854	832	7
-5	1	1	54	37	22
-4	1	1	963	980	7
-3	1	1	295	269	4
-2	1	1	790	778	7
-1	1	1	1590	1562	17
0	1	1	1703	1686	14
1	1	1	399	354	3
2	1	1	63	54	21
3	1	1	293	287	6
4	1	1	746	739	8
5	1	1	867	855	8
6	1	1	773	728	8
7	1	1	178	178	10
8	1	1	246	234	7
9	1	1	421	420	6
10	1	1	131	134	16
11	1	1	299	314	19
-13	2	1	291	270	16
-12	2	1	0	30	1
-11	2	1	190	160	15
-10	2	1	583	572	9
-9	2	1	987	976	8
-8	2	1	419	429	5
-7	2	1	574	588	4
-6	2	1	342	370	5
-5	2	1	405	425	4
9	3	1	404	403	6
10	3	1	491	478	6
11	3	1	167	143	29
-13	4	1	302	330	16
-12	4	1	0	27	1
-11	4	1	473	463	12
-10	4	1	0	27	1
-9	4	1	373	375	6
-8	4	1	100	113	13
-7	4	1	816	823	6
-6	4	1	65	64	15
-5	4	1	796	782	5
-4	4	1	744	774	5
-3	4	1	380	376	4
-2	4	1	2048	2023	14
-1	4	1	871	871	6
0	4	1	774	804	5
1	4	1	1204	1203	9
2	4	1	1899	1937	13
3	4	1	310	312	6
4	4	1	811	800	8
5	4	1	226	200	10
6	4	1	624	588	6
7	4	1	230	234	8
8	4	1	570	554	5
9	4	1	233	228	10
10	4	1	0	33	1
11	4	1	0	21	-1
-13	5	1	188	224	21
-12	5	1	135	161	20
-11	5	1	283	288	25
-10	5	1	209	213	15
-9	5	1	146	138	11
-8	5	1	346	340	5
-7	5	1	845	806	6
-6	5	1	155	166	7
-5	5	1	176	180	8
-4	5	1	408	397	4
-3	5	1	123	109	7
-2	5	1	1344	1348	10
-1	5	1	981	972	7
0	5	1	197	171	6
1	5	1	297	326	8
2	5	1	234	226	5
3	5	1	324	333	6
4	5	1	251	242	5
5	5	1	318	293	5
6	5	1	755	742	6
7	5	1	43	8	43
8	5	1	553	560	6
-3	7	1	1210	1268	9
-2	7	1	728	752	6
-1	7	1	3478	3454	26
0	7	1	760	763	5
1	7	1	890	890	8
2	7	1	1709	1768	15
3	7	1	225	195	9
4	7	1	1032	1097	7
5	7	1	1159	1167	10
6	7	1	355	353	5
7	7	1	113	121	13
8	7	1	735	732	7
9	7	1	882	885	8
10	7	1	235	234	11
11	7	1	67	11	66
12	7	1	501	466	19
-13	8	1	200	202	21
-12	8	1	164	129	24
-11	8	1	50	21	50
-10	8	1	637	633	9
-9	8	1	620	635	8
-8	8	1	321	325	6
-7	8	1	373	370	5
-6	8	1	888	897	7
-5	8	1	1450	1436	11
-4	8	1	293	274	5
-3	8	1	709	720	6
-2	8	1	1953	1931	14
-1	8	1	2265	2254	17
0	8	1	537	529	4
1	8	1	363	376	6
2	8	1	450	458	6
3	8	1	961	1003	8
4	8	1	702	720	6
5	8	1	430	439	5
6	8	1	947	929	7
7	8	1	436	423	7
8	8	1	333	347	8
9	8	1	315	319	8
10	8	1	307	296	9
11	8	1	264	260	15
12	8	1	245	221	29
-13	9	1	55	6	55
-12	9	1	120	148	33
-11	9	1	390	395	12
-10	9	1	271	271	13
-9	9	1	93	106	26
-8	9	1	100	97	18
-7	9	1	223	231	7
-6	9	1	107	122	11
7	10	1	139	134	16
8	10	1	90	63	28
9	10	1	161	130	16
10	10	1	88	125	34
11	10	1	204	244	20
-13	11	1	218	261	20
-12	11	1	631	613	20
-11	11	1	219	248	17
-10	11	1	279	269	11
-9	11	1	208	215	12
-8	11	1	571	570	7
-7	11	1	875	875	8
-6	11	1	411	398	6
-5	11	1	282	298	6
-4	11	1	1061	1102	8
-3	11	1	1861	1894	14
-2	11	1	114	102	11
-1	11	1	217	217	7
0	11	1	1069	1117	10
1	11	1	563	579	5
2	11	1	296	304	8
3	11	1	146	106	11
4	11	1	630	641	7
5	11	1	577	564	7
6	11	1	729	728	8
7	11	1	282	292	9
8	11	1	538	545	9
9	11	1	692	657	9
10	11	1	159	163	18
11	11	1	0	21	1
12	11	1	205	193	29
-13	12	1	369	389	15
-12	12	1	153	123	59
-11	12	1	264	278	16
-10	12	1	872	851	10
-9	12	1	386	395	9
-8	12	1	233	219	12
-7	12	1	54	66	43
-6	12	1	807	824	7
-5	12	1	2001	1996	15
-4	12	1	330	334	5
-3	12	1	67	95	18
-2	12	1	1494	1480	11
-1	12	1	1582	1641	12
0	12	1	271	303	8
1	12	1	565	520	6
2	12	1	1595	1654	14
3	12	1	61	24	42
4	12	1	614	613	15
5	12	1	303	301	8
-8	14	1	0	28	1
-7	14	1	240	219	9
-6	14	1	55	53	54
-5	14	1	1083	1085	10
-4	14	1	212	210	7
-3	14	1	116	102	10
-2	14	1	106	55	23
-1	14	1	218	209	6
0	14	1	101	83	21
1	14	1	226	235	10
2	14	1	580	527	9
3	14	1	497	486	7
4	14	1	901	920	9
5	14	1	207	215	11
6	14	1	714	717	8
7	14	1	59	11	58
8	14	1	133	158	17
9	14	1	29	106	29
10	14	1	207	218	15
11	14	1	167	189	19
12	14	1	95	35	47
-12	15	1	123	112	34
-11	15	1	138	141	27
-10	15	1	0	71	1
-9	15	1	102	90	41
-8	15	1	92	62	27
-7	15	1	47	56	47
-6	15	1	179	147	13
-5	15	1	489	482	13
-4	15	1	563	554	6
-3	15	1	778	751	7
-2	15	1	435	439	10
-1	15	1	838	808	8
0	15	1	418	415	8
1	15	1	344	353	10
2	15	1	1012	965	10
3	15	1	889	850	9
4	15	1	427	445	12
5	15	1	897	911	9
6	15	1	76	45	30
7	15	1	292	294	10
8	15	1	70	78	70
9	15	1	0	97	1
10	15	1	0	71	1
11	15	1	239	254	20
12	15	1	168	165	34
-12	16	1	62	26	61
-11	16	1	199	201	22
-10	16	1	122	95	23
-9	16	1	460	461	9

-4	2	1	709	731	5	9	5	1	0	11	1	-5	9	1	94	76	20	6	12	1	1245	1244	12	-8	16	1	243	240	18
-3	2	1	671	659	5	10	5	1	171	178	12	-4	9	1	926	938	8	7	12	1	1143	1141	11	-7	16	1	731	735	8
-2	2	1	2638	2611	19	11	5	1	0	14	1	-3	9	1	806	808	7	8	12	1	253	240	11	-6	16	1	291	300	8
-1	2	1	1582	1599	12	-13	6	1	79	17	79	-2	9	1	1112	1091	9	9	12	1	244	236	17	-5	16	1	103	107	19
0	2	1	59	73	8	-12	6	1	73	96	73	-1	9	1	518	520	13	10	12	1	376	356	10	-4	16	1	1012	1041	10
1	2	1	1284	1312	9	-11	6	1	143	153	25	0	9	1	905	912	10	11	12	1	330	307	12	-3	16	1	563	558	6
2	2	1	864	861	8	-10	6	1	730	711	9	1	9	1	897	936	9	12	12	1	260	266	20	-2	16	1	1842	1864	14
3	2	1	527	557	6	-9	6	1	397	402	7	2	9	1	387	402	8	-13	13	1	227	236	21	-1	16	1	428	424	7
4	2	1	610	625	7	-8	6	1	30	33	30	3	9	1	614	618	7	-12	13	1	496	484	13	0	16	1	297	320	14
5	2	1	164	200	10	-7	6	1	595	580	6	4	9	1	339	320	5	-11	13	1	346	336	20	1	16	1	282	218	21
6	2	1	733	726	8	-6	6	1	326	350	5	5	9	1	25	32	25	-10	13	1	73	10	47	2	16	1	461	489	5
7	2	1	566	555	7	-5	6	1	1143	1154	8	6	9	1	525	524	5	-9	13	1	363	373	12	3	16	1	784	821	8
8	2	1	638	642	6	-4	6	1	28	12	28	7	9	1	224	224	9	-8	13	1	936	942	10	4	16	1	309	317	9
9	2	1	319	317	7	-3	6	1	619	618	5	8	9	1	647	657	7	-7	13	1	690	700	7	5	16	1	606	606	8
10	2	1	519	515	6	-2	6	1	719	695	8	9	9	1	0	10	1	-6	13	1	745	743	8	6	16	1	657	655	8
11	2	1	670	655	18	-1	6	1	1339	1329	9	10	9	1	0	15	1	-5	13	1	267	268	8	7	16	1	501	491	8
-13	3	1	0	15	-1	0	6	1	1460	1449	9	11	9	1	179	185	17	-4	13	1	104	105	13	8	16	1	217	234	13
-12	3	1	328	302	13	1	6	1	1050	1071	9	12	9	1	176	163	42	-3	13	1	1635	1669	15	9	16	1	21	85	21
-11	3	1	823	795	10	2	6	1	793	820	7	-13	10	1	38	6	38	-2	13	1	1333	1314	13	10	16	1	518	510	20
-10	3	1	207	206	18	3	6	1	88	93	13	-12	10	1	75	21	75	-1	13	1	221	183	15	11	16	1	246	260	14
-9	3	1	883	859	7	4	6	1	719	696	5	-11	10	1	125	143	37	0	13	1	951	970	12	12	16	1	117	170	116
-8	3	1	319	315	5	5	6	1	198	178	6	-10	10	1	97	85	38	1	13	1	495	487	6	-12	17	1	364	388	15
-7	3	1	507	513	6	6	6	1	1009	1000	7	-9	10	1	0	10	1	2	13	1	746	764	8	-11	17	1	485	500	13
-6	3	1	138	146	8	7	6	1	668	673	5	-8	10	1	168	162	11	3	13	1	581	579	7	-10	17	1	99	72	29
-5	3	1	122	129	7	8	6	1	183	176	13	-7	10	1	354	352	6	4	13	1	1621	1642	14	-9	17	1	444	456	9
-4	3	1	1185	1203	7	9	6	1	75	74	32	-6	10	1	123	126	11	5	13	1	173	161	12	-8	17	1	422	427	9
-3	3	1	1401	1392	9	10	6	1	450	447	8	-5	10	1	754	735	6	6	13	1	272	268	9	-7	17	1	566	561	8
-2	3	1	691	668	5	11	6	1	466	455	8	-4	10	1	221	222	6	7	13	1	161	164	15	-6	17	1	528	536	8
-1	3	1	329	312	3	-13	7	1	188	166	17	-3	10	1	1040	1048	14	8	13	1	663	643	9	-5	17	1	464	470	7
0	3	1	2691	2686	18	-12	7	1	360	361	22	-2	10	1	907	902	9	9	13	1	616	584	9	-4	17	1	1514	1555	12
1	3	1	2755	2757	20	-11	7	1	378	357	17	-1	10	1	81	66	14	10	13	1	59	43	58	-3	17	1	1526	1520	12
2	3	1	954	929	10	-10	7	1	206	201	13	0	10	1	39	44	39	11	13	1	207	219	28	-2	17	1	330	276	23
3	3	1	836	853	8	-9	7	1	338	316	9	1	10	1	795	811	6	12	13	1	346	357	15	-1	17	1	1023	1011	10
4	3	1	962	966	9	-8	7	1	1062	1066	8	2	10	1	575	554	6	-13	14	1	119	142	41	0	17	1	1137	1169	12
5	3	1	838	839	8	-7	7	1	774	787	6	3	10	1	246	237	8	-12	14	1	76	107	75	1	17	1	156	183	12

Table D.6. Observed and calculated structure factors for Rutdp

h	k	l	10Fo	10Fc	10s	h	k	l	10Fo	10Fc	10s	h	k	l	10Fo	10Fc	10s	h	k	l	10Fo	10Fc	10s	h	k	l	10Fo	10Fc	10s
2	17	1	0	12	1	-6	21	1	0	31	1	-8	25	1	489	482	10	-3	29	1	299	323	12	-6	34	1	226	200	24
3	17	1	441	408	7	-5	21	1	287	296	9	-7	25	1	339	324	9	-2	29	1	230	211	17	-5	34	1	179	152	15
4	17	1	486	475	7	-4	21	1	217	223	11	-6	25	1	31	17	31	-1	29	1	160	137	22	-4	34	1	111	100	26
5	17	1	828	826	9	-3	21	1	775	774	8	-5	25	1	136	110	36	0	29	1	399	389	14	-3	34	1	379	381	11
6	17	1	605	619	8	-2	21	1	698	704	11	-4	25	1	0	42	1	1	29	1	63	101	63	-2	34	1	165	179	21
7	17	1	69	65	43	-1	21	1	374	388	10	-3	25	1	909	907	12	2	29	1	112	73	30	-1	34	1	94	59	40
8	17	1	231	211	12	0	21	1	689	711	11	-2	25	1	171	154	21	3	29	1	285	293	12	0	34	1	163	172	21
9	17	1	274	244	35	1	21	1	606	627	10	-1	25	1	141	70	20	4	29	1	61	18	61	1	34	1	110	67	35
10	17	1	94	91	94	2	21	1	64	81	63	0	25	1	403	402	19	5	29	1	98	41	98	2	34	1	0	18	1
11	17	1	0	16	1	3	21	1	186	196	13	1	25	1	577	572	10	6	29	1	165	173	19	3	34	1	401	414	13

-12	18	1	25	112	25
-11	18	1	0	31	1
-10	18	1	602	601	9
-9	18	1	234	215	12
-8	18	1	275	276	11
-7	18	1	29	44	29
-6	18	1	472	467	8
-5	18	1	1018	996	10
-4	18	1	321	304	8
-3	18	1	603	586	6
-2	18	1	366	359	9
-1	18	1	1083	1094	10
0	18	1	716	733	9
1	18	1	81	42	36
2	18	1	1665	1678	25
3	18	1	173	166	12
4	18	1	104	120	19
5	18	1	256	239	10
6	18	1	314	321	10
7	18	1	512	501	8
8	18	1	223	207	13
9	18	1	167	195	23
10	18	1	214	248	21
11	18	1	127	104	26
-12	19	1	0	69	-1
-11	19	1	45	18	44
-10	19	1	151	167	20
-9	19	1	0	63	1
-8	19	1	144	147	17
-7	19	1	220	220	11
-6	19	1	539	528	8
-5	19	1	219	209	15
-4	19	1	904	896	10
-3	19	1	460	435	7
-2	19	1	111	125	17
-1	19	1	126	69	16
0	19	1	523	505	8
1	19	1	374	379	7
2	19	1	238	272	10
3	19	1	336	318	8
4	19	1	628	607	8
5	19	1	0	34	1
6	19	1	111	138	22
7	19	1	194	211	14
8	19	1	176	188	16
9	19	1	136	132	31
10	19	1	125	140	35
11	19	1	0	82	1
-12	20	1	0	81	-1
-11	20	1	302	310	17
4	21	1	867	875	9
5	21	1	832	830	12
6	21	1	378	372	9
7	21	1	145	98	20
8	21	1	369	345	11
9	21	1	652	637	12
10	21	1	444	424	14
11	21	1	299	318	14
-11	22	1	187	158	35
-10	22	1	262	278	13
-9	22	1	698	705	14
-8	22	1	381	369	10
-7	22	1	477	478	9
-6	22	1	792	797	9
-5	22	1	114	96	22
-4	22	1	828	823	14
-3	22	1	190	196	13
-2	22	1	1465	1485	13
-1	22	1	675	686	8
0	22	1	126	100	83
1	22	1	502	495	8
2	22	1	480	469	11
3	22	1	1036	1050	10
4	22	1	224	232	12
5	22	1	0	39	1
6	22	1	288	297	11
7	22	1	622	593	9
8	22	1	172	168	17
9	22	1	140	158	28
10	22	1	542	528	15
11	22	1	174	158	36
-11	23	1	440	427	14
-10	23	1	140	166	22
-9	23	1	321	305	11
-8	23	1	261	240	12
-7	23	1	556	530	11
-6	23	1	463	468	8
-5	23	1	639	627	8
-4	23	1	750	743	9
-3	23	1	288	269	10
-2	23	1	345	339	13
-1	23	1	306	298	11
0	23	1	413	422	10
1	23	1	827	837	10
2	23	1	141	127	17
3	23	1	34	71	33
4	23	1	298	294	10
5	23	1	503	495	8
6	23	1	576	567	9
7	23	1	450	439	9
2	25	1	81	29	40
3	25	1	664	649	10
4	25	1	535	541	9
5	25	1	211	195	17
6	25	1	236	216	15
7	25	1	84	127	37
8	25	1	262	232	13
9	25	1	173	187	24
10	25	1	53	13	53
-11	26	1	279	290	23
-10	26	1	393	388	11
-9	26	1	448	468	11
-8	26	1	89	6	69
-7	26	1	405	423	13
-6	26	1	296	282	11
-5	26	1	475	470	9
-4	26	1	238	233	12
-3	26	1	110	95	38
-2	26	1	206	180	13
-1	26	1	548	564	10
1	26	1	647	652	10
2	26	1	941	931	10
3	26	1	199	190	14
4	26	1	212	192	13
5	26	1	297	287	11
6	26	1	699	703	10
7	26	1	354	342	11
8	26	1	371	361	12
9	26	1	120	135	38
10	26	1	461	478	12
-10	27	1	253	296	17
-9	27	1	341	325	12
-8	27	1	530	552	10
-7	27	1	318	322	14
-6	27	1	162	167	18
-5	27	1	184	175	15
-4	27	1	709	701	9
-3	27	1	623	592	9
-2	27	1	434	432	9
-1	27	1	478	486	10
0	27	1	611	615	10
1	27	1	611	622	10
2	27	1	206	183	13
3	27	1	52	60	52
4	27	1	491	472	9
5	27	1	677	659	13
6	27	1	256	251	14
7	27	1	321	349	12
8	27	1	239	238	18
9	27	1	514	518	13
7	29	1	398	417	15
8	29	1	0	64	1
9	29	1	220	218	22
-10	30	1	259	253	21
-9	30	1	319	312	14
-8	30	1	0	34	-1
-7	30	1	256	235	14
-6	30	1	168	168	15
-5	30	1	115	121	75
-4	30	1	78	70	77
-3	30	1	188	161	22
-2	30	1	380	388	10
-1	30	1	577	564	15
0	30	1	136	42	23
1	30	1	251	229	15
2	30	1	295	284	13
3	30	1	474	468	11
4	30	1	292	276	13
5	30	1	186	172	17
6	30	1	300	297	13
7	30	1	182	170	19
8	30	1	226	237	22
9	30	1	134	153	41
-9	31	1	127	151	28
-8	31	1	443	450	11
-7	31	1	402	395	11
-6	31	1	0	5	1
-5	31	1	265	273	16
-4	31	1	527	525	9
-3	31	1	624	617	9
-2	31	1	268	258	14
-1	31	1	440	435	11
0	31	1	489	469	10
1	31	1	857	866	11
2	31	1	645	654	11
3	31	1	195	203	15
4	31	1	535	529	10
5	31	1	288	291	19
6	31	1	0	115	1
7	31	1	91	107	41
8	31	1	380	378	21
-9	32	1	44	34	43
-8	32	1	0	21	1
-7	32	1	96	72	35
-6	32	1	513	494	8
-5	32	1	448	431	8
-4	32	1	79	41	71
-3	32	1	435	437	10
-2	32	1	195	174	26
-1	32	1	431	404	11
4	34	1	52	28	51
5	34	1	79	29	78
6	34	1	61	21	60
7	34	1	442	427	22
-8	35	1	174	204	22
-7	35	1	268	231	15
-6	35	1	104	111	104
-5	35	1	85	112	35
-4	35	1	381	359	13
-3	35	1	360	349	16
-2	35	1	228	157	18
-1	35	1	278	274	21
0	35	1	473	482	12
2	35	1	322	342	15
3	35	1	13	5	13
4	35	1	303	311	15
5	35	1	436	413	11
6	35	1	112	41	35
7	35	1	76	91	76
-7	36	1	343	356	15
-6	36	1	383	396	12
-5	36	1	357	363	11
-4	36	1	312	310	13
-3	36	1	285	294	16
-2	36	1	596	620	17
-1	36	1	529	532	11
0	36	1	139	117	29
1	36	1	274	276	17
2	36	1	299	299	18
3	36	1	579	592	12
4	36	1	461	459	11
5	36	1	191	157	19
6	36	1	357	356	13
7	36	1	204	233	96
-7	37	1	230	194	19
-6	37	1	0	39	1
-5	37	1	242	250	19
-4	37	1	304	313	13
-3	37	1	176	168	23
-2	37	1	133	127	41
-1	37	1	261	262	17
0	37	1	357	353	13
1	37	1	477	471	12
2	37	1	157	151	25
3	37	1	49	131	49
4	37	1	300	273	18
5	37	1	395	381	20
6	37	1	209	207	19
-6	38	1	57	75	56
-5	38	1	127	111	39

-10	20	1	298	310	11
-9	20	1	261	248	12
-8	20	1	190	174	15
-7	20	1	0	9	1
-6	20	1	579	567	8
-5	20	1	353	349	8
-4	20	1	316	310	9
-3	20	1	418	415	11
-2	20	1	443	434	7
-1	20	1	567	574	9
0	20	1	557	553	9
1	20	1	70	5	34
2	20	1	0	56	1
3	20	1	773	770	9
4	20	1	201	190	11
5	20	1	325	314	10
6	20	1	98	119	59
7	20	1	634	617	11
8	20	1	385	387	11
9	20	1	308	286	16
10	20	1	361	370	14
11	20	1	65	59	65
-12	21	1	0	101	1
-11	21	1	197	207	21
-10	21	1	103	88	38
-9	21	1	439	426	10
-8	21	1	706	703	12
-7	21	1	573	559	8
8	23	1	425	443	16
9	23	1	205	234	21
10	23	1	134	102	30
-11	24	1	109	118	81
-10	24	1	188	203	17
-9	24	1	216	206	16
-8	24	1	170	154	17
-7	24	1	384	391	8
-6	24	1	115	119	22
-5	24	1	69	8	50
-4	24	1	579	574	8
-3	24	1	163	110	15
-2	24	1	138	130	18
-1	24	1	184	187	13
0	24	1	205	189	19
1	24	1	169	148	45
2	24	1	482	478	8
3	24	1	152	132	16
4	24	1	0	65	1
5	24	1	349	344	10
6	24	1	31	19	31
7	24	1	40	56	39
8	24	1	0	6	1
9	24	1	309	283	15
10	24	1	146	129	24
-11	25	1	177	171	58
-10	25	1	0	77	1
-9	25	1	208	220	17
10	27	1	287	308	18
-10	28	1	82	113	53
-9	28	1	235	236	16
-8	28	1	103	46	31
-7	28	1	95	108	33
-6	28	1	0	58	1
-5	28	1	120	139	21
-4	28	1	420	414	15
-3	28	1	127	84	21
-2	28	1	409	416	9
-1	28	1	81	36	51
0	28	1	28	50	28
1	28	1	240	268	21
2	28	1	320	320	11
3	28	1	343	330	16
4	28	1	268	261	12
5	28	1	162	124	21
6	28	1	482	480	11
7	28	1	0	29	1
8	28	1	90	120	58
9	28	1	0	60	1
-10	29	1	67	41	67
-9	29	1	114	167	31
-8	29	1	331	344	12
-7	29	1	17	82	16
-6	29	1	85	51	37
-5	29	1	0	71	1
-4	29	1	134	112	19
0	32	1	566	584	11
1	32	1	610	626	15
3	32	1	339	335	12
4	32	1	318	303	12
5	32	1	0	27	1
6	32	1	526	503	13
7	32	1	411	390	12
8	32	1	0	41	1
-9	33	1	117	16	53
-8	33	1	117	93	32
-7	33	1	190	197	18
-6	33	1	219	207	21
-5	33	1	141	141	20
-4	33	1	75	51	38
-3	33	1	120	91	26
-2	33	1	116	73	54
-1	33	1	172	140	22
0	33	1	92	50	40
1	33	1	189	174	21
2	33	1	153	67	30
3	33	1	162	133	22
4	33	1	165	168	20
5	33	1	0	48	1
6	33	1	275	289	15
7	33	1	72	7	71
8	33	1	95	168	95
-8	34	1	141	158	34
-7	34	1	176	175	32
-4	38	1	97	131	48
-3	38	1	125	92	37
-2	38	1	137	116	31
-1	38	1	83	35	82
0	38	1	0	41	1
1	38	1	58	33	58
2	38	1	96	93	57
3	38	1	55	81	54
4	38	1	0	41	1
5	38	1	163	153	24
-6	39	1	191	176	27
-5	39	1	86	94	50
-4	39	1	301	311	28
-3	39	1	159	127	27
-2	39	1	74	17	74
-1	39	1	0	14	-1
0	39	1	225	256	18
1	39	1	119	133	36
2	39	1	64	62	64
3	39	1	148	54	35
4	39	1	86	124	86
5	39	1	310	291	18
-5	40	1	314	311	15
-4	40	1	164	127	29
-3	40	1	161	137	31
-2	40	1	261	238	20
-1	40	1	304	315	16
0	40	1	162	141	28

Table 0.6. Observed and calculated structure factors for Rutdp

h	k	1	10Fo	10Fc	10s
1	40	1	66	34	66
2	40	1	374	371	25
3	40	1	519	557	13
4	40	1	201	153	29
-4	41	1	402	402	15
-3	41	1	359	340	16
-2	41	1	218	221	22
-1	41	1	98	9	56
0	41	1	370	380	33
1	41	1	387	422	15
2	41	1	147	132	50
3	41	1	226	197	24
-3	42	1	21	94	21
-2	42	1	248	225	23
-1	42	1	137	133	36
0	42	1	162	148	45
1	42	1	0	38	1
3	2	2	423	429	6
4	2	2	157	169	10
5	2	2	500	506	8
6	2	2	94	96	17
7	2	2	530	523	7
8	2	2	353	354	9
9	2	2	277	296	10
10	2	2	264	252	15
11	2	2	0	112	1
-14	3	2	140	149	31
-13	3	2	53	8	52
-12	3	2	63	90	62
-11	3	2	253	256	15
-10	3	2	351	340	9
-9	3	2	873	870	7
-8	3	2	70	73	20
-7	3	2	326	307	5
-13	6	2	0	14	1
-12	6	2	120	98	31
-11	6	2	850	826	13
-10	6	2	238	234	14
-9	6	2	458	450	9
-8	6	2	341	346	7
-7	6	2	169	175	8
-6	6	2	274	282	6
-5	6	2	415	424	4
-4	6	2	183	200	6
-3	6	2	1315	1332	9
-2	6	2	760	740	5
-1	6	2	228	203	4
0	6	2	732	730	5
1	6	2	194	219	5
2	6	2	644	675	5
3	6	2	402	416	5
0	9	2	1859	1887	12
1	9	2	274	268	4
2	9	2	1085	1134	10
3	9	2	873	871	7
4	9	2	906	885	9
5	9	2	533	531	5
6	9	2	705	694	7
7	9	2	792	788	8
8	9	2	678	672	7
9	9	2	0	32	1
10	9	2	349	360	11
11	9	2	421	394	13
12	9	2	430	431	20
-13	10	2	111	134	43
-12	10	2	658	671	12
-11	10	2	446	466	12
-10	10	2	77	34	58
10	12	2	86	21	51
11	12	2	8	23	7
12	12	2	169	188	41
-13	13	2	438	447	27
-12	13	2	215	205	32
-11	13	2	0	48	1
-10	13	2	0	111	1
-9	13	2	210	195	12
-8	13	2	662	654	8
-7	13	2	181	178	10
-6	13	2	283	283	6
-5	13	2	117	88	15
-4	13	2	880	896	6
-3	13	2	488	462	5
-2	13	2	1163	1175	8
-1	13	2	1043	1061	7
0	13	2	459	462	5

2	42	1	295	311	20	-6	3	2	333	352	6	4	6	2	539	544	5	-9	10	2	263	266	10	1	13	2	255	260	6
-1	43	1	149	182	35	-5	3	2	86	99	12	5	6	2	30	26	30	-8	10	2	378	377	8	2	13	2	196	193	20
0	43	1	21	58	21	-4	3	2	447	438	7	6	6	2	326	349	8	-7	10	2	1249	1277	11	3	13	2	842	837	8
-14	0	2	0	37	-1	-3	3	2	360	357	5	7	6	2	0	11	1	-6	10	2	266	261	6	4	13	2	698	683	8
-13	0	2	64	98	64	-2	3	2	1327	1310	12	8	6	2	455	460	6	-5	10	2	54	56	54	5	13	2	35	37	35
-12	0	2	0	19	1	-1	3	2	361	356	3	9	6	2	144	139	13	-4	10	2	823	818	6	6	13	2	633	624	11
-11	0	2	1292	1275	24	0	3	2	724	734	6	10	6	2	339	338	8	-3	10	2	1417	1458	10	7	13	2	521	499	9
-10	0	2	833	805	17	1	3	2	2117	2102	16	11	6	2	0	45	1	-2	10	2	795	835	7	8	13	2	245	234	14
-9	0	2	849	843	16	2	3	2	554	554	5	-13	7	2	69	58	69	-1	10	2	222	196	7	9	13	2	133	125	22
-8	0	2	781	789	7	3	3	2	32	52	31	-12	7	2	80	125	56	0	10	2	318	338	4	10	13	2	108	133	36
-7	0	2	1075	1067	12	4	3	2	584	573	7	-11	7	2	190	170	19	1	10	2	715	716	5	11	13	2	166	151	26
-6	0	2	607	603	8	5	3	2	0	67	1	-10	7	2	254	246	17	2	10	2	1037	1060	10	-13	14	2	112	43	37
-5	0	2	1166	1153	20	6	3	2	177	176	16	-9	7	2	0	7	1	3	10	2	373	380	7	-12	14	2	530	510	13
-4	0	2	231	210	4	7	3	2	229	232	10	-8	7	2	0	20	1	4	10	2	782	798	6	-11	14	2	589	590	18
-3	0	2	3736	3678	57	8	3	2	71	81	24	-7	7	2	28	61	28	5	10	2	1275	1274	10	-10	14	2	319	308	14
-2	0	2	2070	2008	32	9	3	2	67	18	51	-6	7	2	442	435	5	6	10	2	754	728	7	-9	14	2	290	278	10
-1	0	2	2950	2878	30	10	3	2	182	195	13	-5	7	2	46	23	29	7	10	2	125	125	16	-8	14	2	466	465	8
0	0	2	899	904	10	11	3	2	225	264	18	-4	7	2	827	813	6	8	10	2	559	557	8	-7	14	2	773	765	7
1	0	2	5858	5696	51	-14	4	2	251	210	20	-3	7	2	171	140	5	9	10	2	279	275	14	-6	14	2	794	798	7
2	0	2	1921	1904	20	-13	4	2	235	216	15	-2	7	2	1379	1356	9	10	10	2	455	441	12	-5	14	2	239	236	6
3	0	2	501	508	8	-12	4	2	323	306	24	-1	7	2	703	695	5	11	10	2	0	19	1	-4	14	2	1169	1181	9
4	0	2	904	923	11	-11	4	2	630	615	18	0	7	2	205	204	5	12	10	2	0	73	1	-3	14	2	1716	1762	12
5	0	2	279	254	13	-10	4	2	113	102	35	1	7	2	665	648	5	-13	11	2	0	16	1	-2	14	2	782	805	7
6	0	2	853	847	11	-9	4	2	0	16	-1	2	7	2	211	230	6	-12	11	2	140	120	26	-1	14	2	314	327	6
7	0	2	559	546	16	-8	4	2	512	495	6	3	7	2	45	10	44	-11	11	2	0	4	1	0	14	2	1209	1247	9
8	0	2	368	370	11	-7	4	2	524	527	5	4	7	2	172	146	8	-10	11	2	143	160	41	1	14	2	544	581	6
9	0	2	191	201	13	-6	4	2	787	788	7	5	7	2	234	235	7	-9	11	2	233	235	11	2	14	2	1348	1326	12
10	0	2	490	495	16	-5	4	2	577	573	5	6	7	2	111	103	13	-8	11	2	34	22	33	3	14	2	399	381	8
-14	1	2	146	158	51	-4	4	2	506	515	5	7	7	2	88	59	27	-7	11	2	540	533	5	4	14	2	776	772	8
-13	1	2	413	397	14	-3	4	2	2520	2510	17	8	7	2	343	351	7	-6	11	2	835	807	6	5	14	2	473	452	8
-12	1	2	334	340	11	-2	4	2	2511	2541	17	9	7	2	126	97	17	-5	11	2	692	695	5	6	14	2	829	830	9
-11	1	2	225	189	22	-1	4	2	1170	1157	8	10	7	2	0	65	1	-4	11	2	475	461	5	7	14	2	277	271	10
-10	1	2	460	459	8	0	4	2	1583	1600	9	11	7	2	56	36	55	-3	11	2	236	238	5	8	14	2	799	792	10
-9	1	2	639	629	10	1	4	2	1163	1158	8	-13	8	2	26	24	26	-2	11	2	1389	1394	9	9	14	2	328	311	12
-8	1	2	690	697	5	2	4	2	423	386	7	-12	8	2	270	272	16	-1	11	2	125	104	8	10	14	2	115	127	36
-7	1	2	403	399	4	3	4	2	760	720	8	-11	8	2	309	310	14	0	11	2	245	232	5	11	14	2	126	33	61
-6	1	2	1059	1064	7	4	4	2	319	319	8	-10	8	2	165	151	20	1	11	2	804	805	7	-13	15	2	192	216	27
-5	1	2	919	929	7	5	4	2	1454	1464	16	-9	8	2	109	116	21	2	11	2	396	379	6	-12	15	2	390	406	14
-4	1	2	148	164	6	6	4	2	785	765	11	-8	8	2	338	338	7	3	11	2	66	39	42	-11	15	2	45	95	45
-3	1	2	73	19	20	7	4	2	72	89	42	-7	8	2	628	619	6	4	11	2	840	867	7	-10	15	2	567	555	14
-2	1	2	1226	1205	14	8	4	2	510	511	7	-6	8	2	345	318	5	5	11	2	88	89	23	-9	15	2	330	318	10
-1	1	2	1361	1319	10	9	4	2	435	415	7	-5	8	2	257	243	8	6	11	2	726	739	7	-8	15	2	299	303	9
0	1	2	501	492	4	10	4	2	457	438	8	-4	8	2	788	765	6	7	11	2	597	577	7	-7	15	2	126	120	16
1	1	2	1401	1414	9	11	4	2	213	228	20	-3	8	2	517	534	4	8	11	2	391	383	12	-6	15	2	259	254	10
2	1	2	1117	1103	8	-14	5	2	283	237	23	-2	8	2	39	27	39	9	11	2	65	23	64	-5	15	2	1080	1121	8
3	1	2	373	387	5	-13	5	2	230	222	15	-1	8	2	602	598	8	10	11	2	49	7	49	-4	15	2	436	449	5
4	1	2	831	839	7	-12	5	2	516	519	12	0	8	2	322	314	6	11	11	2	443	420	13	-3	15	2	602	593	5
5	1	2	295	292	7	-11	5	2	0	6	1	1	8	2	298	284	4	12	11	2	226	265	29	-2	15	2	904	905	9
6	1	2	107	120	15	-10	5	2	495	521	8	2	8	2	693	724	6	-13	12	2	118	50	63	-1	15	2	747	758	6
7	1	2	760	767	7	-9	5	2	1040	1039	9	3	8	2	445	438	6	-12	12	2	107	77	107	0	15	2	961	970	8

8	1	2	533	522	7
9	1	2	0	10	1
10	1	2	219	207	18
11	1	2	457	436	13
-14	2	2	98	20	61
-13	2	2	0	13	1
-12	2	2	219	222	15
-11	2	2	121	150	46
-10	2	2	0	24	1
-9	2	2	126	128	13
-8	2	2	156	140	10
-7	2	2	221	236	6
-6	2	2	653	651	5
-5	2	2	42	42	26
-4	2	2	195	200	5
-3	2	2	72	29	15
-2	2	2	521	529	5
-1	2	2	594	563	5
0	2	2	1865	1870	13
1	2	2	2082	2048	14
2	2	2	1545	1519	12
-8	5	2	626	626	7
-7	5	2	387	381	5
-6	5	2	709	742	6
-5	5	2	1152	1201	8
-4	5	2	184	172	7
-3	5	2	260	258	4
-2	5	2	895	912	6
-1	5	2	760	769	5
0	5	2	172	166	5
1	5	2	519	502	4
2	5	2	965	966	8
3	5	2	1595	1632	14
4	5	2	1316	1354	12
5	5	2	214	195	9
6	5	2	617	633	8
7	5	2	1040	1019	14
8	5	2	373	378	7
9	5	2	83	104	25
10	5	2	341	336	12
11	5	2	619	616	18
-14	6	2	89	88	57
4	8	2	982	990	8
5	8	2	73	50	20
6	8	2	174	180	9
7	8	2	721	704	7
8	8	2	205	209	15
9	8	2	447	468	8
10	8	2	201	175	14
11	8	2	204	182	15
-13	9	2	143	165	28
-12	9	2	297	278	21
-11	9	2	0	114	1
-10	9	2	1028	996	14
-9	9	2	1047	1038	34
-8	9	2	191	182	9
-7	9	2	466	463	5
-6	9	2	301	306	5
-5	9	2	2421	2391	16
-4	9	2	923	942	10
-3	9	2	1399	1380	9
-2	9	2	493	489	6
-1	9	2	926	946	6
-11	12	2	150	171	23
-10	12	2	82	78	52
-9	12	2	183	192	14
-8	12	2	0	7	1
-7	12	2	45	2	44
-6	12	2	84	102	16
-5	12	2	166	185	8
-4	12	2	369	352	5
-3	12	2	1040	1039	7
-2	12	2	816	788	7
-1	12	2	169	158	9
0	12	2	659	665	5
1	12	2	167	174	7
2	12	2	765	763	8
3	12	2	774	785	8
4	12	2	666	661	8
5	12	2	535	547	7
6	12	2	31	12	31
7	12	2	496	487	8
8	12	2	118	117	20
9	12	2	169	179	16
1	15	2	682	683	6
2	15	2	805	850	8
3	15	2	634	642	8
4	15	2	495	500	8
5	15	2	491	480	9
6	15	2	677	678	8
7	15	2	537	540	8
8	15	2	814	795	12
9	15	2	0	57	1
10	15	2	0	25	1
11	15	2	207	198	24
-13	16	2	0	7	1
-12	16	2	259	275	18
-11	16	2	0	9	1
-10	16	2	0	21	1
-9	16	2	0	54	1
-8	16	2	479	465	8
-7	16	2	861	854	10
-6	16	2	83	72	20
-5	16	2	286	302	6
-4	16	2	15	43	15

Table D.6. Observed and calculated structure factors for Rutdp

h	k	l	10Fo	10Fc	10s
-3	16	2	743	743	6
-2	16	2	476	489	6
-1	16	2	399	404	5
0	16	2	712	723	9
1	16	2	109	95	11
2	16	2	421	403	10
3	16	2	956	952	10
4	16	2	638	631	8
5	16	2	541	522	8
6	16	2	41	36	41
7	16	2	21	26	21
8	16	2	338	334	12
9	16	2	77	129	44
10	16	2	255	268	17
11	16	2	66	95	65
-13	17	2	109	151	42
-12	17	2	0	67	1
-11	17	2	226	213	18
-10	17	2	89	42	56
-9	17	2	0	48	1
-8	17	2	230	210	11
-7	17	2	48	5	47
-6	17	2	48	15	48
-5	17	2	61	43	47
-12	20	2	101	120	101
-11	20	2	399	416	20
-10	20	2	71	128	70
-9	20	2	211	207	16
-8	20	2	58	34	57
-7	20	2	263	251	10
-6	20	2	341	339	7
-5	20	2	115	122	16
-4	20	2	1011	996	7
-3	20	2	1364	1368	9
-2	20	2	139	94	11
-1	20	2	170	163	9
0	20	2	778	780	8
1	20	2	585	619	8
2	20	2	232	257	13
3	20	2	91	86	26
4	20	2	59	52	59
5	20	2	760	759	9
6	20	2	771	772	9
7	20	2	211	226	18
8	20	2	470	452	10
9	20	2	312	304	13
10	20	2	394	379	15
-12	21	2	118	143	40
7	23	2	301	280	12
8	23	2	418	406	11
9	23	2	83	105	82
10	23	2	126	119	63
-11	24	2	289	288	23
-10	24	2	173	192	19
-9	24	2	0	32	1
-8	24	2	667	651	12
-7	24	2	773	762	12
-6	24	2	247	215	9
-5	24	2	217	183	15
-4	24	2	587	603	7
-3	24	2	820	817	9
-2	24	2	538	544	7
-1	24	2	497	488	7
0	24	2	488	508	13
1	24	2	725	734	10
2	24	2	359	366	9
3	24	2	0	24	1
4	24	2	266	237	11
5	24	2	779	759	12
6	24	2	585	579	9
7	24	2	30	81	30
8	24	2	288	269	13
8	27	2	67	19	67
9	27	2	272	287	18
-10	28	2	265	260	14
-9	28	2	0	55	1
-8	28	2	512	511	10
-7	28	2	586	601	9
-6	28	2	492	490	9
-5	28	2	81	14	30
-4	28	2	348	342	10
-3	28	2	410	390	8
-2	28	2	306	308	10
-1	28	2	383	359	11
0	28	2	396	380	15
1	28	2	471	460	16
2	28	2	681	688	10
3	28	2	94	41	29
4	28	2	417	414	10
5	28	2	390	388	10
6	28	2	279	264	27
7	28	2	0	53	1
8	28	2	274	253	19
9	28	2	477	450	21
-10	29	2	524	519	12
-9	29	2	434	438	11
-1	32	2	177	146	21
0	32	2	134	43	27
1	32	2	440	437	17
2	32	2	473	483	11
3	32	2	0	74	1
4	32	2	192	173	20
5	32	2	230	196	15
6	32	2	8	68	7
7	32	2	84	56	84
8	32	2	0	14	-1
-9	33	2	404	399	12
-8	33	2	299	310	14
-7	33	2	120	126	28
-6	33	2	507	483	16
-5	33	2	379	377	9
-4	33	2	214	206	15
-3	33	2	140	132	20
-2	33	2	537	546	11
-1	33	2	615	618	16
0	33	2	460	435	12
1	33	2	257	244	15
2	33	2	305	319	13
3	33	2	522	524	12
4	33	2	484	476	11

-4	17	2	422	400	9	-11	21	2	73	55	72	9	24	2	504	519	13	-8	29	2	0	38	1	5	33	2	190	156	19
-3	17	2	195	196	7	-10	21	2	47	116	47	10	24	2	315	313	17	-7	29	2	105	135	28	6	33	2	222	235	18
-2	17	2	429	424	5	-9	21	2	400	404	10	-11	25	2	265	264	19	-6	29	2	92	62	31	7	33	2	378	357	13
-1	17	2	322	310	5	-8	21	2	0	49	1	-10	25	2	239	274	16	-5	29	2	566	558	8	-8	34	2	286	299	14
0	17	2	163	134	10	-7	21	2	55	30	55	-9	25	2	408	395	11	-4	29	2	507	512	8	-7	34	2	321	314	13
1	17	2	164	156	9	-6	21	2	0	12	1	-8	25	2	303	292	12	-3	29	2	417	403	8	-6	34	2	183	181	23
2	17	2	86	99	23	-5	21	2	413	409	9	-7	25	2	243	233	13	-2	29	2	0	80	1	-5	34	2	115	40	28
3	17	2	799	800	9	-4	21	2	353	343	10	-6	25	2	409	405	8	-1	29	2	318	304	15	-4	34	2	153	154	41
4	17	2	257	251	10	-3	21	2	163	128	43	-5	25	2	357	357	8	0	29	2	656	639	18	-3	34	2	280	299	24
5	17	2	328	330	10	-2	21	2	43	33	43	-4	25	2	363	358	8	1	29	2	200	184	47	-2	34	2	258	266	16
6	17	2	185	175	18	-1	21	2	263	236	8	-3	25	2	225	185	13	2	29	2	584	605	15	-1	34	2	212	210	17
7	17	2	57	50	56	0	21	2	294	297	7	-2	25	2	500	487	8	3	29	2	475	459	9	0	34	2	413	396	12
8	17	2	129	143	21	1	21	2	145	171	36	-1	25	2	1305	1327	14	4	29	2	334	323	11	1	34	2	462	476	14
9	17	2	0	79	1	2	21	2	393	386	8	0	25	2	101	108	29	5	29	2	187	180	21	2	34	2	514	510	13
10	17	2	287	301	16	3	21	2	460	466	12	1	25	2	218	196	15	6	29	2	615	611	12	3	34	2	119	34	58
11	17	2	0	19	1	4	21	2	52	5	52	2	25	2	42	18	41	7	29	2	512	502	11	4	34	2	309	306	13
-12	18	2	208	193	23	5	21	2	47	35	47	3	25	2	652	647	9	8	29	2	328	320	14	5	34	2	465	465	14
-11	18	2	298	280	16	6	21	2	25	24	25	4	25	2	776	768	9	9	29	2	90	92	67	6	34	2	130	127	27
-10	18	2	459	416	19	7	21	2	232	224	13	5	25	2	263	260	12	-10	30	2	0	22	1	7	34	2	188	137	23
-9	18	2	394	395	9	8	21	2	148	158	21	6	25	2	160	170	22	-9	30	2	71	79	70	-8	35	2	129	131	29
-8	18	2	140	104	18	9	21	2	176	196	24	7	25	2	372	379	11	-8	30	2	190	183	17	-7	35	2	34	56	33
-7	18	2	499	493	8	10	21	2	106	74	63	8	25	2	451	445	11	-7	30	2	424	431	10	-6	35	2	36	17	36
-6	18	2	408	416	7	-12	22	2	34	83	33	9	25	2	175	209	25	-6	30	2	130	123	19	-5	35	2	360	345	15
-5	18	2	350	341	7	-11	22	2	0	29	1	10	25	2	106	133	46	-5	30	2	382	397	8	-4	35	2	454	450	10
-4	18	2	1730	1722	12	-10	22	2	0	18	1	-11	26	2	272	297	18	-4	30	2	664	680	8	-3	35	2	120	99	34
-3	18	2	443	427	5	-9	22	2	76	72	75	-10	26	2	0	49	1	-3	30	2	765	753	9	-2	35	2	48	50	47
-2	18	2	366	360	6	-8	22	2	82	77	33	-9	26	2	229	238	15	-2	30	2	157	177	18	-1	35	2	257	269	33
-1	18	2	192	200	8	-7	22	2	427	421	9	-8	26	2	179	178	28	-1	30	2	312	324	13	0	35	2	520	508	12
0	18	2	628	641	7	-6	22	2	55	54	55	-7	26	2	108	90	25	0	30	2	652	653	11	1	35	2	195	158	24
1	18	2	58	125	29	-5	22	2	485	489	7	-6	26	2	581	589	7	1	30	2	550	552	10	2	35	2	186	187	21
2	18	2	68	39	33	-4	22	2	550	527	7	-5	26	2	453	451	10	2	30	2	288	283	31	3	35	2	130	135	59
3	18	2	268	263	9	-3	22	2	787	774	6	-4	26	2	414	420	7	3	30	2	106	126	29	4	35	2	275	290	26
4	18	2	136	148	20	-2	22	2	254	256	8	-3	26	2	587	584	7	4	30	2	271	241	13	5	35	2	98	63	67
5	18	2	1311	1312	12	-1	22	2	105	37	15	-2	26	2	448	444	11	5	30	2	421	422	11	6	35	2	93	111	43
6	18	2	488	491	10	0	22	2	759	753	10	-1	26	2	233	184	17	6	30	2	59	17	59	-8	36	2	84	14	83
7	18	2	0	13	1	1	22	2	286	291	12	0	26	2	345	364	31	7	30	2	129	146	27	-7	36	2	18	55	18
8	18	2	177	151	16	2	22	2	403	388	8	1	26	2	395	401	11	8	30	2	162	152	27	-6	36	2	235	266	15
9	18	2	463	462	12	3	22	2	177	174	14	2	26	2	94	73	28	-10	31	2	0	127	1	-5	36	2	0	22	1
10	18	2	126	125	97	4	22	2	438	453	9	3	26	2	129	88	21	-9	31	2	109	105	41	-4	36	2	91	3	46
11	18	2	0	9	1	5	22	2	455	462	10	4	26	2	338	353	13	-8	31	2	13	66	13	-3	36	2	249	266	17
-12	19	2	0	111	1	6	22	2	368	383	10	5	26	2	255	235	13	-7	31	2	217	204	15	-2	36	2	129	122	52
-11	19	2	133	163	30	7	22	2	192	173	16	6	26	2	0	27	1	-6	31	2	149	136	19	-1	36	2	31	5	31
-10	19	2	422	432	10	8	22	2	0	37	1	7	26	2	232	257	14	-5	31	2	171	165	15	0	36	2	99	61	74
-9	19	2	472	458	11	9	22	2	289	313	16	8	26	2	104	31	88	-4	31	2	98	103	48	1	36	2	127	143	32
-8	19	2	439	439	9	10	22	2	165	172	28	9	26	2	57	110	56	-3	31	2	226	198	25	2	36	2	73	65	73
-7	19	2	141	139	17	-12	23	2	71	119	71	-11	27	2	88	29	87	-2	31	2	204	186	48	3	36	2	113	120	55
-6	19	2	943	952	8	-11	23	2	75	114	74	-10	27	2	0	45	1	-1	31	2	236	224	15	4	36	2	155	183	28
-5	19	2	618	622	7	-10	23	2	449	447	10	-9	27	2	251	252	14	0	31	2	132	133	69	5	36	2	0	8	1
-4	19	2	1120	1117	8	-9	23	2	447	436	15	-8	27	2	509	495	10	1	31	2	109	10	35	6	36	2	150	189	26
-3	19	2	258	223	13	-8	23	2	446	448	10	-7	27	2	211	207	14	2	31	2	39	51	39	-7	37	2	28	30	28

-2	19	2	1036	1056	10	-7	23	2	106	70	25	-6	27	2	702	695	11	3	31	2	159	160	20	-6	37	2	0	29	1
-1	19	2	791	827	7	-6	23	2	603	614	7	-5	27	2	303	297	9	4	31	2	76	70	53	-5	37	2	279	302	31
0	19	2	560	582	7	-5	23	2	928	925	8	-4	27	2	68	29	44	5	31	2	225	234	15	-4	37	2	265	258	16
1	19	2	235	211	10	-4	23	2	931	923	8	-3	27	2	408	420	7	6	31	2	303	285	16	-3	37	2	84	13	76
2	19	2	355	331	8	-3	23	2	86	26	63	-2	27	2	69	26	40	7	31	2	0	20	1	-2	37	2	317	314	15
3	19	2	973	990	10	-2	23	2	456	452	8	-1	27	2	544	557	10	8	31	2	104	168	39	-1	37	2	318	315	15
4	19	2	970	974	10	-1	23	2	888	868	8	0	27	2	490	491	13	-9	32	2	128	112	28	0	37	2	102	63	43
5	19	2	237	243	11	0	23	2	988	971	11	1	27	2	139	105	24	-8	32	2	196	207	18	1	37	2	171	89	25
6	19	2	88	88	30	1	23	2	217	207	14	2	27	2	241	228	12	-7	32	2	440	452	10	2	37	2	252	248	19
7	19	2	341	314	10	2	23	2	502	517	8	3	27	2	79	17	38	-6	32	2	328	323	12	3	37	2	381	375	15
8	19	2	741	730	9	3	23	2	854	849	9	4	27	2	0	33	1	-5	32	2	40	42	39	4	37	2	112	79	40
9	19	2	215	230	14	4	23	2	384	370	9	5	27	2	241	233	14	-4	32	2	329	348	9	5	37	2	31	91	31
10	19	2	323	345	15	5	23	2	123	113	23	6	27	2	340	330	11	-3	32	2	301	298	11	-7	38	2	142	92	34
11	19	2	216	234	17	6	23	2	68	30	53	7	27	2	104	137	33	-2	32	2	582	592	11	-6	38	2	261	253	21

Table D.6. Observed and calculated structure factors for Rutdp

h	k	l	10Fo	10Fc	10s	h	k	l	10Fo	10Fc	10s	h	k	l	10Fo	10Fc	10s	h	k	l	10Fo	10Fc	10s	h	k	l	10Fo	10Fc	10s
-5	38	2	86	19	85	3	2	3	1166	1142	9	-13	6	3	229	213	43	-3	9	3	1272	1275	10	9	12	3	262	255	13
-4	38	2	266	279	15	4	2	3	645	669	6	-12	6	3	36	50	36	-2	9	3	448	431	4	10	12	3	145	161	32
-3	38	2	349	365	23	5	2	3	1004	981	8	-11	6	3	67	60	67	-1	9	3	243	264	5	11	12	3	252	269	28
-2	38	2	261	267	17	6	2	3	362	371	8	-10	6	3	274	279	10	0	9	3	236	227	5	-13	13	3	285	291	27
-1	38	2	171	120	26	7	2	3	527	518	7	-9	6	3	895	873	15	1	9	3	100	83	9	-12	13	3	392	398	13
0	38	2	384	410	14	8	2	3	518	504	15	-8	6	3	422	422	7	2	9	3	561	578	6	-11	13	3	599	607	23
1	38	2	626	634	13	9	2	3	289	314	13	-7	6	3	214	211	8	3	9	3	251	262	8	-10	13	3	180	200	18
2	38	2	248	221	23	10	2	3	157	180	25	-6	6	3	75	38	14	4	9	3	599	599	7	-9	13	3	452	438	10
3	38	2	85	46	84	11	2	3	227	228	16	-5	6	3	1266	1292	9	5	9	3	160	148	10	-8	13	3	138	115	18
4	38	2	279	258	18	-14	3	3	138	146	32	-4	6	3	777	781	6	6	9	3	145	146	12	-7	13	3	1003	1008	9
5	38	2	478	492	26	-13	3	3	99	37	49	-3	6	3	833	821	6	7	9	3	321	328	8	-6	13	3	1151	1158	8
-6	39	2	493	481	15	-12	3	3	103	106	103	-2	6	3	568	561	6	8	9	3	450	437	8	-5	13	3	29	63	29
-5	39	2	58	101	57	-11	3	3	435	428	9	-1	6	3	695	700	5	9	9	3	274	277	12	-4	13	3	172	179	7
-4	39	2	223	222	21	-10	3	3	1341	1303	13	0	6	3	306	329	4	10	9	3	231	232	14	-3	13	3	1369	1392	10
-3	39	2	361	322	15	-9	3	3	170	186	13	1	6	3	484	500	4	11	9	3	43	10	43	-2	13	3	989	992	7
-2	39	2	299	285	16	-8	3	3	606	625	7	2	6	3	831	856	9	-14	10	3	152	137	66	-1	13	3	58	90	18
-1	39	2	518	546	18	-7	3	3	957	964	8	3	6	3	1150	1173	10	-13	10	3	310	322	21	0	13	3	171	124	7
0	39	2	268	248	35	-6	3	3	223	254	6	4	6	3	245	265	9	-12	10	3	252	273	16	1	13	3	620	630	5
1	39	2	59	86	58	-5	3	3	290	306	5	5	6	3	298	301	11	-11	10	3	169	150	22	2	13	3	641	659	6
2	39	2	65	50	65	-4	3	3	1121	1127	11	6	6	3	185	181	14	-10	10	3	305	327	19	3	13	3	346	355	10
3	39	2	372	335	17	-3	3	3	1572	1609	13	7	6	3	455	454	7	-9	10	3	341	325	9	4	13	3	482	469	8
4	39	2	413	397	15	-2	3	3	318	309	4	8	6	3	225	227	9	-8	10	3	125	136	19	5	13	3	599	594	8
-5	40	2	99	44	77	-1	3	3	101	94	9	9	6	3	174	192	13	-7	10	3	366	357	6	6	13	3	794	788	9
-4	40	2	152	96	32	0	3	3	885	881	7	10	6	3	0	19	-1	-6	10	3	529	516	5	7	13	3	0	23	-1
-3	40	2	373	358	14	1	3	3	1025	1054	7	11	6	3	378	368	15	-5	10	3	240	228	5	8	13	3	243	272	13
-2	40	2	364	379	14	2	3	3	2258	2261	15	-14	7	3	348	339	16	-4	10	3	1204	1213	12	9	13	3	388	377	10
-1	40	2	0	1	-1	3	3	3	1371	1373	12	-13	7	3	221	228	18	-3	10	3	116	76	17	10	13	3	229	211	20
0	40	2	72	123	71	4	3	3	916	917	8	-12	7	3	478	488	18	-2	10	3	119	93	8	11	13	3	185	217	38
1	40	2	115	130	39	5	3	3	643	641	7	-11	7	3	621	590	12	-1	10	3	53	48	19	-13	14	3	135	158	33
2	40	2	35	106	35	6	3	3	644	622	7	-10	7	3	63	106	63	0	10	3	211	190	6	-12	14	3	224	235	21
3	40	2	0	25	1	7	3	3	185	187	12	-9	7	3	170	198	18	1	10	3	231	240	5	-11	14	3	139	150	85

```
   4 40  2  114   73  72       8  3  3  200  196  16      -8  7  3  265  255   8       2 10  3  168  130  12     -10 14  3  534  541  14
  -4 41  2  116  103  47       9  3  3  263  276  14      -7  7  3 1337 1362  11       3 10  3   68   29  37      -9 14  3  188  208  14
  -3 41  2  104  101 104      10  3  3  600  578   8      -6  7  3  401  416   5       4 10  3  644  636   7      -8 14  3   84  100  26
  -2 41  2  151  131  31      11  3  3  276  286  22      -5  7  3 1064 1050   7       5 10  3  521  510   7      -7 14  3  237  234   9
  -1 41  2  153  117  33     -14  4  3  109  129 108      -4  7  3  796  785   6       6 10  3    0   19   1      -6 14  3  251  238   7
   0 41  2  128  118  39     -13  4  3  199  209  20      -3  7  3 1242 1270   8       7 10  3  167  177  12      -5 14  3  574  567   5
   1 41  2  141   31  33     -12  4  3  655  623  12      -2  7  3 1190 1219   8       8 10  3  235  231  11      -4 14  3  476  473   5
   2 41  2  108   60 107     -11  4  3  152  157  16      -1  7  3  985 1008   7       9 10  3  224  213  20      -3 14  3  191  160  18
   3 41  2  134   21  62     -10  4  3  357  346   9       0  7  3  817  834   5      10 10  3    0   21   1      -2 14  3   49   41  34
  -3 42  2  176  209  28      -9  4  3   85   56  25       1  7  3 1160 1173   7      11 10  3  130  170  56      -1 14  3  363  357   5
  -2 42  2  164  180  29      -8  4  3  615  610   7       2  7  3  982 1025   6     -13 11  3   41   36  40       0 14  3  167  155   8
  -1 42  2  170   16  39      -7  4  3  368  386   5       3  7  3  330  333   7     -12 11  3  407  395  13       1 14  3  803  744   7
   0 42  2  110  185  59      -6  4  3  686  681   6       4  7  3  169  165   8     -11 11  3  618  601  12       2 14  3  101  119  18
   1 42  2  385  377  16      -5  4  3  478  464   5       5  7  3  971  976   7     -10 11  3  638  642  11       3 14  3    0  127   1
 -14  1  3  130  181  32      -4  4  3  234  187  19       6  7  3 1424 1432  10      -9 11  3  126  116  18       4 14  3  108  115  20
 -13  1  3  100   83  44      -3  4  3 1088 1089   7       7  7  3  110  128  16      -8 11  3  713  702   7       5 14  3  368  361   8
 -12  1  3  317  311  10      -2  4  3  851  861   6       8  7  3   62   56  39      -7 11  3  682  673   7       6 14  3  103  106  24
 -11  1  3  329  321  17      -1  4  3 1044 1050   6       9  7  3  444  443   8      -6 11  3 1086 1085   9       7 14  3  372  385   9
 -10  1  3  603  601  10       0  4  3 1037 1021  12      10  7  3  601  609   9      -5 11  3  226  218   6       8 14  3  266  284  12
  -9  1  3  178  168  17       1  4  3 1385 1401   9      11  7  3  370  361  15      -4 11  3  455  459   8       9 14  3  264  281  13
  -8  1  3  354  363   8       2  4  3  168  182  11     -14  8  3  176  159  28      -3 11  3  642  676   6      10 14  3  233  239  32
  -7  1  3  504  486   5       3  4  3 1563 1567  14     -13  8  3  379  389  30      -2 11  3  830  865   6      11 14  3   97   24  97
  -6  1  3  318  290   4       4  4  3  381  382   7     -12  8  3  272  263  16      -1 11  3  475  474   4     -13 15  3   33    5  32
  -5  1  3  122  135   7       5  4  3  253  258   9     -11  8  3  120   16  88       0 11  3   31   14  31     -12 15  3  145  147  30
  -4  1  3  717  716   7       6  4  3  202  201   9     -10  8  3  259  241  14       1 11  3   44   21  33     -11 15  3  230  243  29
  -3  1  3  290  296   5       7  4  3    0   28   1      -9  8  3  726  728  11       2 11  3  761  783   7     -10 15  3  248  222  28
  -2  1  3  195  177   5       8  4  3   56   65  56      -8  8  3  582  574   6       3 11  3 1595 1598  13      -9 15  3  308  304  10
  -1  1  3  866  866   7       9  4  3  254  246  10      -7  8  3  676  672   8       4 11  3  723  752   8      -8 15  3   98   97  34
   0  1  3  545  561   5      10  4  3  185  204  15      -6  8  3  230  197   8       5 11  3  695  685   7      -7 15  3  369  381  10
   1  1  3 1639 1667  11      11  4  3    0   37   1      -5  8  3 1524 1546  10       6 11  3  435  440   7      -6 15  3  764  769   6
   2  1  3  589  595   4     -14  5  3    0   31   1      -4  8  3 1182 1194   8       7 11  3  494  491   7      -5 15  3  541  556   6
   3  1  3  425  405   6     -13  5  3  125  120  31      -3  8  3   45   54  37       8 11  3   73   50  36      -4 15  3  572  588   6
   4  1  3   40   20  39     -12  5  3    0   29   1      -2  8  3  282  294   4       9 11  3  406  414  14      -3 15  3  643  634   6
   5  1  3  452  447   7     -11  5  3    0   48   1      -1  8  3  471  476   4      10 11  3  342  333  15      -2 15  3  979  966   7
   6  1  3  844  847   8     -10  5  3  202  219  13       0  8  3  929  961   7      11 11  3  163  192  41      -1 15  3  520  511   6
   7  1  3  160  150  16      -9  5  3  288  289   9       1  8  3  244  237   5     -13 12  3  475  505  13       0 15  3  482  465   5
   8  1  3  516  509  11      -8  5  3  111   88  15       2  8  3  308  293   5     -12 12  3  495  480  16       1 15  3  681  699   6
   9  1  3  135  177  26      -7  5  3  414  418   6       3  8  3  448  434   7     -11 12  3  144  146  26       2 15  3  184  190  10
  10  1  3  400  399  17      -6  5  3  104  113  10       4  8  3 1017 1028   8     -10 12  3  294  297  21       3 15  3  127  143  19
  11  1  3  256  248  17      -5  5  3  341  319   4       5  8  3  484  478   6      -9 12  3  621  602  10       4 15  3  863  865  10
 -14  2  3  249  280  26      -4  5  3  228  218   5       6  8  3  163  166  12      -8 12  3  671  671   7       5 15  3  107   73  22
 -13  2  3  572  564  10      -3  5  3  400  391   8       7  8  3  597  574   6      -7 12  3  344  330   7       6 15  3  412  408   9
 -12  2  3  328  280  14      -2  5  3  127  109   7       8  8  3  116   80  16      -6 12  3  137  130   9       7 15  3   59   12  59
 -11  2  3  122   96  21      -1  5  3  792  808   5       9  8  3  131  152  21      -5 12  3  761  767   6       8 15  3  368  351  10
 -10  2  3  256  246  10       0  5  3  147  146   5      10  8  3  105   97  31      -4 12  3 1437 1446  10       9 15  3   73  128  54
  -9  2  3  558  545  11       1  5  3   34   53  33      11  8  3  124  149  43      -3 12  3  373  357   5      10 15  3  132  109  57
  -8  2  3  824  829  10       2  5  3  485  436   6     -14  9  3  231  231  20      -2 12  3  192  153   6      11 15  3    0   65   1
  -7  2  3  560  573   5       3  5  3  227  204  10     -13  9  3    0   34   1      -1 12  3 1654 1673  11     -13 16  3  430  422  15
  -6  2  3  803  798   6       4  5  3   51   83  50     -12  9  3   82  115  50       0 12  3  732  772   6     -12 16  3  533  541  20
  -5  2  3 1657 1699  10       5  5  3   13   90  13     -11  9  3  132  125  28       1 12  3  473  512   5     -11 16  3    0    3  -1
```

-4	2	3	847	873	8
-3	2	3	2120	2120	18
-2	2	3	685	666	5
-1	2	3	775	771	6
0	2	3	1274	1267	9
1	2	3	739	734	6
2	2	3	842	835	7
6	5	3	473	477	8
7	5	3	366	362	9
8	5	3	152	136	12
9	5	3	556	539	8
10	5	3	0	71	-1
11	5	3	132	106	33
-14	6	3	315	279	14
-10	9	3	442	440	11
-9	9	3	377	384	15
-8	9	3	733	732	7
-7	9	3	286	278	7
-6	9	3	378	377	6
-5	9	3	372	383	5
-4	9	3	116	46	8
2	12	3	822	818	7
3	12	3	1438	1412	13
4	12	3	1075	1072	10
5	12	3	386	396	7
6	12	3	279	280	9
7	12	3	732	725	8
8	12	3	347	336	9
-10	16	3	327	351	20
-9	16	3	125	132	19
-8	16	3	327	326	17
-7	16	3	102	71	22
-6	16	3	932	928	7
-5	16	3	713	719	6
-4	16	3	147	172	8

Table 0.6. Observed and calculated structure factors for Rutdp

h	k	l	10Fo	10Fc	10s
-3	16	3	541	557	5
-2	16	3	150	161	12
-1	16	3	1211	1223	8
0	16	3	416	456	6
1	16	3	539	550	6
2	16	3	287	274	9
3	16	3	676	675	10
4	16	3	1238	1233	12
5	16	3	375	370	9
6	16	3	0	20	1
7	16	3	513	515	12
8	16	3	465	470	9
9	16	3	114	99	27
10	16	3	83	64	83
11	16	3	197	197	43
-13	17	3	0	74	1
-12	17	3	226	214	20
-11	17	3	511	498	13
-10	17	3	528	531	18
-9	17	3	118	96	48
-8	17	3	362	357	9
-7	17	3	139	134	17
-6	17	3	279	268	9
-5	17	3	137	144	10
-4	17	3	639	632	6
-3	17	3	856	865	10
-2	17	3	1134	1144	8
-1	17	3	178	207	7
0	17	3	767	769	12
1	17	3	1080	1073	10
2	17	3	584	588	9
3	17	3	667	665	10
4	17	3	334	321	11
5	17	3	660	643	9
6	17	3	575	565	9
7	17	3	223	223	15
8	17	3	107	43	28
9	17	3	589	595	10
-10	20	3	111	123	36
-9	20	3	537	524	9
-8	20	3	337	330	10
-7	20	3	71	89	41
-6	20	3	385	388	8
-5	20	3	253	259	8
-4	20	3	486	468	6
-3	20	3	371	358	6
-2	20	3	284	291	6
-1	20	3	547	558	5
0	20	3	354	353	10
1	20	3	150	158	20
2	20	3	316	315	9
3	20	3	721	724	10
4	20	3	989	973	10
5	20	3	0	30	-1
6	20	3	64	73	63
7	20	3	75	86	74
8	20	3	397	393	10
9	20	3	395	410	12
10	20	3	120	18	90
-12	21	3	209	229	22
-11	21	3	324	353	16
-10	21	3	419	413	13
-9	21	3	311	315	11
-8	21	3	121	93	22
-7	21	3	382	366	9
-6	21	3	612	600	8
-5	21	3	226	221	9
-4	21	3	1044	1047	8
-3	21	3	680	663	6
-2	21	3	640	643	6
-1	21	3	624	635	6
0	21	3	100	130	29
1	21	3	1192	1188	13
2	21	3	401	420	17
3	21	3	0	30	1
4	21	3	90	110	30
-12	24	3	0	122	1
-11	24	3	306	328	16
-10	24	3	133	27	47
-9	24	3	0	13	1
-8	24	3	75	59	75
-7	24	3	0	15	1
-6	24	3	746	764	9
-5	24	3	225	183	11
-4	24	3	72	52	71
-3	24	3	58	38	33
-2	24	3	772	775	8
-1	24	3	107	114	54
0	24	3	690	675	10
1	24	3	99	132	32
2	24	3	434	444	9
3	24	3	127	99	22
4	24	3	142	120	20
5	24	3	91	76	39
6	24	3	148	160	20
7	24	3	310	297	13
8	24	3	0	38	1
9	24	3	51	101	50
-11	25	3	299	295	27
-10	25	3	348	357	28
-9	25	3	227	224	15
-8	25	3	169	168	18
-7	25	3	218	233	19
-6	25	3	43	39	43
-5	25	3	668	676	7
-4	25	3	324	327	8
-3	25	3	105	91	23
-2	25	3	916	914	8
-1	25	3	133	111	20
0	25	3	330	334	14
1	25	3	245	251	21
2	25	3	495	489	13
3	25	3	266	247	11
4	25	3	312	313	11
-7	28	3	307	276	14
-6	28	3	167	170	17
-5	28	3	582	576	7
-4	28	3	51	29	50
-3	28	3	132	110	20
-2	28	3	144	101	18
-1	28	3	207	213	16
0	28	3	79	45	71
1	28	3	48	25	47
2	28	3	77	59	63
3	28	3	413	430	10
4	28	3	227	188	15
5	28	3	175	180	18
6	28	3	66	113	65
7	28	3	163	168	21
8	28	3	209	225	19
-10	29	3	0	88	1
-9	29	3	127	128	37
-8	29	3	72	30	58
-7	29	3	195	188	16
-6	29	3	55	58	54
-5	29	3	471	477	8
-4	29	3	268	269	9
-3	29	3	120	44	30
-2	29	3	502	504	9
-1	29	3	386	374	17
0	29	3	171	189	20
1	29	3	341	319	34
2	29	3	509	500	11
3	29	3	51	40	51
4	29	3	160	168	19
5	29	3	170	150	19
6	29	3	106	109	34
7	29	3	135	161	26
8	29	3	119	140	33
-10	30	3	129	144	28
-9	30	3	258	257	15
-8	30	3	144	158	22
7	32	3	202	237	24
-9	33	3	103	99	40
-8	33	3	100	88	68
-7	33	3	132	128	34
-6	33	3	116	150	32
-5	33	3	118	106	22
-4	33	3	231	213	25
-3	33	3	53	35	52
-2	33	3	121	111	29
-1	33	3	185	208	29
0	33	3	63	53	62
1	33	3	84	81	66
2	33	3	115	102	39
3	33	3	223	244	37
4	33	3	160	152	32
5	33	3	118	116	29
6	33	3	0	18	1
7	33	3	135	149	66
-9	34	3	251	251	21
-8	34	3	248	228	16
-7	34	3	101	72	34
-6	34	3	51	50	50
-5	34	3	307	310	13
-4	34	3	381	391	13
-3	34	3	246	218	14
-2	34	3	335	325	14
-1	34	3	132	136	28
0	34	3	62	126	62
1	34	3	59	83	59
2	34	3	48	29	47
3	34	3	236	211	20
4	34	3	255	286	19
5	34	3	74	13	74
6	34	3	60	104	59
-8	35	3	206	203	18
-7	35	3	398	395	12
-6	35	3	377	369	14
-5	35	3	149	154	30

10	17	3	400	348	22
-13	18	3	370	362	18
-12	18	3	219	217	20
-11	18	3	129	145	87
-10	18	3	101	75	57
-9	18	3	396	408	9
-8	18	3	519	528	8
-7	18	3	475	477	8
-6	18	3	65	22	37
-5	18	3	690	689	6
-4	18	3	986	985	7
-3	18	3	130	92	10
-2	18	3	377	377	5
-1	18	3	707	680	6
0	18	3	582	580	10
1	18	3	1073	1082	12
2	18	3	0	33	1
3	18	3	797	760	16
4	18	3	562	560	8
5	18	3	280	273	11
6	18	3	299	306	11
7	18	3	254	248	13
8	18	3	408	376	10
9	18	3	227	200	17
10	18	3	0	106	-1
-13	19	3	123	95	38
-12	19	3	126	81	34
-10	19	3	24	56	23
-9	19	3	67	12	67
-8	19	3	114	115	21
-7	19	3	123	113	21
-6	19	3	46	31	45
-5	19	3	338	324	7
-4	19	3	271	243	7
-3	19	3	50	21	36
-2	19	3	436	419	5
-1	19	3	21	30	21
0	19	3	393	404	8
1	19	3	598	604	9
2	19	3	275	277	12
3	19	3	140	101	16
4	19	3	35	32	35
5	19	3	361	366	10
6	19	3	304	319	11
7	19	3	175	210	16
8	19	3	0	4	1
9	19	3	104	137	40
10	19	3	85	70	85
-12	20	3	314	325	16
-11	20	3	0	90	1
5	21	3	640	623	9
6	21	3	428	436	10
7	21	3	209	237	15
8	21	3	91	52	37
9	21	3	164	172	22
10	21	3	513	502	21
-12	22	3	476	462	14
-11	22	3	82	88	81
-10	22	3	280	291	25
-9	22	3	423	431	10
-8	22	3	451	443	9
-7	22	3	473	471	9
-6	22	3	314	325	8
-5	22	3	747	742	7
-4	22	3	192	151	12
-3	22	3	760	759	6
-2	22	3	360	367	6
-1	22	3	1378	1387	11
0	22	3	1083	1084	12
1	22	3	110	105	24
2	22	3	191	157	16
3	22	3	739	744	9
4	22	3	758	741	9
5	22	3	81	100	35
6	22	3	0	6	1
7	22	3	463	440	14
8	22	3	564	565	13
9	22	3	222	229	16
-12	23	3	0	74	1
-11	23	3	170	131	24
-10	23	3	180	165	23
-9	23	3	52	39	52
-8	23	3	421	437	9
-7	23	3	149	148	19
-6	23	3	227	232	14
-5	23	3	1164	1156	10
-4	23	3	921	914	8
-3	23	3	707	703	6
-2	23	3	99	77	30
-1	23	3	55	6	55
0	23	3	87	82	87
1	23	3	343	380	16
2	23	3	446	448	11
3	23	3	145	157	17
4	23	3	165	166	16
5	23	3	89	112	43
6	23	3	567	543	9
7	23	3	284	278	13
8	23	3	47	21	47
9	23	3	251	257	15
5	25	3	461	459	12
6	25	3	284	283	13
7	25	3	310	301	13
8	25	3	37	19	36
9	25	3	372	356	13
-11	26	3	223	212	22
-10	26	3	171	216	42
-9	26	3	457	450	10
-8	26	3	604	594	11
-7	26	3	121	103	22
-6	26	3	450	447	9
-5	26	3	436	420	12
-4	26	3	398	397	7
-3	26	3	343	345	9
-2	26	3	115	76	37
-1	26	3	587	602	10
0	26	3	337	356	11
1	26	3	426	440	11
2	26	3	312	304	13
3	26	3	861	838	10
4	26	3	387	369	10
5	26	3	335	329	12
6	26	3	245	238	19
7	26	3	514	509	12
8	26	3	393	363	12
9	26	3	324	326	52
-11	27	3	415	400	15
-10	27	3	382	384	20
-9	27	3	216	225	16
-8	27	3	392	391	10
-7	27	3	774	782	13
-6	27	3	736	740	9
-5	27	3	731	724	8
-4	27	3	378	391	9
-3	27	3	320	309	9
-2	27	3	585	583	8
-1	27	3	486	484	22
0	27	3	124	120	26
1	27	3	629	633	12
2	27	3	555	544	10
3	27	3	253	256	12
4	27	3	326	325	11
5	27	3	446	437	10
6	27	3	432	427	10
7	27	3	221	219	17
8	27	3	240	246	16
-11	28	3	206	229	23
-10	28	3	363	353	12
-9	28	3	86	128	41
-8	28	3	112	100	40
-7	30	3	110	22	29
-6	30	3	311	304	12
-5	30	3	475	462	8
-4	30	3	90	66	27
-3	30	3	543	541	9
-2	30	3	180	104	44
-1	30	3	258	242	14
0	30	3	768	761	12
1	30	3	0	46	1
2	30	3	378	332	27
3	30	3	283	283	14
4	30	3	504	498	12
5	30	3	365	357	11
6	30	3	171	142	21
7	30	3	409	381	12
8	30	3	55	134	54
-10	31	3	162	170	23
-9	31	3	75	12	75
-8	31	3	190	234	16
-7	31	3	712	700	10
-6	31	3	782	792	10
-5	31	3	433	424	8
-4	31	3	111	77	25
-3	31	3	500	495	9
-2	31	3	704	713	13
-1	31	3	148	95	24
0	31	3	224	200	31
1	31	3	127	136	31
2	31	3	577	591	11
3	31	3	535	545	20
4	31	3	203	196	19
5	31	3	380	378	16
6	31	3	175	185	20
7	31	3	149	126	31
-9	32	3	507	495	11
-8	32	3	187	226	36
-7	32	3	177	181	21
-6	32	3	195	175	17
-5	32	3	583	579	8
-4	32	3	832	833	10
-3	32	3	217	220	14
-2	32	3	653	655	16
-1	32	3	215	198	17
0	32	3	375	392	13
1	32	3	542	556	11
2	32	3	170	160	30
3	32	3	518	517	11
4	32	3	317	304	12
5	32	3	206	213	17
6	32	3	50	79	50
-4	35	3	88	48	41
-3	35	3	318	354	20
-2	35	3	253	241	18
-1	35	3	159	139	24
0	35	3	157	65	41
1	35	3	414	442	18
2	35	3	383	362	13
3	35	3	134	100	33
4	35	3	156	93	30
5	35	3	355	343	13
6	35	3	385	379	13
-8	36	3	475	484	12
-7	36	3	502	520	11
-6	36	3	178	195	50
-5	36	3	650	653	13
-4	36	3	335	341	18
-3	36	3	192	156	21
-2	36	3	124	108	124
-1	36	3	593	597	11
0	36	3	663	678	12
1	36	3	121	79	44
2	36	3	66	85	66
3	36	3	52	140	51
4	36	3	340	328	18
5	36	3	393	400	15
-7	37	3	253	262	16
-6	37	3	306	299	18
-5	37	3	211	186	23
-4	37	3	264	247	17
-3	37	3	305	333	19
-2	37	3	350	338	14
-1	37	3	84	56	83
0	37	3	154	106	39
1	37	3	272	245	22
2	37	3	353	367	14
3	37	3	199	194	24
4	37	3	99	68	98
5	37	3	234	234	27
-7	38	3	103	127	56
-6	38	3	146	179	35
-5	38	3	0	72	1
-4	38	3	157	167	22
-3	38	3	155	197	58
-2	38	3	184	243	22
-1	38	3	164	168	27
0	38	3	72	90	72
1	38	3	185	159	25
2	38	3	81	28	81
3	38	3	79	71	78
4	38	3	0	41	1

Table D.6. Observed and calculated structure factors for Rutdp

h	k	l	10Fo	10Fc	10s	h	k	l	10Fo	10Fc	10s	h	k	l	10Fo	10Fc	10s	h	k	l	10Fo	10Fc	10s	h	k	l	10Fo	10Fc	10s
-6	39	3	185	119	27	-9	2	4	52	16	51	1	5	4	1264	1272	9	11	8	4	181	184	27	-4	12	4	511	502	5
-5	39	3	230	178	32	-8	2	4	103	79	27	2	5	4	393	390	5	-14	9	4	89	71	88	-3	12	4	65	17	17
-4	39	3	148	25	49	-7	2	4	51	49	50	3	5	4	1001	999	7	-13	9	4	396	386	14	-2	12	4	517	504	5
-3	39	3	137	164	47	-6	2	4	568	566	11	4	5	4	1033	1037	9	-12	9	4	488	480	12	-1	12	4	183	172	7
-2	39	3	0	13	1	-5	2	4	0	30	1	5	5	4	536	528	9	-11	9	4	371	385	13	0	12	4	266	269	17
-1	39	3	201	192	26	-4	2	4	465	477	6	6	5	4	128	129	25	-10	9	4	169	187	14	1	12	4	598	599	6
0	39	3	85	29	84	-3	2	4	324	336	5	7	5	4	0	14	1	-9	9	4	895	893	10	2	12	4	301	304	9
1	39	3	241	264	21	-2	2	4	360	379	5	8	5	4	701	696	11	-8	9	4	827	804	8	3	12	4	43	88	43
2	39	3	95	76	67	-1	2	4	292	267	6	9	5	4	463	467	8	-7	9	4	212	231	9	4	12	4	0	29	1
3	39	3	20	28	19	0	2	4	125	108	8	10	5	4	232	224	14	-6	9	4	102	59	13	5	12	4	912	913	8
4	39	3	99	99	98	1	2	4	667	633	6	11	5	4	190	188	17	-5	9	4	369	396	6	6	12	4	11	45	10
-5	40	3	100	213	52	2	2	4	702	699	5	-14	6	4	497	488	26	-4	9	4	1427	1399	10	7	12	4	113	101	19
-4	40	3	521	528	17	3	2	4	812	788	7	-13	6	4	0	136	1	-3	9	4	1800	1788	12	8	12	4	49	39	48
-3	40	3	298	278	29	4	2	4	37	64	36	-12	6	4	179	181	21	-2	9	4	263	271	5	9	12	4	70	81	69
-2	40	3	323	299	16	5	2	4	255	267	13	-11	6	4	71	129	70	-1	9	4	73	74	13	10	12	4	69	43	68
-1	40	3	285	268	19	6	2	4	423	428	10	-10	6	4	282	277	10	0	9	4	476	487	5	-13	13	4	250	270	28
0	40	3	182	182	24	7	2	4	128	157	23	-9	6	4	185	182	15	1	9	4	1022	1073	7	-12	13	4	601	614	18
1	40	3	142	132	33	8	2	4	237	237	22	-8	6	4	250	245	10	2	9	4	179	194	7	-11	13	4	436	429	12
2	40	3	162	109	33	9	2	4	85	130	85	-7	6	4	482	500	6	3	9	4	1178	1188	8	-10	13	4	228	250	16
3	40	3	288	280	18	10	2	4	78	111	78	-6	6	4	178	176	8	4	9	4	887	878	7	-9	13	4	270	256	21
-4	41	3	223	209	59	11	2	4	122	127	27	-5	6	4	0	19	1	5	9	4	483	482	6	-8	13	4	130	118	16
-3	41	3	525	561	13	-14	3	4	111	152	32	-4	6	4	54	30	33	6	9	4	84	89	23	-7	13	4	241	235	8
-2	41	3	321	321	18	-13	3	4	201	211	21	-3	6	4	927	936	7	7	9	4	431	423	8	-6	13	4	141	103	24
-1	41	3	135	117	35	-12	3	4	65	14	65	-2	6	4	122	149	8	8	9	4	324	320	11	-5	13	4	217	230	7
0	41	3	0	23	1	-11	3	4	234	231	12	-1	6	4	1492	1503	8	9	9	4	535	527	13	-4	13	4	581	580	5
1	41	3	357	351	40	-10	3	4	176	145	13	0	6	4	676	659	6	10	9	4	261	230	18	-3	13	4	654	643	5
2	41	3	312	324	19	-9	3	4	491	485	10	1	6	4	702	709	5	11	9	4	307	305	18	-2	13	4	40	52	39
-3	42	3	159	140	66	-8	3	4	218	221	12	2	6	4	912	890	10	-14	10	4	441	412	16	-1	13	4	254	278	7
-2	42	3	0	65	1	-7	3	4	309	311	6	3	6	4	794	809	9	-13	10	4	349	310	15	0	13	4	1251	1273	9
-1	42	3	377	348	16	-6	3	4	265	249	6	4	6	4	0	30	1	-12	10	4	111	94	53	1	13	4	483	488	7
0	42	3	119	127	95	-5	3	4	227	252	6	5	6	4	943	938	9	-11	10	4	795	777	13	2	13	4	262	271	9
-14	0	4	855	878	22	-4	3	4	692	651	8	6	6	4	359	342	9	-10	10	4	672	671	12	3	13	4	238	251	12
-13	0	4	115	105	115	-3	3	4	198	188	4	7	6	4	266	261	14	-9	10	4	75	79	32	4	13	4	450	458	7
-12	0	4	210	220	17	-2	3	4	110	79	10	8	6	4	167	155	23	-8	10	4	399	384	7	5	13	4	533	529	7
-11	0	4	168	152	29	-1	3	4	621	607	5	9	6	4	152	160	18	-7	10	4	568	563	6	6	13	4	83	87	27
-10	0	4	1276	1270	22	0	3	4	396	385	5	10	6	4	392	389	10	-6	10	4	965	966	8	7	13	4	508	513	8
-9	0	4	1060	1048	19	1	3	4	1167	1170	10	11	6	4	376	381	15	-5	10	4	834	823	6	8	13	4	464	459	42
-8	0	4	973	974	17	2	3	4	702	695	5	-14	7	4	89	29	88	-4	10	4	186	124	36	9	13	4	355	356	23
-7	0	4	321	315	7	3	3	4	545	554	5	-13	7	4	114	124	38	-3	10	4	1551	1518	10	10	13	4	140	158	31
-6	0	4	2238	2220	23	4	3	4	434	445	7	-12	7	4	0	40	-1	-2	10	4	1247	1272	9	-13	14	4	344	352	16
-5	0	4	1238	1259	20	5	3	4	259	260	9	-11	7	4	0	73	1	-1	10	4	1028	1058	7	-12	14	4	0	16	1
-4	0	4	1224	1198	20	6	3	4	183	196	16	-10	7	4	381	365	9	0	10	4	586	569	6	-11	14	4	374	384	13
-3	0	4	155	138	9	7	3	4	88	108	40	-9	7	4	705	694	9	1	10	4	493	503	5	-10	14	4	588	561	11
-2	0	4	1144	1160	12	8	3	4	140	143	24	-8	7	4	8	32	7	2	10	4	674	694	5	-9	14	4	427	418	11
-1	0	4	736	746	13	9	3	4	0	47	-1	-7	7	4	450	443	6	3	10	4	686	697	7	-8	14	4	79	3	24
0	0	4	336	341	7	10	3	4	65	52	65	-6	7	4	129	104	10	4	10	4	212	224	8	-7	14	4	723	733	7

1	0	4	1315	1327	14	11	3	4	165	169	19	-5	7	4	523	516	6	5	10	4	895	886	7	-6	14	4	947	958	9
2	0	4	2096	2074	19	-14	4	4	425	421	11	-4	7	4	389	372	4	6	10	4	185	184	12	-5	14	4	400	414	5
3	0	4	1904	1913	17	-13	4	4	291	269	16	-3	7	4	481	456	4	7	10	4	777	771	12	-4	14	4	305	285	5
4	0	4	153	165	13	-12	4	4	0	54	1	-2	7	4	190	185	5	8	10	4	232	236	13	-3	14	4	1044	1050	9
5	0	4	759	764	14	-11	4	4	585	577	9	-1	7	4	195	204	5	9	10	4	259	242	14	-2	14	4	1112	1153	10
6	0	4	8	32	7	-10	4	4	604	580	9	0	7	4	611	601	5	10	10	4	351	360	28	-1	14	4	662	668	7
7	0	4	166	180	27	-9	4	4	339	316	9	1	7	4	129	131	9	11	10	4	330	341	43	0	14	4	156	146	9
8	0	4	161	168	31	-8	4	4	111	103	40	2	7	4	44	51	43	-14	11	4	180	127	48	1	14	4	442	446	6
9	0	4	174	226	33	-7	4	4	946	947	9	3	7	4	530	536	6	-13	11	4	159	205	35	2	14	4	660	663	9
10	0	4	314	268	24	-6	4	4	897	909	8	4	7	4	694	701	10	-12	11	4	160	186	24	3	14	4	1192	1189	11
11	0	4	403	430	19	-5	4	4	1033	1047	10	5	7	4	110	109	18	-11	11	4	0	77	1	4	14	4	58	93	58
-14	1	4	0	29	1	-4	4	4	959	906	10	6	7	4	381	378	8	-10	11	4	189	157	33	5	14	4	716	726	9
-13	1	4	235	245	14	-3	4	4	208	205	5	7	7	4	0	29	1	-9	11	4	483	468	8	6	14	4	228	206	12
-12	1	4	418	409	10	-2	4	4	553	544	4	8	7	4	325	326	17	-8	11	4	55	91	44	7	14	4	652	630	9
-11	1	4	311	299	12	-1	4	4	848	880	6	9	7	4	208	219	17	-7	11	4	197	209	9	8	14	4	0	39	1
-10	1	4	217	218	15	0	4	4	132	138	10	10	7	4	96	7	59	-6	11	4	355	363	6	9	14	4	324	318	18
-9	1	4	527	511	10	1	4	4	905	928	7	11	7	4	0	7	1	-5	11	4	1116	1129	10	10	14	4	497	483	13
-8	1	4	852	849	11	2	4	4	1764	1751	11	-14	8	4	61	90	60	-4	11	4	1002	1022	7	-13	15	4	507	521	14
-7	1	4	317	336	6	3	4	4	216	206	8	-13	8	4	31	100	31	-3	11	4	785	784	6	-12	15	4	422	415	13
-6	1	4	926	887	11	4	4	4	470	453	6	-12	8	4	240	261	17	-2	11	4	814	810	6	-11	15	4	202	216	19
-5	1	4	593	617	11	5	4	4	169	175	13	-11	8	4	414	399	29	-1	11	4	403	412	5	-10	15	4	176	171	19
-4	1	4	1608	1591	14	6	4	4	160	163	13	-10	8	4	23	66	22	0	11	4	464	477	5	-9	15	4	343	348	14
-3	1	4	281	293	4	7	4	4	339	323	18	-9	8	4	48	17	48	1	11	4	464	466	5	-8	15	4	718	696	17
-2	1	4	476	482	5	8	4	4	127	122	29	-8	8	4	131	110	13	2	11	4	738	737	5	-7	15	4	232	249	9
-1	1	4	1026	1041	8	9	4	4	408	404	17	-7	8	4	533	533	6	3	11	4	246	245	9	-6	15	4	231	217	10
0	1	4	1228	1248	9	10	4	4	433	461	9	-6	8	4	461	456	6	4	11	4	151	126	25	-5	15	4	565	568	5
1	1	4	2673	2645	30	11	4	4	357	373	11	-5	8	4	1031	1001	7	5	11	4	971	960	9	-4	15	4	646	669	6
2	1	4	591	591	6	-14	5	4	123	117	36	-4	8	4	684	654	6	6	11	4	339	319	8	-3	15	4	372	383	5
3	1	4	52	19	51	-13	5	4	428	436	27	-3	8	4	633	638	5	7	11	4	239	248	14	-2	15	4	591	545	5
4	1	4	698	695	7	-12	5	4	690	664	28	-2	8	4	352	364	4	8	11	4	661	666	9	-1	15	4	1034	1040	7
5	1	4	280	273	9	-11	5	4	318	290	14	-1	8	4	305	302	4	9	11	4	399	403	10	0	15	4	548	559	6
6	1	4	152	99	55	-10	5	4	0	7	1	0	8	4	339	318	5	10	11	4	269	279	15	1	15	4	777	785	8
7	1	4	318	314	13	-9	5	4	535	523	13	1	8	4	633	612	5	-14	12	4	0	115	1	2	15	4	551	558	8
8	1	4	578	566	10	-8	5	4	963	962	10	2	8	4	872	839	5	-13	12	4	0	2	1	3	15	4	543	544	10
9	1	4	289	304	15	-7	5	4	772	770	7	3	8	4	939	960	6	-12	12	4	108	59	107	4	15	4	443	430	15
10	1	4	0	59	1	-6	5	4	35	4	35	4	8	4	265	261	7	-11	12	4	91	5	45	5	15	4	708	720	9
11	1	4	163	170	19	-5	5	4	1027	1050	9	5	8	4	527	530	6	-10	12	4	23	29	22	6	15	4	152	155	22
-14	2	4	0	62	1	-4	5	4	2365	2349	16	6	8	4	86	69	28	-9	12	4	573	575	11	7	15	4	263	264	12
-13	2	4	0	65	1	-3	5	4	188	209	5	7	8	4	173	161	14	-8	12	4	582	569	7	8	15	4	517	513	12
-12	2	4	231	244	13	-2	5	4	997	996	6	8	8	4	411	404	9	-7	12	4	572	556	6	9	15	4	750	752	12
-11	2	4	373	357	10	-1	5	4	725	745	6	9	8	4	66	90	65	-6	12	4	739	743	7	10	15	4	166	150	124
-10	2	4	265	241	12	0	5	4	391	422	5	10	8	4	406	395	11	-5	12	4	246	227	7	-13	16	4	70	120	69

Table D.6. Observed and calculated structure factors for Rutdp

h	k	l	10Fo	10Fc	10s	h	k	l	10Fo	10Fc	10s	h	k	l	10Fo	10Fc	10s	h	k	l	10Fo	10Fc	10s	h	k	l	10Fo	10Fc	10s
-12	16	4	75	61	75	4	19	4	654	650	9	4	23	4	456	448	10	-11	28	4	296	298	18	4	32	4	169	176	27
-11	16	4	336	340	19	5	19	4	339	327	10	5	23	4	51	85	50	-10	28	4	259	288	18	5	32	4	92	75	40
-10	16	4	214	199	30	6	19	4	0	103	1	6	23	4	106	41	65	-9	28	4	350	346	12	6	32	4	120	106	43

-9	16	4	0	80	1
-8	16	4	494	502	11
-7	16	4	176	181	11
-6	16	4	1055	1080	9
-5	16	4	341	338	5
-4	16	4	100	89	13
-3	16	4	157	147	8
-2	16	4	57	91	24
-1	16	4	749	734	6
0	16	4	296	299	6
1	16	4	377	387	8
2	16	4	469	480	9
3	16	4	424	422	8
4	16	4	96	33	26
5	16	4	566	559	8
6	16	4	113	114	23
7	16	4	545	536	9
8	16	4	0	26	1
9	16	4	360	349	17
10	16	4	36	117	36
-13	17	4	0	3	1
-12	17	4	248	236	17
-11	17	4	57	12	57
-10	17	4	39	70	39
-9	17	4	321	342	13
-8	17	4	80	70	34
-7	17	4	86	82	25
-6	17	4	297	296	8
-5	17	4	82	44	17
-4	17	4	27	73	27
-3	17	4	554	539	5
-2	17	4	320	303	5
-1	17	4	517	508	5
0	17	4	146	147	10
1	17	4	798	790	8
2	17	4	452	450	8
3	17	4	338	315	11
4	17	4	647	623	10
5	17	4	211	215	13
6	17	4	0	48	1
7	17	4	69	65	68
8	17	4	0	11	-1
9	17	4	295	262	17
10	17	4	127	139	88
-13	18	4	201	230	33
-12	18	4	125	21	57
-11	18	4	391	411	13
-10	18	4	468	484	16
-9	18	4	41	39	41
-8	18	4	230	242	11
7	19	4	163	133	24
8	19	4	472	467	11
9	19	4	511	512	13
-12	20	4	187	195	26
-11	20	4	152	130	51
-10	20	4	613	603	12
-9	20	4	378	373	10
-8	20	4	0	20	1
-7	20	4	110	91	22
-6	20	4	341	326	9
-5	20	4	288	282	6
-4	20	4	140	135	12
-3	20	4	713	709	6
-2	20	4	416	428	6
-1	20	4	306	322	6
0	20	4	183	193	12
1	20	4	640	641	10
2	20	4	612	628	8
3	20	4	249	261	12
4	20	4	43	61	43
5	20	4	302	301	11
6	20	4	303	287	12
7	20	4	574	582	12
8	20	4	134	104	25
9	20	4	175	210	26
-12	21	4	75	111	74
-11	21	4	135	157	29
-10	21	4	228	235	18
-9	21	4	39	8	39
-8	21	4	596	582	9
-7	21	4	416	419	9
-6	21	4	454	446	8
-5	21	4	65	52	27
-4	21	4	32	9	31
-3	21	4	628	608	6
-2	21	4	235	208	8
-1	21	4	461	481	7
0	21	4	38	39	38
1	21	4	148	155	19
2	21	4	238	234	15
3	21	4	0	46	1
4	21	4	300	291	11
5	21	4	242	265	13
6	21	4	115	130	25
7	21	4	11	19	10
8	21	4	131	152	26
9	21	4	46	59	46
-12	22	4	48	81	47
-11	22	4	52	60	52
-10	22	4	217	234	18
7	23	4	0	91	1
8	23	4	314	310	13
9	23	4	436	420	15
-12	24	4	140	97	140
-11	24	4	299	311	16
-10	24	4	476	474	16
-9	24	4	318	300	11
-8	24	4	0	68	1
-7	24	4	545	537	9
-6	24	4	1215	1227	12
-5	24	4	476	487	7
-4	24	4	273	278	7
-3	24	4	849	838	7
-2	24	4	606	618	8
-1	24	4	597	605	8
0	24	4	430	421	11
1	24	4	506	512	15
2	24	4	833	832	11
3	24	4	383	392	10
4	24	4	83	70	42
5	24	4	78	45	44
6	24	4	589	579	13
7	24	4	512	496	10
8	24	4	0	36	1
9	24	4	68	81	67
-11	25	4	77	67	77
-10	25	4	209	254	30
-9	25	4	387	408	11
-8	25	4	458	446	9
-7	25	4	556	547	12
-6	25	4	202	168	27
-5	25	4	353	349	8
-4	25	4	427	421	7
-3	25	4	208	165	19
-2	25	4	482	482	7
-1	25	4	72	37	72
0	25	4	662	669	10
1	25	4	470	480	10
2	25	4	88	94	87
3	25	4	366	357	10
4	25	4	576	564	9
5	25	4	391	374	10
6	25	4	350	362	12
7	25	4	138	111	25
8	25	4	361	354	13
-11	26	4	98	112	51
-10	26	4	0	48	-1
-9	26	4	24	105	23
-8	26	4	259	249	14
-7	26	4	128	104	21
-8	28	4	70	52	69
-7	28	4	471	460	20
-6	28	4	593	585	9
-5	28	4	295	287	9
-4	28	4	171	114	17
-3	28	4	44	67	43
-2	28	4	716	704	9
-1	28	4	416	400	11
0	28	4	404	400	12
1	28	4	293	276	29
2	28	4	453	442	11
3	28	4	663	666	11
4	28	4	69	44	69
5	28	4	446	448	10
6	28	4	360	345	13
7	28	4	238	229	16
8	28	4	158	169	25
-10	29	4	31	12	31
-9	29	4	507	490	10
-8	29	4	598	606	10
-7	29	4	324	321	11
-6	29	4	325	290	19
-5	29	4	327	326	11
-4	29	4	826	803	10
-3	29	4	273	273	11
-2	29	4	205	198	14
-1	29	4	296	292	13
0	29	4	263	232	22
1	29	4	452	434	24
2	29	4	105	106	37
3	29	4	439	417	13
4	29	4	629	613	17
5	29	4	393	397	11
6	29	4	0	14	1
7	29	4	343	351	14
-10	30	4	277	288	18
-9	30	4	0	59	1
-8	30	4	154	117	21
-7	30	4	112	68	27
-6	30	4	1051	1056	11
-5	30	4	150	154	20
-4	30	4	230	222	14
-3	30	4	94	68	29
-2	30	4	348	365	17
-1	30	4	192	181	28
0	30	4	66	41	65
1	30	4	218	182	18
2	30	4	408	414	33
3	30	4	384	362	13
4	30	4	186	173	22
-9	33	4	303	315	13
-8	33	4	177	216	28
-7	33	4	293	292	13
-6	33	4	208	169	15
-5	33	4	442	420	13
-4	33	4	688	695	16
-3	33	4	336	311	11
-2	33	4	119	36	30
-1	33	4	114	21	36
0	33	4	533	529	21
1	33	4	501	499	12
2	33	4	198	141	21
3	33	4	453	432	19
4	33	4	429	453	14
5	33	4	395	411	15
6	33	4	253	259	17
-9	34	4	216	219	25
-8	34	4	0	13	1
-7	34	4	429	447	11
-6	34	4	480	477	13
-5	34	4	176	172	24
-4	34	4	156	142	19
-3	34	4	461	468	10
-2	34	4	783	789	15
-1	34	4	439	439	12
0	34	4	94	31	94
1	34	4	161	135	27
2	34	4	485	510	13
3	34	4	511	495	32
4	34	4	236	228	21
5	34	4	300	298	17
-8	35	4	323	355	14
-7	35	4	101	125	37
-6	35	4	0	110	1
-5	35	4	224	153	44
-4	35	4	207	218	17
-3	35	4	192	193	21
-2	35	4	92	79	92
-1	35	4	137	111	32
0	35	4	343	334	14
1	35	4	361	358	15
2	35	4	0	57	1
3	35	4	138	94	44
4	35	4	168	169	29
5	35	4	252	236	21
-8	36	4	171	185	22
-7	36	4	104	15	50
-6	36	4	65	102	64
-5	36	4	303	299	16
-4	36	4	0	28	1

-7	18	4	334	340	9	-9	22	4	65	36	64	-6	26	4	165	167	16	5	30	4	168	177	22	-3	36	4	155	155	26
-6	18	4	447	452	6	-8	22	4	199	187	14	-5	26	4	475	477	7	6	30	4	327	337	13	-2	36	4	0	36	1
-5	18	4	935	927	7	-7	22	4	55	23	54	-4	26	4	194	170	11	7	30	4	352	348	13	-1	36	4	104	87	41
-4	18	4	196	191	8	-6	22	4	450	459	9	-3	26	4	755	762	7	-10	31	4	91	20	61	0	36	4	161	141	25
-3	18	4	1110	1115	8	-5	22	4	99	77	17	-2	26	4	334	338	8	-9	31	4	95	118	38	1	36	4	124	143	35
-2	18	4	544	534	5	-4	22	4	78	58	20	-1	26	4	322	331	13	-8	31	4	90	64	52	2	36	4	52	54	52
-1	18	4	430	443	5	-3	22	4	330	316	7	0	26	4	371	369	12	-7	31	4	210	209	16	3	36	4	55	121	54
0	18	4	234	231	9	-2	22	4	539	545	6	1	26	4	0	46	1	-6	31	4	186	171	31	4	36	4	89	78	88
1	18	4	1026	1025	15	-1	22	4	69	28	35	2	26	4	60	50	59	-5	31	4	143	133	19	5	36	4	191	159	41
2	18	4	1138	1152	11	0	22	4	189	169	25	3	26	4	0	25	1	-4	31	4	0	48	1	-7	37	4	60	117	60
3	18	4	87	14	29	1	22	4	132	162	21	4	26	4	62	45	61	-3	31	4	340	341	10	-6	37	4	137	164	36
4	18	4	43	48	42	2	22	4	55	10	54	5	26	4	120	118	37	-2	31	4	125	50	50	-5	37	4	193	163	22
5	18	4	175	165	14	3	22	4	486	497	9	6	26	4	175	172	30	-1	31	4	352	365	12	-4	37	4	408	383	14
6	18	4	748	735	9	4	22	4	154	140	17	7	26	4	0	46	1	0	31	4	91	120	46	-3	37	4	364	348	15
7	18	4	331	342	11	5	22	4	316	321	11	8	26	4	0	24	1	1	31	4	371	381	26	-2	37	4	190	179	24
8	18	4	95	51	78	6	22	4	241	224	14	-11	27	4	281	318	19	2	31	4	44	57	43	-1	37	4	445	441	13
9	18	4	89	93	67	7	22	4	117	95	31	-10	27	4	70	21	70	3	31	4	49	31	49	0	37	4	309	317	16
10	18	4	380	404	16	8	22	4	0	85	1	-9	27	4	48	31	48	4	31	4	124	57	33	1	37	4	46	12	46
-13	19	4	452	448	15	9	22	4	60	43	60	-8	27	4	115	101	43	5	31	4	0	19	1	2	37	4	45	102	45
-12	19	4	742	735	13	-12	23	4	402	383	15	-7	27	4	194	185	14	6	31	4	46	88	46	3	37	4	0	116	1
-11	19	4	179	203	48	-11	23	4	307	307	18	-6	27	4	590	564	9	7	31	4	233	229	18	4	37	4	457	447	15
-10	19	4	67	84	66	-10	23	4	48	23	47	-5	27	4	380	372	8	-10	32	4	187	230	36	-7	38	4	264	279	20
-9	19	4	446	449	9	-9	23	4	308	335	11	-4	27	4	427	419	12	-9	32	4	107	99	32	-6	38	4	196	209	23
-8	19	4	183	175	14	-8	23	4	641	646	9	-3	27	4	440	456	7	-8	32	4	102	66	46	-5	38	4	227	263	28
-7	19	4	659	649	9	-7	23	4	707	727	9	-2	27	4	237	204	14	-7	32	4	283	299	13	-4	38	4	181	203	23
-6	19	4	93	54	22	-6	23	4	90	47	36	-1	27	4	375	364	11	-6	32	4	249	255	14	-3	38	4	278	280	17
-5	19	4	842	866	11	-5	23	4	287	280	8	0	27	4	696	702	10	-5	32	4	420	390	13	-2	38	4	390	371	15
-4	19	4	441	458	5	-4	23	4	387	380	6	1	27	4	418	412	11	-4	32	4	239	228	15	-1	38	4	300	342	21
-3	19	4	861	850	7	-3	23	4	1082	1089	8	2	27	4	114	95	32	-3	32	4	268	277	16	0	38	4	108	111	47
-2	19	4	413	394	5	-2	23	4	185	189	9	3	27	4	218	225	19	-2	32	4	380	393	17	1	38	4	367	370	15
-1	19	4	639	639	6	-1	23	4	963	950	8	4	27	4	193	191	16	-1	32	4	332	340	14	2	38	4	416	431	20
0	19	4	948	965	9	0	23	4	587	580	10	5	27	4	69	60	68	0	32	4	190	170	21	3	38	4	148	185	50
1	19	4	770	760	10	1	23	4	280	271	13	6	27	4	79	41	78	1	32	4	98	23	45	-6	39	4	81	76	80
2	19	4	0	18	1	2	23	4	389	393	11	7	27	4	473	456	11	2	32	4	345	325	14	-5	39	4	470	468	26
3	19	4	270	265	17	3	23	4	369	369	9	8	27	4	221	221	19	3	32	4	263	245	17	-4	39	4	240	241	28

Table D.6. Observed and calculated structure factors for Rutdp

h	k	l	10Fo	10Fc	10s	h	k	l	10Fo	10Fc	10s	h	k	l	10Fo	10Fc	10s	h	k	l	10Fo	10Fc	10s	h	k	l	10Fo	10Fc	10s
-3	39	4	131	50	36	4	3	5	768	782	10	-8	7	5	72	84	33	5	10	5	318	329	7	-6	14	5	272	269	8
-2	39	4	151	66	48	5	3	5	0	73	1	-7	7	5	876	848	9	6	10	5	154	143	15	-5	14	5	447	445	5
-1	39	4	166	166	26	6	3	5	618	620	16	-6	7	5	947	980	10	7	10	5	0	60	1	-4	14	5	349	351	5
0	39	4	499	495	13	7	3	5	961	961	13	-5	7	5	1295	1343	9	8	10	5	133	144	25	-3	14	5	255	265	6
1	39	4	431	415	15	8	3	5	72	97	71	-4	7	5	288	302	5	9	10	5	150	183	22	-2	14	5	395	374	5
2	39	4	115	68	47	9	3	5	0	42	1	-3	7	5	791	798	6	10	10	5	24	5	23	-1	14	5	181	164	10
3	39	4	236	209	22	10	3	5	129	129	30	-2	7	5	514	507	4	-14	11	5	384	361	15	0	14	5	275	291	7
-5	40	4	49	92	49	-14	4	5	97	100	50	-1	7	5	1653	1678	9	-13	11	5	359	373	21	1	14	5	719	735	8
-4	40	4	209	214	33	-13	4	5	274	271	16	0	7	5	748	739	5	-12	11	5	78	28	77	2	14	5	297	307	8
-3	40	4	116	124	116	-12	4	5	443	435	10	1	7	5	66	44	22	-11	11	5	389	370	13	3	14	5	638	656	8

-2	40	4	135	115	37
-1	40	4	285	267	18
0	40	4	111	104	48
1	40	4	60	95	60
2	40	4	207	219	23
-4	41	4	302	313	26
-3	41	4	52	38	52
-2	41	4	0	43	1
-1	41	4	0	65	1
0	41	4	136	119	36
-14	1	5	332	346	17
-13	1	5	285	270	11
-12	1	5	184	178	16
-11	1	5	343	339	12
-10	1	5	404	407	16
-9	1	5	788	778	11
-8	1	5	49	9	49
-7	1	5	739	732	10
-6	1	5	813	777	10
-5	1	5	1220	1239	14
-4	1	5	233	244	5
-3	1	5	838	854	7
-2	1	5	451	440	5
-1	1	5	406	406	6
0	1	5	123	144	12
1	1	5	679	642	6
2	1	5	475	478	4
3	1	5	483	495	5
4	1	5	0	11	-1
5	1	5	111	19	43
6	1	5	0	36	1
7	1	5	644	649	11
8	1	5	243	233	23
9	1	5	218	232	30
10	1	5	122	109	42
-14	2	5	0	45	1
-13	2	5	344	368	12
-12	2	5	289	261	11
-11	2	5	189	171	17
-10	2	5	175	183	18
-9	2	5	73	75	72
-8	2	5	1040	1039	13
-7	2	5	415	407	9
-6	2	5	1092	1108	10
-5	2	5	1050	1002	9
-4	2	5	1060	1036	8
-3	2	5	1062	1082	8
-2	2	5	448	465	5
-1	2	5	834	846	7
0	2	5	1997	1981	15
-11	4	5	415	414	9
-10	4	5	637	631	9
-9	4	5	402	407	10
-8	4	5	422	414	9
-7	4	5	320	320	19
-6	4	5	605	587	7
-5	4	5	637	634	7
-4	4	5	901	883	7
-3	4	5	161	159	5
-2	4	5	357	364	4
-1	4	5	168	169	7
0	4	5	713	694	6
1	4	5	611	575	6
2	4	5	854	859	6
3	4	5	184	173	13
4	4	5	810	820	11
5	4	5	26	111	26
6	4	5	398	380	11
7	4	5	211	208	19
8	4	5	60	127	60
9	4	5	292	321	18
10	4	5	39	25	39
-14	5	5	0	67	1
-13	5	5	289	280	15
-12	5	5	96	68	37
-11	5	5	0	90	1
-10	5	5	517	519	9
-9	5	5	374	369	10
-8	5	5	356	358	8
-7	5	5	519	501	15
-6	5	5	624	604	7
-5	5	5	648	664	7
-4	5	5	645	586	5
-3	5	5	809	816	8
-2	5	5	407	404	4
-1	5	5	209	227	5
0	5	5	290	276	6
1	5	5	468	434	6
2	5	5	538	506	5
3	5	5	458	460	5
4	5	5	0	24	1
5	5	5	386	363	15
6	5	5	315	319	13
7	5	5	94	120	37
8	5	5	183	163	21
9	5	5	0	24	1
10	5	5	129	144	23
-14	6	5	156	160	29
-13	6	5	302	294	15
-12	6	5	136	118	25
2	7	5	722	720	6
3	7	5	1348	1354	12
4	7	5	79	97	28
5	7	5	241	233	15
6	7	5	268	291	22
7	7	5	993	985	10
8	7	5	652	641	9
9	7	5	0	19	1
10	7	5	428	418	18
-14	8	5	43	11	42
-13	8	5	310	317	21
-12	8	5	491	478	14
-11	8	5	234	240	16
-10	8	5	125	132	21
-9	8	5	158	138	16
-8	8	5	499	485	8
-7	8	5	458	465	6
-6	8	5	1047	1052	9
-5	8	5	231	216	5
-4	8	5	513	530	5
-3	8	5	1463	1521	10
-2	8	5	58	77	20
-1	8	5	778	775	5
0	8	5	856	845	6
1	8	5	837	862	6
2	8	5	285	274	6
3	8	5	341	343	11
4	8	5	562	548	6
5	8	5	53	64	52
6	8	5	82	86	81
7	8	5	356	373	9
8	8	5	657	656	8
9	8	5	431	423	9
10	8	5	177	202	25
-14	9	5	0	99	1
-13	9	5	231	227	18
-12	9	5	198	197	33
-11	9	5	255	267	15
-10	9	5	47	24	47
-9	9	5	704	730	11
-8	9	5	658	653	13
-7	9	5	767	782	7
-6	9	5	389	380	6
-5	9	5	207	213	6
-4	9	5	0	28	1
-3	9	5	56	10	22
-2	9	5	332	322	5
-1	9	5	1098	1084	9
0	9	5	690	685	6
1	9	5	641	643	5
-10	11	5	86	81	31
-9	11	5	550	546	12
-8	11	5	754	755	9
-7	11	5	244	229	10
-6	11	5	1120	1137	12
-5	11	5	832	823	8
-4	11	5	809	802	6
-3	11	5	248	231	6
-2	11	5	1439	1468	11
-1	11	5	803	818	6
0	11	5	105	113	18
1	11	5	698	685	6
2	11	5	79	82	19
3	11	5	712	716	7
4	11	5	844	835	8
5	11	5	0	7	1
6	11	5	605	600	9
7	11	5	543	526	11
8	11	5	344	343	14
9	11	5	113	4	31
10	11	5	230	227	17
-14	12	5	101	77	46
-13	12	5	584	576	19
-12	12	5	541	524	13
-11	12	5	800	811	13
-10	12	5	417	415	13
-9	12	5	201	197	13
-8	12	5	919	929	13
-7	12	5	842	824	10
-6	12	5	37	10	36
-5	12	5	79	49	18
-4	12	5	738	755	6
-3	12	5	341	345	5
-2	12	5	692	701	6
-1	12	5	364	359	5
0	12	5	726	735	6
1	12	5	1096	1129	11
2	12	5	367	359	7
3	12	5	127	114	17
4	12	5	158	129	12
5	12	5	680	661	8
6	12	5	354	357	10
7	12	5	278	270	13
8	12	5	661	668	10
9	12	5	565	565	10
10	12	5	296	320	19
-14	13	5	243	218	30
-13	13	5	289	276	18
-12	13	5	363	375	14
-11	13	5	520	520	16
4	14	5	445	436	8
5	14	5	185	183	12
6	14	5	0	25	1
7	14	5	149	126	21
8	14	5	88	33	80
9	14	5	0	105	1
-13	15	5	145	106	33
-12	15	5	119	149	33
-11	15	5	67	41	67
-10	15	5	441	403	18
-9	15	5	0	27	1
-8	15	5	39	50	39
-7	15	5	120	130	20
-6	15	5	21	9	21
-5	15	5	436	432	6
-4	15	5	321	335	5
-3	15	5	536	518	5
-2	15	5	597	595	5
-1	15	5	166	163	8
0	15	5	57	76	56
1	15	5	92	57	23
2	15	5	847	874	9
3	15	5	154	152	17
4	15	5	191	209	13
5	15	5	200	216	13
6	15	5	139	162	24
7	15	5	276	297	33
8	15	5	0	27	1
9	15	5	203	182	23
-13	16	5	183	208	23
-12	16	5	555	544	13
-11	16	5	592	571	12
-10	16	5	126	112	28
-9	16	5	190	200	24
-8	16	5	258	250	9
-7	16	5	713	708	7
-6	16	5	186	181	12
-5	16	5	467	465	5
-4	16	5	852	860	7
-3	16	5	521	539	5
-2	16	5	459	455	6
-1	16	5	378	370	6
0	16	5	1174	1171	11
1	16	5	1092	1111	10
2	16	5	440	442	8
3	16	5	141	135	17
4	16	5	172	180	15
5	16	5	621	608	11
6	16	5	107	87	35
7	16	5	210	215	24

1	2	5	1200	1200	9	-11	6	5	234	248	13	2	9	5	350	340	5	-10	13	5	683	678	16	8	16	5	438	443	15
2	2	5	553	536	5	-10	6	5	35	79	34	3	9	5	281	281	7	-9	13	5	700	710	9	9	16	5	561	557	13
3	2	5	455	446	7	-9	6	5	161	152	14	4	9	5	113	94	15	-8	13	5	253	261	10	-13	17	5	318	337	16
4	2	5	767	770	10	-8	6	5	1153	1140	14	5	9	5	344	345	8	-7	13	5	49	34	48	-12	17	5	142	135	29
5	2	5	787	785	11	-7	6	5	855	864	7	6	9	5	277	292	10	-6	13	5	806	798	12	-11	17	5	317	326	17
6	2	5	862	860	13	-6	6	5	911	897	9	7	9	5	0	41	1	-5	13	5	683	689	6	-10	17	5	397	399	19
7	2	5	369	355	17	-5	6	5	523	527	6	8	9	5	65	53	64	-4	13	5	137	143	10	-9	17	5	687	682	12
8	2	5	418	412	17	-4	6	5	946	949	7	9	9	5	0	32	1	-3	13	5	350	301	5	-8	17	5	470	480	9
9	2	5	690	682	27	-3	6	5	651	634	5	10	9	5	94	97	45	-2	13	5	850	843	6	-7	17	5	410	401	7
10	2	5	157	130	28	-2	6	5	73	21	13	-14	10	5	160	169	28	-1	13	5	740	756	6	-6	17	5	660	653	7
-14	3	5	555	540	11	-1	6	5	733	714	6	-13	10	5	167	99	26	0	13	5	209	206	8	-5	17	5	662	652	6
-13	3	5	424	421	15	0	6	5	485	460	5	-12	10	5	0	27	1	1	13	5	72	71	25	-4	17	5	236	254	7
-12	3	5	156	168	23	1	6	5	726	723	8	-11	10	5	426	435	18	2	13	5	99	107	16	-3	17	5	72	54	25
-11	3	5	155	146	17	2	6	5	576	597	7	-10	10	5	84	51	30	3	13	5	1062	1071	9	-2	17	5	946	953	7
-10	3	5	118	53	22	3	6	5	645	623	11	-9	10	5	48	37	48	4	13	5	360	365	8	-1	17	5	857	882	7
-9	3	5	673	681	10	4	6	5	256	242	11	-8	10	5	149	131	15	5	13	5	72	15	41	0	17	5	337	347	10
-8	3	5	532	531	9	5	6	5	450	456	15	-7	10	5	255	229	8	6	13	5	419	423	9	1	17	5	284	286	15
-7	3	5	1232	1247	14	6	6	5	785	771	11	-6	10	5	255	237	7	7	13	5	423	427	10	2	17	5	739	717	10
-6	3	5	1379	1392	15	7	6	5	0	8	1	-5	10	5	517	501	5	8	13	5	323	303	12	3	17	5	553	545	8
-5	3	5	231	236	8	8	6	5	279	279	12	-4	10	5	645	638	6	9	13	5	121	118	40	4	17	5	173	183	15
-4	3	5	224	197	5	9	6	5	287	313	11	-3	10	5	549	541	5	10	13	5	441	427	16	5	17	5	163	185	17
-3	3	5	100	100	16	10	6	5	174	162	17	-2	10	5	105	105	10	-13	14	5	119	105	35	6	17	5	592	584	9
-2	3	5	608	619	5	-14	7	5	368	361	15	-1	10	5	279	261	5	-12	14	5	0	64	1	7	17	5	372	358	14
-1	3	5	678	685	5	-13	7	5	246	242	17	0	10	5	996	987	7	-11	14	5	205	191	19	8	17	5	282	276	17
0	3	5	1095	1098	10	-12	7	5	223	225	18	1	10	5	392	409	5	-10	14	5	351	368	15	9	17	5	103	111	56
1	3	5	441	414	6	-11	7	5	514	509	13	2	10	5	631	615	5	-9	14	5	386	401	15	-13	18	5	266	261	19
2	3	5	1036	1046	7	-10	7	5	825	806	10	3	10	5	317	316	6	-8	14	5	502	525	7	-12	18	5	239	263	19
3	3	5	1213	1213	9	-9	7	5	169	147	15	4	10	5	317	311	8	-7	14	5	266	271	9	-11	18	5	271	292	16

Table D.6. Observed and calculated structure factors for Rutdp

h	k	1	10Fo	10Fc	10s	h	k	1	10Fo	10Fc	10s	h	k	1	10Fo	10Fc	10s	h	k	l	10Fo	10Fc	10s	h	k	1	10Fo	10Fc	10s
-10	18	5	0	69	1	-11	22	5	447	450	18	-6	26	5	88	45	34	-9	31	5	228	227	16	-6	37	5	160	164	29
-9	18	5	56	22	56	-10	22	5	86	52	85	-5	26	5	474	473	9	-8	31	5	182	153	19	-5	37	5	127	167	40
-8	18	5	580	574	8	-9	22	5	371	384	13	-4	26	5	778	762	7	-7	31	5	232	252	14	-4	37	5	0	10	1
-7	18	5	501	494	7	-8	22	5	770	798	9	-3	26	5	227	221	11	-6	31	5	598	593	10	-3	37	5	47	58	47
-6	18	5	217	198	10	-7	22	5	736	753	12	-2	26	5	499	494	7	-5	31	5	338	334	14	-2	37	5	239	243	76
-5	18	5	486	494	6	-6	22	5	70	60	37	-1	26	5	0	47	1	-4	31	5	247	220	13	-1	37	5	394	349	18
-4	18	5	611	594	6	-5	22	5	466	464	7	0	26	5	872	876	17	-3	31	5	97	75	29	0	37	5	192	133	26
-3	18	5	323	330	7	-4	22	5	80	83	24	1	26	5	387	357	12	-2	31	5	613	609	11	1	37	5	0	42	1
-2	18	5	556	562	6	-3	22	5	709	709	6	2	26	5	221	232	23	-1	31	5	544	537	11	2	37	5	157	210	33
-1	18	5	145	173	10	-2	22	5	614	616	7	3	26	5	341	332	15	0	31	5	179	175	24	3	37	5	414	386	16
0	18	5	730	732	8	-1	22	5	215	193	11	4	26	5	557	531	10	1	31	5	167	175	22	-6	38	5	58	116	57
1	18	5	601	580	8	0	22	5	676	684	8	5	26	5	556	536	10	2	31	5	492	489	13	-5	38	5	104	65	50
2	18	5	82	112	39	1	22	5	965	976	17	6	26	5	274	285	14	3	31	5	638	617	12	-4	38	5	0	16	-1
3	18	5	121	137	20	2	22	5	320	324	13	7	26	5	156	146	32	4	31	5	324	328	16	-3	38	5	0	4	1
4	18	5	494	499	9	3	22	5	498	498	9	-11	27	5	113	155	112	5	31	5	236	228	22	-2	38	5	51	42	51
5	18	5	536	540	12	4	22	5	582	572	13	-10	27	5	508	508	13	6	31	5	281	302	17	-1	38	5	49	9	49
6	18	5	40	41	39	5	22	5	526	514	11	-9	27	5	298	292	15	-9	32	5	79	94	68	0	38	5	120	144	119

7	18	5	120	86	34
8	18	5	0	22	1
9	18	5	355	376	17
-13	19	5	137	115	38
-12	19	5	62	56	61
-11	19	5	0	75	1
-10	19	5	100	62	36
-9	19	5	35	12	34
-8	19	5	339	338	10
-7	19	5	389	393	9
-6	19	5	208	197	11
-5	19	5	294	297	7
-4	19	5	238	225	7
-3	19	5	91	69	28
-2	19	5	0	25	1
-1	19	5	114	139	18
0	19	5	219	234	11
1	19	5	70	109	69
2	19	5	324	318	12
3	19	5	627	638	9
4	19	5	208	204	15
5	19	5	130	113	21
6	19	5	215	252	14
7	19	5	172	183	26
8	19	5	235	236	21
9	19	5	0	2	1
-13	20	5	152	75	31
-12	20	5	347	346	26
-11	20	5	241	247	24
-10	20	5	51	47	51
-9	20	5	249	271	15
-8	20	5	451	423	9
-7	20	5	982	981	13
-6	20	5	170	173	11
-5	20	5	306	306	7
-4	20	5	108	115	14
-3	20	5	364	352	6
-2	20	5	638	637	6
-1	20	5	478	471	7
0	20	5	833	848	9
1	20	5	160	133	21
2	20	5	339	341	12
3	20	5	225	230	11
4	20	5	371	359	10
5	20	5	338	330	11
6	20	5	0	30	1
7	20	5	24	32	23
8	20	5	0	44	1
9	20	5	317	322	17
-12	21	5	117	115	40
6	22	5	356	366	11
7	22	5	87	71	70
8	22	5	245	193	21
-12	23	5	21	67	21
-11	23	5	0	13	1
-10	23	5	290	299	15
-9	23	5	270	273	16
-8	23	5	263	255	11
-7	23	5	806	832	10
-6	23	5	63	55	63
-5	23	5	153	131	13
-4	23	5	750	752	7
-3	23	5	374	370	6
-2	23	5	818	818	8
-1	23	5	729	731	8
0	23	5	213	224	13
1	23	5	85	69	46
2	23	5	638	625	12
3	23	5	434	424	11
4	23	5	0	59	1
5	23	5	345	349	11
6	23	5	184	194	18
7	23	5	306	322	16
8	23	5	0	39	1
-12	24	5	0	10	1
-11	24	5	0	52	1
-10	24	5	200	196	21
-9	24	5	214	209	18
-8	24	5	57	55	56
-7	24	5	272	261	13
-6	24	5	194	142	14
-5	24	5	111	71	16
-4	24	5	468	460	6
-3	24	5	128	122	13
-2	24	5	494	497	7
-1	24	5	387	396	9
0	24	5	410	413	11
1	24	5	491	497	11
2	24	5	0	40	1
3	24	5	0	25	1
4	24	5	0	27	1
5	24	5	68	87	68
6	24	5	86	14	68
7	24	5	0	78	1
8	24	5	302	295	20
-12	25	5	48	17	47
-11	25	5	161	156	43
-10	25	5	147	122	28
-9	25	5	399	414	13
-8	25	5	265	258	16
-8	27	5	323	321	11
-7	27	5	309	309	11
-6	27	5	504	502	9
-5	27	5	632	609	9
-4	27	5	136	61	15
-3	27	5	390	385	8
-2	27	5	110	126	17
-1	27	5	332	307	25
0	27	5	325	323	20
1	27	5	233	240	17
2	27	5	620	623	11
3	27	5	572	573	11
4	27	5	318	304	15
5	27	5	185	178	17
6	27	5	335	331	13
7	27	5	419	416	12
-11	28	5	173	204	26
-10	28	5	0	24	1
-9	28	5	103	44	57
-8	28	5	227	245	17
-7	28	5	0	49	1
-6	28	5	177	152	16
-5	28	5	193	171	14
-4	28	5	440	444	9
-3	28	5	446	444	7
-2	28	5	64	55	64
-1	28	5	131	144	28
0	28	5	81	19	81
1	28	5	203	177	19
2	28	5	433	455	12
3	28	5	330	327	14
4	28	5	257	236	17
5	28	5	182	159	19
6	28	5	220	199	18
7	28	5	106	20	35
-11	29	5	0	3	1
-10	29	5	0	47	1
-9	29	5	76	49	75
-8	29	5	17	41	16
-7	29	5	0	39	1
-6	29	5	423	424	10
-5	29	5	118	110	33
-4	29	5	237	213	13
-3	29	5	134	139	16
-2	29	5	0	39	1
-1	29	5	395	419	17
0	29	5	91	30	49
1	29	5	128	94	34
2	29	5	101	79	40
3	29	5	175	186	47
-8	32	5	515	528	10
-7	32	5	120	129	36
-6	32	5	0	21	1
-5	32	5	243	282	22
-4	32	5	508	498	10
-3	32	5	570	575	9
-2	32	5	204	169	20
-1	32	5	177	173	21
0	32	5	365	323	14
1	32	5	350	319	15
2	32	5	246	294	17
3	32	5	0	74	1
4	32	5	245	262	20
5	32	5	549	521	27
-9	33	5	43	46	43
-8	33	5	161	145	22
-7	33	5	244	232	17
-6	33	5	274	246	16
-5	33	5	36	26	36
-4	33	5	0	54	1
-3	33	5	134	142	23
-2	33	5	186	159	21
-1	33	5	159	133	24
0	33	5	156	95	27
1	33	5	93	87	93
2	33	5	108	5	41
3	33	5	149	194	32
4	33	5	112	71	44
5	33	5	0	7	1
-9	34	5	73	48	73
-8	34	5	0	50	1
-7	34	5	325	346	15
-6	34	5	0	55	1
-5	34	5	174	200	25
-4	34	5	175	190	21
-3	34	5	201	188	26
-2	34	5	138	129	28
-1	34	5	257	262	17
0	34	5	226	184	20
1	34	5	46	108	46
2	34	5	131	57	43
3	34	5	176	203	27
4	34	5	136	186	35
5	34	5	177	190	46
-8	35	5	0	63	1
-7	35	5	83	62	82
-6	35	5	320	331	30
-5	35	5	346	337	15
-4	35	5	109	93	43
-3	35	5	200	185	21
1	38	5	207	189	22
2	38	5	0	47	1
-5	39	5	237	229	20
-4	39	5	171	180	37
-3	39	5	175	153	34
-2	39	5	143	153	32
-1	39	5	86	69	85
0	39	5	105	82	54
1	39	5	41	63	40
-4	40	5	245	280	31
-3	40	5	348	376	17
-2	40	5	243	235	21
-1	40	5	194	200	52
0	40	5	365	352	16
-2	41	5	306	321	27
-14	0	6	336	340	16
-13	0	6	863	846	15
-12	0	6	360	359	17
-11	0	6	259	249	21
-10	0	6	507	514	15
-9	0	6	1538	1591	25
-8	0	6	1308	1301	22
-7	0	6	70	18	70
-6	0	6	974	954	17
-5	0	6	1000	1015	13
-4	0	6	476	474	7
-3	0	6	221	214	9
-2	0	6	703	702	9
-1	0	6	762	757	10
0	0	6	693	719	9
1	0	6	212	197	25
2	0	6	614	629	12
3	0	6	482	452	17
5	0	6	209	221	21
6	0	6	690	685	15
7	0	6	785	794	17
8	0	6	212	207	30
9	0	6	0	64	1
-14	1	6	116	169	26
-13	1	6	0	31	1
-12	1	6	68	136	67
-11	1	6	208	217	20
-10	1	6	798	796	11
-9	1	6	244	212	13
-8	1	6	499	510	14
-7	1	6	1325	1363	15
-6	1	6	77	72	36
-5	1	6	638	608	5
-4	1	6	715	709	6
-3	1	6	412	417	5

-11	21	5	113	145	60
-10	21	5	512	502	13
-9	21	5	276	258	15
-8	21	5	166	150	22
-7	21	5	160	138	16
-6	21	5	299	295	8
-5	21	5	912	901	8
-4	21	5	274	283	7
-3	21	5	691	700	6
-2	21	5	467	470	6
-1	21	5	474	468	7
0	21	5	729	740	8
1	21	5	146	147	30
2	21	5	826	842	11
3	21	5	118	95	23
4	21	5	112	105	28
5	21	5	0	15	1
6	21	5	518	511	10
7	21	5	477	446	13
8	21	5	399	371	16
-12	22	5	413	415	15
-7	25	5	158	123	16
-6	25	5	819	822	9
-5	25	5	369	368	10
-4	25	5	125	100	17
-3	25	5	496	491	7
-2	25	5	370	373	8
-1	25	5	665	683	8
0	25	5	69	31	68
1	25	5	332	339	12
2	25	5	327	314	13
3	25	5	221	225	17
4	25	5	156	152	19
5	25	5	164	205	19
6	25	5	375	379	11
7	25	5	329	318	16
8	25	5	241	233	24
-11	26	5	300	316	27
-10	26	5	160	170	28
-9	26	5	182	225	25
-8	26	5	627	637	9
-7	26	5	550	554	10
4	29	5	138	136	44
5	29	5	43	39	43
6	29	5	107	101	59
-10	30	5	139	177	50
-9	30	5	243	250	14
-8	30	5	303	308	13
-7	30	5	192	206	16
-6	30	5	172	155	17
-5	30	5	0	8	1
-4	30	5	851	856	10
-3	30	5	403	404	10
-2	30	5	252	249	15
-1	30	5	133	123	27
0	30	5	237	254	17
1	30	5	759	739	12
2	30	5	209	213	20
3	30	5	150	107	29
4	30	5	227	210	34
5	30	5	232	218	22
6	30	5	305	293	14
-10	31	5	321	355	17
-2	35	5	416	415	13
-1	35	5	314	314	15
0	35	5	226	230	20
1	35	5	0	110	1
2	35	5	458	455	35
3	35	5	251	276	19
4	35	5	206	251	26
-8	36	5	341	353	18
-7	36	5	212	201	22
-6	36	5	364	384	18
-5	36	5	69	97	69
-4	36	5	641	638	13
-3	36	5	430	437	15
-2	36	5	46	101	46
-1	36	5	65	58	65
0	36	5	411	441	14
1	36	5	608	599	12
2	36	5	247	245	21
3	36	5	277	236	20
4	36	5	330	318	27
-7	37	5	0	76	1
-2	1	6	1324	1321	10
-1	1	6	55	85	55
0	1	6	460	496	7
1	1	6	644	644	7
2	1	6	837	812	7
3	1	6	703	699	7
4	1	6	0	71	1
5	1	6	871	868	16
6	1	6	189	160	18
7	1	6	205	232	21
8	1	6	48	31	48
9	1	6	355	404	22
-14	2	6	311	294	14
-13	2	6	0	31	1
-12	2	6	163	156	17
-11	2	6	59	71	59
-10	2	6	206	186	15
-9	2	6	559	567	10
-8	2	6	283	282	11
-7	2	6	442	439	10
-6	2	6	330	361	10

Table D.6. Observed and calculated structure factors for Rutdp

h	k	1	10Fo	10Fc	10s
-5	2	6	176	174	9
-4	2	6	1095	1116	8
-3	2	6	533	522	9
-2	2	6	510	523	5
-1	2	6	116	143	11
0	2	6	279	274	7
1	2	6	435	421	6
2	2	6	143	120	12
3	2	6	520	519	6
4	2	6	35	67	34
5	2	6	416	417	11
6	2	6	164	174	21
7	2	6	489	477	11
8	2	6	165	156	27
9	2	6	0	30	1
-14	3	6	41	81	41
-13	3	6	0	19	-1
-12	3	6	145	160	19
-11	3	6	0	36	1
-10	3	6	305	306	20
-9	3	6	319	326	11
-8	3	6	505	491	10
-7	3	6	123	116	22
-6	3	6	170	193	14
-13	6	6	362	339	14
-12	6	6	0	14	-1
-11	6	6	0	52	1
-10	6	6	407	391	9
-9	6	6	236	239	21
-8	6	6	265	264	10
-7	6	6	64	23	63
-6	6	6	1059	1083	9
-5	6	6	284	315	7
-4	6	6	57	38	22
-3	6	6	769	755	7
-2	6	6	465	454	4
-1	6	6	711	696	6
0	6	6	731	744	8
1	6	6	133	111	12
2	6	6	455	465	7
3	6	6	745	705	8
4	6	6	544	532	15
5	6	6	84	110	84
6	6	6	308	293	14
7	6	6	439	447	12
8	6	6	80	152	42
9	6	6	0	100	1
-14	7	6	63	95	63
3	9	6	92	76	18
4	9	6	348	370	15
5	9	6	553	551	7
6	9	6	714	726	11
7	9	6	132	138	22
8	9	6	341	355	12
9	9	6	183	211	19
-14	10	6	158	166	60
-13	10	6	306	294	15
-12	10	6	25	24	25
-11	10	6	42	10	41
-10	10	6	853	832	10
-9	10	6	919	901	10
-8	10	6	319	319	10
-7	10	6	190	188	16
-6	10	6	540	510	6
-5	10	6	405	422	7
-4	10	6	1088	1096	8
-3	10	6	75	49	16
-2	10	6	630	623	5
-1	10	6	1523	1513	10
0	10	6	739	739	6
1	10	6	215	220	8
2	10	6	293	306	12
-5	13	6	385	376	9
-4	13	6	184	149	8
-3	13	6	280	299	6
-2	13	6	136	162	9
-1	13	6	244	225	8
0	13	6	463	464	6
1	13	6	726	715	7
2	13	6	482	486	7
3	13	6	463	460	7
4	13	6	131	130	21
5	13	6	420	434	10
6	13	6	206	199	15
7	13	6	146	114	23
8	13	6	225	250	17
9	13	6	279	275	15
-14	14	6	222	199	30
-13	14	6	329	296	16
-12	14	6	288	285	25
-11	14	6	182	166	40
-10	14	6	498	498	16
-9	14	6	486	485	11
-8	14	6	614	618	9
-7	14	6	157	174	12
-6	14	6	1046	1048	9
-9	17	6	82	35	48
-8	17	6	98	87	23
-7	17	6	331	315	8
-6	17	6	58	61	47
-5	17	6	175	186	14
-4	17	6	99	109	17
-3	17	6	101	101	16
-2	17	6	0	45	1
-1	17	6	193	189	12
0	17	6	438	449	8
1	17	6	329	344	9
2	17	6	97	95	67
3	17	6	320	317	12
4	17	6	77	68	54
5	17	6	347	350	13
6	17	6	126	151	35
7	17	6	124	86	102
8	17	6	51	38	50
-13	18	6	245	253	20
-12	18	6	172	202	23
-11	18	6	132	82	43
-10	18	6	501	513	12
-9	18	6	953	933	19
-8	18	6	274	238	12

-5	3	6	503	463	6
-4	3	6	442	442	5
-3	3	6	166	165	8
-2	3	6	362	346	6
-1	3	6	351	348	5
0	3	6	569	515	6
1	3	6	0	55	1
2	3	6	91	111	33
3	3	6	544	541	6
4	3	6	489	517	13
5	3	6	452	466	14
6	3	6	553	548	21
7	3	6	348	346	14
8	3	6	163	161	25
9	3	6	150	180	30
-14	4	6	344	341	16
-13	4	6	364	358	11
-12	4	6	327	337	11
-11	4	6	423	391	11
-10	4	6	310	310	12
-9	4	6	889	912	17
-8	4	6	480	478	15
-7	4	6	533	516	9
-6	4	6	191	167	12
-5	4	6	157	198	10
-4	4	6	765	815	6
-3	4	6	429	435	5
-2	4	6	357	354	5
-1	4	6	1025	1038	7
0	4	6	723	749	7
1	4	6	144	138	11
2	4	6	488	468	7
3	4	6	1262	1267	11
4	4	6	210	242	15
5	4	6	166	190	20
6	4	6	385	382	12
7	4	6	527	556	17
8	4	6	519	506	12
9	4	6	229	215	15
-14	5	6	273	279	18
-13	5	6	29	74	29
-12	5	6	406	396	10
-11	5	6	590	591	9
-10	5	6	546	533	9
-9	5	6	175	204	13
-8	5	6	378	369	10
-7	5	6	1301	1296	15
-6	5	6	348	378	8
-5	5	6	108	102	14
-4	5	6	423	396	5
-13	7	6	200	241	23
-12	7	6	309	308	11
-11	7	6	138	148	24
-10	7	6	140	104	18
-9	7	6	138	119	19
-8	7	6	304	310	9
-7	7	6	274	265	9
-6	7	6	1099	1079	12
-5	7	6	38	80	37
-4	7	6	906	884	7
-3	7	6	45	13	29
-2	7	6	103	100	9
-1	7	6	703	695	5
0	7	6	756	749	7
1	7	6	436	450	9
2	7	6	0	10	1
3	7	6	809	829	9
4	7	6	214	222	17
5	7	6	172	178	18
6	7	6	46	41	46
7	7	6	41	32	40
8	7	6	0	21	1
9	7	6	138	152	26
-14	8	6	185	158	26
-13	8	6	182	187	39
-12	8	6	350	363	14
-11	8	6	194	185	14
-10	8	6	491	490	11
-9	8	6	0	49	1
-8	8	6	686	681	9
-7	8	6	224	223	11
-6	8	6	884	884	8
-5	8	6	394	405	7
-4	8	6	100	100	11
-3	8	6	825	809	6
-2	8	6	428	437	5
-1	8	6	711	736	5
0	8	6	90	76	13
1	8	6	0	51	1
2	8	6	71	35	25
3	8	6	139	150	17
4	8	6	400	430	11
5	8	6	0	13	1
6	8	6	268	280	10
7	8	6	263	250	13
8	8	6	318	346	10
9	8	6	214	247	15
-14	9	6	316	328	16
-13	9	6	0	37	1
-12	9	6	282	286	16
3	10	6	438	439	6
4	10	6	1137	1141	9
5	10	6	199	196	12
6	10	6	539	553	9
7	10	6	411	413	9
8	10	6	470	461	11
9	10	6	216	206	18
-14	11	6	45	103	45
-13	11	6	245	276	34
-12	11	6	264	234	23
-11	11	6	118	149	28
-10	11	6	383	376	9
-9	11	6	346	361	9
-8	11	6	817	816	9
-7	11	6	267	250	8
-6	11	6	316	310	8
-5	11	6	0	38	-1
-4	11	6	395	387	5
-3	11	6	1203	1181	8
-2	11	6	1213	1212	8
-1	11	6	377	368	8
0	11	6	49	40	48
1	11	6	371	387	8
2	11	6	679	703	7
3	11	6	92	79	19
4	11	6	0	55	1
5	11	6	0	50	1
6	11	6	474	490	12
7	11	6	209	227	16
8	11	6	260	219	14
9	11	6	289	290	15
-14	12	6	0	14	1
-13	12	6	131	163	29
-12	12	6	35	6	34
-11	12	6	129	99	32
-10	12	6	309	324	10
-9	12	6	368	375	9
-8	12	6	335	343	9
-7	12	6	669	657	8
-6	12	6	604	594	7
-5	12	6	220	223	8
-4	12	6	262	270	6
-3	12	6	418	411	6
-2	12	6	622	612	5
-1	12	6	649	637	6
0	12	6	210	196	8
1	12	6	439	444	7
2	12	6	70	74	29
3	12	6	255	262	10
4	12	6	72	75	45
-5	14	6	636	637	7
-4	14	6	654	650	6
-3	14	6	495	515	5
-2	14	6	1456	1455	10
-1	14	6	1637	1650	12
0	14	6	602	608	7
1	14	6	86	50	25
2	14	6	534	545	7
3	14	6	186	171	11
4	14	6	852	848	10
5	14	6	166	136	17
6	14	6	427	415	13
7	14	6	522	508	12
8	14	6	194	200	19
9	14	6	131	90	44
-13	15	6	127	151	43
-12	15	6	469	455	18
-11	15	6	472	489	13
-10	15	6	259	276	19
-9	15	6	131	167	19
-8	15	6	639	649	9
-7	15	6	738	744	9
-6	15	6	738	729	7
-5	15	6	84	94	35
-4	15	6	1160	1177	8
-3	15	6	681	681	6
-2	15	6	427	409	5
-1	15	6	225	223	8
0	15	6	765	761	8
1	15	6	912	913	9
2	15	6	640	626	8
3	15	6	278	258	10
4	15	6	141	118	25
5	15	6	373	357	10
6	15	6	693	691	12
7	15	6	0	6	1
8	15	6	287	273	18
9	15	6	443	455	15
-13	16	6	241	285	20
-12	16	6	110	122	38
-11	16	6	83	79	82
-10	16	6	283	286	14
-9	16	6	333	327	23
-8	16	6	69	95	40
-7	16	6	57	29	49
-6	16	6	343	352	7
-5	16	6	236	241	8
-4	16	6	439	444	5
-3	16	6	200	190	8
-2	16	6	122	123	12
-7	18	6	229	215	11
-6	18	6	210	210	10
-5	18	6	325	320	7
-4	18	6	640	626	6
-3	18	6	430	436	6
-2	18	6	721	719	6
-1	18	6	298	301	14
0	18	6	457	465	8
1	18	6	582	592	8
2	18	6	268	271	13
3	18	6	435	439	19
4	18	6	317	298	11
5	18	6	35	11	34
6	18	6	190	199	21
7	18	6	290	292	22
8	18	6	191	195	29
-13	19	6	60	103	60
-12	19	6	240	276	20
-11	19	6	549	534	20
-10	19	6	269	275	35
-9	19	6	57	43	57
-8	19	6	287	311	13
-7	19	6	406	404	7
-6	19	6	562	582	7
-5	19	6	575	573	7
-4	19	6	593	574	6
-3	19	6	782	757	9
-2	19	6	1185	1194	9
-1	19	6	465	472	9
0	19	6	769	755	9
1	19	6	477	488	8
2	19	6	321	309	14
3	19	6	278	267	14
4	19	6	386	387	10
5	19	6	651	645	11
6	19	6	225	204	20
7	19	6	204	187	24
8	19	6	164	152	32
-13	20	6	393	390	16
-12	20	6	30	107	30
-11	20	6	119	37	61
-10	20	6	190	207	20
-9	20	6	581	601	12
-8	20	6	320	332	17
-7	20	6	69	44	44
-6	20	6	242	241	9
-5	20	6	294	280	8
-4	20	6	690	682	6
-3	20	6	269	271	7
-2	20	6	500	503	7

-3	5	6	1417	1424	8
-2	5	6	1275	1312	9
-1	5	6	833	795	7
0	5	6	294	312	6
1	5	6	646	658	6
2	5	6	864	872	8
3	5	6	113	105	16
4	5	6	896	886	11
5	5	6	1029	1047	18
6	5	6	356	372	18
7	5	6	68	44	67
8	5	6	240	238	19
9	5	6	410	407	10
-14	6	6	100	109	51
-11	9	6	434	418	10
-10	9	6	776	780	10
-9	9	6	229	216	17
-8	9	6	1124	1130	12
-7	9	6	1087	1074	11
-6	9	6	934	944	8
-5	9	6	65	71	24
-4	9	6	843	882	6
-3	9	6	921	922	7
-2	9	6	528	527	5
-1	9	6	0	10	1
0	9	6	430	440	5
1	9	6	880	887	6
2	9	6	659	652	6
5	12	6	101	85	27
6	12	6	157	155	19
7	12	6	37	36	36
8	12	6	142	157	23
9	12	6	85	23	57
-14	13	6	108	99	43
-13	13	6	0	54	1
-12	13	6	108	104	56
-11	13	6	569	570	12
-10	13	6	531	535	9
-9	13	6	288	267	12
-8	13	6	669	661	9
-7	13	6	392	380	7
-6	13	6	249	262	8
-1	16	6	287	272	7
0	16	6	136	111	16
1	16	6	435	438	8
2	16	6	222	233	12
3	16	6	92	55	27
4	16	6	320	324	13
5	16	6	162	115	23
6	16	6	60	24	59
7	16	6	0	32	1
8	16	6	280	303	20
-13	17	6	152	204	48
-12	17	6	0	5	1
-11	17	6	344	354	14
-10	17	6	430	430	19
-1	20	6	955	969	9
0	20	6	746	761	11
1	20	6	49	56	48
2	20	6	942	927	18
3	20	6	330	305	13
4	20	6	346	350	13
5	20	6	190	140	22
6	20	6	93	107	54
7	20	6	423	413	14
8	20	6	252	279	22
-12	21	6	237	288	20
-11	21	6	313	329	25
-10	21	6	113	137	30
-9	21	6	38	83	38

Table D.6. Observed and calculated structure factors for Rutdp

h	k	l	10Fo	10Fc	10s
-8	21	6	207	220	13
-7	21	6	125	128	19
-6	21	6	0	22	-1
-5	21	6	607	609	7
-4	21	6	72	77	24
-3	21	6	174	165	10
-2	21	6	581	576	7
-1	21	6	65	110	57
0	21	6	301	277	13
1	21	6	469	456	10
2	21	6	149	139	26
3	21	6	145	144	25
4	21	6	24	65	23
5	21	6	73	84	73
6	21	6	202	201	22
7	21	6	170	189	29
8	21	6	174	205	32
-12	22	6	106	81	46
-11	22	6	231	206	19
-10	22	6	220	219	18
-9	22	6	393	417	22
-8	22	6	122	114	64
-7	22	6	222	213	14
-6	22	6	80	78	25
-5	22	6	869	872	8
-4	22	6	48	61	48
-3	22	6	171	170	10
-2	22	6	0	35	1
-1	22	6	426	426	8
0	22	6	605	628	15
1	22	6	304	317	13
-1	25	6	0	71	1
0	25	6	43	69	42
1	25	6	511	519	11
2	25	6	262	270	16
3	25	6	0	7	-1
4	25	6	294	286	16
5	25	6	424	431	11
6	25	6	129	155	41
7	25	6	393	375	21
-11	26	6	0	65	1
-10	26	6	121	66	31
-9	26	6	135	141	27
-8	26	6	136	141	36
-7	26	6	301	308	11
-6	26	6	124	140	20
-5	26	6	162	172	17
-4	26	6	436	443	11
-3	26	6	80	1	28
-2	26	6	153	151	15
-1	26	6	182	182	14
0	26	6	160	186	21
1	26	6	289	299	14
2	26	6	303	327	21
3	26	6	118	101	39
4	26	6	39	73	39
5	26	6	215	183	22
6	26	6	178	183	28
-11	27	6	122	40	52
-10	27	6	257	254	18
-9	27	6	207	265	18
-8	27	6	333	339	11
-2	30	6	306	285	14
-1	30	6	77	58	76
0	30	6	206	172	20
1	30	6	171	160	25
2	30	6	383	378	14
3	30	6	402	410	14
4	30	6	402	380	17
5	30	6	0	35	-1
-10	31	6	128	86	37
-9	31	6	107	172	71
-8	31	6	136	153	23
-7	31	6	110	20	34
-6	31	6	268	284	31
-5	31	6	106	28	37
-4	31	6	107	75	36
-3	31	6	138	107	20
-2	31	6	0	90	1
-1	31	6	441	483	12
0	31	6	122	134	33
1	31	6	152	168	44
2	31	6	106	26	44
3	31	6	92	127	75
4	31	6	84	19	84
5	31	6	112	102	48
-9	32	6	72	84	72
-8	32	6	182	186	19
-7	32	6	0	35	1
-6	32	6	234	225	44
-5	32	6	286	288	16
-4	32	6	203	213	20
-3	32	6	144	140	25
-6	37	6	206	213	24
-5	37	6	0	49	-1
-4	37	6	267	221	27
-3	37	6	163	185	39
-2	37	6	196	161	25
-1	37	6	70	15	69
0	37	6	358	395	15
1	37	6	185	182	28
2	37	6	63	111	62
-6	38	6	246	245	21
-5	38	6	440	453	15
-4	38	6	295	285	26
-3	38	6	55	22	55
-2	38	6	264	238	20
-1	38	6	383	389	15
0	38	6	344	342	30
1	38	6	0	89	1
-5	39	6	129	31	66
-4	39	6	318	336	27
-3	39	6	474	461	20
-2	39	6	346	328	22
-1	39	6	46	110	45
0	39	6	191	231	38
-14	1	7	200	206	16
-13	1	7	375	398	11
-12	1	7	297	271	14
-11	1	7	47	47	47
-10	1	7	111	127	26
-9	1	7	494	483	10
-8	1	7	725	706	15
-7	1	7	265	271	16
3	3	7	701	699	7
4	3	7	341	364	12
5	3	7	491	501	11
6	3	7	162	161	24
7	3	7	393	346	19
8	3	7	441	475	24
9	3	7	0	32	1
-14	4	7	0	91	-1
-13	4	7	251	238	14
-12	4	7	111	92	28
-11	4	7	663	643	10
-10	4	7	410	416	11
-9	4	7	163	150	18
-8	4	7	682	701	11
-7	4	7	248	245	12
-6	4	7	475	495	15
-5	4	7	96	51	18
-4	4	7	375	377	5
-3	4	7	725	705	6
-2	4	7	408	425	5
-1	4	7	266	265	7
0	4	7	732	729	[illegible]
1	4	7	614	590	7
2	4	7	0	13	1
3	4	7	294	296	8
4	4	7	85	37	84
5	4	7	600	599	16
6	4	7	353	341	20
7	4	7	174	167	25
8	4	7	115	97	40
9	4	7	0	43	1

2	22	6	261	248	38
3	22	6	163	154	73
4	22	6	357	357	16
5	22	6	0	106	1
6	22	6	170	192	26
7	22	6	147	117	39
-12	23	6	273	255	18
-11	23	6	434	419	14
-10	23	6	158	171	46
-9	23	6	61	86	60
-8	23	6	408	429	9
-7	23	6	727	706	9
-6	23	6	392	405	8
-5	23	6	169	174	13
-4	23	6	426	426	6
-3	23	6	219	214	10
-2	23	6	489	496	8
-1	23	6	529	533	12
0	23	6	306	310	10
1	23	6	463	449	11
2	23	6	66	46	65
3	23	6	51	33	50
4	23	6	252	219	21
5	23	6	500	482	19
6	23	6	317	302	17
7	23	6	78	40	77
-12	24	6	146	123	37
-11	24	6	108	98	38
-10	24	6	210	213	42
-9	24	6	687	690	12
-8	24	6	337	355	10
-7	24	6	171	167	16
-6	24	6	329	333	11
-5	24	6	727	720	8
-4	24	6	856	849	7
-3	24	6	125	113	17
-2	24	6	571	566	8
-1	24	6	587	591	8
0	24	6	677	669	9
1	24	6	97	125	97
2	24	6	361	328	13
3	24	6	337	327	14
4	24	6	398	415	14
5	24	6	15	80	15
6	24	6	147	104	31
7	24	6	420	396	15
-12	25	6	177	196	94
-11	25	6	446	455	14
-10	25	6	332	342	15
-9	25	6	149	149	25
-7	27	6	46	68	45
-6	27	6	73	69	41
-5	27	6	474	458	9
-4	27	6	525	515	13
-3	27	6	762	773	8
-2	27	6	354	363	9
-1	27	6	141	122	18
0	27	6	121	111	29
1	27	6	31	79	31
2	27	6	267	270	16
3	27	6	52	2	52
4	27	6	172	185	25
5	27	6	0	33	1
6	27	6	258	253	21
-11	28	6	0	45	1
-10	28	6	294	305	16
-9	28	6	373	357	18
-8	28	6	377	395	11
-7	28	6	0	31	1
-6	28	6	622	620	9
-5	28	6	642	647	12
-4	28	6	85	47	33
-3	28	6	57	71	56
-2	28	6	70	64	70
-1	28	6	453	455	11
0	28	6	283	263	22
1	28	6	278	276	22
2	28	6	259	257	17
3	28	6	376	349	17
4	28	6	391	408	14
5	28	6	67	3	67
6	28	6	339	339	17
-10	29	6	220	230	21
-9	29	6	0	32	1
-8	29	6	234	232	21
-7	29	6	504	509	10
-6	29	6	290	290	13
-5	29	6	213	224	18
-4	29	6	418	420	14
-3	29	6	389	379	11
-2	29	6	141	145	19
-1	29	6	122	85	31
0	29	6	378	384	13
1	29	6	760	728	12
2	29	6	318	311	15
3	29	6	127	111	55
4	29	6	185	187	39
5	29	6	569	570	13
6	29	6	399	391	23
-10	30	6	0	60	1
-2	32	6	283	290	17
-1	32	6	240	231	17
0	32	6	144	134	29
1	32	6	141	149	39
2	32	6	142	82	34
3	32	6	350	364	16
4	32	6	235	230	25
-9	33	6	48	56	47
-8	33	6	397	391	22
-7	33	6	296	292	17
-6	33	6	236	256	18
-5	33	6	172	130	25
-4	33	6	204	223	20
-3	33	6	661	667	11
-2	33	6	232	242	20
-1	33	6	152	160	28
0	33	6	219	222	25
1	33	6	499	485	13
2	33	6	533	521	15
3	33	6	63	49	63
4	33	6	441	415	15
-8	34	6	265	261	16
-7	34	6	131	28	48
-6	34	6	372	394	15
-5	34	6	520	507	18
-4	34	6	352	342	21
-3	34	6	91	147	91
-2	34	6	240	229	26
-1	34	6	606	635	17
0	34	6	400	394	15
1	34	6	48	3	47
2	34	6	262	300	19
3	34	6	385	389	16
4	34	6	441	430	21
-8	35	6	126	151	126
-7	35	6	114	117	46
-6	35	6	64	14	63
-5	35	6	49	118	48
-4	35	6	240	180	29
-3	35	6	110	106	110
-2	35	6	234	234	19
-1	35	6	134	125	32
0	35	6	146	161	30
1	35	6	447	430	14
2	35	6	0	22	1
3	35	6	49	122	49
-7	36	6	20	17	19
-6	36	6	142	123	31
-5	36	6	111	108	37
-4	36	6	112	83	65
-6	1	7	540	533	10
-5	1	7	224	222	6
-4	1	7	393	410	5
-3	1	7	732	722	6
-2	1	7	99	115	18
-1	1	7	606	618	8
0	1	7	333	316	8
1	1	7	288	280	7
2	1	7	299	299	7
3	1	7	481	467	7
4	1	7	354	386	20
5	1	7	185	190	19
6	1	7	170	207	22
7	1	7	324	335	17
8	1	7	266	274	19
9	1	7	0	77	1
-14	2	7	235	243	16
-13	2	7	53	48	52
-12	2	7	315	301	17
-11	2	7	948	929	13
-10	2	7	215	224	15
-9	2	7	797	771	12
-8	2	7	168	120	19
-7	2	7	635	635	10
-6	2	7	692	697	10
-5	2	7	35	54	34
-4	2	7	475	479	6
-3	2	7	1166	1145	9
-2	2	7	1473	1463	11
-1	2	7	779	756	7
0	2	7	484	485	6
1	2	7	694	673	7
2	2	7	627	631	7
3	2	7	622	607	8
4	2	7	0	14	1
5	2	7	602	597	11
6	2	7	623	634	11
7	2	7	379	408	21
8	2	7	69	110	69
9	2	7	342	372	16
-14	3	7	178	224	19
-13	3	7	523	508	10
-12	3	7	662	661	12
-11	3	7	316	305	24
-10	3	7	486	471	16
-9	3	7	705	698	11
-8	3	7	958	950	12
-7	3	7	412	415	10
-6	3	7	241	242	15
-5	3	7	1244	1277	15
-14	5	7	33	66	32
-13	5	7	62	49	62
-12	5	7	223	233	14
-11	5	7	104	90	41
-10	5	7	415	414	10
-9	5	7	291	290	10
-8	5	7	222	230	14
-7	5	7	684	658	10
-6	5	7	124	111	23
-5	5	7	941	954	9
-4	5	7	402	396	4
-3	5	7	97	138	12
-2	5	7	914	894	8
-1	5	7	390	391	6
0	5	7	416	421	6
1	5	7	278	269	8
2	5	7	136	129	14
3	5	7	80	71	33
4	5	7	0	38	1
5	5	7	246	285	24
6	5	7	200	184	22
7	5	7	48	23	48
8	5	7	71	82	70
9	5	7	71	80	71
-14	6	7	350	347	15
-13	6	7	21	128	21
-12	6	7	257	263	12
-11	6	7	560	565	9
-10	6	7	134	120	18
-9	6	7	145	142	30
-8	6	7	256	251	20
-7	6	7	513	515	8
-6	6	7	459	481	9
-5	6	7	733	736	7
-4	6	7	96	63	11
-3	6	7	1248	1254	7
-2	6	7	847	830	7
-1	6	7	163	141	10
0	6	7	0	40	1
1	6	7	535	510	7
2	6	7	794	801	7
3	6	7	306	312	12
4	6	7	623	646	15
5	6	7	168	193	43
6	6	7	654	685	17
7	6	7	348	368	21
8	6	7	242	205	14
9	6	7	219	210	17
-14	7	7	184	185	23
-13	7	7	463	430	21

-8	25	6	274	302	12	-9	30	6	299	312	17	-3	36	6	79	64	79	-4	3	7	1408	1404	11	-12	7	7	469	465	10
-7	25	6	800	791	10	-8	30	6	104	102	45	-2	36	6	144	129	77	-3	3	7	83	19	17	-11	7	7	216	171	20
-6	25	6	198	199	14	-7	30	6	122	95	34	-1	36	6	155	176	29	-2	3	7	628	630	6	-10	7	7	753	768	9
-5	25	6	13	38	13	-6	30	6	230	184	22	0	36	6	168	73	27	-1	3	7	234	222	10	-9	7	7	821	844	12
-4	25	6	83	22	24	-5	30	6	587	599	12	1	36	6	0	74	1	0	3	7	305	334	7	-8	7	7	840	832	10
-3	25	6	614	610	7	-4	30	6	439	438	18	2	36	6	0	43	1	1	3	7	1012	1029	8	-7	7	7	140	109	16
-2	25	6	700	701	8	-3	30	6	23	76	22	-7	37	6	327	332	39	2	3	7	232	247	9	-6	7	7	444	447	8

Table D.6. Observed and calculated structure factors for Rutdp

h	k	l	10Fo	10Fc	10s	h	k	l	10Fo	10Fc	10s	h	k	l	10Fo	10Fc	10s	h	k	l	10Fo	10Fc	10s	h	k	l	10Fo	10Fc	10s
-5	7	7	348	361	6	-9	11	7	396	386	10	-12	15	7	112	27	44	-10	19	7	111	97	31	-3	23	7	98	100	26
-4	7	7	966	984	7	-8	11	7	26	20	26	-11	15	7	0	39	1	-9	19	7	0	33	1	-2	23	7	85	88	36
-3	7	7	335	332	5	-7	11	7	591	596	8	-10	15	7	210	173	14	-8	19	7	337	335	10	-1	23	7	583	577	15
-2	7	7	185	179	7	-6	11	7	93	40	19	-9	15	7	302	316	15	-7	19	7	54	52	54	0	23	7	732	724	9
-1	7	7	863	855	10	-5	11	7	899	909	8	-8	15	7	268	240	14	-6	19	7	442	440	7	1	23	7	127	109	39
0	7	7	1243	1217	11	-4	11	7	305	315	6	-7	15	7	155	142	25	-5	19	7	114	84	17	2	23	7	109	24	36
1	7	7	126	102	14	-3	11	7	687	667	6	-6	15	7	95	63	25	-4	19	7	160	158	12	3	23	7	240	213	22
2	7	7	488	493	7	-2	11	7	56	18	39	-5	15	7	256	254	8	-3	19	7	724	732	9	4	23	7	221	207	19
3	7	7	766	749	11	-1	11	7	768	767	6	-4	15	7	435	435	6	-2	19	7	89	14	27	5	23	7	214	192	23
4	7	7	1052	1051	13	0	11	7	1035	1030	8	-3	15	7	288	287	10	-1	19	7	0	37	1	6	23	7	79	117	78
5	7	7	116	110	33	1	11	7	92	104	23	-2	15	7	597	583	7	0	19	7	0	20	1	-12	24	7	0	141	1
6	7	7	230	247	18	2	11	7	296	296	7	-1	15	7	404	413	7	1	19	7	52	87	52	-11	24	7	163	151	27
7	7	7	267	265	12	3	11	7	357	344	10	0	15	7	256	261	10	2	19	7	439	445	11	-10	24	7	287	316	16
8	7	7	450	461	9	4	11	7	681	675	9	1	15	7	346	343	9	3	19	7	65	31	64	-9	24	7	124	173	28
-14	8	7	471	490	14	5	11	7	456	446	10	2	15	7	257	256	12	4	19	7	265	245	17	-8	24	7	0	4	1
-13	8	7	167	162	35	6	11	7	114	94	29	3	15	7	609	628	11	5	19	7	25	100	25	-7	24	7	43	53	43
-12	8	7	102	88	47	7	11	7	335	319	17	4	15	7	281	291	18	6	19	7	123	22	36	-6	24	7	220	251	10
-11	8	7	534	529	17	8	11	7	489	487	11	5	15	7	0	43	1	7	19	7	93	19	93	-5	24	7	0	36	1
-10	8	7	346	333	10	-14	12	7	421	431	15	6	15	7	0	47	1	-13	20	7	326	326	19	-4	24	7	259	287	14
-9	8	7	157	183	15	-13	12	7	206	175	25	7	15	7	241	262	20	-12	20	7	134	165	48	-3	24	7	332	334	9
-8	8	7	869	863	12	-12	12	7	228	237	18	8	15	7	124	89	46	-11	20	7	406	409	14	-2	24	7	78	99	38
-7	8	7	670	660	13	-11	12	7	485	471	10	-13	16	7	188	194	24	-10	20	7	249	255	22	-1	24	7	330	340	10
-6	8	7	598	607	6	-10	12	7	707	719	9	-12	16	7	140	135	27	-9	20	7	52	54	51	0	24	7	48	5	48
-5	8	7	222	227	8	-9	12	7	179	173	17	-11	16	7	640	651	13	-8	20	7	62	32	54	1	24	7	46	28	46
-4	8	7	366	361	5	-8	12	7	289	289	10	-10	16	7	730	737	12	-7	20	7	281	264	8	2	24	7	251	248	17
-3	8	7	639	620	5	-7	12	7	624	630	9	-9	16	7	124	146	20	-6	20	7	707	717	7	3	24	7	102	67	44
-2	8	7	1270	1283	8	-6	12	7	624	633	7	-8	16	7	404	417	9	-5	20	7	0	25	1	4	24	7	49	2	48
-1	8	7	207	196	7	-5	12	7	596	600	7	-7	16	7	278	262	25	-4	20	7	509	520	9	5	24	7	85	99	84
0	8	7	96	110	25	-4	12	7	182	201	8	-6	16	7	386	392	7	-3	20	7	127	131	17	6	24	7	155	122	46
1	8	7	458	445	11	-3	12	7	1090	1084	8	-5	16	7	225	219	9	-2	20	7	48	78	48	-11	25	7	78	105	77
2	8	7	409	427	11	-2	12	7	681	677	7	-4	16	7	176	180	12	-1	20	7	948	962	10	-10	25	7	295	308	16
3	8	7	80	66	33	-1	12	7	292	291	7	-3	16	7	679	682	7	0	20	7	289	281	11	-9	25	7	263	289	17
4	8	7	169	178	29	0	12	7	54	44	53	-2	16	7	1013	1008	10	1	20	7	624	640	11	-8	25	7	338	339	14
5	8	7	772	784	8	1	12	7	710	716	7	-1	16	7	648	629	8	2	20	7	497	491	11	-7	25	7	271	258	12
6	8	7	407	424	9	2	12	7	954	960	9	0	16	7	322	331	14	3	20	7	292	303	15	-6	25	7	105	97	20
7	8	7	142	160	24	3	12	7	112	114	26	1	16	7	403	389	9	4	20	7	97	93	97	-5	25	7	696	702	8
8	8	7	0	82	1	4	12	7	190	201	22	2	16	7	674	672	9	5	20	7	314	325	19	-4	25	7	249	231	15
-14	9	7	108	66	42	5	12	7	399	406	10	3	16	7	597	580	11	6	20	7	304	303	17	-3	25	7	0	36	-1

-13	9	7	122	149	35
-12	9	7	253	243	16
-11	9	7	321	302	11
-10	9	7	599	599	11
-9	9	7	185	207	14
-8	9	7	197	190	13
-7	9	7	378	390	8
-6	9	7	66	74	26
-5	9	7	822	804	7
-4	9	7	0	25	1
-3	9	7	556	540	5
-2	9	7	100	83	23
-1	9	7	104	100	14
0	9	7	619	628	5
1	9	7	75	79	22
2	9	7	129	110	14
3	9	7	64	28	38
4	9	7	369	372	8
5	9	7	261	256	11
6	9	7	275	275	11
7	9	7	238	211	13
8	9	7	135	158	24
-14	10	7	351	343	30
-13	10	7	98	15	46
-12	10	7	155	120	25
-11	10	7	83	85	47
-10	10	7	765	765	10
-9	10	7	287	289	11
-8	10	7	145	155	16
-7	10	7	328	332	9
-6	10	7	38	42	38
-5	10	7	138	143	11
-4	10	7	238	232	7
-3	10	7	259	255	6
-2	10	7	223	200	7
-1	10	7	347	342	6
0	10	7	303	298	6
1	10	7	70	76	29
2	10	7	85	85	21
3	10	7	24	53	23
4	10	7	297	305	10
5	10	7	35	20	34
6	10	7	79	93	35
7	10	7	250	258	12
8	10	7	99	42	58
-14	11	7	73	25	73
-13	11	7	266	277	33
-12	11	7	682	669	13
-11	11	7	101	110	28
-10	11	7	487	489	15
6	12	7	653	650	10
7	12	7	376	342	16
8	12	7	219	201	21
-14	13	7	101	133	53
-13	13	7	72	77	72
-12	13	7	602	610	20
-11	13	7	0	110	1
-10	13	7	321	320	13
-9	13	7	328	330	12
-8	13	7	937	937	10
-7	13	7	105	92	22
-6	13	7	248	244	8
-5	13	7	598	582	7
-4	13	7	396	412	5
-3	13	7	364	373	6
-2	13	7	128	118	14
-1	13	7	925	909	8
0	13	7	838	849	8
1	13	7	604	606	8
2	13	7	424	420	8
3	13	7	337	327	27
4	13	7	655	642	9
5	13	7	287	305	13
6	13	7	196	189	22
7	13	7	265	270	23
8	13	7	191	213	21
-14	14	7	73	79	72
-13	14	7	225	236	20
-12	14	7	116	103	53
-11	14	7	118	83	30
-10	14	7	147	167	18
-9	14	7	385	383	10
-8	14	7	268	244	11
-7	14	7	382	381	9
-6	14	7	315	317	7
-5	14	7	113	106	16
-4	14	7	434	439	6
-3	14	7	179	185	9
-2	14	7	433	421	7
-1	14	7	202	228	15
0	14	7	124	135	18
1	14	7	150	152	14
2	14	7	801	801	8
3	14	7	0	27	-1
4	14	7	180	201	20
5	14	7	102	90	32
6	14	7	125	166	26
7	14	7	0	13	1
8	14	7	112	22	111
-13	15	7	285	288	41
4	16	7	0	4	1
5	16	7	351	335	27
6	16	7	345	357	26
7	16	7	195	176	26
8	16	7	0	43	1
-13	17	7	234	236	32
-12	17	7	457	443	14
-11	17	7	113	138	32
-10	17	7	456	477	21
-9	17	7	742	759	12
-8	17	7	488	472	9
-7	17	7	0	78	1
-6	17	7	181	178	12
-5	17	7	941	934	8
-4	17	7	596	597	7
-3	17	7	206	198	10
-2	17	7	321	308	10
-1	17	7	686	682	8
0	17	7	1037	1046	10
1	17	7	118	107	21
2	17	7	70	67	70
3	17	7	701	697	11
4	17	7	421	416	17
5	17	7	200	184	20
6	17	7	0	34	1
7	17	7	275	281	23
-13	18	7	158	121	27
-12	18	7	171	179	24
-11	18	7	495	493	13
-10	18	7	422	419	17
-9	18	7	0	20	1
-8	18	7	69	63	42
-7	18	7	119	99	16
-6	18	7	430	415	9
-5	18	7	94	38	21
-4	18	7	622	621	7
-3	18	7	507	500	7
-2	18	7	394	384	8
-1	18	7	383	379	9
0	18	7	454	453	8
1	18	7	867	876	9
2	18	7	821	803	16
3	18	7	217	227	17
4	18	7	64	84	64
5	18	7	217	258	20
6	18	7	294	280	18
7	18	7	0	8	1
-13	19	7	0	49	-1
-12	19	7	42	6	41
-11	19	7	90	72	51
7	20	7	0	7	-1
-12	21	7	91	83	56
-11	21	7	58	117	58
-10	21	7	177	178	22
-9	21	7	797	805	13
-8	21	7	617	613	12
-7	21	7	127	102	16
-6	21	7	0	23	1
-5	21	7	300	288	12
-4	21	7	741	734	8
-3	21	7	341	357	11
-2	21	7	387	390	9
-1	21	7	611	619	8
0	21	7	863	856	9
1	21	7	767	747	9
2	21	7	29	92	29
3	21	7	599	597	11
4	21	7	436	435	13
5	21	7	250	253	18
6	21	7	99	29	58
7	21	7	154	166	34
-12	22	7	33	63	32
-11	22	7	463	480	19
-10	22	7	499	508	13
-9	22	7	210	214	19
-8	22	7	501	521	12
-7	22	7	627	637	7
-6	22	7	730	755	8
-5	22	7	164	172	14
-4	22	7	163	160	14
-3	22	7	345	342	9
-2	22	7	897	890	9
-1	22	7	362	347	11
0	22	7	650	656	9
1	22	7	594	570	9
2	22	7	489	480	12
3	22	7	406	387	13
4	22	7	236	263	19
5	22	7	313	296	16
6	22	7	181	183	29
7	22	7	122	128	79
-12	23	7	126	139	35
-11	23	7	248	232	30
-10	23	7	94	79	40
-9	23	7	392	376	18
-8	23	7	192	200	18
-7	23	7	126	134	32
-6	23	7	196	225	11
-5	23	7	0	72	1
-4	23	7	364	367	9
-2	25	7	90	98	72
-1	25	7	198	183	14
0	25	7	591	592	9
1	25	7	274	288	16
2	25	7	239	237	25
3	25	7	252	263	20
4	25	7	315	323	16
5	25	7	268	263	29
6	25	7	0	44	1
-11	26	7	454	481	14
-10	26	7	394	419	15
-9	26	7	175	220	38
-8	26	7	259	267	15
-7	26	7	695	700	9
-6	26	7	361	357	10
-5	26	7	313	319	10
-4	26	7	241	203	29
-3	26	7	829	812	11
-2	26	7	165	161	17
-1	26	7	548	536	9
0	26	7	68	128	68
1	26	7	504	520	12
2	26	7	536	523	20
3	26	7	280	270	18
4	26	7	49	78	49
5	26	7	160	189	29
6	26	7	552	528	21
-11	27	7	146	178	33
-10	27	7	84	84	84
-9	27	7	386	421	14
-8	27	7	291	297	15
-7	27	7	80	65	39
-6	27	7	213	225	22
-5	27	7	457	447	9
-4	27	7	805	807	11
-3	27	7	286	285	11
-2	27	7	396	384	10
-1	27	7	421	414	10
0	27	7	182	171	22
1	27	7	0	44	-1
2	27	7	158	151	26
3	27	7	427	425	14
4	27	7	534	564	34
5	27	7	131	150	38
-11	28	7	0	122	1
-10	28	7	46	25	45
-9	28	7	161	190	25
-8	28	7	193	218	20
-7	28	7	173	188	17
-6	28	7	312	330	11

Table D.6. Observed and calculated structure factors for Rutdp

h	k	1	10Fo	10Fc	10s
-5	28	7	319	316	11
-4	28	7	260	211	15
-3	28	7	458	464	9
-2	28	7	263	235	18
-1	28	7	0	21	1
0	28	7	348	347	13
1	28	7	124	169	32
2	28	7	162	192	46
3	28	7	381	350	29
4	28	7	203	206	24
5	28	7	248	255	22
-10	29	7	0	73	1
-9	29	7	85	76	60
-8	29	7	118	160	35
-7	29	7	99	118	63
-6	29	7	145	166	43
-5	29	7	292	258	22
-4	29	7	107	37	32
-3	29	7	97	101	27
-2	29	7	66	5	65
-1	29	7	0	71	-1
0	29	7	429	438	13
1	29	7	255	239	26
2	29	7	0	41	1
3	29	7	107	92	45
4	29	7	126	135	70
5	29	7	75	15	75
-10	30	7	353	356	16
-9	30	7	104	114	43
-8	30	7	236	256	18
-7	30	7	484	483	17
-6	30	7	323	294	15
-5	30	7	300	287	22
-4	30	7	91	82	49
-3	30	7	466	437	12
-2	30	7	432	428	10
-1	30	7	191	166	21
0	30	7	129	134	32
1	30	7	233	209	21
2	30	7	448	424	14
3	30	7	206	223	23,
4	30	7	156	117	45
-10	31	7	117	142	83
-9	31	7	133	206	34
-8	31	7	164	184	25
-7	31	7	271	236	47
-3	34	7	0	85	1
-2	34	7	157	192	31
-1	34	7	127	140	36
0	34	7	204	252	48
1	34	7	168	149	34
2	34	7	207	209	29
-7	35	7	97	66	96
-6	35	7	134	94	53
-5	35	7	204	192	33
-4	35	7	382	366	21
-3	35	7	187	199	39
-2	35	7	172	171	28
-1	35	7	306	308	17
0	35	7	192	163	26
1	35	7	313	315	18
2	35	7	197	183	30
-7	36	7	364	386	31
-6	36	7	219	225	31
-5	36	7	168	286	33
-4	36	7	101	68	90
-3	36	7	477	451	19
-2	36	7	377	380	15
-1	36	7	104	94	58
0	36	7	263	293	20
1	36	7	130	180	81
-6	37	7	137	28	49
-5	37	7	241	242	30
-4	37	7	358	297	24
-3	37	7	132	39	63
-2	37	7	108	112	50
-1	37	7	323	355	17
0	37	7	350	373	17
-5	38	7	87	79	86
-4	38	7	0	4	1
-3	38	7	157	142	47
-2	38	7	0	16	1
-1	38	7	8	7	7
-14	0	8	279	288	18
-13	0	8	316	256	22
-12	0	8	752	733	17
-11	0	8	91	112	91
-10	0	8	126	129	42
-9	0	8	174	183	23
-8	0	8	1011	999	19
-7	0	8	272	250	18
-6	0	8	71	18	71
-8	2	8	671	674	11
-7	2	8	403	383	11
-6	2	8	468	474	10
-5	2	8	391	390	10
-4	2	8	72	62	25
-3	2	8	1180	1162	9
-2	2	8	220	197	16
-1	2	8	370	366	7
0	2	8	97	104	19
1	2	8	0	5	1
2	2	8	85	63	24
3	2	8	79	48	27
4	2	8	0	46	1
5	2	8	144	114	27
6	2	8	0	78	1
7	2	8	0	92	1
8	2	8	89	27	88
-14	3	8	0	78	1
-13	3	8	196	180	23
-12	3	8	191	184	17
-11	3	8	78	110	55
-10	3	8	105	109	32
-9	3	8	505	513	13
-8	3	8	490	487	16
-7	3	8	482	488	10
-6	3	8	349	326	32
-5	3	8	306	292	8
-4	3	8	519	510	6
-3	3	8	157	138	15
-2	3	8	465	449	6
-1	3	8	206	202	9
0	3	8	89	48	19
1	3	8	204	194	10
2	3	8	377	375	9
3	3	8	18	8	18
4	3	8	254	264	15
5	3	8	375	404	13
6	3	8	223	252	20
7	3	8	108	121	47
8	3	8	54	68	53
-14	4	8	0	4	1
-13	4	8	350	348	16
-12	4	8	460	461	10
-11	4	8	300	308	11
-10	4	8	0	70	1
-9	4	8	78	21	49
-12	6	8	381	383	11
-11	6	8	179	180	17
-10	6	8	0	20	1
-9	6	8	501	496	9
-8	6	8	107	92	23
-7	6	8	75	78	36
-6	6	8	282	258	10
-5	6	8	293	294	7
-4	6	8	1253	1265	10
-3	6	8	413	409	5
-2	6	8	995	993	8
-1	6	8	348	323	8
0	6	8	291	271	9
1	6	8	744	744	13
2	6	8	176	155	22
3	6	8	339	335	25
4	6	8	708	732	16
5	6	8	474	479	12
6	6	8	188	168	22
7	6	8	184	184	17
8	6	8	190	229	17
-14	7	8	0	43	1
-13	7	8	154	165	21
-12	7	8	67	16	67
-11	7	8	306	310	13
-10	7	8	95	138	26
-9	7	8	297	283	20
-8	7	8	89	93	28
-7	7	8	471	485	20
-6	7	8	70	79	56
-5	7	8	393	391	6
-4	7	8	23	3	22
-3	7	8	165	151	8
-2	7	8	329	336	8
-1	7	8	186	198	10
0	7	8	0	40	1
1	7	8	385	378	7
2	7	8	393	388	10
3	7	8	58	11	58
4	7	8	501	538	11
5	7	8	199	161	19
6	7	8	141	176	24
7	7	8	88	121	37
8	7	8	0	31	1
-14	8	8	42	36	41
-13	8	8	244	229	16
7	9	8	275	274	12
-14	10	8	18	8	18
-13	10	8	445	397	22
-12	10	8	565	554	12
-11	10	8	200	206	15
-10	10	8	373	377	10
-9	10	8	573	573	11
-8	10	8	324	318	10
-7	10	8	928	911	10
-6	10	8	11	29	10
-5	10	8	744	735	7
-4	10	8	480	482	14
-3	10	8	714	725	7
-2	10	8	897	883	7
-1	10	8	996	989	7
0	10	8	922	923	7
1	10	8	194	184	11
2	10	8	168	195	12
3	10	8	107	109	18
4	10	8	838	819	9
5	10	8	661	674	8
6	10	8	0	51	1
7	10	8	359	362	11
-14	11	8	297	318	29
-13	11	8	245	245	19
-12	11	8	230	242	24
-11	11	8	233	241	14
-10	11	8	218	238	17
-9	11	8	717	715	9
-8	11	8	156	152	17
-7	11	8	581	575	13
-6	11	8	473	468	8
-5	11	8	428	420	7
-4	11	8	163	156	13
-3	11	8	525	532	6
-2	11	8	831	813	7
-1	11	8	52	12	52
0	11	8	315	323	9
1	11	8	315	309	10
2	11	8	159	171	14
3	11	8	230	237	10
4	11	8	374	391	9
5	11	8	0	77	1
6	11	8	454	446	11
7	11	8	194	197	19
-14	12	8	108	120	45

-6	31	7	316	338	15	-5	0	8	806	764	16	-8	4	8	840	835	12	-12	8	8	236	230	14	-13	12	8	234	248	18
-5	31	7	663	651	16	-4	0	8	1623	1611	25	-7	4	8	705	700	11	-11	8	8	442	440	19	-12	12	8	134	61	107
-4	31	7	452	414	17	-3	0	8	1375	1353	15	-6	4	8	759	758	11	-10	8	8	277	267	14	-11	12	8	68	37	68
-3	31	7	266	223	16	-2	0	8	641	657	9	-5	4	8	701	691	8	-9	8	8	477	449	9	-10	12	8	219	237	13
-2	31	7	198	200	22	-1	0	8	185	151	15	-4	4	8	494	482	6	-8	8	8	148	147	17	-9	12	8	386	378	12
-1	31	7	408	424	28	0	0	8	275	281	11	-3	4	8	951	949	8	-7	8	8	444	452	9	-8	12	8	214	226	18
0	31	7	310	309	16	1	0	8	1106	1101	13	-2	4	8	341	345	7	-6	8	8	343	348	9	-7	12	8	54	82	54
1	31	7	0	123	1	2	0	8	160	161	31	-1	4	8	715	709	7	-5	8	8	759	733	8	-6	12	8	351	356	7
2	31	7	236	222	29	3	0	8	512	518	10	0	4	8	948	956	8	-4	8	8	738	728	7	-5	12	8	73	95	28
3	31	7	371	382	16	4	0	8	397	416	16	1	4	8	34	25	33	-3	8	8	235	226	7	-4	12	8	270	274	12
4	31	7	467	469	14	5	0	8	439	435	17	2	4	8	84	95	23	-2	8	8	735	730	6	-3	12	8	610	596	6
-9	32	7	251	264	19	7	0	8	243	239	26	3	4	8	363	363	9	-1	8	8	178	187	9	-2	12	8	177	175	11
-8	32	7	152	204	26	8	0	8	508	490	21	4	4	8	912	929	12	0	8	8	314	319	9	-1	12	8	186	175	9
-7	32	7	429	429	13	-14	1	8	256	243	16	5	4	8	358	381	13	1	8	8	190	177	17	0	12	8	114	98	17
-6	32	7	437	436	14	-13	1	8	471	483	11	6	4	8	0	43	1	2	8	8	114	58	21	1	12	8	117	118	23
-5	32	7	422	417	18	-12	1	8	301	299	14	7	4	8	248	280	19	3	8	8	234	218	12	2	12	8	83	87	37
-4	32	7	122	20	50	-11	1	8	383	381	12	8	4	8	98	124	59	4	8	8	220	236	37	3	12	8	0	3	1
-3	32	7	570	579	23	-10	1	8	479	476	14	-14	5	8	362	361	26	5	8	8	140	110	19	4	12	8	82	8	44
-2	32	7	320	279	16	-9	1	8	209	203	16	-13	5	8	481	464	10	6	8	8	36	15	36	5	12	8	29	26	29
-1	32	7	99	68	45	-8	1	8	515	523	10	-12	5	8	300	315	12	7	8	8	115	28	25	6	12	8	38	3	38
0	32	7	103	117	49	-7	1	8	145	127	18	-11	5	8	633	628	10	8	8	8	248	205	35	7	12	8	0	47	-1
1	32	7	224	204	21	-6	1	8	1122	1121	14	-10	5	8	832	818	13	-14	9	8	537	535	14	-14	13	8	170	202	42
2	32	7	184	172	26	-5	1	8	592	584	10	-9	5	8	238	245	11	-13	9	8	466	471	20	-13	13	8	31	55	31
3	32	7	0	8	1	-4	1	8	415	409	6	-8	5	8	112	60	27	-12	9	8	384	367	14	-12	13	8	127	118	37
-9	33	7	80	37	80	-3	1	8	59	88	59	-7	5	8	465	470	10	-11	9	8	461	452	15	-11	13	8	198	195	16
-8	33	7	0	17	1	-2	1	8	679	655	7	-6	5	8	1071	1059	13	-10	9	8	534	547	9	-10	13	8	737	751	10
-7	33	7	106	24	69	-1	1	8	763	759	7	-5	5	8	386	384	6	-9	9	8	674	658	9	-9	13	8	554	562	9
-6	33	7	98	46	97	0	1	8	87	74	20	-4	5	8	224	227	8	-8	9	8	119	134	21	-8	13	8	180	187	14
-5	33	7	225	200	32	1	1	8	443	420	8	-3	5	8	355	350	6	-7	9	8	455	464	8	-7	13	8	500	498	9
-4	33	7	243	245	30	2	1	8	409	408	7	-2	5	8	1276	1270	10	-6	9	8	393	393	9	-6	13	8	377	373	7
-3	33	7	227	168	28	3	1	8	433	423	7	-1	5	8	539	543	6	-5	9	8	732	736	7	-5	13	8	256	276	8
-2	33	7	68	91	68	4	1	8	457	507	16	0	5	8	125	102	15	-4	9	8	356	341	8	-4	13	8	0	9	1
-1	33	7	241	241	36	5	1	8	319	319	14	1	5	8	467	461	7	-3	9	8	816	813	7	-3	13	8	460	470	7
0	33	7	0	52	-1	6	1	8	342	354	21	2	5	8	594	588	7	-2	9	8	989	989	7	-2	13	8	1081	1071	9
1	33	7	286	279	22	7	1	8	0	13	1	3	5	8	345	329	10	-1	9	8	561	547	5	-1	13	8	762	767	8
2	33	7	175	194	29	8	1	8	34	54	33	4	5	8	293	309	14	0	9	8	605	598	5	0	13	8	169	175	13
3	33	7	0	33	-1	-14	2	8	0	53	-1	5	5	8	443	459	17	1	9	8	233	231	9	1	13	8	335	341	8
-8	34	7	0	67	1	-13	2	8	194	205	17	6	5	8	713	744	17	2	9	8	679	675	7	2	13	8	265	251	12
-7	34	7	162	120	26	-12	2	8	275	277	15	7	5	8	261	286	18	3	9	8	479	484	7	3	13	8	332	329	11
-6	34	7	368	339	20	-11	2	8	169	173	36	8	5	8	67	60	66	4	9	8	33	44	32	4	13	8	287	322	13
-5	34	7	0	38	1	-10	2	8	152	112	29	-14	6	8	0	63	1	5	9	8	365	358	10	5	13	8	95	92	34
-4	34	7	45	123	45	-9	2	8	262	267	14	-13	6	8	282	257	17	6	9	8	358	353	14	6	13	8	100	152	37

Table D.6. Observed and calculated structure factors for Rutdp

h	k	1	10Fo	10Fc	10s	h	k	1	10Fo	10Fc	10s	h	k	1	10Fo	10Fc	10s	h	k	1	10Fo	10Fc	10s	h	k	1	10Fo	10Fc	10s
7	13	8	148	130	27	-9	18	8	335	352	13	2	22	8	120	57	35	4	27	8	0	18	1	1	34	8	386	400	26
-13	14	8	235	292	30	-8	18	8	544	555	9	3	22	8	0	24	1	-10	28	8	0	83	1	-7	35	8	110	139	77
-12	14	8	587	587	13	-7	18	8	304	262	25	4	22	8	0	22	1	-9	28	8	237	250	41	-6	35	8	127	106	65

-11	14	8	441	437	10
-10	14	8	160	181	29
-9	14	8	579	576	9
-8	14	8	256	234	11
-7	14	8	280	283	10
-6	14	8	174	171	12
-5	14	8	495	500	7
-4	14	8	854	857	9
-3	14	8	502	485	6
-2	14	8	180	164	11
-1	14	8	870	868	9
0	14	8	645	635	8
1	14	8	677	673	8
2	14	8	200	221	12
3	14	8	430	416	10
4	14	8	287	302	13
5	14	8	468	488	11
6	14	8	248	251	16
7	14	8	249	258	18
-13	15	8	101	122	100
-12	15	8	110	122	110
-11	15	8	435	422	13
-10	15	8	578	595	13
-9	15	8	254	245	14
-8	15	8	0	3	1
-7	15	8	288	271	10
-6	15	8	562	562	7
-5	15	8	834	842	8
-4	15	8	209	207	14
-3	15	8	582	571	7
-2	15	8	555	546	7
-1	15	8	117	121	22
0	15	8	51	35	50
1	15	8	320	308	12
2	15	8	451	455	8
3	15	8	756	777	10
4	15	8	135	145	24
5	15	8	0	45	1
6	15	8	408	404	14
7	15	8	311	309	22
-13	16	8	115	46	38
-12	16	8	178	209	25
-11	16	8	27	10	27
-10	16	8	190	195	16
-9	16	8	0	48	1
-8	16	8	108	92	23
-7	16	8	613	620	9
-6	16	8	101	108	19
-5	16	8	421	426	8
-4	16	8	336	335	9
-6	18	8	0	2	1
-5	18	8	154	152	28
-4	18	8	686	706	8
-3	18	8	504	501	7
-2	18	8	73	80	40
-1	18	8	657	652	8
0	18	8	616	598	11
1	18	8	332	312	10
2	18	8	103	76	27
3	18	8	413	436	12
4	18	8	464	458	16
5	18	8	355	344	15
6	18	8	177	124	31
-13	19	8	340	305	17
-12	19	8	0	42	1
-11	19	8	372	366	15
-10	19	8	565	566	16
-9	19	8	218	210	14
-8	19	8	171	200	15
-7	19	8	237	224	19
-6	19	8	424	403	7
-5	19	8	450	450	8
-4	19	8	674	660	8
-3	19	8	292	262	10
-2	19	8	458	449	9
-1	19	8	692	675	9
0	19	8	288	284	11
1	19	8	965	960	10
2	19	8	661	662	11
3	19	8	493	478	12
4	19	8	368	337	14
5	19	8	346	345	16
6	19	8	498	512	21
-12	20	8	330	355	16
-11	20	8	130	172	31
-10	20	8	0	34	1
-9	20	8	418	420	13
-8	20	8	429	441	10
-7	20	8	204	203	13
-6	20	8	83	76	25
-5	20	8	140	131	17
-4	20	8	469	449	9
-3	20	8	197	197	15
-2	20	8	149	131	17
-1	20	8	385	393	10
0	20	8	475	447	9
1	20	8	741	721	9
2	20	8	94	132	45
3	20	8	456	446	13
4	20	8	327	352	16
5	22	8	117	135	116
-12	23	8	0	64	1
-11	23	8	176	200	25
-10	23	8	331	348	15
-9	23	8	188	192	20
-8	23	8	141	127	24
-7	23	8	415	425	9
-6	23	8	720	700	8
-5	23	8	589	590	16
-4	23	8	64	8	63
-3	23	8	526	517	29
-2	23	8	361	377	15
-1	23	8	79	71	40
0	23	8	164	162	45
1	23	8	438	435	12
2	23	8	596	589	12
3	23	8	231	187	32
4	23	8	66	29	65
5	23	8	54	106	54
-12	24	8	307	365	25
-11	24	8	170	205	24
-10	24	8	0	62	1
-9	24	8	332	356	14
-8	24	8	544	558	12
-7	24	8	453	453	9
-6	24	8	71	54	43
-5	24	8	282	268	14
-4	24	8	525	501	11
-3	24	8	671	655	13
-2	24	8	110	99	33
-1	24	8	508	486	9
0	24	8	491	489	9
1	24	8	499	486	12
2	24	8	69	73	69
3	24	8	273	284	17
4	24	8	348	351	21
5	24	8	328	327	18
-11	25	8	65	136	64
-10	25	8	515	545	13
-9	25	8	90	82	51
-8	25	8	95	41	43
-7	25	8	368	380	10
-6	25	8	626	633	9
-5	25	8	360	378	12
-4	25	8	99	60	35
-3	25	8	167	113	22
-2	25	8	503	497	9
-1	25	8	576	549	9
0	25	8	252	237	13
1	25	8	188	224	40
-8	28	8	303	290	15
-7	28	8	438	417	10
-6	28	8	125	13	48
-5	28	8	501	479	27
-4	28	8	533	514	11
-3	28	8	268	238	16
-2	28	8	81	98	81
-1	28	8	309	310	11
0	28	8	439	411	15
1	28	8	122	85	38
2	28	8	178	181	34
3	28	8	196	230	24
4	28	8	377	373	17
-10	29	8	438	477	16
-9	29	8	50	84	50
-8	29	8	113	101	33
-7	29	8	347	311	21
-6	29	8	441	441	18
-5	29	8	517	536	22
-4	29	8	144	48	43
-3	29	8	657	614	13
-2	29	8	673	673	9
-1	29	8	311	310	13
0	29	8	222	209	21
1	29	8	0	49	1
2	29	8	632	626	12
3	29	8	315	311	18
-10	30	8	161	219	29
-9	30	8	23	95	22
-8	30	8	264	275	18
-7	30	8	371	357	21
-6	30	8	127	53	53
-5	30	8	393	391	19
-4	30	8	373	372	13
-3	30	8	456	471	12
-2	30	8	74	105	73
-1	30	8	313	285	20
0	30	8	0	57	1
1	30	8	178	177	25
2	30	8	210	201	22
3	30	8	154	93	33
-9	31	8	0	84	-1
-8	31	8	0	32	1
-7	31	8	223	210	32
-6	31	8	0	83	-1
-5	31	8	73	7	73
-4	31	8	194	207	20
-3	31	8	82	79	81
-2	31	8	170	156	21
-1	31	8	156	166	29
-5	35	8	307	292	23
-4	35	8	134	94	55
-3	35	8	291	247	25
-2	35	8	158	151	49
-1	35	8	40	19	39
0	35	8	87	73	86
-6	36	8	93	148	93
-5	36	8	70	99	69
-4	36	8	0	25	1
-3	36	8	292	266	26
-2	36	8	37	24	36
-1	36	8	0	65	1
-4	37	8	0	64	1
-3	37	8	287	301	27
-14	1	9	103	65	50
-13	1	9	257	285	17
-12	1	9	483	481	12
-11	1	9	294	267	21
-10	1	9	214	226	31
-9	1	9	125	134	26
-8	1	9	495	511	11
-7	1	9	543	540	11
-6	1	9	58	11	58
-5	1	9	599	563	15
-4	1	9	925	903	8
-3	1	9	313	292	7
-2	1	9	649	631	7
-1	1	9	70	34	48
0	1	9	716	717	7
1	1	9	189	175	11
2	1	9	190	204	12
3	1	9	101	31	27
4	1	9	234	209	18
5	1	9	165	181	25
6	1	9	154	210	28
7	1	9	72	146	72
-14	2	9	606	615	11
-13	2	9	217	205	16
-12	2	9	312	303	14
-11	2	9	309	308	18
-10	2	9	410	373	12
-9	2	9	139	120	23
-8	2	9	419	403	11
-7	2	9	330	324	12
-6	2	9	1166	1154	14
-5	2	9	1228	1212	15
-4	2	9	432	427	8
-3	2	9	261	285	9
-2	2	9	731	717	7
-1	2	9	1120	1107	9

-3	16	8	204	211	10	5	20	8	169	180	27	2	25	8	237	227	19	0	31	8	287	287	18	0	2	9	442	451	7
-2	16	8	373	355	9	6	20	8	192	193	27	3	25	8	250	261	20	1	31	8	158	184	29	1	2	9	334	318	8
-1	16	8	861	857	9	-12	21	8	214	197	22	4	25	8	238	218	22	2	31	8	0	61	1	2	2	9	291	252	13
0	16	8	540	527	11	-11	21	8	0	22	-1	5	25	8	391	367	18	3	31	8	0	17	-1	3	2	9	567	590	9
1	16	8	325	329	10	-10	21	8	274	317	16	-11	26	8	152	182	28	-9	32	8	134	128	36	4	2	9	444	459	12
2	16	8	126	142	21	-9	21	8	49	61	49	-10	26	8	107	22	64	-8	32	8	70	120	69	5	2	9	73	60	72
3	16	8	38	44	37	-8	21	8	51	90	50	-9	26	8	44	67	43	-7	32	8	153	109	41	6	2	9	336	337	21
4	16	8	332	322	15	-7	21	8	79	28	78	-8	26	8	155	182	25	-6	32	8	46	35	46	7	2	9	259	296	24
5	16	8	232	207	21	-6	21	8	290	301	9	-7	26	8	32	25	31	-5	32	8	173	188	40	-14	3	9	146	149	24
6	16	8	83	23	82	-5	21	8	70	76	41	-6	26	8	0	35	1	-4	32	8	243	246	18	-13	3	9	350	351	12
7	16	8	111	112	53	-4	21	8	361	363	9	-5	26	8	20	2	19	-3	32	8	213	192	20	-12	3	9	662	655	13
-13	17	8	179	193	25	-3	21	8	147	125	16	-4	26	8	215	215	18	-2	32	8	170	83	44	-11	3	9	408	396	12
-12	17	8	149	173	26	-2	21	8	317	319	12	-3	26	8	101	97	36	-1	32	8	172	160	30	-10	3	9	201	195	21
-11	17	8	148	167	28	-1	21	8	0	38	1	-2	26	8	84	107	83	0	32	8	199	226	29	-9	3	9	146	162	22
-10	17	8	273	306	16	0	21	8	0	54	1	-1	26	8	40	16	39	1	32	8	95	120	94	-8	3	9	483	476	16
-9	17	8	215	238	14	1	21	8	150	144	18	0	26	8	0	44	1	2	32	8	27	55	27	-7	3	9	559	533	11
-8	17	8	198	202	13	2	21	8	299	296	15	1	26	8	0	45	-1	-8	33	8	29	70	29	-6	3	9	177	167	18
-7	17	8	212	236	12	3	21	8	177	178	26	2	26	8	27	128	27	-7	33	8	393	343	22	-5	3	9	214	208	30
-6	17	8	80	38	26	4	21	8	0	27	1	3	26	8	123	140	37	-6	33	8	434	427	20	-4	3	9	1168	1151	9
-5	17	8	87	35	27	5	21	8	194	213	25	4	26	8	107	137	52	-5	33	8	274	258	28	-3	3	9	1225	1230	10
-4	17	8	140	137	16	6	21	8	82	101	82	-11	27	8	52	49	52	-4	33	8	69	39	69	-2	3	9	44	45	43
-3	17	8	155	138	13	-12	22	8	181	171	25	-10	27	8	105	97	42	-3	33	8	413	401	13	-1	3	9	471	471	7
-2	17	8	349	363	9	-11	22	8	15	79	15	-9	27	8	286	248	16	-2	33	8	551	565	18	0	3	9	89	108	23
-1	17	8	541	521	8	-10	22	8	0	25	1	-8	27	8	116	140	33	-1	33	8	366	382	16	1	3	9	427	411	10
0	17	8	43	11	43	-9	22	8	246	248	16	-7	27	8	162	188	23	0	33	8	146	210	33	2	3	9	749	763	8
1	17	8	0	68	1	-8	22	8	263	256	12	-6	27	8	72	32	72	1	33	8	0	22	1	3	3	9	320	305	11
2	17	8	166	174	18	-7	22	8	0	59	1	-5	27	8	35	89	34	2	33	8	260	236	36	4	3	9	386	403	13
3	17	8	194	201	20	-6	22	8	284	288	9	-4	27	8	349	338	16	-7	34	8	277	324	25	5	3	9	330	371	19
4	17	8	0	74	1	-5	22	8	89	62	48	-3	27	8	217	202	18	-6	34	8	148	41	46	6	3	9	297	298	36
5	17	8	0	48	1	-4	22	8	272	282	13	-2	27	8	295	307	11	-5	34	8	320	328	24	7	3	9	54	25	53
6	17	8	0	76	1	-3	22	8	273	292	21	-1	27	8	107	49	29	-4	34	8	504	480	18	-14	4	9	253	281	15
-13	18	8	543	523	14	-2	22	8	203	183	14	0	27	8	324	357	14	-3	34	8	354	352	22	-13	4	9	51	13	50
-12	18	8	182	200	23	-1	22	8	0	6	-1	1	27	8	434	463	15	-2	34	8	199	125	40	-12	4	9	73	119	73
-11	18	8	41	92	40	0	22	8	118	88	24	2	27	8	225	185	33	-1	34	8	169	148	28	-11	4	9	382	393	13
-10	18	8	157	182	24	1	22	8	192	180	16	3	27	8	245	252	20	0	34	8	309	288	20	-10	4	9	796	777	12

Table D.6. Observed and calculated structure factors for Rutdp

h	k	1	10Fo	10Fc	10s	h	k	1	10Fo	10Fc	10s	h	k	1	10Fo	10Fc	10s	h	k	1	10Fo	10Fc	10s	h	k	1	10Fo	10Fc	10s
-9	4	9	231	259	15	-9	8	9	405	394	9	-4	12	9	743	752	9	4	16	9	401	426	15	0	21	9	309	298	11
-8	4	9	127	100	26	-8	8	9	0	66	1	-3	12	9	323	328	7	5	16	9	0	25	1	1	21	9	584	582	9
-7	4	9	623	626	11	-7	8	9	230	240	13	-2	12	9	774	774	7	-13	17	9	276	252	27	2	21	9	413	417	13
-6	4	9	640	633	11	-6	8	9	701	699	9	-1	12	9	510	505	8	-12	17	9	285	336	24	3	21	9	87	116	86
-5	4	9	556	556	10	-5	8	9	845	842	9	0	12	9	133	163	35	-11	17	9	431	434	20	4	21	9	368	364	16
-4	4	9	250	244	11	-4	8	9	290	289	9	1	12	9	65	70	43	-10	17	9	146	129	20	5	21	9	389	382	24
-3	4	9	682	683	7	-3	8	9	404	402	5	2	12	9	578	580	8	-9	17	9	67	84	67	-12	22	9	454	469	24
-2	4	9	240	245	10	-2	8	9	644	632	6	3	12	9	894	889	10	-8	17	9	835	842	17	-11	22	9	290	309	31
-1	4	9	402	420	7	-1	8	9	719	714	6	4	12	9	384	397	15	-7	17	9	574	582	9	-10	22	9	288	284	16
0	4	9	48	59	48	0	8	9	229	217	10	5	12	9	163	169	22	-6	17	9	107	117	54	-9	22	9	330	391	21

1	4	9	330	338	9
2	4	9	245	222	12
3	4	9	475	510	11
4	4	9	363	363	13
5	4	9	82	90	81
6	4	9	51	19	51
7	4	9	56	82	56
-14	5	9	357	357	13
-13	5	9	30	85	30
-12	5	9	121	126	25
-11	5	9	147	58	19
-10	5	9	308	315	11
-9	5	9	431	439	9
-8	5	9	166	168	15
-7	5	9	93	18	58
-6	5	9	15	109	15
-5	5	9	208	201	17
-4	5	9	429	440	6
-3	5	9	84	95	23
-2	5	9	0	26	1
-1	5	9	113	105	18
0	5	9	0	54	1
1	5	9	221	211	15
2	5	9	108	75	25
3	5	9	127	70	23
4	5	9	73	107	73
5	5	9	0	61	1
6	5	9	91	8	90
7	5	9	91	37	91
-14	6	9	445	441	12
-13	6	9	350	337	12
-12	6	9	84	125	38
-11	6	9	215	208	15
-10	6	9	315	318	12
-9	6	9	429	424	9
-8	6	9	45	80	45
-7	6	9	876	869	13
-6	6	9	760	749	9
-5	6	9	597	612	10
-4	6	9	676	662	7
-3	6	9	329	330	7
-2	6	9	624	617	9
-1	6	9	184	163	11
0	6	9	343	336	14
1	6	9	303	305	10
2	6	9	265	229	35
3	6	9	564	579	11
4	6	9	0	8	1
5	6	9	182	157	25
6	6	9	51	79	51
1	8	9	445	441	11
2	8	9	886	879	10
3	8	9	413	437	10
4	8	9	347	361	10
5	8	9	116	149	24
6	8	9	387	432	12
-14	9	9	173	145	41
-13	9	9	88	144	42
-12	9	9	64	48	63
-11	9	9	238	210	13
-10	9	9	206	204	14
-9	9	9	426	436	12
-8	9	9	529	530	9
-7	9	9	160	179	15
-6	9	9	230	229	11
-5	9	9	178	160	17
-4	9	9	279	281	10
-3	9	9	104	112	15
-2	9	9	578	589	5
-1	9	9	161	167	10
0	9	9	0	46	1
1	9	9	0	13	1
2	9	9	278	269	8
3	9	9	73	29	31
4	9	9	207	178	14
5	9	9	380	417	12
6	9	9	0	48	1
-14	10	9	0	26	1
-13	10	9	95	123	35
-12	10	9	55	46	55
-11	10	9	50	14	50
-10	10	9	0	15	1
-9	10	9	144	119	18
-8	10	9	271	248	12
-7	10	9	55	4	54
-6	10	9	441	442	14
-5	10	9	193	194	12
-4	10	9	158	137	17
-3	10	9	224	200	11
-2	10	9	475	477	6
-1	10	9	64	11	31
0	10	9	83	99	22
1	10	9	109	119	18
2	10	9	180	189	12
3	10	9	163	185	14
4	10	9	67	53	56
5	10	9	0	10	-1
6	10	9	0	64	1
-14	11	9	0	67	1
-13	11	9	104	43	82
6	12	9	0	80	1
-13	13	9	106	110	49
-12	13	9	257	273	14
-11	13	9	765	776	13
-10	13	9	191	199	15
-9	13	9	149	117	17
-8	13	9	301	303	13
-7	13	9	743	754	9
-6	13	9	279	311	13
-5	13	9	524	508	8
-4	13	9	552	544	8
-3	13	9	105	129	18
-2	13	9	273	273	9
-1	13	9	253	264	9
0	13	9	849	832	8
1	13	9	338	356	15
2	13	9	133	134	18
3	13	9	64	59	64
4	13	9	312	320	12
5	13	9	545	539	11
6	13	9	108	172-	36
-13	14	9	342	328	20
-12	14	9	97	111	47
-11	14	9	78	146	77
-10	14	9	48	105	48
-9	14	9	0	8	1
-8	14	9	283	281	11
-7	14	9	0	13	1
-6	14	9	224	230	15
-5	14	9	97	104	25
-4	14	9	39	45	39
-3	14	9	0	3	1
-2	14	9	355	363	8
-1	14	9	309	313	10
0	14	9	93	130	23
1	14	9	165	172	14
2	14	9	281	276	16
3	14	9	176	171	23
4	14	9	183	175	19
5	14	9	135	131	26
6	14	9	84	65	62
-13	15	9	115	124	39
-12	15	9	279	292	17
-11	15	9	45	69	44
-10	15	9	0	52	1
-9	15	9	55	15	54
-8	15	9	127	149	21
-7	15	9	0	67	1
-6	15	9	0	66	1
-5	15	9	254	251	11
-5	17	9	120	118	20
-4	17	9	788	783	9
-3	17	9	883	869	12
-2	17	9	218	230	12
-1	17	9	144	162	20
0	17	9	486	483	9
1	17	9	862	864	10
2	17	9	393	395	19
3	17	9	202	178	38
4	17	9	565	564	13
5	17	9	437	471	22
-13	18	9	168	153	42
-12	18	9	0	98	-1
-11	18	9	0	46	1
-10	18	9	371	385	11
-9	18	9	506	501	15
-8	18	9	0	27	1
-7	18	9	146	125	23
-6	18	9	372	370	11
-5	18	9	522	508	8
-4	18	9	108	98	23
-3	18	9	381	369	12
-2	18	9	322	322	19
-1	18	9	624	623	9
0	18	9	109	117	25
1	18	9	102	101	30
2	18	9	452	450	10
3	18	9	473	463	13
4	18	9	121	27	40
5	18	9	310	305	23
-12	19	9	212	179	23
-11	19	9	0	30	1
-10	19	9	149	134	59
-9	19	9	99	69	42
-8	19	9	55	25	54
-7	19	9	149	151	21
-6	19	9	68	53	41
-5	19	9	374	381	9
-4	19	9	86	107	32
-3	19	9	205	194	24
-2	19	9	140	146	24
-1	19	9	455	450	9
0	19	9	129	133	31
1	19	9	65	53	65
2	19	9	115	137	36
3	19	9	35	84	35
4	19	9	81	70	80
5	19	9	171	147	29
-12	20	9	363	351	16
-11	20	9	28	73	28
-8	22	9	269	241	12
-7	22	9	265	268	22
-6	22	9	888	891	10
-5	22	9	512	515	11
-4	22	9	70	64	70
-3	22	9	51	92	50
-2	22	9	208	209	14
-1	22	9	594	586	9
0	22	9	647	654	9
1	22	9	185	165	28
2	22	9	468	476	13
3	22	9	314	321	17
4	22	9	260	237	21
-11	23	9	167	188	25
-10	23	9	83	121	82
-9	23	9	67	71	67
-8	23	9	538	549	10
-7	23	9	412	415	12
-6	23	9	219	201	13
-5	23	9	171	114	20
-4	23	9	105	96	36
-3	23	9	371	368	21
-2	23	9	94	5	31
-1	23	9	187	193	16
0	23	9	0	78	1
1	23	9	604	609	10
2	23	9	452	447	15
3	23	9	143	158	34
4	23	9	232	205	25
-11	24	9	0	16	1
-10	24	9	0	53	1
-9	24	9	0	106	1
-8	24	9	160	134	32
-7	24	9	126	98	41
-6	24	9	55	55	55
-5	24	9	125	82	30
-4	24	9	136	124	26
-3	24	9	155	124	24
-2	24	9	41	82	40
-1	24	9	121	120	24
0	24	9	265	256	13
1	24	9	106	8	43
2	24	9	254	263	19
3	24	9	70	4	69
4	24	9	0	58	1
-11	25	9	329	344	18
-10	25	9	0	107	1
-9	25	9	126	155	44
-8	25	9	395	373	18
-7	25	9	341	358	13

7	6	9	421	429	10
-14	7	9	116	112	36
-13	7	9	235	223	15
-12	7	9	593	580	12
-11	7	9	541	542	10
-10	7	9	119	110	23
-9	7	9	205	208	13
-8	7	9	436	417	9
-7	7	9	1222	1234	16
-6	7	9	590	595	9
-5	7	9	380	375	8
-4	7	9	830	827	9
-3	7	9	586	588	5
-2	7	9	395	389	7
-1	7	9	246	258	9
0	7	9	958	951	8
1	7	9	455	442	9
2	7	9	308	312	11
3	7	9	167	180	17
4	7	9	479	487	12
5	7	9	588	589	12
6	7	9	89	91	37
7	7	9	158	183	41
-14	8	9	191	215	23
-13	8	9	297	288	16
-12	8	9	0	97	1
-11	8	9	439	434	13
-10	8	9	349	340	10
-12	11	9	428	439	10
-11	11	9	663	654	10
-10	11	9	254	258	12
-9	11	9	230	208	19
-8	11	9	242	213	12
-7	11	9	0	31	1
-6	11	9	499	505	11
-5	11	9	152	141	16
-4	11	9	631	620	8
-3	11	9	739	727	7
-2	11	9	208	187	11
-1	11	9	90	34	20
0	11	9	305	309	8
1	11	9	681	675	7
2	11	9	214	195	12
3	11	9	0	32	1
4	11	9	272	284	12
5	11	9	364	390	14
6	11	9	0	99	1
-13	12	9	344	321	31
-12	12	9	88	93	39
-11	12	9	189	188	17
-10	12	9	480	483	13
-9	12	9	810	807	16
-8	12	9	268	275	11
-7	12	9	176	122	15
-6	12	9	429	425	11
-5	12	9	809	812	9
-4	15	9	336	335	9
-3	15	9	521	520	11
-2	15	9	110	127	24
-1	15	9	590	585	8
0	15	9	181	194	15
1	15	9	325	324	9
2	15	9	0	56	1
3	15	9	39	76	39
4	15	9	80	65	53
5	15	9	168	157	21
6	15	9	183	195	31
-13	16	9	175	212	42
-12	16	9	317	311	23
-11	16	9	151	190	102
-10	16	9	549	561	11
-9	16	9	524	525	10
-8	16	9	277	266	32
-7	16	9	43	84	42
-6	16	9	549	539	11
-5	16	9	384	381	9
-4	16	9	83	91	30
-3	16	9	66	90	66
-2	16	9	171	187	17
-1	16	9	682	672	9
0	16	9	157	169	17
1	16	9	360	361	10
2	16	9	583	573	9
3	16	9	522	561	13
-10	20	9	193	281	32
-9	20	9	246	264	12
-8	20	9	41	26	40
-7	20	9	58	87	58
-6	20	9	150	152	17
-5	20	9	761	746	13
-4	20	9	415	370	11
-3	20	9	340	358	17
-2	20	9	73	71	72
-1	20	9	285	299	12
0	20	9	120	77	51
1	20	9	59	55	58
2	20	9	225	236	20
3	20	9	274	305	18
4	20	9	63	87	63
5	20	9	102	80	60
-12	21	9	404	406	15
-11	21	9	234	247	26
-10	21	9	91	156	46
-9	21	9	192	166	31
-8	21	9	633	645	12
-7	21	9	632	641	11
-6	21	9	405	397	9
-5	21	9	260	248	11
-4	21	9	405	401	11
-3	21	9	357	346	12
-2	21	9	111	98	31
-1	21	9	203	193	16
-6	25	9	264	238	15
-5	25	9	95	123	44
-4	25	9	303	295	13
-3	25	9	589	576	17
-2	25	9	305	296	12
-1	25	9	0	54	1
0	25	9	27	54	27
1	25	9	273	256	18
2	25	9	184	203	26
3	25	9	0	56	1
4	25	9	181	204	49
-11	26	9	0	10	1
-10	26	9	483	486	19
-9	26	9	515	502	13
-8	26	9	131	158	45
-7	26	9	162	145	36
-6	26	9	527	548	12
-5	26	9	412	381	12
-4	26	9	411	412	12
-3	26	9	176	186	20
-2	26	9	696	681	12
-1	26	9	344	335	11
0	26	9	93	96	36
1	26	9	118	82	38
2	26	9	319	300	17
3	26	9	484	456	14
-10	27	9	0	23	1
-9	27	9	207	206	20

Table D.6. Observed and calculated structure factors for Rutdp

h	k	l	10Fo	10Fc	10s
-8	27	9	264	248	22
-6	27	9	208	166	19
-5	27	9	391	393	13
-4	27	9	526	499	12
-3	27	9	528	521	12
-2	27	9	388	371	13
-1	27	9	237	212	21
0	27	9	405	434	14
1	27	9	431	407	14
2	27	9	129	101	43
3	27	9	158	164	38
-10	28	9	78	176	77
-9	28	9	110	36	65
-8	28	9	233	197	28
-6	28	9	400	391	13
-5	28	9	0	8	1
-4	28	9	21	32	21
2	0	10	672	677	11
3	0	10	307	334	21
4	0	10	239	282	26
5	0	10	267	283	26
6	0	10	229	210	32
-14	1	10	370	366	14
-13	1	10	479	477	13
-12	1	10	397	392	14
-11	1	10	193	170	20
-10	1	10	487	450	12
-9	1	10	278	274	14
-8	1	10	157	143	20
-7	1	10	476	481	11
-6	1	10	41	45	41
-5	1	10	944	929	19
-4	1	10	90	93	26
-3	1	10	194	176	11
6	4	10	578	569	13
-14	5	10	154	193	28
-13	5	10	560	587	13
-12	5	10	383	378	11
-11	5	10	0	21	1
-10	5	10	377	394	15
-9	5	10	542	543	9
-8	5	10	348	349	10
-7	5	10	230	231	15
-6	5	10	715	711	11
-5	5	10	1013	998	20
-4	5	10	65	19	65
-3	5	10	77	61	26
-2	5	10	286	270	14
-1	5	10	669	667	9
0	5	10	645	645	14
1	5	10	276	286	19
-6	9	10	833	824	12
-5	9	10	890	857	12
-4	9	10	613	601	8
-3	9	10	25	62	25
-2	9	10	707	688	6
-1	9	10	297	292	7
0	9	10	378	371	7
1	9	10	312	322	8
2	9	10	299	303	14
3	9	10	625	622	7
4	9	10	362	392	10
5	9	10	161	147	19
-13	10	10	133	64	26
-12	10	10	356	356	14
-11	10	10	643	606	13
-10	10	10	506	498	10
-9	10	10	401	403	10
-13	14	10	0	91	1
-12	14	10	304	344	13
-11	14	10	416	406	11
-10	14	10	457	451	10
-9	14	10	0	42	1
-8	14	10	700	711	16
-7	14	10	742	739	12
-6	14	10	335	321	12
-5	14	10	376	390	9
-4	14	10	346	344	10
-3	14	10	519	513	9
-2	14	10	446	442	9
-1	14	10	0	60	1
0	14	10	505	496	8
1	14	10	737	746	9
2	14	10	540	526	8
3	14	10	37	59	36

-3	28	9	25	7	25
-2	28	9	239	245	18
-1	28	9	226	237	25
0	28	9	356	352	14
1	28	9	49	95	48
2	28	9	0	11	1
3	28	9	0	73	1
-9	29	9	139	31	55
-6	29	9	274	270	17
-5	29	9	136	123	30
-4	29	9	188	198	22
-3	29	9	134	94	31
-2	29	9	101	51	64
-1	29	9	61	88	60
0	29	9	75	116	75
1	29	9	125	137	45
-9	30	9	252	280	29
-6	30	9	375	357	19
-5	30	9	397	378	13
-4	30	9	194	183	24
-3	30	9	0	61	1
-2	30	9	268	270	17
-1	30	9	239	244	28
0	30	9	218	223	23
1	30	9	217	210	24
2	30	9	231	198	37
-6	31	9	252	186	29
-5	31	9	334	333	18
-4	31	9	542	548	12
-3	31	9	525	510	17
-2	31	9	273	237	35
-1	31	9	217	258	23
0	31	9	389	383	16
1	31	9	409	392	16
-6	32	9	283	265	24
-5	32	9	311	277	24
-4	32	9	290	263	16
-3	32	9	271	229	35
-2	32	9	587	601	13
-1	32	9	247	252	24
0	32	9	127	116	42
-5	33	9	179	98	45
-4	33	9	205	185	23
-3	33	9	183	134	25
-2	33	9	152	122	47
-1	33	9	125	101	52
0	33	9	205	208	48
-6	34	9	0	73	1
-5	34	9	186	206	38
-4	34	9	101	27	100
-2	1	10	94	102	23
-1	1	10	780	786	8
0	1	10	365	355	8
1	1	10	0	94	1
2	1	10	273	268	11
3	1	10	392	407	14
4	1	10	327	331	22
5	1	10	79	80	78
6	1	10	112	144	48
-14	2	10	164	155	23
-13	2	10	62	23	62
-12	2	10	179	174	23
-11	2	10	154	169	23
-10	2	10	13	29	13
-9	2	10	0	5	1
-8	2	10	105	69	30
-7	2	10	202	196	25
-6	2	10	314	326	12
-5	2	10	88	39	77
-4	2	10	72	54	37
-3	2	10	51	97	50
-2	2	10	91	92	21
-1	2	10	267	268	9
0	2	10	105	118	21
1	2	10	389	386	8
2	2	10	139	170	21
3	2	10	95	10	40
4	2	10	0	14	1
5	2	10	0	124	1
6	2	10	80	102	80
-14	3	10	51	109	50
-13	3	10	0	55	1
-12	3	10	167	194	19
-11	3	10	44	3	43
-10	3	10	90	179	40
-9	3	10	155	132	22
-8	3	10	551	543	14
-7	3	10	367	363	12
-6	3	10	480	476	11
-5	3	10	0	66	1
-4	3	10	127	132	18
-3	3	10	36	68	36
-2	3	10	146	123	14
-1	3	10	390	388	8
0	3	10	392	399	8
1	3	10	210	203	12
2	3	10	206	182	16
3	3	10	277	272	13
4	3	10	0	107	1
5	3	10	109	100	65
2	5	10	575	567	11
3	5	10	587	592	18
4	5	10	249	241	20
5	5	10	115	115	45
-14	6	10	316	317	14
-13	6	10	258	248	15
-12	6	10	397	406	11
-11	6	10	122	144	24
-10	6	10	290	282	12
-9	6	10	238	238	12
-8	6	10	259	257	11
-7	6	10	533	517	11
-6	6	10	589	603	11
-5	6	10	188	176	19
-4	6	10	74	66	36
-3	6	10	369	370	7
-2	6	10	777	777	8
-1	6	10	368	361	8
0	6	10	482	461	9
1	6	10	338	345	15
2	6	10	389	395	10
3	6	10	137	132	45
4	6	10	208	220	20
5	6	10	294	315	17
-14	7	10	76	96	75
-13	7	10	0	72	1
-12	7	10	71	104	71
-11	7	10	147	120	21
-10	7	10	331	341	11
-9	7	10	220	252	13
-8	7	10	300	319	10
-7	7	10	121	35	27
-6	7	10	147	127	28
-5	7	10	639	645	11
-4	7	10	75	104	74
-3	7	10	101	117	37
-2	7	10	112	107	26
-1	7	10	103	105	19
0	7	10	0	84	1
1	7	10	84	83	34
2	7	10	129	135	23
3	7	10	31	71	31
4	7	10	188	184	24
5	7	10	259	290	13
-14	8	10	0	30	1
-13	8	10	0	22	1
-12	8	10	0	7	1
-11	8	10	228	224	14
-10	8	10	233	226	13
-9	8	10	70	63	70
-8	10	10	663	677	9
-7	10	10	682	666	11
-6	10	10	1112	1087	14
-5	10	10	336	344	13
-4	10	10	910	906	13
-3	10	10	0	34	1
-2	10	10	362	344	7
-1	10	10	421	400	7
0	10	10	423	410	7
1	10	10	652	657	7
2	10	10	129	143	16
3	10	10	68	7	41
4	10	10	55	52	55
5	10	10	274	309	13
-13	11	10	371	384	12
-12	11	10	238	239	16
-11	11	10	163	145	19
-10	11	10	207	219	15
-9	11	10	269	272	20
-8	11	10	450	430	9
-7	11	10	82	94	46
-6	11	10	92	103	92
-5	11	10	446	431	11
-4	11	10	203	212	17
-3	11	10	683	687	9
-2	11	10	160	142	12
-1	11	10	57	38	57
0	11	10	137	144	15
1	11	10	201	203	11
2	11	10	289	295	10
3	11	10	249	241	15
4	11	10	83	82	42
5	11	10	218	241	18
-13	12	10	153	209	29
-12	12	10	52	79	52
-11	12	10	0	77	1
-10	12	10	93	117	32
-9	12	10	231	256	13
-8	12	10	109	101	69
-7	12	10	79	81	48
-6	12	10	0	66	1
-5	12	10	116	143	26
-4	12	10	0	8	1
-3	12	10	165	154	23
-2	12	10	528	529	6
-1	12	10	0	24	-1
0	12	10	54	46	53
1	12	10	168	179	22
2	12	10	32	16	31
3	12	10	42	46	41
4	14	10	195	223	20
5	14	10	300	302	15
-13	15	10	493	482	23
-12	15	10	82	68	81
-11	15	10	60	3	59
-10	15	10	360	376	15
-9	15	10	728	723	14
-8	15	10	600	589	17
-7	15	10	0	90	1
-6	15	10	483	464	11
-5	15	10	597	608	9
-4	15	10	537	534	8
-3	15	10	246	245	16
-2	15	10	533	514	9
-1	15	10	216	201	14
0	15	10	390	393	10
1	15	10	0	50	1
2	15	10	229	239	12
3	15	10	453	440	11
4	15	10	99	148	39
5	15	10	63	154	62
-13	16	10	104	112	103
-12	16	10	158	191	29
-11	16	10	199	214	16
-10	16	10	116	44	32
-9	16	10	139	149	24
-8	16	10	0	7	-1
-7	16	10	0	50	1
-6	16	10	421	428	12
-5	16	10	292	296	10
-4	16	10	762	764	9
-3	16	10	0	62	1
-2	16	10	324	327	10
-1	16	10	582	595	14
0	16	10	344	333	11
1	16	10	507	507	10
2	16	10	113	37	28
3	16	10	0	70	1
4	16	10	113	86	61
-12	17	10	132	140	35
-11	17	10	143	187	22
-10	17	10	0	50	-1
-9	17	10	180	190	17
-8	17	10	56	28	56
-7	17	10	138	157	25
-6	17	10	76	60	54
-5	17	10	111	102	27
-4	17	10	456	466	10
-3	17	10	165	119	20
-2	17	10	0	50	1

-3	34	9	166	125	27	6	3	10	264	269	21	-8	8	10	64	67	63	4	12	10	165	119	40	-1	17	10	85	81	48
-2	34	9	208	159	41	-14	4	10	41	108	41	-7	8	10	504	518	11	5	12	10	17	52	16	0	17	10	152	139	20
-1	34	9	54	113	53	-13	4	10	96	95	36	-6	8	10	301	312	12	-13	13	10	210	206	23	1	17	10	156	86	26
-4	35	9	263	234	29	-12	4	10	190	201	21	-5	8	10	169	144	19	-12	13	10	192	206	17	2	17	10	0	61	1
-3	35	9	353	333	24	-11	4	10	471	479	14	-4	8	10	132	135	18	-11	13	10	0	54	1	3	17	10	0	29	1
-14	0	10	420	402	15	-10	4	10	315	304	12	-3	8	10	122	124	16	-10	13	10	202	175	16	4	17	10	316	301	18
-13	0	10	336	328	21	-9	4	10	0	53	1	-2	8	10	314	319	7	-9	13	10	259	254	12	-12	18	10	453	468	20
-12	0	10	202	185	28	-8	4	10	348	330	13	-1	8	10	264	277	7	-8	13	10	381	383	27	-11	18	10	248	272	18
-11	0	10	401	400	18	-7	4	10	811	810	12	0	8	10	97	58	28	-7	13	10	0	52	1	-10	18	10	86	80	40
-10	0	10	409	415	18	-6	4	10	591	564	11	1	8	10	334	338	11	-6	13	10	716	713	11	-9	18	10	0	13	1
-9	0	10	348	347	19	-5	4	10	779	783	12	2	8	10	390	399	10	-5	13	10	419	418	11	-8	18	10	252	275	17
-8	0	10	742	751	17	-4	4	10	1019	1021	10	3	8	10	170	179	14	-4	13	10	244	205	11	-7	18	10	645	665	12
-7	0	10	814	796	17	-3	4	10	317	310	10	4	8	10	272	262	28	-3	13	10	532	528	8	-6	18	10	318	293	13
-6	0	10	513	512	16	-2	4	10	227	225	10	5	8	10	419	407	10	-2	13	10	108	104	24	-5	18	10	148	164	26
-5	0	10	429	438	16	-1	4	10	313	325	12	-13	9	10	542	529	11	-1	13	10	538	523	8	-4	18	10	195	176	18
-4	0	10	681	675	16	0	4	10	409	395	8	-12	9	10	338	340	12	0	13	10	532	520	8	-3	18	10	558	538	12
-3	0	10	885	877	11	1	4	10	987	983	9	-11	9	10	0	71	1	1	13	10	52	90	51	-2	18	10	57	20	56
-2	0	10	1070	1055	13	2	4	10	559	575	10	-10	9	10	274	250	12	2	13	10	288	286	10	-1	18	10	51	71	50
-1	0	10	202	214	17	3	4	10	223	209	14	-9	9	10	707	716	12	3	13	10	312	308	13	0	18	10	174	176	18
0	0	10	546	530	11	4	4	10	268	258	42	-8	9	10	596	610	9	4	13	10	309	328	13	1	18	10	475	470	10
1	0	10	564	585	11	5	4	10	389	438	20	-7	9	10	283	280	16	5	13	10	308	269	15	2	18	10	389	391	11

Table D.6. Observed and calculated structure factors for Rutdp

h	k	l	10Fo	10Fc	10s	h	k	l	10Fo	10Fc	10s	h	k	l	10Fo	10Fc	10s	h	k	l	10Fo	10Fc	10s	h	k	l	10Fo	10Fc	10s
3	18	10	73	52	73	-5	24	10	92	72	47	-4	1	11	321	314	13	-6	6	11	361	351	17	-8	11	11	428	440	12
4	18	10	144	165	34	-4	24	10	170	161	22	-3	1	11	559	560	7	-5	6	11	211	175	24	-7	11	11	393	359	14
-12	19	10	411	408	15	-3	24	10	530	502	17	-2	1	11	101	80	21	-4	6	11	400	393	12	-6	11	11	282	293	14
-11	19	10	0	74	1	-2	24	10	384	389	13	-1	1	11	208	196	13	-3	6	11	276	273	9	-5	11	11	346	330	12
-10	19	10	484	472	10	-1	24	10	0	15	1	0	1	11	208	231	12	-2	6	11	339	339	8	-4	11	11	42	17	41
-9	19	10	433	439	17	0	24	10	178	192	19	1	1	11	540	537	11	-1	6	11	408	412	8	-3	11	11	299	290	11
-8	19	10	596	574	12	1	24	10	421	418	15	2	1	11	336	344	14	0	6	11	465	471	15	-2	11	11	700	673	11
-7	19	10	0	42	1	2	24	10	254	251	20	3	1	11	63	99	62	1	6	11	263	265	13	-1	11	11	397	401	8
-6	19	10	571	596	11	3	24	10	18	118	18	4	1	11	41	82	40	2	6	11	78	76	57	0	11	11	180	175	14
-5	19	10	715	714	9	-10	25	10	242	285	30	-13	2	11	459	445	12	3	6	11	212	224	16	1	11	11	336	344	9
-4	19	10	92	69	55	-9	25	10	273	278	23	-12	2	11	444	444	13	4	6	11	248	260	20	2	11	11	244	245	11
-3	19	10	296	290	16	-8	25	10	283	268	15	-11	2	11	375	397	13	-13	7	11	190	212	19	3	11	11	118	103	25
-2	19	10	214	209	25	-7	25	10	99	80	62	-10	2	11	303	287	15	-12	7	11	0	57	1	4	11	11	0	33	1
-1	19	10	325	324	14	-6	25	10	383	365	18	-9	2	11	869	868	18	-11	7	11	577	582	10	-13	12	11	286	294	15
0	19	10	709	693	11	-5	25	10	620	607	12	-8	2	11	396	385	22	-10	7	11	581	572	10	-12	12	11	376	369	12
1	19	10	42	98	41	-4	25	10	227	221	18	-7	2	11	521	537	11	-9	7	11	246	286	16	-11	12	11	73	47	57
2	19	10	461	466	13	-3	25	10	143	58	42	-6	2	11	221	229	16	-8	7	11	207	215	18	-10	12	11	115	123	51
3	19	10	427	448	14	-2	25	10	104	16	37	-5	2	11	300	269	13	-7	7	11	536	528	11	-9	12	11	378	393	13
4	19	10	276	247	20	-1	25	10	539	507	10	-4	2	11	339	322	23	-6	7	11	957	942	13	-8	12	11	437	441	12
-12	20	10	332	353	18	0	25	10	487	481	11	-3	2	11	484	484	7	-5	7	11	297	256	13	-7	12	11	0	12	1
-11	20	10	0	113	1	1	25	10	126	77	38	-2	2	11	52	31	52	-4	7	11	59	36	58	-6	12	11	360	392	24
-10	20	10	238	247	28	2	25	10	176	153	28	-1	2	11	522	505	16	-3	7	11	354	344	9	-5	12	11	122	139	26
-9	20	10	203	220	27	-10	26	10	176	136	39	0	2	11	846	853	9	-2	7	11	296	292	7	-4	12	11	801	794	9
-8	20	10	413	407	12	-9	26	10	164	99	32	1	2	11	320	326	18	-1	7	11	386	369	11	-3	12	11	476	463	9

-7	20	10	473	467	14
-6	20	10	0	14	1
-5	20	10	66	36	65
-4	20	10	468	474	11
-3	20	10	644	633	11
-2	20	10	430	448	18
-1	20	10	151	158	19
0	20	10	247	242	14
1	20	10	574	594	10
2	20	10	484	476	13
3	20	10	80	9	80
4	20	10	351	361	26
-12	21	10	0	68	1
-11	21	10	0	25	1
-10	21	10	0	6	1
-9	21	10	158	161	26
-8	21	10	144	160	45
-7	21	10	141	156	30
-6	21	10	0	80	1
-5	21	10	0	48	1
-4	21	10	213	225	17
-3	21	10	0	57	1
-2	21	10	377	344	13
-1	21	10	343	348	11
0	21	10	225	257	15
1	21	10	101	101	34
2	21	10	244	250	21
3	21	10	274	265	21
-11	22	10	100	73	100
-10	22	10	90	106	64
-9	22	10	0	5	1
-8	22	10	213	225	19
-7	22	10	367	369	13
-6	22	10	264	258	15
-5	22	10	219	194	18
-4	22	10	90	119	49
-3	22	10	83	59	55
-2	22	10	171	173	23
-1	22	10	142	139	21
0	22	10	80	81	55
1	22	10	105	67	53
2	22	10	107	141	106
3	22	10	98	68	67
-11	23	10	0	17	1
-10	23	10	249	258	24
-9	23	10	454	451	19
-8	23	10	368	339	13
-7	23	10	0	94	1
-6	23	10	286	299	21
-5	23	10	460	456	12
-8	26	10	88	80	87
-7	26	10	97	64	96
-6	26	10	99	33	62
-5	26	10	79	66	79
-4	26	10	52	81	51
-3	26	10	223	204	19
-2	26	10	27	37	27
-1	26	10	45	45	45
0	26	10	0	48	1
1	26	10	90	119	89
2	26	10	139	112	39
-9	27	10	104	119	104
-7	27	10	108	26	57
-6	27	10	202	222	29
-5	27	10	200	173	25
-4	27	10	143	141	28
-3	27	10	0	51	1
-2	27	10	211	243	19
-1	27	10	305	297	20
0	27	10	249	242	16
1	27	10	117	87	49
-9	28	10	134	150	45
-7	28	10	192	228	27
-6	28	10	366	335	19
-5	28	10	94	35	52
-4	28	10	424	407	13
-3	28	10	475	462	17
-2	28	10	280	287	18
-1	28	10	93	25	57
0	28	10	367	381	16
1	28	10	455	448	15
-9	29	10	420	417	20
-6	29	10	338	301	19
-5	29	10	345	324	16
-4	29	10	445	428	21
-3	29	10	173	135	26
-2	29	10	398	397	14
-1	29	10	539	537	13
0	29	10	165	174	41
-6	30	10	361	348	21
-5	30	10	91	122	62
-4	30	10	290	265	16
-3	30	10	305	292	16
-2	30	10	283	289	18
-1	30	10	56	20	55
0	30	10	173	221	35
-5	31	10	0	63	1
-4	31	10	0	14	1
-3	31	10	136	49	71
-2	31	10	0	23	1
2	2	11	96	135	32
3	2	11	189	214	23
4	2	11	246	295	19
-13	3	11	164	183	26
-12	3	11	307	307	12
-11	3	11	416	412	18
-10	3	11	509	529	12
-9	3	11	249	239	16
-8	3	11	82	61	81
-7	3	11	593	575	16
-6	3	11	237	244	16
-5	3	11	87	43	44
-4	3	11	178	163	20
-3	3	11	533	523	7
-2	3	11	929	910	10
-1	3	11	491	484	8
0	3	11	571	554	8
1	3	11	423	443	11
2	3	11	436	434	10
3	3	11	325	335	15
4	3	11	0	119	1
-13	4	11	195	218	18
-12	4	11	160	154	20
-11	4	11	73	87	72
-10	4	11	185	187	17
-9	4	11	537	532	10
-8	4	11	188	224	18
-7	4	11	92	71	66
-6	4	11	87	38	79
-5	4	11	363	358	12
-4	4	11	580	571	11
-3	4	11	261	249	11
-2	4	11	499	491	7
-1	4	11	418	419	8
0	4	11	519	517	8
1	4	11	115	66	30
2	4	11	275	292	13
3	4	11	137	152	36
4	4	11	107	151	107
-13	5	11	207	215	17
-12	5	11	53	27	52
-11	5	11	112	162	38
-10	5	11	142	152	28
-9	5	11	0	35	1
-8	5	11	101	38	101
-7	5	11	238	242	15
-6	5	11	239	238	15
-5	5	11	70	48	69
-4	5	11	127	115	26
-3	5	11	94	51	23
0	7	11	103	16	54
1	7	11	520	518	10
2	7	11	530	519	10
3	7	11	145	150	21
4	7	11	101	117	79
-13	8	11	304	320	14
-12	8	11	373	336	12
-11	8	11	111	88	28
-10	8	11	238	233	18
-9	8	11	824	842	13
-8	8	11	389	381	15
-7	8	11	62	84	61
-6	8	11	506	480	12
-5	8	11	631	621	18
-4	8	11	739	740	9
-3	8	11	312	310	10
-2	8	11	173	182	11
-1	8	11	563	566	10
0	8	11	600	608	8
1	8	11	475	463	8
2	8	11	86	123	33
3	8	11	285	293	14
4	8	11	320	323	13
-13	9	11	0	31	1
-12	9	11	0	6	1
-11	9	11	0	66	1
-10	9	11	135	163	23
-9	9	11	0	46	1
-8	9	11	408	437	12
-7	9	11	615	625	11
-6	9	11	530	529	11
-5	9	11	0	32	-1
-4	9	11	90	29	41
-3	9	11	250	261	15
-2	9	11	395	381	6
-1	9	11	0	44	1
0	9	11	304	289	9
1	9	11	25	28	25
2	9	11	74	63	41
3	9	11	73	88	48
4	9	11	41	38	41
-13	10	11	158	184	37
-12	10	11	95	137	68
-11	10	11	35	102	35
-10	10	11	101	60	58
-9	10	11	256	259	16
-8	10	11	237	230	16
-7	10	11	116	58	29
-6	10	11	0	25	1
-5	10	11	195	203	19
-2	12	11	124	112	31
-1	12	11	765	751	8
0	12	11	580	588	11
1	12	11	252	263	12
2	12	11	242	239	13
3	12	11	254	275	16
4	12	11	526	519	11
-13	13	11	0	117	1
-12	13	11	262	264	14
-11	13	11	380	388	11
-10	13	11	667	648	12
-9	13	11	201	208	21
-8	13	11	476	478	12
-7	13	11	422	410	19
-6	13	11	555	562	11
-5	13	11	66	14	65
-4	13	11	195	185	15
-3	13	11	558	576	13
-2	13	11	219	231	17
-1	13	11	203	183	14
0	13	11	194	183	14
1	13	11	423	416	10
2	13	11	452	449	10
3	13	11	133	145	28
4	13	11	53	32	53
-12	14	11	0	4	1
-11	14	11	86	3	58
-10	14	11	0	33	1
-9	14	11	218	202	19
-8	14	11	196	193	76
-7	14	11	276	275	14
-6	14	11	65	86	64
-5	14	11	64	42	64
-4	14	11	602	603	9
-3	14	11	216	213	17
-2	14	11	61	40	61
-1	14	11	194	174	16
0	14	11	0	5	1
1	14	11	125	119	25
2	14	11	126	83	23
3	14	11	0	85	1
-12	15	11	144	166	25
-11	15	11	296	308	13
-10	15	11	85	109	69
-9	15	11	0	19	1
-8	15	11	380	387	19
-7	15	11	357	360	16
-6	15	11	0	34	1
-5	15	11	334	345	12
-4	15	11	195	173	15

-4	23	10	572	560	11
-3	23	10	146	119	27
-2	23	10	301	293	17
-1	23	10	360	340	11
0	23	10	290	298	13
1	23	10	90	119	40
2	23	10	0	108	1
3	23	10	257	253	21
-11	24	10	435	438	15
-10	24	10	258	294	25
-9	24	10	0	78	1
-8	24	10	254	260	16
-7	24	10	524	557	12
-6	24	10	379	354	20
-1	31	10	111	150	79
-5	32	10	164	114	29
-4	32	10	151	145	47
-3	32	10	121	101	77
-2	32	10	239	144	43
-4	33	10	394	399	18
-13	1	11	135	137	31
-12	1	11	0	73	1
-11	1	11	457	458	13
-10	1	11	448	442	12
-9	1	11	144	107	41
-8	1	11	157	147	23
-7	1	11	445	455	12
-6	1	11	69	52	68
-2	5	11	303	306	14
-1	5	11	80	58	31
0	5	11	365	348	13
1	5	11	55	135	55
2	5	11	0	32	1
3	5	11	79	80	57
4	5	11	0	22	1
-13	6	11	355	368	13
-12	6	11	373	357	13
-11	6	11	56	87	56
-10	6	11	111	143	26
-9	6	11	332	330	14
-8	6	11	828	826	13
-7	6	11	359	363	17
-4	10	11	0	62	1
-3	10	11	35	72	35
-2	10	11	105	93	25
-1	10	11	339	358	10
0	10	11	145	120	15
1	10	11	106	129	22
2	10	11	49	63	49
3	10	11	162	177	19
4	10	11	49	130	49
-13	11	11	154	113	24
-12	11	11	0	47	1
-11	11	11	270	248	13
-10	11	11	489	496	12
-9	11	11	357	368	17
-3	15	11	391	406	12
-2	15	11	591	587	11
-1	15	11	0	39	1
0	15	11	101	36	33
1	15	11	0	44	1
2	15	11	299	303	11
3	15	11	8	127	7
-12	16	11	226	245	16
-11	16	11	287	283	16
-10	16	11	118	115	36
-9	16	11	472	478	13
-8	16	11	527	515	17
-7	16	11	198	180	36
-6	16	11	258	249	15

Table D.6. Observed and calculated structure factors for Rutdp

h	k	l	10Fo	10Fc	10s
-5	16	11	410	412	12
-4	16	11	627	620	14
-3	16	11	21	57	21
-2	16	11	85	48	49
-1	16	11	403	397	14
0	16	11	648	651	10
1	16	11	396	368	11
2	16	11	260	240	15
3	16	11	323	354	17
-12	17	11	162	198	29
-11	17	11	321	313	15
-10	17	11	425	409	13
-9	17	11	147	207	47
-8	17	11	352	349	22
-7	17	11	769	767	12
-6	17	11	497	487	29
-5	17	11	167	127	20
-4	17	11	316	318	14
-3	17	11	562	551	11
-2	17	11	493	480	13
-1	17	11	279	280	13
0	17	11	97	68	34
1	17	11	468	483	11
2	17	11	556	575	11
3	17	11	377	374	20
-12	18	11	96	149	54
-11	18	11	0	27	1
-10	18	11	119	99	36
-9	18	11	409	402	14
-8	18	11	607	613	12
-7	18	11	312	316	15
-6	22	11	140	128	39
-5	22	11	631	601	17
-4	22	11	569	538	12
-3	22	11	54	19	53
-2	22	11	145	108	39
-1	22	11	298	292	16
0	22	11	500	483	10
1	22	11	305	327	21
2	22	11	216	195	27
-10	23	11	367	363	22
-9	23	11	315	312	48
-8	23	11	0	78	1
-7	23	11	525	513	18
-6	23	11	259	220	23
-5	23	11	113	89	55
-4	23	11	58	52	57
-3	23	11	51	106	50
-2	23	11	240	230	18
-1	23	11	64	9	64
0	23	11	162	184	23
1	23	11	0	14	1
-10	24	11	131	125	56
-9	24	11	126	152	75
-8	24	11	135	136	54
-7	24	11	0	87	1
-6	24	11	137	96	44
-5	24	11	143	120	40
-4	24	11	185	171	22
-3	24	11	174	131	25
-2	24	11	104	33	43
-1	24	11	100	68	64
-1	0	12	661	645	25
0	0	12	27	87	27
1	0	12	300	360	22
2	0	12	441	451	19
3	0	12	355	378	25
-13	1	12	229	240	16
-12	1	12	410	388	16
-11	1	12	426	419	13
-10	1	12	195	180	21
-9	1	12	518	527	12
-8	1	12	429	430	14
-7	1	12	205	191	18
-6	1	12	220	216	17
-5	1	12	122	98	29
-4	1	12	569	549	11
-3	1	12	256	249	16
-2	1	12	69	89	42
-1	1	12	236	243	11
0	1	12	592	605	8
1	1	12	328	301	12
2	1	12	8	116	7
3	1	12	86	125	85
-13	2	12	205	196	33
-12	2	12	70	67	70
-11	2	12	0	81	1
-10	2	12	75	27	75
-9	2	12	197	201	19
-8	2	12	84	102	83
-7	2	12	87	9	46
-6	2	12	0	84	1
-5	2	12	79	94	52
2	5	12	155	140	33
3	5	12	265	280	19
-13	6	12	446	428	12
-12	6	12	53	55	52
-11	6	12	527	540	13
-10	6	12	248	252	29
-9	6	12	298	274	16
-8	6	12	65	85	65
-7	6	12	152	147	24
-6	6	12	236	216	18
-5	6	12	497	477	12
-4	6	12	0	38	1
-3	6	12	381	373	10
-2	6	12	532	524	8
-1	6	12	434	434	9
0	6	12	59	6	58
1	6	12	237	242	15
2	6	12	283	299	14
3	6	12	62	72	61
-13	7	12	67	46	66
-12	7	12	60	98	59
-11	7	12	115	114	36
-10	7	12	0	56	1
-9	7	12	72	80	72
-8	7	12	0	31	-1
-7	7	12	488	489	12
-6	7	12	0	14	-1
-5	7	12	138	58	26
-4	7	12	137	148	23
-3	7	12	77	77	76
-2	7	12	97	62	30
-9	11	12	296	315	16
-8	11	12	512	515	14
-7	11	12	210	215	20
-6	11	12	52	38	51
-5	11	12	225	211	25
-4	11	12	362	340	24
-3	11	12	405	383	13
-2	11	12	0	59	1
-1	11	12	314	324	10
0	11	12	138	143	20
1	11	12	50	51	50
2	11	12	145	143	20
-12	12	12	0	5	-1
-11	12	12	0	56	1
-10	12	12	104	75	43
-9	12	12	147	154	25
-8	12	12	48	56	48
-7	12	12	296	264	19
-6	12	12	0	67	1
-5	12	12	158	154	23
-4	12	12	205	203	25
-3	12	12	127	63	92
-2	12	12	81	120	81
-1	12	12	0	32	1
0	12	12	97	94	30
1	12	12	136	106	20
2	12	12	45	91	45
-12	13	12	215	212	24
-11	13	12	205	190	22
-10	13	12	83	45	61
-9	13	12	405	399	16

-6	18	11	411	400	12	0	24	11	116	136	33	-4	2	12	194	184	19	-1	7	12	98	94	24	-8	13	12	353	316	21
-5	18	11	289	293	21	1	24	11	0	15	1	-3	2	12	127	115	45	0	7	12	180	210	17	-7	13	12	194	182	21
-4	18	11	427	429	18	-9	25	11	241	227	27	-2	2	12	182	189	13	1	7	12	80	3	79	-6	13	12	322	331	14
-3	18	11	84	45	56	-8	25	11	229	193	31	-1	2	12	52	49	51	2	7	12	104	58	24	-5	13	12	299	314	29
-2	18	11	169	138	24	-7	25	11	292	279	22	0	2	12	160	134	21	3	7	12	60	53	59	-4	13	12	352	355	13
-1	18	11	168	155	18	-6	25	11	291	305	23	1	2	12	105	37	47	-13	8	12	111	88	46	-3	13	12	191	147	29
0	18	11	451	444	13	-5	25	11	233	231	25	2	2	12	143	98	30	-12	8	12	0	35	-1	-2	13	12	0	68	1
1	18	11	292	269	14	-4	25	11	152	116	29	3	2	12	63	84	63	-11	8	12	163	168	26	-1	13	12	274	270	31
2	18	11	285	282	18	-3	25	11	165	183	41	-13	3	12	80	110	57	-10	8	12	319	338	14	0	13	12	244	254	13
3	18	11	206	234	24	-2	25	11	374	361	15	-12	3	12	0	60	1	-9	8	12	199	177	21	1	13	12	328	324	11
-11	19	11	204	206	21	-1	25	11	277	265	18	-11	3	12	78	79	48	-8	8	12	0	58	1	2	13	12	125	149	24
-10	19	11	148	171	28	0	25	11	0	71	1	-10	3	12	118	146	34	-7	8	12	140	74	27	-12	14	12	0	76	-1
-9	19	11	174	180	24	-9	26	11	408	431	21	-9	3	12	124	114	85	-6	8	12	511	505	12	-11	14	12	388	401	14
-8	19	11	246	234	24	-8	26	11	583	579	19	-8	3	12	120	122	33	-5	8	12	272	303	14	-10	14	12	412	435	13
-7	19	11	177	165	53	-7	26	11	160	161	36	-7	3	12	328	338	14	-4	8	12	359	356	25	-9	14	12	423	416	13
-6	19	11	0	3	1	-6	26	11	333	291	22	-6	3	12	67	8	67	-3	8	12	185	173	17	-8	14	12	119	116	32
-5	19	11	105	67	57	-5	26	11	344	351	15	-5	3	12	394	385	13	-2	8	12	61	51	61	-7	14	12	381	394	13
-4	19	11	181	130	21	-4	26	11	277	288	25	-4	3	12	313	294	13	-1	8	12	261	249	9	-6	14	12	376	378	13
-3	19	11	139	123	25	-3	26	11	261	272	17	-3	3	12	0	31	1	0	8	12	204	219	13	-5	14	12	382	384	13
-2	19	11	153	110	26	-2	26	11	86	5	85	-2	3	12	95	104	26	1	8	12	170	114	15	-4	14	12	171	115	35
-1	19	11	123	134	34	-1	26	11	389	395	15	-1	3	12	107	72	24	2	8	12	146	145	18	-3	14	12	479	472	12
0	19	11	176	173	27	0	26	11	416	432	12	0	3	12	286	293	17	3	8	12	96	91	77	-2	14	12	665	657	12
1	19	11	156	137	23	-7	27	11	350	341	22	1	3	12	167	152	19	-12	9	12	527	538	11	-1	14	12	497	474	12
2	19	11	112	147	49	-6	27	11	340	305	23	2	3	12	132	100	64	-11	9	12	254	239	18	0	14	12	43	42	43
-11	20	11	144	154	47	-5	27	11	325	270	20	3	3	12	0	29	1	-10	9	12	119	124	38	1	14	12	302	300	11
-10	20	11	64	43	63	-4	27	11	208	223	78	-13	4	12	0	35	1	-9	9	12	381	385	14	2	14	12	299	296	14
-9	20	11	305	299	16	-3	27	11	334	325	15	-12	4	12	0	19	1	-8	9	12	560	553	12	-11	15	12	204	199	23
-8	20	11	276	299	16	-2	27	11	357	364	15	-11	4	12	392	429	11	-7	9	12	429	430	12	-10	15	12	122	140	57
-7	20	11	0	31	1	-1	27	11	400	396	15	-10	4	12	570	568	12	-6	9	12	310	311	14	-9	15	12	218	213	19
-6	20	11	110	28	36	-7	28	11	144	99	46	-9	4	12	341	359	14	-5	9	12	343	326	14	-8	15	12	430	428	21
-5	20	11	198	161	29	-6	28	11	159	120	43	-8	4	12	127	107	30	-4	9	12	280	264	16	-7	15	12	296	287	15
-4	20	11	331	328	15	-5	28	11	376	389	14	-7	4	12	271	266	15	-3	9	12	518	489	13	-6	15	12	0	16	1
-3	20	11	96	101	44	-4	28	11	164	166	45	-6	4	12	661	653	12	-2	9	12	176	184	17	-5	15	12	483	478	12
-2	20	11	0	11	1	-3	28	11	53	57	52	-5	4	12	570	567	15	-1	9	12	417	429	8	-4	15	12	171	175	36
-1	20	11	224	219	34	-2	28	11	92	78	92	-4	4	12	0	5	1	0	9	12	432	425	8	-3	15	12	676	674	12
0	20	11	277	283	14	-1	28	11	167	145	50	-3	4	12	423	421	15	1	9	12	110	135	23	-2	15	12	146	105	28
1	20	11	66	58	66	-7	29	11	125	87	48	-2	4	12	518	518	9	2	9	12	148	161	19	-1	15	12	306	246	16
2	20	11	131	114	60	-6	29	11	175	209	36	-1	4	12	282	267	12	3	9	12	146	169	23	0	15	12	418	413	11
-11	21	11	292	335	28	-5	29	11	118	73	45	0	4	12	195	191	17	-12	10	12	185	175	24	1	15	12	308	324	12
-10	21	11	285	307	22	-4	29	11	100	72	48	1	4	12	235	218	15	-11	10	12	251	263	18	2	15	12	100	125	35
-9	21	11	291	267	15	-3	29	11	83	8	82	2	4	12	496	489	13	-10	10	12	646	625	13	-11	16	12	66	90	66
-8	21	11	253	273	17	-2	29	11	128	83	38	3	4	12	356	368	16	-9	10	12	355	368	14	-10	16	12	280	310	22
-7	21	11	697	698	12	-6	30	11	67	4	67	-13	5	12	217	236	18	-8	10	12	76	103	76	-9	16	12	133	29	43
-6	21	11	444	430	19	-5	30	11	166	231	26	-12	5	12	357	369	12	-7	10	12	354	337	13	-8	16	12	178	182	22
-5	21	11	379	351	21	-4	30	11	342	317	16	-11	5	12	341	334	15	-6	10	12	251	222	24	-7	16	12	215	258	17
-4	21	11	0	5	1	-3	30	11	115	139	49	-10	5	12	180	168	22	-5	10	12	738	731	12	-6	16	12	0	48	1
-3	21	11	326	302	14	-13	0	12	345	336	23	-9	5	12	442	426	13	-4	10	12	353	357	13	-5	16	12	429	395	19
-2	21	11	409	403	13	-12	0	12	114	80	68	-8	5	12	658	675	17	-3	10	12	505	501	9	-4	16	12	217	238	26
-1	21	11	157	143	25	-11	0	12	601	613	19	-7	5	12	417	410	14	-2	10	12	685	706	12	-3	16	12	251	256	17
0	21	11	42	10	41	-10	0	12	403	391	19	-6	5	12	40	11	39	-1	10	12	505	509	7	-2	16	12	25	9	25

1	21	11	260	227	24	-9	0	12	641	635	18	-5	5	12	517	517	12	0	10	12	200	180	16	-1	16	12	189	157	23
2	21	11	631	635	13	-8	0	12	110	28	57	-4	5	12	878	864	13	1	10	12	176	169	15	0	16	12	170	191	34
-11	22	11	307	313	27	-6	0	12	431	416	18	-3	5	12	403	401	9	2	10	12	399	395	9	1	16	12	288	293	14
-10	22	11	103	154	89	-5	0	12	543	560	16	-2	5	12	118	147	19	3	10	12	0	72	1	2	16	12	422	433	12
-9	22	11	501	492	20	-4	0	12	115	45	49	-1	5	12	441	443	9	-12	11	12	225	186	22	-11	17	12	120	138	40
-8	22	11	405	416	13	-3	0	12	372	386	18	0	5	12	632	640	12	-11	11	12	352	356	14	-10	17	12	25	19	25
-7	22	11	224	207	19	-2	0	12	737	721	11	1	5	12	543	529	10	-10	11	12	115	81	41	-9	17	12	0	109	1

Table D.6. Observed and calculated structure factors for Rutdp

h	k	1	10Fo	10Fc	10s	h	k	1	10Fo	10Fc	10s	h	k	1	10Fo	10Fc	10s	h	k	1	10Fo	10Fc	10s	h	k	1	10Fo	10Fc	10s
-8	17	12	136	167	35	-5	25	12	152	149	42	-8	6	13	302	275	15	-1	12	13	366	362	23	-5	21	13	269	254	27
-7	17	12	285	311	19	-4	25	12	426	414	14	-7	6	13	698	706	12	0	12	13	234	246	14	-4	21	13	210	171	33
-6	17	12	163	165	25	-3	25	12	152	142	31	-6	6	13	307	311	14	1	12	13	294	286	12	-3	21	13	113	64	112
-5	17	12	0	54	1	-2	25	12	126	71	37	-5	6	13	207	212	25	-11	13	13	72	87	72	-2	21	13	365	345	24
-4	17	12	94	43	68	-7	26	12	45	137	44	-4	6	13	258	245	17	-10	13	13	242	278	19	-7	22	13	448	409	20
-3	17	12	0	21	1	-6	26	12	203	229	30	-3	6	13	440	442	12	-9	13	13	631	625	13	-6	22	13	130	173	48
-2	17	12	68	19	68	-5	26	12	95	76	95	-2	6	13	381	381	18	-8	13	13	67	88	66	-5	22	13	0	124	1
-1	17	12	0	43	1	-4	26	12	69	79	69	-1	6	13	109	101	32	-7	13	13	418	412	13	-4	22	13	461	486	20
0	17	12	201	192	18	-3	26	12	243	226	22	0	6	13	224	215	16	-6	13	13	270	260	15	-3	22	13	369	367	23
1	17	12	0	63	-1	-6	27	12	95	44	95	1	6	13	240	233	17	-5	13	13	398	403	15	-6	23	13	371	385	21
-11	18	12	260	214	45	-5	27	12	39	10	39	-12	7	13	101	108	52	-4	13	13	221	185	28	-5	23	13	113	126	62
-10	18	12	278	296	18	-4	27	12	219	224	22	-11	7	13	59	39	59	-3	13	13	279	239	25	-4	23	13	164	176	41
-9	18	12	150	57	55	-12	1	13	85	113	84	-10	7	13	475	487	13	-2	13	13	375	387	14	-11	0	14	122	36	59
-8	18	12	179	191	23	-11	1	13	40	10	39	-9	7	13	708	724	13	-1	13	13	118	128	37	-10	0	14	432	463	20
-7	18	12	178	164	23	-10	1	13	304	288	16	-8	7	13	67	56	66	0	13	13	195	181	17	-9	0	14	465	452	19
-6	18	12	397	381	13	-9	1	13	358	352	14	-7	7	13	203	181	20	-11	14	13	122	86	36	-8	0	14	378	395	21
-5	18	12	141	88	44	-8	1	13	228	218	30	-6	7	13	418	444	13	-10	14	13	37	56	36	-7	0	14	285	257	23
-4	18	12	103	76	63	-7	1	13	127	107	82	-5	7	13	773	785	13	-9	14	13	125	80	31	-6	0	14	189	184	33
-3	18	12	365	362	14	-6	1	13	252	236	18	-4	7	13	507	520	16	-8	14	13	54	118	54	-5	0	14	487	446	19
-2	18	12	686	662	12	-5	1	13	162	161	24	-3	7	13	289	249	31	-7	14	13	246	252	52	-4	0	14	162	17	37
-1	18	12	247	228	21	-4	1	13	329	330	14	-2	7	13	559	545	12	-6	14	13	153	130	24	-3	0	14	146	11	39
0	18	12	0	20	1	-3	1	13	45	44	45	-1	7	13	410	420	20	-5	14	13	148	76	44	-2	0	14	0	41	1
1	18	12	146	83	26	-2	1	13	475	471	8	0	7	13	265	254	11	-4	14	13	157	149	40	-1	0	14	435	432	14
-11	19	12	391	411	18	-1	1	13	448	473	9	1	7	13	118	108	24	-3	14	13	264	256	26	0	0	14	388	390	21
-10	19	12	120	140	39	0	1	13	137	120	36	-12	8	13	397	420	22	-2	14	13	154	110	28	-11	1	14	359	366	16
-9	19	12	536	535	27	1	1	13	79	63	78	-11	8	13	219	229	20	-1	14	13	116	131	73	-10	1	14	470	472	15
-8	19	12	469	458	23	2	1	13	164	119	56	-10	8	13	154	172	28	0	14	13	134	119	33	-9	1	14	153	142	27
-7	19	12	45	120	45	-12	2	13	403	411	15	-9	8	13	176	169	22	-10	15	13	281	284	18	-8	1	14	435	437	14
-6	19	12	234	250	29	-11	2	13	477	479	14	-8	8	13	507	503	25	-9	15	13	307	320	19	-7	1	14	435	442	22
-5	19	12	601	583	18	-10	2	13	317	337	15	-7	8	13	484	479	13	-8	15	13	267	289	17	-6	1	14	225	270	19
-4	19	12	750	745	12	-9	2	13	138	141	29	-6	8	13	241	252	17	-7	15	13	127	108	32	-5	1	14	93	23	92
-3	19	12	334	311	15	-8	2	13	503	513	13	-5	8	13	128	27	29	-6	15	13	256	248	18	-4	1	14	334	301	15
-2	19	12	91	48	53	-7	2	13	300	303	15	-4	8	13	567	582	12	-4	15	13	216	182	27	-3	1	14	488	498	13
-1	19	12	197	201	22	-6	2	13	337	324	15	-3	8	13	515	517	12	-3	15	13	182	140	24	-2	1	14	155	128	25
0	19	12	459	468	11	-5	2	13	115	75	33	-2	8	13	204	202	32	-2	15	13	385	391	15	-1	1	14	126	114	41
1	19	12	360	364	14	-4	2	13	499	489	12	-1	8	13	335	332	12	-1	15	13	393	408	15	0	1	14	0	69	1
-10	20	12	98	71	62	-3	2	13	580	561	12	0	8	13	290	330	11	0	15	13	153	122	30	-11	2	14	0	53	1
-9	20	12	270	236	17	-2	2	13	311	316	16	1	8	13	223	225	13	-10	16	13	301	294	16	-10	2	14	85	106	84

```
 -8 20 12   123   100   33
 -7 20 12   404   414   14
 -6 20 12   533   527   18
 -5 20 12   188   193   27
 -4 20 12    75    20   75
 -3 20 12   189   213   34
 -2 20 12   596   596   13
 -1 20 12   294   302   17
  0 20 12   118   102   33
-10 21 12     0    34    1
 -9 21 12   123   140   34
 -8 21 12   190   187   22
 -7 21 12     0    75    1
 -6 21 12   183   118   34
 -5 21 12   415   432   19
 -4 21 12     0    14    1
 -3 21 12   117    69   38
 -2 21 12    54    36   53
 -1 21 12   150   131   35
  0 21 12   211   210   20
 -9 22 12     0    30    1
 -8 22 12    93   135   92
 -7 22 12    29    18   29
 -6 22 12   249   259   27
 -5 22 12   201   189   30
 -4 22 12    41    94   41
 -3 22 12    48    74   48
 -2 22 12    46    25   46
 -1 22 12    76   104   76
  0 22 12   118    52   77
 -9 23 12   228   273   43
 -8 23 12   443   436   21
 -7 23 12   312   306   25
 -6 23 12     0    31    1
 -5 23 12   397   397   20
 -4 23 12   400   400   26
 -3 23 12   359   359   15
 -2 23 12   320   297   16
 -1 23 12   129   117   37
 -8 24 12   206   193   35
 -7 24 12   317   323   22
 -6 24 12   425   440   20
 -5 24 12   374   385   20
 -4 24 12   179   193   25
 -3 24 12   201   172   74
 -2 24 12   603   595   16
 -1 24 12   195   226   37
 -8 25 12   205   248   37
 -7 25 12   151    81   42
 -6 25 12   299   247   24

 -1  2 13     0    48    1
  0  2 13   366   375   12
  1  2 13   463   488   14
  2  2 13     0    93    1
-12  3 13   230   199   20
-11  3 13   406   386   14
-10  3 13   558   561   13
 -9  3 13   316   332   15
 -8  3 13   300   279   37
 -7  3 13   202   172   23
 -6  3 13   410   400   13
 -5  3 13   282   289   15
 -4  3 13   151   133   71
 -3  3 13   408   421   14
 -2  3 13   472   473   12
 -1  3 13   438   447   11
  0  3 13   280   291   14
  1  3 13   149   155   25
-12  4 13   371   361   23
-11  4 13   176   216   25
-10  4 13    30    89   30
 -9  4 13   165   173   25
 -8  4 13   270   271   22
 -7  4 13   103    41   36
 -6  4 13   114    54   37
 -5  4 13    85    11   52
 -4  4 13   147   123   52
 -3  4 13   386   411   13
 -2  4 13   199   199   32
 -1  4 13     0    64    1
  0  4 13   173   160   20
  1  4 13   330   343   12
-12  5 13     0     7    1
-11  5 13     0    13    1
-10  5 13   165   191   41
 -9  5 13    98    43   63
 -8  5 13    94    95   48
 -7  5 13   189   164   21
 -6  5 13   272   268   17
 -5  5 13   245   241   18
 -4  5 13    49    63   48
 -3  5 13    94   107   42
 -2  5 13   137   138   35
 -1  5 13     0    20    1
  0  5 13    52    73   52
  1  5 13    50   110   50
-12  6 13   377   375   20
-11  6 13   308   330   17
-10  6 13    55    61   54
 -9  6 13   138   149   28

-12  9 13   109   162   86
-11  9 13   232   227   34
-10  9 13   237   225   18
 -9  9 13    43   131   42
 -8  9 13   136   122   30
 -7  9 13   321   316   14
 -6  9 13   147   150   52
 -5  9 13   394   413   13
 -4  9 13   218   210   23
 -3  9 13     0    56    1
 -2  9 13   176   155   23
 -1  9 13   129   113   25
  0  9 13    66    83   66
  1  9 13     0    22    1
-11 10 13    50    31   50
-10 10 13     0     7    1
 -9 10 13    80    41   80
 -8 10 13   157   151   25
 -7 10 13   204   231   30
 -6 10 13    67    67   67
 -5 10 13   224   221   19
 -4 10 13   157   126   25
 -3 10 13    94    59   94
 -2 10 13   129   135   30
 -1 10 13    67    20   67
  0 10 13     0    92    1
  1 10 13     0     7    1
-11 11 13   234   259   20
-10 11 13   455   460   13
 -9 11 13   388   399   14
 -8 11 13   194   243   21
 -7 11 13    61    83   60
 -6 11 13   320   301   20
 -5 11 13   483   485   13
 -4 11 13    46    83   46
 -3 11 13   125   125   44
 -2 11 13   220   228   21
 -1 11 13   515   512   13
  0 11 13   208   236   16
  1 11 13   108    74   29
-11 12 13   405   392   15
-10 12 13   104   149   44
 -9 12 13   208   245   24
 -8 12 13   333   309   14
 -7 12 13   635   617   12
 -6 12 13     0    66    1
 -5 12 13   116    95   46
 -4 12 13   409   397   20
 -3 12 13   750   753   18
 -2 12 13   390   394   14

 -9 16 13   177   159   25
 -8 16 13   167   161   25
 -7 16 13   498   490   12
 -6 16 13    98   105   41
 -5 16 13   228   177   28
 -4 16 13   490   505   19
 -3 16 13   629   614   12
 -2 16 13   141    97   32
 -1 16 13   210   203   22
  0 16 13   172   164   47
-10 17 13   415   421   15
 -9 17 13   368   366   15
 -8 17 13   188   200   46
 -7 17 13    52    97   51
 -6 17 13   607   585   19
 -5 17 13   476   460   19
 -4 17 13     0    36    1
 -3 17 13   278   295   18
 -2 17 13   359   361   15
 -1 17 13   357   327   24
-10 18 13   125   152   52
 -9 18 13   176   169   26
 -8 18 13    72    60   72
 -7 18 13   488   512   13
 -6 18 13   166   178   36
 -5 18 13     0    82    1
 -4 18 13   392   389   21
 -3 18 13   369   385   15
 -2 18 13    74   100   74
 -1 18 13    98   116   98
 -9 19 13   122    27   36
 -8 19 13   189   196   42
 -7 19 13     0    48    1
 -6 19 13   216   164   32
 -5 19 13   124    12   54
 -4 19 13   140    76   43
 -3 19 13   145   135   31
 -2 19 13    41    37   40
 -1 19 13     0    57    1
 -9 20 13     0    23    1
 -8 20 13     0    68    1
 -7 20 13   174   211   39
 -6 20 13   166   154   38
 -5 20 13   212   209   33
 -4 20 13   357   326   22
 -3 20 13   220   238   23
 -2 20 13   170   158   28
 -8 21 13   283   297   26
 -7 21 13   172   191   38
 -6 21 13   466   447   20

 -9  2 14     0    23    1
 -8  2 14   223   217   20
 -7  2 14   113    11   37
 -6  2 14   212   209   19
 -5  2 14     0     8    1
 -4  2 14   113     3   56
 -3  2 14   119    83   32
 -2  2 14   204   212   19
 -1  2 14   174   222   24
  0  2 14    79    29   79
-11  3 14     0    96    1
-10  3 14   131   155   34
 -9  3 14    27    67   27
 -8  3 14   213   220   19
 -7  3 14   245   256   18
 -6  3 14   276   285   17
 -5  3 14     0    15   -1
 -4  3 14   440   432   13
 -3  3 14   502   496   13
 -2  3 14   186   172   22
 -1  3 14   114    43   38
  0  3 14   191   181   20
-11  4 14   100    73   57
-10  4 14   289   268   23
 -9  4 14   617   611   13
 -8  4 14   418   442   14
 -7  4 14    88    74   58
 -6  4 14   320   313   15
 -5  4 14   531   556   13
 -4  4 14   421   422   13
 -3  4 14     0     7    1
 -2  4 14   353   338   22
 -1  4 14   297   299   17
-11  5 14   438   458   15
-10  5 14   286   305   17
 -9  5 14   104    60   45
 -8  5 14   310   314   16
 -7  5 14   415   418   14
 -6  5 14   423   415   17
 -5  5 14   108    68   40
 -4  5 14   431   423   14
 -3  5 14   521   536   13
 -2  5 14   268   262   25
 -1  5 14   137   141   32
-11  6 14   102    10  101
-10  6 14   295   271   18
 -9  6 14   259   266   32
 -8  6 14    64    63   63
 -7  6 14   108    17   42
 -6  6 14   201   188   21
```

Table 0.6. Observed and calculated structure factors for Rutdp

h	k	1	10Fo	10Fc	10s	h	k	1	10Fo	10Fc	10s	h	k	1	10Fo	10Fc	10s	h	k	1	10Fo	10Fc	10s	h	k	1	10Fo	10Fc	10s
-5	6	14	424	433	14	-6	9	14	377	389	15	-5	12	14	153	178	43	-4	16	14	215	184	30	-7	4	15	90	113	62
-4	6	14	457	445	13	-5	9	14	0	49	1	-4	12	14	107	124	67	-7	17	14	222	201	32	-6	4	15	137	69	31
-3	6	14	190	131	34	-4	9	14	306	311	22	-3	12	14	102	62	102	-6	17	14	89	53	89	-5	4	15	66	39	66
-2	6	14	108	202	59	-3	9	14	345	398	21	-2	12	14	0	37	1	-5	17	14	184	201	36	-4	4	15	159	146	27
-1	6	14	377	374	15	-2	9	14	217	256	32	-9	13	14	208	248	52	-4	17	14	120	132	65	-3	4	15	110	136	70
-11	7	14	154	170	49	-1	9	14	80	86	79	-8	13	14	183	160	26	-7	18	14	33	35	32	-8	5	15	112	13	45
-10	7	14	112	166	42	-10	10	14	104	105	43	-7	13	14	211	203	21	-6	18	14	377	356	24	-7	5	15	139	108	31
-9	7	14	39	40	39	-9	10	14	430	437	14	-6	13	14	0	52	1	-9	1	15	220	233	22	-6	5	15	279	241	18
-8	7	14	175	183	43	-8	10	14	175	203	24	-5	13	14	139	105	45	-8	1	15	234	190	23	-5	5	15	91	53	59
-7	7	14	169	142	24	-7	10	14	144	163	29	-4	13	14	237	186	28	-7	1	15	261	245	23	-4	5	15	260	255	18
-6	7	14	202	190	20	-6	10	14	253	268	18	-3	13	14	308	279	25	-6	1	15	208	207	20	-8	6	15	125	96	35
-5	7	14	173	149	25	-5	10	14	525	533	16	-2	13	14	136	124	34	-5	1	15	290	302	18	-7	6	15	337	311	50
-4	7	14	49	70	48	-4	10	14	655	634	19	-9	14	14	363	348	16	-4	1	15	101	11	47	-6	6	15	440	430	14
-3	7	14	281	221	27	-3	10	14	160	96	40	-8	14	14	169	179	47	-3	1	15	103	58	48	-5	6	15	180	173	32
-2	7	14	90	14	89	-2	10	14	183	198	33	-7	14	14	54	63	54	-9	2	15	50	67	50	-4	6	15	0	52	1
-1	7	14	0	15	1	-1	10	14	360	367	16	-6	14	14	309	293	25	-8	2	15	236	216	21	-8	7	15	476	477	14
-10	8	14	191	244	25	-10	11	14	0	25	1	-5	14	14	482	455	20	-7	2	15	322	347	19	-7	7	15	205	171	24
-9	8	14	257	249	19	-9	11	14	232	206	21	-4	14	14	412	398	21	-6	2	15	363	329	15	-6	7	15	312	303	30
-8	8	14	112	136	39	-8	11	14	238	266	19	-3	14	14	111	96	66	-5	2	15	225	207	20	-5	7	15	488	484	26
-7	8	14	54	21	53	-7	11	14	261	294	26	-2	14	14	194	165	37	-4	2	15	153	150	26	-4	7	15	519	555	20
-6	8	14	174	118	25	-6	11	14	179	142	23	-9	15	14	0	46	1	-3	2	15	254	257	22	-8	8	15	158	58	42
-5	8	14	547	535	13	-5	11	14	25	13	25	-8	15	14	434	464	14	-9	3	15	367	356	23	-7	8	15	430	435	15
-4	8	14	270	267	17	-4	11	14	61	13	61	-7	15	14	238	242	36	-8	3	15	285	310	18	-6	8	15	521	530	13
-3	8	14	244	231	26	-3	11	14	253	264	28	-5	15	14	51	15	51	-7	3	15	345	348	16	-5	8	15	275	288	20
-2	8	14	140	89	42	-2	11	14	259	300	19	-4	15	14	207	249	34	-6	3	15	263	285	18	-4	8	15	0	18	1
-1	8	14	0	30	1	-10	12	14	160	57	28	-3	15	14	527	531	20	-5	3	15	301	320	16	-7	9	15	0	105	1
-10	9	14	269	255	32	-9	12	14	93	50	93	-8	16	14	221	239	23	-4	3	15	190	196	36	-6	9	15	236	199	20
-9	9	14	176	172	30	-8	12	14	125	113	34	-7	16	14	281	302	18	-3	3	15	320	361	23	-5	9	15	99	92	49
-8	9	14	414	413	32	-7	12	14	169	149	54	-6	16	14	87	33	86	-9	4	15	64	122	63	-7	10	15	120	135	71
-7	9	14	412	438	14	-6	12	14	137	117	31	-5	16	14	201	171	31	-8	4	15	153	122	29	-6	10	15	188	144	33

LIST OF REFERENCES

[1] Interrante, L. V.; Casper, L. A.; Ellis, A. B. Adv. Chem. Ser. **1995**, 245, Materials Chemistry.

[2] Abruña, H. D. in Electroresponsive Molecular and Polymeric Systems; Skotheim, T. A. (Ed.); Marcel Dekker: New York; 1988; vol. 1; p. 97.

[3] Natan, M. J.; Wrighton, M. S. Prog. Inorg. Chem. **1989**, 37, 391.

[4]Molecular Electronic Devices II; Carter, F. L. (Ed.); Marcel Dekker: New York; 1987.

[5] Bowden, M. J. Adv. Chem. Ser., **1988**, 218, 1.

[6] Moses, P. R.; Murray, R.W.; Anal. Chem., **1975**, 47, 1882.

[7] Murray, R. W. in Molecular Design of Electrode Surfaces; Murray, R. W. (Ed.); Wiley and Sons: New York; 1992, p. 1.

[8] Andrieux, C. P.; Savéant, J.-M. in Molecular Design of Electrode Surfaces; Murray, R. W. (Ed.); Wiley and Sons: New York; 1992, p. 207.

[9] Murray, R. W.; Ewing, A. G.; Durst, R. A.; Anal. Chem., **1987**, 59, 379A.

[10] Haussling, L.; Ringsdorf, H.; Schmitt, T. J.; Knoll, W. Langmuir, **1991**, 7, 1837.

[11] Elliot, C. M.; Schmittle, S. J.; Redepenning, J. G.; Balk, E. M. J. Macromol. Sci., Chem., **1988**, A25, 1215.

[12] Bell, C. M.; Yang, H. C.; Mallouk, T. E. Adv. Chem. Ser. **1995**, 245, 211.

[13] Blodgett, K. B.; Langmuir, I. Phys. Rev., **1937**, 51, 964.

[14] Kondo, T.; Yamada, H.; Nishiyama, K.; Suga, K.; Fujihira, M. Thin Solid Films, **1989**, 179, 463.

[15] Lane, R. F.; Hubbard, A. T. J. Phys. Chem., **1973**, 77, 1411.

[16] Anson, F. C.; Brown, A. P. J. Electroanal. Chem., **1978**, 92, 133.

[17] Meyer, T. J.; Meyer, G. J.; Pfennig, B. W.; Schoonover, J. R.; Timpson, C. J.; Wall, J. F.; Kobusch, C.; Chen, X.; Peek, B. M.; Wall, C. G.; Ou, W. Erickson, B. W.; Bignozzi, C. A. Inorg. Chem., **1994**, 33, 3952.

[18] Silane Coupling Agents, Pleuddeman, E. P. Plenum Press: New York, 1991.

[19] Lenhard, J. R.; Murray, R. W.; J. Am. Chem. Soc., **1978**, 100, 7870.

[20] Bain, C. D.; Whitesides, G. M. J. Am. Chem. Soc., **1989**, 111, 7164.

[21] Roszyani, L. F.; Wrighton, M. S. Langmuir, **1995**, 11, 3913.

[22] Li, D.; Ratner, M. A.; Marks, T. J.; Zhang, C. H.; Yang, J.; Wang, G. K. J. Am. Chem. Soc., **1990**, 112, 7389.

[23] Mallouk, T. E.; Lee, H.; Kepley, L. J.; Hong, H.-G.; J. Am. Chem. Soc., **1988**, 110, 618.

[24] Cao, G; Mallouk, T. E. Inorg. Chem., **1991**, 30, 1434.

[25] Kepley, L. J.; Sackett, D. D.; Bell, C. M.; Mallouk, T. E. Thin Solid Films, **1992**, 208, 132.

[26] Katz, H. E.; Scheller, G.; Putvinski, T. M.; Schilling, M. L.; Wilson, W. L.; Chidsey, C. E. D. Science, **1991**, 254, 1485.

[27] Greene, R. L.; Street, G. B. Science, **1984**, 226, 651.

[28] Chidsey, C. E. D.; Murray, R. W. J. Phys. Chem., **1986**, 90, 1479.

[29] Shigehara, K.; Oyama, N.; Anson, F. C. J. Am. Chem. Soc., **1981**, 103, 2552.

[30] Calvert, J. M.; Meyer, T. J. Inorg. Chem., **1981**, 20, 27.

[31] Merz, A.; Bard, A. J. J. Am. Chem. Soc., **1978**, 100, 3223.

[32] Oyama, N.; Anson, F. C. J. Electrochem. Soc., **1980**, 127, 247.

[33] Denisevich, P.; Abruña, H. D.; Leidner, C. R.; Meyer, T. J.; Murray, R. W. Inorg. Chem., **1982**, 21, 2153.

[34] Leidner, C. R.; Sullivan, B. P.; Reed, R. A.; White, B. A.; Crimmins, M. T.; Murray, R. W.; Meyer, T. J. Inorg. Chem., **1987**, 26, 882.

[35] Lewis, T. J.; White, H. S.; Wrighton, M. S. J. Am. Chem. Soc., **1984**, 106, 6947.

[36] Bettelheim, A.; White, B. A.; Raybuck, S. A.; Murray, R. W.; Inorg. Chem., **1987**, 26, 1009.

[37] Juris, A.; Balzani, V.; Barigelletti, F.; Campagna, S.; Belser, P.; Von Zelewsky, A. Coord. Chem. Rev., **1988**, 84, 85.

[38] Calvert, J. M.; Caspar, J. V.,; Binstead, R. A.; Westmoreland, T. D.; Meyer, T. J. J. Am. Chem. Soc., **1982**, 104, 6620.

[39] Introduction to Microlithography, Thompson, L. F.; Wilson, C. G.; Bowden, M. J. (Eds.); American Chemical Society: Washington, D.C., 1994, 2nd Edition.

[40] O'Toole, T. R.; Sullivan, B. P.; Meyer, T. J.; J. Am. Chem. Soc., **1989**, 111, 5699.

[41] Gould, S.; Gray, K. H.; Linton, R. W.; Meyer, T. J. Inorg. Chem., **1992**, 31, 5521.

[42] Leasure, R. M.; Moss, J. A.; Meyer, T. J. Inorg. Chem., **1994**, 33, 1247.

[43] Gould, S.; O'Toole, T. R.; Meyer, T. J. J. Am. Chem. Soc., **1990**, 112, 9490.

[44] VanHouten, J.; Watts, W. J.; Inorg. Chem., **1978**, 17, 3381.

[45] Durham, B.; Caspar, J. V.; Nagle, J. V.; Meyer, T. J. J. Am. Chem. Soc., **1982**, 104, 4803.

[46] Leasure, R. M.; Ou, W.; Moss, J. A.; Linton, R. W.; Meyer, T. J. Chem. Mater., **1996**, 8, 264.

[47] Wu, Y.; Pfennig, B. W.; Bocarsly, A.B.; Vicenzi, E. P. Inorg. Chem., **1995**, 34, 4262.

[48] Pfennig, B.W.; Bocarsly, A. B. J. Phys. Chem., **1992**, 96, 226.

[49] Bergstedt, T. S.; Hauser, B. T.; Schanze, K. S. J. Am. Chem. Soc., **1994**, 116, 8380.

[50] Bergstedt, T. S.; Hauser, B. T.; Schanze, K. S. Proc. Poly. Mat. Sci. Eng., **1995**, 72, 561.

[51] Tomlinson, W. J.; Chandross, E. A. Adv. in Photochem., **1980**, 12, 201.

[52] Jenkins, F. A.; White, H. E. Fundamentals of Optics; McGraw-Hill: New York, 1957.

[53] Nelson, K. A.; Casalegno. R.; Miller, R. J. D.; Fayer, M. D. J. Chem Phys., **1982**, 77, 1144.

[54] Prasad, P. N.; Williams, D. J. Introduction to Nonlinear Optical Effects in Molecules and Polymers; John Wiley and Sons: New York, 1991.

[55] Dagani, R. Chem. Eng. News, **1996**, 74, 22.

[56] Tachinaba, Y.; Sakurai, Y.; Yokoyama, M. Chem. Lett., **1994**, 1119.

[57] Miller, R. D.; Michl, J. Chem. Rev., **1989**, 89, 1359.

[58] West, R. J. Organomet. Chem., **1986**, 300, 327.

[59] Miller, R. D.; Hofer, D.; Fickes, G. N.; Willson, C. G.; Marinero, E.; Trefonas, P.; and West, R. Poly. Eng. Sci., **1986**, 26, 1129.

[60] Watanbe, A.; Ito, O. J. Phys. Chem., **1994**, 98, 7736.

[61] Calvert, J. M.; Schmehl, R. H.; Sullivan, B. P.; Facci, J. S.; Meyer, T. J.; Murray, R. W. Inorg. Chem., **1983**, 22, 2151.

[62] Hauser, B. T.; Schanze, K. S. unpublished results.

[63] Bard, A. J.; Faulkner, L. R. Electrochemical Methods; John Wiley and Sons: New York, 1980, p. 91.

[64] Gould, S.; Strouse, G. F.; Meyer, T. J.; Sullivan, B. P. Inorg. Chem., **1991**, 30, 2942.

[65] Bergstedt, T. Ph.D. Dissertation, University of Florida, 1996.

[66] Daum, P.; Murray, R. W. J. Phys. Chem., **1981**, 85, 389.

[67] Ellis, C. D.; Murphy, W. R.; Meyer, T. J. J. Am. Chem. Soc., **1981**, 103, 7480.

[68] Delahay, P. New Instrumental Methods in Electrochemistry; Interscience: New York, 1954, p.119.

[69] Daum, P.; Lenhard, J. R.; Rolison, D.; Murray, R. W. J. Am. Chem. Soc., **1980**, 102, 4649.

[70] Pickup, P. G.; Osteryoung, R. A. J. Electroanal. Chem., **1985**, 195, 271.

[71] Fayer, M. D. Ann. Rev. Phys. Chem., **1982**, 33, 63.

[72] Meerholz, K.; Volodin, B. L.; Sandalphon, B. K.; Peyghambarian, N. Nature, **1994**, 371, 497.

[73] Moerner, W. E.; Silence, S. M. Chem. Rev., **1994**, 94, 127.

[74] Zhang, J.; Carlen, C. C.; Palmer, S.; Sponsler, M. B. J. Am. Chem. Soc., **1994**, 116, 7055.

[75] Ghosh, P. K.; Spiro, T. G. J. Am. Chem. Soc., **1980**, 102, 5543.

[76] Abruña, H. D. Inorg. Chem., **1985**, 24, 987.

[77] Guarr, T. F.; Anson, F. C. J. Phys. Chem., **1987**, 91, 4037.

[78] Cznarik, A.W. Acc. Chem. Res., **1994**, 27, 302.

[79] Fabrizzi, L.; Poggi, A. Chem. Soc. Rev., **1995**, 24, 197.

[80] Meyer, T. J. Pure App. Chem., **1986**, 58, 1193.

[81] Kalyanasundaram, K. Photochemistry of Polypyridine and Porphyrin Complexes, Academic Press: London, 1991.

[82] Hartshorn, R. M.; Barton, J. K. J. Am. Chem. Soc., **1992**, 114, 5919.

[83] Pyle, A. M.; Barton, J. K. Prog. Inorg. Chem., **1990**, 38, 413.

[84] Turro, N. J.; Barton, J. K.; Tomalia, D. A. Acc. Chem. Res., **1991**, 24, 332.

[85] Xu, W; McDonough, R. C.; Langsdorf, B.; Demas, J. N.; DeGraff, B. A. Anal. Chem., **1994**, 66, 4133.

[86] Bacon, J. R.; Demas, J. N. Anal. Chem., **1987**, 59, 2780.

[87] Labelle, R. D.; Garvey, S. D. IEEE Bulletin, **1995**, 30.1.

[88] Kavandi, J.; Callis, J.; Gouterman, M; Khalil, G.; Wright, D.; Green, E.; Burns, D.; McLachlan, B. Rev. Sci. Instrum., **1990**, 61, 3340.

[89] Gallery, J.; Gouterman, M.; Callis, J.; Khalil, G.; McLachlan, B.; Bell, J. Rev. Sci. Instrum., **1994**, 65, 712.

[90] Hubner, J. P.; Carroll, B. F., unpublished results.

[91] Demas, J. N.; DeGraff, B. A. Anal. Chem., **1991**, 63, 829A.

[92] Caspar, J. V. Ph.D. Dissertation, University of North Carolina, Chapel Hill, **1982**.

[93] Crosby G. A. Acc. Chem. Res., **1975**, 8, 231.

[94] Allen, G. H.; White, R. P.; Rillema, D. P.; Meyer, T. J. J. Am. Chem. Soc., **1984**, 106, 2613.

[95] Klassen, D. M.; Crosby, G. A. J. Chem. Phys., **1968**, 48, 1853.

[96] Stone, M. L.; Crosby, G. A. Chem. Phys. Lett., **1981**, 79, 169.

[97] Agnew, S. F.; Stone, M. L.; Crosby, G. A. Chem. Phys. Lett., **1982**, 85, 57.

[98] Winkler, J. R.; Netzel, T. L.; Creutz, C.; Sutin, N. J. Am. Chem. Soc., **1987**, 109, 2381.

[99] Hecker, C. R.; Gushurst, A. K. I.; McMillin, Inorg. Chem., **1991**, 30, 538.

[100] Beley, M; Collin, J.-P.; Sauvage, J.-P.; Sugihara, H.; Heisel, F.; Miehe, A. J. Chem. Soc. Dalton Trans., **1991**, 3157.

[101] Berger, R. M.; McMillin, D. R.; Inorg. Chem., **1988**, 27, 4245.

[102] Maestri, M.; Armaroli, N.; Balzani, V.; Constable, E. C.; Cargill Thompson, A. M. W. Inorg. Chem., **1995**, 34, 2759.

[103] Collin, J.-P.; Beley, M.; Sauvage, J.-P.; Barigelletti, F. Inorg. Chim. Acta, **1991**, 186, 91.

[104] Adcock, P. A.; Keene, F. R.; Smythe, R. S.; Snow, M. R. Inorg. Chem., **1984**, 23, 2336.

[105] Thummel, R. P.; Jahng, Y. Inorg. Chem., **1986**, 25, 2527.

[106] Wickramashinghe, W. A.; Bird, P. H.; Serpone, N. Inorg. Chem., **1982**, 21, 2694.

[107] Beran, G.; Carty, A. J.; Patel, H. A.; Palenik, G. J. J. Chem. Soc. Dalton Trans., **1970**, 222.

[108] Einstein, F. W. B.; Penfold, B. R. Acta Crystallogr., **1966**, 20, 924.

[109] Einstein, F. W. B.; Penfold, B. R. J. Chem. Soc., **1968**, 3019.

[110] Trofimenko, S. Prog. Inorg. Chem., **1986**, 34, 115.

[111] Byers, P. K.; Canty, A. J.; Honeyman, R. T. J. Organomet. Chem., **1990**, 385, 417.

[112] Fajardo, M.; de la Hoz, A.; Diéz-Barra, E.; Jalón, F. A.; Otero, A.; Rodríguez, A; Tejeda, J.; Belletti, D.; Lanfranchi, M.; Pellinghelli, M. A. J. Chem. Soc. Dalton Trans., **1993**, 1935.

[113] Llobet, A.; Doppelt, P.; Meyer, T. J. Inorg. Chem., **1988**, 27, 514.

[114] Barqawi, K. R.; Llobet, A.; Meyer, T. J. J. Am. Chem. Soc., **1988**, 110.

[115] Jones, W. E.; Bignozzi, C. A.; Chen, P.; Meyer, T. J. Inorg. Chem., **1993**, 32, 1167.

[116] Wacholtz, W. F.; Auerbach, R. A.; Schmehl, R. H. Inorg. Chem., **1986**, 25, 227.

[117] Young, R. C.; Nagle, J. K.; Meyer, T. J.; Whitten, D. G. J. Am. Chem. Soc., **1978**, 100, 4773.

[118] Crosby, G. A. Acc. Chem. Res., **1975**, 8, 231.

[119] Caspar, J. V.; Meyer, T. J. Inorg. Chem., **1983**, 22, 2444.

[120] Wrighton, M.; Morse, D. L. J. Am. Chem. Soc., **1974**, 96, 998.

[121] Braddock, J. N.; Meyer, T. J. J. Am. Chem. Soc., **1973**, 95, 3158.

[122] Leising, R. A.; Kubow, S. A.; Churchill, M. R.; Buttrey, L. A.; Ziller, J. W.; Takeuchi, K. J. Inorg. Chem., **1990**, 29, 1306.

[123] Gupta, N.; Grover, N.; Neyhart, G. A.; Singh, P.; Thorp, H. H. Inorg. Chem., **1993**, 32, 310.

[124] Sheldrick, G. M. SHELXTL5, **1995**, Siemens Analytical Instrumentation, Madison, Wisconsin.

[125] O'Connor, D. V.; Phillips, D. Time-Correlated Single Photon Counting; Academic Press: Orlando, 1984.

BIOGRAPHICAL SKETCH

Brian Timothy Hauser was born June 4, 1969 at Chester County Hospital in West Chester, PA, a suburb of Philadelphia. He and his older sister Lauren, who started to teach him to read at age 4, are the only two children born to William and Patricia Hauser. His father, a Lutheran minister, served several congregations, moving the family from West Chester to Akron, OH and finally to Pittsburgh, PA, in 1977, where his family still resides. As a child, Brian did well in school, graduating from Penn Hills High School in 1987 as one of eleven valedictorians. At age 6, Brian clamored to play the drums and after much searching, his mother finally found an instructor who didn't feel he was too young. Playing the drums would become a great love of Brian's through high school and college, and even to the present. After graduating from high school, Brian enrolled at the University of Richmond, Virginia, and because of his interest in the sciences, decided to major in chemistry. After a disappointing fall academic semester his sophomore year, he began to get back on track with the help of chemistry professor Dr. Raymond Dominey. Dr. Dominey suggested that he get involved in undergraduate chemistry research to see if it appealed to him. With Dr. Dominey's encouragement, he spent a summer at the University of Florida doing research in the group of Dr. Kirk Schanze. A summer's worth of hard work in the lab helping a graduate student complete his synthetic endeavors was enough to inspire Brian to apply to graduate school. After applying to many institutions, he felt most comfortable going back to Florida to work for Dr. Schanze in the area of photochemistry. After graduation from Richmond with a B.S. in chemistry in May 1991, he immediately began graduate school at Florida (and turned into an enormous Gator fan!). In the summer of 1992, he fell victim to a friend's cupid-playing, meeting Robin

Camposano, a medical student at the University of Florida. After three years of relentless courtship and a few peanut butter pies, he convinced her to marry him. Upon completion of his thesis and successful Ph.D. defense, he will continue in the Schanze group as a postdoctoral fellow working on a collaborative project with NASA, until his wife finishes her residency in pediatrics.

I certify that I have read this study and that in my opinion it conforms to acceptable standards of scholarly presentation and is fully adequate, in scope and quality, as a dissertation for the degree of Doctor of Philosophy.

Kirk S. Schanze

Kirk S. Schanze, Chair
Associate Professor of Chemistry

I certify that I have read this study and that in my opinion it conforms to acceptable standards of scholarly presentation and is fully adequate, in scope and quality, as a dissertation for the degree of Doctor of Philosophy.

Daniel R. Talham
Associate Professor of Chemistry

I certify that I have read this study and that in my opinion it conforms to acceptable standards of scholarly presentation and is fully adequate, in scope and quality, as a dissertation for the degree of Doctor of Philosophy.

James M Boncella

James M. Boncella
Associate Professor of Chemistry

I certify that I have read this study and that in my opinion it conforms to acceptable standards of scholarly presentation and is fully adequate, in scope and quality, as a dissertation for the degree of Doctor of Philosophy.

John R. Reynolds
Professor of Chemistry

I certify that I have read this study and that in my opinion it conforms to acceptable standards of scholarly presentation and is fully adequate, in scope and quality, as a dissertation for the degree of Doctor of Philosophy.

Joseph H. Simmons
Professor of Materials Science and
Engineering

This dissertation was submitted to the Graduate Faculty of the Department of Chemistry in the College of Liberal Arts and Sciences and to the Graduate School and was accepted as partial fulfillment of the requirements for the degree of Doctor of Philosophy.

December, 1996

Dean, Graduate School

LD
1780
1996
.H376

UNIVERSITY OF FLORIDA
3 1262 06554 9250